SAIMM

JOURNAL OF THE SOUTHERN AFRICAN INSTITUTE OF MINING AND METALLURGY

CAPACI OCCASIO

FOUNDED 1894

VOLUME 118 NO. 1 JANUARY 2018

We strive to offer you the lowest cost of ownership

Weir Minerals is a leading designer and manufacturer of mine dewatering solutions, slurry pumps, hydrocyclones, valves, screens, centrifuges, crushers, feeders, washers, conveyers, rubber lining, hoses and wear-resistant linings for the global mining and minerals processing, sand and aggregate, and power and general industrial sectors.

For more information contact us on +27 11 9292600

WEIR

Minerals
www.minerals.weir
www.weirafricastore.com

2018 INFACON XV
15TH INTERNATIONAL FERRO-ALLOYS CONGRESS
CAPE TOWN, SOUTH AFRICA

Infacon XV: International Ferro-Alloys Congress

25-28 February 2018

Century City Conference Centre and Hotel, Cape Town, South Africa

INFACON (International Ferro-Alloys Congress) was founded in South Africa in 1974 by the SAIMM (Southern African Institute of Mining and Metallurgy), Mintek (then the National Institute for Metallurgy), and the Ferro Alloys Producers' Association (FAPA) when the first INFACON was held in Johannesburg.
The intention of INFACON is to stimulate technical interchange on all aspects of ferro-alloy production.

Topics for discussion:

Topics include but are not limited to

- Operational updates from ferro-alloy producers
- Technical aspects of ferro-alloy production
- Status of the ferro-alloys markets
- FeCr, FeMn, FeNi, FeV, FeSi, SiMn, *etc.*
- Effects of electricity cost and availability
- Energy efficiency and recovery
- Pre-treatment technologies
- New technologies and processes
- Safety
- Environmental issues
- Carbon dioxide emissions and climate change
- Government policies affecting ferro-alloys
- Carbon tax
- Export restrictions or subsidies
- Sustainability
- Use of natural gas
- Sale of ore versus ferro-alloy production
- Market supply and demand
- Future of the ferro-alloys industry in South Africa
- The impact of UG2 chromite from the PGM industry
- Fines, tailings, and low-grade ores
- Volatility of ore and ferro-alloy prices
- Approach to a circular economy
- How to extract maximum value from resources
- Other topics of relevance to ferro-alloy production

Who should attend

- Metallurgists
- Ferro-alloy producers
- Steel and stainless steel producers
- Smelter operations managers
- Plant general managers
- Engineers, technicians, and scientists
- Process engineers
- Engineering companies
- Furnace equipment and refractory suppliers
- Researchers / Academics
- Specialists in production, economics, and the environment
- Policy makers
- Investors
- Students

SAIMM
THE SOUTHERN AFRICAN INSTITUTE OF MINING AND METALLURGY

For further information please contact:

Gugu Charlie • Conference Co-ordinator • E-mail: gugu@saimm.co.za
Website: http://infacon15.com

Announcement

The Southern African Institute of Mining and Metallurgy

OFFICE BEARERS AND COUNCIL FOR THE 2017/2018 SESSION

Honorary President
Mxolis Donald Mbuyisa Mgojo
President, Chamber of Mines of South Africa

Honorary Vice-Presidents
Mosebenzi Joseph Zwane
Minister of Mineral Resources, South Africa

Rob Davies
Minister of Trade and Industry, South Africa

Naledi Pandor
Minister of Science and Technology, South Africa

President
S. Ndlovu

President Elect
A.S. Macfarlane

Senior Vice-President
M.I. Mthenjane

Junior Vice-President
Z. Botha

Immediate Past President
C. Musingwini

Honorary Treasurer
J.L. Porter

Ordinary Members on Council

V.G. Duke
I.J. Geldenhuys
M.F. Handley
W.C. Joughin
E. Matinde
M. Motuku
D.D. Munro
G. Njowa
S.M Rupprecht
A.G. Smith
M.H. Solomon
D. Tudor
D.J. van Niekerk
A.T. van Zyl

Past Presidents Serving on Council

N.A. Barcza
R.D. Beck
J.R. Dixon
M. Dworzanowski
H.E. James
R.T. Jones
G.V.R. Landman
R.G.B. Pickering
S.J. Ramokgopa
M.H. Rogers
D.A.J. Ross-Watt
G.L. Smith
W.H. van Niekerk
R.P.H. Willis

G.R. Lane–TPC Mining Chairperson
Z. Botha–TPC Metallurgy Chairperson

A.S. Nhleko–YPC Chairperson
K.M. Letsoalo–YPC Vice-Chairperson

Branch Chairpersons

Botswana	L.E. Dimbungu
DRC	S. Maleba
Johannesburg	J.A. Luckmann
Namibia	N.M. Namate
Northern Cape	W.J. Mans
Pretoria	R.J. Mostert
Western Cape	R.D. Beck
Zambia	D. Muma
Zimbabwe	S. Matutu
Zululand	C.W. Mienie

Corresponding Members of Council

Australia:	I.J. Corrans, R.J. Dippenaar, A. Croll, C. Workman-Davies
Austria:	H. Wagner
Botswana:	S.D. Williams
United Kingdom:	J.J.L. Cilliers, N.A. Barcza
USA:	J-M.M. Rendu, P.C. Pistorius

PAST PRESIDENTS

*Deceased

* W. Bettel (1894–1895)
* A.F. Crosse (1895–1896)
* W.R. Feldtmann (1896–1897)
* C. Butters (1897–1898)
* J. Loevy (1898–1899)
* J.R. Williams (1899–1903)
* S.H. Pearce (1903–1904)
* W.A. Caldecott (1904–1905)
* W. Cullen (1905–1906)
* E.H. Johnson (1906–1907)
* J. Yates (1907–1908)
* R.G. Bevington (1908–1909)
* A. McA. Johnston (1909–1910)
* J. Moir (1910–1911)
* C.B. Saner (1911–1912)
* W.R. Dowling (1912–1913)
* A. Richardson (1913–1914)
* G.H. Stanley (1914–1915)
* J.E. Thomas (1915–1916)
* J.A. Wilkinson (1916–1917)
* G. Hildick-Smith (1917–1918)
* H.S. Meyer (1918–1919)
* J. Gray (1919–1920)
* J. Chilton (1920–1921)
* F. Wartenweiler (1921–1922)
* G.A. Watermeyer (1922–1923)
* F.W. Watson (1923–1924)
* C.J. Gray (1924–1925)
* H.A. White (1925–1926)
* H.R. Adam (1926–1927)
* Sir Robert Kotze (1927–1928)
* J.A. Woodburn (1928–1929)
* H. Pirow (1929–1930)
* J. Henderson (1930–1931)
* A. King (1931–1932)
* V. Nimmo-Dewar (1932–1933)
* P.N. Lategan (1933–1934)
* E.C. Ranson (1934–1935)
* R.A. Flugge-De-Smidt (1935–1936)
* T.K. Prentice (1936–1937)
* R.S.G. Stokes (1937–1938)
* P.E. Hall (1938–1939)
* E.H.A. Joseph (1939–1940)
* J.H. Dobson (1940–1941)
* Theo Meyer (1941–1942)
* John V. Muller (1942–1943)
* C. Biccard Jeppe (1943–1944)
* P.J. Louis Bok (1944–1945)
* J.T. McIntyre (1945–1946)
* M. Falcon (1946–1947)
* A. Clemens (1947–1948)
* F.G. Hill (1948–1949)
* O.A.E. Jackson (1949–1950)
* W.E. Gooday (1950–1951)
* C.J. Irving (1951–1952)
* D.D. Stitt (1952–1953)
* M.C.G. Meyer (1953–1954)
* L.A. Bushell (1954–1955)
* H. Britten (1955–1956)
* Wm. Bleloch (1956–1957)
* H. Simon (1957–1958)
* M. Barcza (1958–1959)
* R.J. Adamson (1959–1960)
* W.S. Findlay (1960–1961)
* D.G. Maxwell (1961–1962)
* J. de V. Lambrechts (1962–1963)
* J.F. Reid (1963–1964)
* D.M. Jamieson (1964–1965)
* H.E. Cross (1965–1966)
* D. Gordon Jones (1966–1967)
* P. Lambooy (1967–1968)
* R.C.J. Goode (1968–1969)
* J.K.E. Douglas (1969–1970)
* V.C. Robinson (1970–1971)
* D.D. Howat (1971–1972)
* J.P. Hugo (1972–1973)
* P.W.J. van Rensburg (1973–1974)
* R.P. Plewman (1974–1975)
* R.E. Robinson (1975–1976)
* M.D.G. Salamon (1976–1977)
* P.A. Von Wielligh (1977–1978)
* M.G. Atmore (1978–1979)
* D.A. Viljoen (1979–1980)
* P.R. Jochens (1980–1981)

G.Y. Nisbet (1981–1982)
A.N. Brown (1982–1983)

* R.P. King (1983–1984)

J.D. Austin (1984–1985)
H.E. James (1985–1986)
H. Wagner (1986–1987)

* B.C. Alberts (1987–1988)

C.E. Fivaz (1988–1989)
O.K.H. Steffen (1989–1990)

* H.G. Mosenthal (1990–1991)

R.D. Beck (1991–1992)

* J.P. Hoffman (1992–1993)
* H. Scott-Russell (1993–1994)

J.A. Cruise (1994–1995)
D.A.J. Ross-Watt (1995–1996)
N.A. Barcza (1996–1997)

* R.P. Mohring (1997–1998)

J.R. Dixon (1998–1999)
M.H. Rogers (1999–2000)
L.A. Cramer (2000–2001)

* A.A.B. Douglas (2001–2002)

S.J. Ramokgopa (2002-2003)
T.R. Stacey (2003–2004)
F.M.G. Egerton (2004–2005)
W.H. van Niekerk (2005–2006)
R.P.H. Willis (2006–2007)
R.G.B. Pickering (2007–2008)
A.M. Garbers-Craig (2008–2009)
J.C. Ngoma (2009–2010)
G.V.R. Landman (2010–2011)
J.N. van der Merwe (2011–2012)
G.L. Smith (2012–2013)
M. Dworzanowski (2013–2014)
J.L. Porter (2014–2015)
R.T. Jones (2015–2016)
C. Musingwini (2016–2017)

Honorary Legal Advisers
Scop Incorporated

Auditors
Genesis Chartered Accountants

Secretaries
The Southern African Institute of Mining and Metallurgy
Fifth Floor, Chamber of Mines Building
5 Hollard Street, Johannesburg 2001 • P.O. Box 61127, Marshalltown 2107
Telephone (011) 834-1273/7 • Fax (011) 838-5923 or (011) 833-8156
E-mail: journal@saimm.co.za

Typeset and Published by
The Southern African Institute of Mining and Metallurgy
P.O. Box 61127
Marshalltown 2107
Telephone (011) 834-1273/7
Fax (011) 838-5923
E-mail: journal@saimm.co.za

Printed by
Camera Press, Johannesburg

Advertising Representative
Barbara Spence
Avenue Advertising
Telephone (011) 463-7940
E-mail: barbara@avenue.co.za

The Secretariat
The Southern African Institute of Mining and Metallurgy

ISSN 2225-6253 (print)
ISSN 2411-9717 (online)

SAIMM
JOURNAL OF THE SOUTHERN AFRICAN INSTITUTE OF MINING AND METALLURGY
VOLUME 118 NO. 1 JANUARY 2018

Contents

PAPERS OF GENERAL INTEREST

SAIMM
JOURNAL OF THE SOUTHERN AFRICAN INSTITUTE OF MINING AND METALLURGY
VOLUME 118 NO. 1 JANUARY 2018

Contents *(continued)*

The SAIMM organizes a number of conferences every year to promote technological developments in the mining- and metallurgy-related sectors. Selected papers from each of these conferences are published in the SAIMM *Journal* throughout the year. The SAIMM *Journal* is not only one of the top journals but also one of the most popular journals in the field of mining and metallurgy, and it continuously receives scientific papers from international researchers who wish to publish their output. The Publications Committee receives an average of 300 scientific research papers annually, and the current trends show that the numbers are increasing.

Every *Journal* edition has a theme that is usually associated with a specific conference topic, and every effort is made to include research papers on related topics that were submitted for consideration by the *Journal* in that specific edition. Despite these efforts, the *Journal* continues to have a backlog of research papers awaiting publication. It can take up to a year for a paper of general interest to appear in the *Journal* from the date that the paper is received. This is not a desirable situation, especially from an academic perspective, as researchers would like to see their findings published as quickly as possible.

Apart from the papers that can be matched to a specific conference edition of the *Journal*, to speed up the publishing of the remaining papers, an edition devoted to papers of general interest is produced at least once every year. The themes for this particular edition of the *Journal* are new developments in underground coal mining, froth flotation, and diamond recovery. Eleven papers have been selected covering topics ranging from diamond recovery to mine-to-mill optimization, some new developments in underground coal mining, and froth flotation. Furthermore, papers about resource estimation in marble quarrying, support for roadways in soft rock, and ground control in steep-seam coal mines in China are some of the interesting reads.

Enjoy reading the general papers in this month's *Journal*.

B. Genc

Report calls for open standard for 3D applications in mining industry

User interviews and analysis highlight common challenges

Wednesday, 15 November 2017

According to a new report released by the Global Mining Standards and Guideline Group (GMSG), a survey of more than 18 3D software applications shows that users experience significant difficulties and delays working with the software, collaborating with peers, and learning multiple proprietary programs. An open mining format (OMF) that encompasses a set of guidelines and recommended steps would solve these difficulties.

Currently, mining companies use multiple applications to manage and manipulate their 3D models. Many job functions, including those of surveyors, geologists, mine engineers, and managers, need to be able to move from one 3D data application to another with consistency and relative ease in order to manipulate 3D projects while collaborating with clients and colleagues. This is where issues arise, as many of these applications and software packages do not allow for easy, clean, and accurate movement of 3D information. 'If you're importing a model from one software to another and not double-checking that the variables are imported correctly, you could totally [mess up] pit operations,' says one report interviewee

Using multiple applications creates common technical and process challenges that can result in significant setbacks. Some technical challenges are more common than others. These issues revolve around scripts, ASCII, flat files, name conventions, rotation of 3D images, validity, colour models, managing coordinate systems, and file size, while the significant process challenges are loss of time, reverse engineering, restricted use of available technology, additional costs, and increased risk.

The report says an OMF is a better solution to transferring, managing, and manipulating 3D information and would improve the compatibility of mining software packages, resulting in fewer issues with manipulating 3D information.

The report is based on interviews of five representatives from the mining industry and two additional interviews with industry stakeholders. Some of the representatives included were from industry leaders such as Teck, Barrick Gold, and Newmont. These interviews discussed the current state of interoperability in 3D application technology.

The complete report is available at http://www.globalminingstandards.org/wp-content/uploads/2017/11/GMSG-3D-Data-Exchange-Report.pdf

About GMSG

The Global Mining Standards and Guidelines Group (GMSG) is a non-profit organization established to oversee the development of guidelines designed to be supported and used by mining stakeholders to improve safety, operational, environmental, and financial performance of the mining industry. Through our Future Mining Forum series and hands-on workshops, GMSG facilitates open collaboration between mining industry leaders to create solutions for common industry problems.

For more information, contact Heather Ednie: hednie@globalminingstandards.org

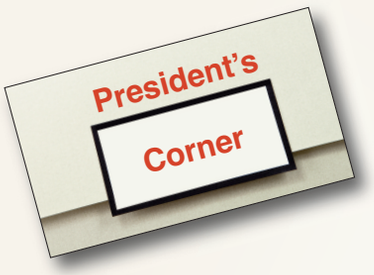

A new year, new reflections

The start of a new year is always worth celebrating. We celebrate the achievements of the previous year. We also celebrate making it through the previous year's challenges and, with optimism, look forward to twelve more fruitful months ahead. However, the fact that a year of our life has just passed by also usually leads to introspection. We question our decisions, actions, ambitions (or lack thereof), as well as many other things we have done or not done in the previous year. The start of the year is an ideal time to reflect on the past and anticipate the future. Hence, the tradition of the New Year resolutions, which are meant to motivate us to do better than what we have done in the past. These resolutions come through self-reflection; we make these resolutions based on the inadequacies that we have acknowledged exist within us. Self-reflection is about questioning, in a positive way, what we do and why we do it and then deciding whether there is a better, or more efficient way of doing it in the future. Because this process is like looking into a mirror and describing what you see, it is not an easy process; it does not come naturally and can even be painful at times.

Self-reflection and self-appraisal is not limited to individuals, but also applies to organizations. It is vital for organizations to occasionally stop and think about where they are coming from and where they want to be in the future. This is essential for effectively and efficiently strategizing for the bigger picture and for the future. Organizational appraisal and analysis involve an intense examination of the organization's internal strengths and weaknesses, identifying gaps in performance between what the organization would like to achieve and what it is actually achieving. Linking the strengths and weaknesses to environmental opportunities and threats can be an effective method of strategic decision-making. From a value perspective, this is essentially recognizing what is not in alignment, disclosing the challenge, and seeking a solution. Although organizational appraisals are not easy; requiring careful planning, consultations, and endless meetings, they become more relevant during volatile times in a changing industrial landscape and when successfully conducted, yield huge returns.

In the past month, the SAIMM embarked on a retrospective analysis. The new year might be the right time for the Institute to forge ahead with this initiative by taking a good look at its current offerings and position within the mining and metallurgical industry, especially since the industrial landscape is changing. It might be a good time to look at both the internal experiences and the external environment through fresh New Year-ready eyes. Maybe it is the time to assess, in detail, the Institute's strengths and weaknesses and to ask some difficult questions. Is the Institute still relevant and doing right by its members? Is it doing what it does in an impactful way? Is it engaged with the members and the industry that it serves? Is it aligned with current events in the industry? How does it position itself so that it is always ready for the changes happening in the industry? Is it meeting the member needs? What are members' perceptions of the Institute? Do they identify with the Institute? These are some of the questions the SAIMM might need to consider as it looks to the future.

As with the reflection that you don't want to see in the mirror, the answers might be hard to swallow. However, change for the better will only come through asking difficult questions, having the courage to answer them honestly, and doing something positive with those answers.

The answers we get might mean that the Institute needs to change what it does and the way it does things. But nevertheless, its core focus and purpose must be maintained. If we don't do this, we run the risk of mission-drift. Purpose is what drives us but holding on to that purpose does not mean that our journey to that purpose shies away from essential and meaningful turns. The start of the year might be that pivotal point where, as an Institute, we embrace that sense of readiness and purpose in order to refresh the SAIMM's aspirations and approach to serving and meeting the needs of its members.

A very happy and productive 2018 to you all!

S. Ndlovu
President, SAIMM

The Society of Mining Professors (SOMP) in collaboration with the Mining Engineering Education South Africa (MEESA) and The Southern African Institute of Mining and Metallurgy (SAIMM) is proud to host

Society of Mining Professors 6th Regional Conference 2018

Overcoming challenges in the Mining Industry through sustainable mining practices

12–13 March 2018 — Conference
14 March 2018— Technical Visit

Birchwood Hotel and Conference Centre, Johannesburg, South Africa

BACKGROUND

The Mining Engineering Education South Africa (MEESA) will host the Society of Mining Professors (SOMP) 6th Regional Conference with the theme: *Overcoming challenges in the Mining Industry through sustainable mining practices*. The Society of Mining Professors is a vibrant Society representing the global academic community and committed to making a significant contribution to the future of the minerals disciplines. The main goal of the Society is to guarantee the scientific, technical, academic and professional knowledge required to ensure a sustainable supply of minerals for mankind. The Society facilitates information exchange, research and teaching partnerships and other collaborative activities among its members. MEESA is comprised of the School of Mining Engineering at the University of Witwatersrand, the Department of Mining Engineering at the University of Pretoria, the Department of Mining Engineering at the University of Johannesburg and the Department of Mining Engineering at the University of South Africa.

The 6th Regional Conference gives a platform to academics, researchers, government officials, Minerals Industry professionals and other stakeholders an opportunity to interact, exchange and analyse the challenges and opportunities within the Minerals Industry. For any country to develop technologically and economically there must be a strong link between its industry, government & academic institutions. This conference will put together the role-players of the Mineral Industry from within and outside South Africa.

RATIONALE FOR SOCIETY OF MINING PROFESSORS (SOMP) REGIONAL CONFERENCE

The main aim of this conference is to facilitate information exchange. It is known that the mining industry is currently faced with big challenges ranging from the technical skills shortage, deep ore bodies, declining ore grades, challenges linked to processing ores with complex mineralogy, water quality and supply to the ever escalating energy costs and sustainability amongst others (Musiyarira et al., 2014). To address some of these challenges there must be a strong link between its industry, government & academic institutions. This will only happen when all the role-players collaboratively work together. The set-up of this conference is such that it allows the interaction between the Minerals Industry players and the academics.

CONFERENCE APPROACH

The conference will feature peer reviewed technical presentations from academic, government and Industry professionals on a wide range of topics. While outlining the Conference programme, great emphasis is laid on participants' interaction in addition to the presentations. The conference will be structured as follows:

FEATURES

- Two-day technical programme with peer-reviewed papers
- Relevant discussion workshops
- Field trips and site tours
- Networking opportunities
- Keynote lecturers

FACILITATOR

The Conference is being organised by Society of Mining Professors (SOMP) in collaboration with the Mining Engineering Education South Africa (MEESA) and The Southern African Institute of Mining and Metallurgy (SAIMM). The Conference presenters are well-known and highly respected experts in their fields, and will cover a wide range of topics. Presentations will be followed by discussions.

TARGET AUDIENCE

The Conference will be of benefit to the Minerals Industry professionals, academics, non-government, government officers and other stakeholders.

EVENT MANAGEMENT SAIMM

For all enquiries please contact:
Chair: Associate Prof Rudrajit Mitra
Telephone: +27 (011) 717 7572 I Email: rudrajit.mitra@wits.ac.za

Head of SOMP Committee on Capacity Building: Dr Harmony Musiyarira

Head of Conferencing: Camielah Jardine
SAIMM, P O Box 61127, Marshalltown 2107
Tel: +27 (0) 11 834-1273/7 · E-mail: camielah@saimm.co.za
Website: http://www.saimm.co.za

Society of Mining Professors
Societät der Bergbaukunde

SAIMM
THE SOUTHERN AFRICAN INSTITUTE OF MINING AND METALLURGY

Conference Announcement

http://dx.doi.org/10.17159/2411-9717/2018/v118n1a1

Application of diamond size frequency distribution and XRT technology at a large diamond producer

by F. Sasman, B. Deetlefs, and P. van der Westhuyzen

Synopsis

Diamond size frequency distribution (SFD) curves, combined with the associated dollar per carat per size class, play an important role in the diamond industry. Value per size class is unique for each deposit and typically varies from less than a dollar per carat to several thousands of dollars per carat for special stones. Recovery of large stone therefore contributes significantly to the bottom line of a large diamond producer. While the design of the process plant should prevent damage and possible breakage of large stones, it should also ensure adequate liberation of the finer diamonds.

Innovative solutions are required to protect and recover type I and II diamonds if prominent within the resource. X-ray transmission (XRT) sorting presents the opportunity to develop flow sheet designs that incorporate a balance between exploitation of the resource and process efficiency, as well as practical capital and operating costs.

This paper serves to illustrate the role and application of SFD curves in determining optimum cut-off and re-crush sizes within the flow sheet of a large diamond producer. A thorough understanding of the unique technical and economic aspects of a deposit provides the basis from where new and innovative technologies can be proposed, allowing mining companies to maintain and improve profit margins. It highlights the results of various plant trials and newly commissioned XRT sorters for larger size fractions. It also provides recommendations for future applications of XRT machines in the diamond process flow sheet.

Keywords

Diamond size frequency distribution, XRT, large diamond producer.

Introduction

Diamond particle size is described in terms of a size frequency distribution (SFD), expressed in terms of the number of stones or carats per size class. SFD curves, in combination with the value profile, are used in resource estimation, cut-off size and re-crush size selections, as well as plant performance tracking and control. The focus here is on the use of SFD curves to optimize cut-off and re-crush size selections. An understanding of the financial drivers of an operation, combined with technical knowledge and experience, provide a sound basis for optimum flow sheet development and fit-for-purpose technology selection.

Technology advances bring forward new options and combinations for diamond processing and are necessary in today's harsh economic environment. The diamond recovery step in particular has undergone vast changes over the last few years as technology from related process industries enters the minerals processing industry; specifically, the inclusion of X-ray transmission (XRT) machines into the flow sheet.

XRT machines operate on the principle of the feed material's ability to absorb X-ray radiation. As diamonds consist of carbon, which is a light element possessing an atomic number of six, they absorb less X-ray radiation than heavier elements such as silicon, calcium, and magnesium. Varying X-ray energies allow the machines to discriminate between various materials based on a combination of density, thickness, and elemental composition.

Large and exceptional stones should be recovered as early as possible in the flow sheet to minimize revenue in circulation and prevent possible diamond damage (van der Westhuyzen, Bouwer, and Jakins, 2014). XRT technology is starting to prove itself in this application by limiting damage to large stones as well as allowing the recovery of type II diamonds. Type II diamonds are more susceptible to damage due to their brittle nature and since they contain very little or no nitrogen, type II diamonds do not luminesce.

Test work was carried out at a diamond mine in Southern Africa to evaluate the use of XRT machines in the recovery circuit, and the results are presented herein. The application of XRT technology in the preconcentration and concentration stages is also documented.

SFD application

The objective of any diamond operation is to obtain maximum liberation; however, given the unique size-revenue profile of diamonds, minimizing diamond damage is equally important in optimizing revenue (Rider and Roodt, 2003). Although much work has been done in mineral processing to quantify the

* *Lycopodium ADP, Cape Town, South Africa.*

 ISSN 2225-6253. Paper received Feb. 2016; revised paper received Feb. 2017.

degree of liberation at different stages of the flow sheet, determining the inputs required for the established formulae is challenging due to the unique attributes of diamonds (Machowski, 2007). However, since the objective is ultimately to know whether a certain size diamond in a certain size host particle is going to be locked or liberated, the size ratio of diamond particle to host rock particle in combination with the preferential liberation factor (PLF) can be used as a proxy. The PLF can be defined as the size ratio of a diamond particle to host rock particle above which the diamond particle will definitely be liberated from the host rock. The mathematical expression and interpretation of the size ratio in relation with the PLF is as follows:

$$\frac{d_{diamond}}{D_{host\ rock}} < PLF \quad [1]$$

$$\frac{d_{diamond}}{D_{host\ rock}} > PLF \quad [2]$$

If the ratio in Equation [1] is true, the diamond will remain locked in the host rock. If not (Equation [2]), the diamond will be liberated from the host rock.

The SFD graph indicates the number of stones or carats per size class. Given the non-uniform class widths and wide range associated with a typical distribution, practice is to convert to unit intervals using the lower critical stone size. Normalizing the size distribution is important as it ensures that the data is presented in a manner that is statistically correct. A typical SFD curve of a recovered diamond parcel (+2 mm diamonds) from a large diamond producer is shown in Figure 1.

Using the SFD as per Figure 1, a diamond deportment exercise was performed to determine the liberation effectiveness of +2 mm diamonds. The diamond deportment exercise prepares a rectangular array, consisting of diamond size on the one axis and host rock particle size on the other axis. Each element in the array indicates a locked or liberated state. The diamond deportment is performed in parallel with the flow sheet mass balance in the process simulation package LIMN, allowing one to track the diamonds across the different streams and unit processes. Once the diamond distributions of the product streams are known, the dollar value per carat per size class is used to calculate revenue and revenue recovery.

The flow sheet in Figure 2 and data as per Table I summarize the results from the diamond deportment exercise.

The results from the diamond deportment exercise as reflected in Table I are typical for a large diamond producer,

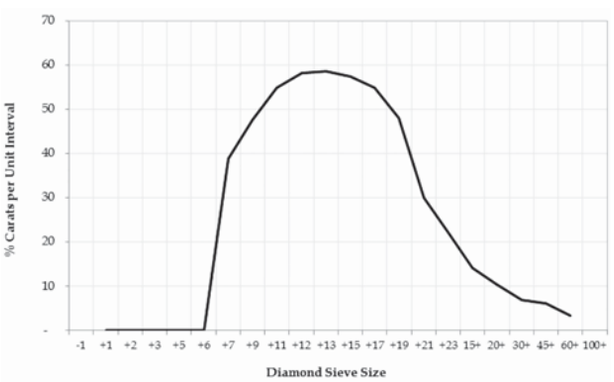

Figure 1—Diamond size frequency distribution indicating percentage carats per unit interval

Table I

Base case diamond and revenue recoveries

	Description	Value	Units
Feed	Liberated diamonds Locked diamonds Total diamonds Total revenue	5 7 12 32 064	cts / h cts / h cts / h $ / h
Product	Diamonds Revenue	8 30 981	cts / h $ / h
Recovery	Diamonds Revenue	66 97	% %

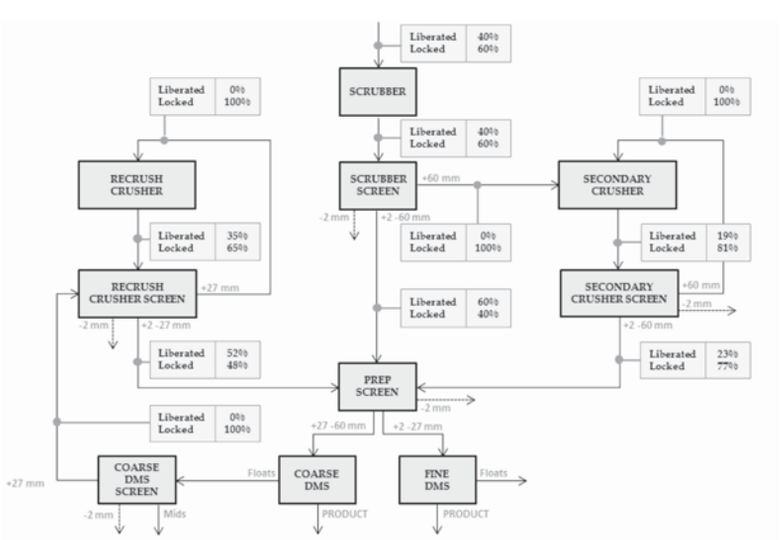

Figure 2—Base case flow sheet indicating per cent liberated and per cent locked carats throughout the flow sheet

with 97% revenue recovery even though more than 30% of the diamonds are not recovered. However, it is important to keep in mind that *in situ* diamond content is not accurately reflected by the recovered diamond parcel. Size distributions based on sales parcels or production samples are not a total content curve and as such not a true reflection of the diamond and revenue recovery potential of a deposit. The illustrated diamond deportment calculation also assumed 100% recovery of liberated diamonds and zero recovery of locked diamonds in the process plant and recovery circuit. The assumptions on which the diamond deportment exercise and subsequent revenue analysis are based are important and dictate whether the results should be interpreted on an absolute or comparative basis.

Impact of cut-off size on diamond and revenue recoveries

Bottom cut-off size (BCOS)

BCOS refers to the smallest diamond the plant is designed to recover and in this exercise is equal to a bottom screen size aperture of 2 mm. Increasing the BCOS to 5 mm will result in a lower diamond and revenue recovery, but on the upside, the operational cost required to recover the diamonds decreases.

Table II indicates that even though the diamond recovery decreases significantly from 66% to 39% when increasing the BCOS from 2 mm to 5 mm, the decrease in revenue recovery is less than 2%.

The distribution in Figure 3 illustrates that most of the revenue is associated with the larger diamonds and therefore the revenue recovery is still acceptable at a relative coarse BCOS of 5 mm. The BCOS is typically determined by the mineral resource management department and is dependent on market conditions.

Middle cut-off size (MCOS)

The MCOS dictates the size fraction that reports to the re-crush stage and is driven by the requirement to attain maximum liberation without causing diamond damage. The base case evaluation was performed at a MCOS of 27 mm.

The decrease in MCOS brings about a small increase in liberation and subsequent diamond and revenue recoveries. However, decisions pertaining to MCOS selection are complex, encompassing a number of aspects such as the risk of diamond damage, capital and operating cost implications, recycle loads, and plant stability. The result as per Table III is just one of the aspects to be included in the trade-off decision.

Table II

Diamond and revenue recoveries at a BCOS of 2 mm and 5 mm

Description	BCOS at 2 mm	BCOS at 5 mm
Diamond recovery	66%	39%
Revenue recovery	97%	95%

XRT applications

XRT machines can be applied at three areas within a diamond process flow sheet. Figure 4 illustrates the inclusion of XRT machines in the preconcentration, concentration, and recovery steps. Although large diamonds are extremely rare and valuable, many operations do not specifically cater for upstream equipment to recover them. Recently, however, there has been a renewed interest from diamond mining operators in recovering larger diamonds as a single large diamond represents significant value compared to the same stone broken into smaller pieces (Webb, 2014).

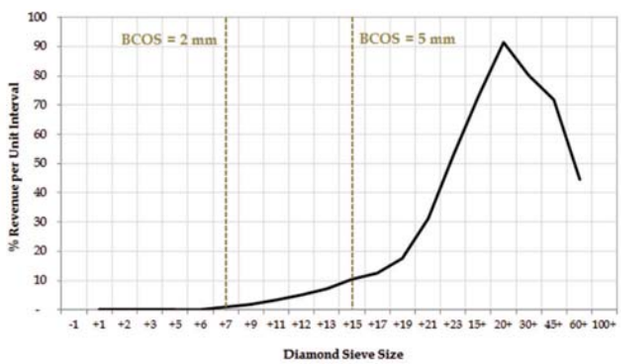

Figure 3—Revenue distribution per unit interval

Table III

Diamond and revenue recoveries at a MCOS of 27 mm and 24 mm

Description	MCOS at 27 mm	MCOS at 24 mm
Diamond recovery	66%	67%
Revenue recovery	97%	97%

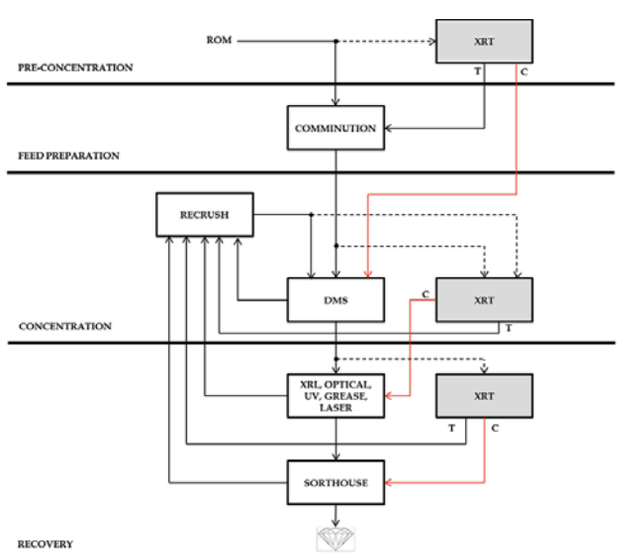

Figure 4—XRT placement in a typical diamond flow sheet

XRT in preconcentration

Waste sorter application

Open pit diamond mines are associated with high stripping ratios. As a result, the preconcentration of run-of-mine (ROM) ore using XRT technology can potentially offer huge economic benefits, including lower operating costs, energy savings, increased throughput, and improved steady-state operations due to less recirculation of the harder constituents. Typically, the ROM is scalped and the undersize fraction is fed to the XRT machines. This step greatly reduces the amount of waste material entering the main treatment plant by applying the discrimination principle on the diamond-bearing ores upfront.

Bulk sorter application

XRT machines can also be used as bulk sorters to recover large diamonds in the preconcentration step. Extraction of large diamonds as early as possible in the flow sheet has the advantage of increasing the recovery of larger diamonds as well as an overall reduction in diamond damage by avoiding exposing the diamonds to subsequent crushing operations.

XRT in concentration

The conventional diamond processing flow sheet employs dense medium separation (DMS) in the concentration step. The advantages and disadvantages of using XRT machines in the concentration step are listed in Table IV.

XRT in recovery

Several methods exist to treat diamond ores in the recovery step. These include separation technologies based on the principles of X-ray luminescence (XRL), X-ray transmission, hydrophobicity (grease tables/belts/drums), infrared (heat conduction), optical (scattering of light and specula reflection of light by diamonds), and laser and ultraviolet discrimination. XRL separation is one of the most basic and common methods of treating diamond ores, and has been applied successfully in diamond plants for more than 40 years (Tirmyaev *et al.*, 2007). XRL operates on the principle of a diamond's property of luminescing under irradiation by an incident X-ray beam.

The advantages and disadvantages of XRL technology in the recovery step are listed in Table V.

A typical large diamond recovery process applies XRT machines post-DMS. The DMS concentrate is fed to recovery; where it is initially sized to XRT feed stream specifications. Generally, this follows a 3:1 feed size distribution. This implies that the top cut-off size (TCOS) is three times the BCOS (*e.g.*, +5 mm -15 mm). The advantages and disadvantages of using XRT in the recovery step are listed in Table VI.

A typical XRT recovery flow sheet is presented in Figure 5. Concentrate is sized into middles +5 mm to 15 mm and coarse +15 mm to 60 mm fractions and fed to two separate XRT machines. The XRT concentrate streams are dried and report to a sort house. The XRT tails fraction is sent to re-crush for recycling. The tails could also be reprocessed through the recovery stage to increase process efficiency.

XRT test work

The primary aim of the XRT test work was to evaluate the unit's ability to recover all diamonds (type I and II) and tracers all the time. The secondary aim was to increase mine revenue by using appropriate technology to improve recovery, reduce diamond damage, increase operational efficiencies, and enhance security of the product.

Table IV

Advantages and disadvantages of XRT in the concentration step

Advantages	Disadvantages
- Lower capital expenditure (CAPEX) than DMS for diamond recovery from larger size fractions	- Higher CAPEX than alternative bulk sorting techniques
- Efficient recovery of all diamond types (I and II)	- Restriction on BCOS
- Potentially low-yielding process	
- Maximizes the recovery of large, high-value stones and minimizes breakage	
- Does not require the material to be exposed to be detected	
- Environmentally friendly technology	

Table V

Advantages and disadvantages of XRL in the recovery step

Advantages	Disadvantages
- Proven technology within the diamond industry	- Traditionally lower throughputs: a monolayer of feed material is required to be presented to the X-ray source
- Recovers high-luminescing diamonds efficiently	- Susceptible to contaminants: for example calcites and sea shells in alluvial diamond applications
- Lower capital expenditure when compared to XRT and DMS	- Inability to detect type II diamonds and other low-luminescing diamonds - Dependant on material temperature – diamond luminescence is a function of temperature

Table VI

Advantages and disadvantages of XRT in the recovery step

Advantages	Disadvantages
- Redefined flow sheet: simplifies the diamond recovery process while significantly reducing operating costs	- High initial costs (CAPEX)
- Automation: minimal or no manual handling required during preconcentration and recovery	- Restriction on BCOS
- Increased recovery rates: technology produces highly efficient sorting by recovering liberated and unliberated diamonds as well as luminescent and non-luminescent diamonds (type I and II)	- Susceptible to carbon-based contaminants: these include plastics and screen panel pins
- Water requirements: little or no water required	
- Higher throughputs: dependent on feed size range	
- Diamond surface properties: less influenced by dust and slime on the surface of the diamond	
- Large diamond recovery: large diamonds can be recovered before secondary and tertiary crushing	

Table VII

Large diamond recovery XRT application test work: summary of results

Test description	Middles fraction +5 mm -15 mm	Coarse fraction +15 mm -60 mm
1. Tracers only	100%	100%
2. Tracers with gravel	100%	100%
3. Diamonds only	100%	100%
4. Diamonds with gravel	100%	100%

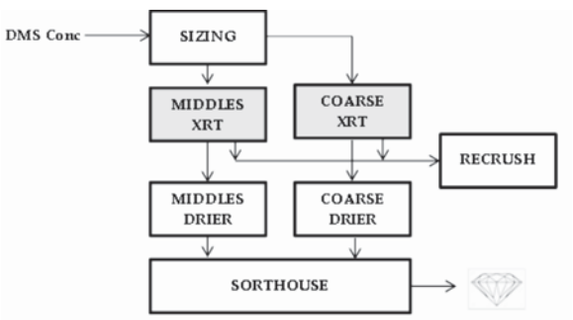

Figure 5—Typical XRT recovery flow sheet

Figure 6—Gem-quality, boart, and type I and type II diamonds used in XRT test work

Test work outline

Four different tests were carried out, and each test was repeated three times to aid in assessing the performance repeatability of the XRT machine. Test 1 was carried out using tracers only, test 2 utilized tracers with gravel, test 3 utilized diamonds only, and test 4 used diamonds with gravel. Table VII summarizes the test work outline and results.

The diamonds used during the test work consisted of different coloured gem-quality stones, boart diamonds, and type I and II diamonds (see Figure 6). For tests carried out with gravel, the sample feed constituted of 100 kg of pre-screened (–15 mm) material. During each test the XRT machines recovered all of the tracers and diamonds from both the middles and the coarse fraction.

XRT yields and grams per ejection

A single test, based on operating the entire recovery plant, was carried out to evaluate the yield of the middles and coarse XRT machines. The middles machine yielded 0.03% and the coarse machine 0.27%.

Grams per ejection can be defined as the associated mass of material ejected once the XRT machine has detected carbon-based matter and triggers the jet of air used to move the detected material from its normal process path to the concentrate chute. Only the middles XRT machine was tested for associated grams per ejection, and it was found that the minimum associated mass per ejection was 0.7 g, with a maximum of 1.7 g. This attribute is a function of feed size distribution and can therefore increase, depending on the TCOS.

Conclusion

Basic diamond process plant design principles utilized in conjunction with SFD and revenue distribution data have proved to be a powerful analytical tool for process design engineers. This method allows the engineer to make improved decisions when faced with the risks and complexities associated with the incorporation of new technology into proven flow sheets. As with the addition of any new technology, risks related to process efficiency, and capital/operating costs should be traded off and the ultimate

decision should be made on applicability and appropriateness.

The XRT algorithm selected during the large diamond recovery test work resulted in 100% of the diamonds being discriminated and ejected to the concentrate stream. For future XRT applications in flow sheets for recovering large diamonds, it is recommended that attention is given to the feed preparation step. Upstream product degradation resulting in additional fines generation could cause the XRT machine to produce much higher yields than initially expected, which could significantly and unnecessarily affect the sizing of downstream equipment.

From the large diamond recovery test work presented, it can be concluded that there is a noticeable role for XRT machines within a traditional diamond process flow sheet. It goes without saying that the addition of XRT machines should follow the systematic approach of process design, including ore dressing studies, development of design criteria, trade-off studies, and the ultimate establishment of applicable and appropriate flow sheets.

References

Anon. 2013. Diamonds sensor-based ore sorting since 1988. www.tomra.com [Accessed 12 October 2015].

file:///C:/Users/User/AppData/Local/Temp/TSMI_11_Segment%20Guide%20-%20Diamonds_english_WEB-2.pdf

Bush, D. 2010. An overview of the estimation of kimberlite diamond deposits. *Proceedings of Diamonds - Source to Use 2017*, Gaborone, Botswana, 1–3 March 2010. Southern African Institute of Mining and Metallurgy, Johannesburg. pp. 73–84.

Ferreira, J. 2013. Sampling and estimation of diamond content in kimberlite based on microdiamonds. Doctoral thesis, Ecole Nationale Supérieure des Mines de Paris.

Machowski, R. 2007. Technique for estimation of diamond lockup in a diamond processing plant. *Proceedings of Dianinds – Source to Use 2007*. Southern African Institute of Mining and Metallurgy, Johannesburg.

Rider, P.J. and Roodt, A. 2003. Diamond value management - knowledge management and the measurement of value addition. *Journal of the South African Institute of Mining and Metallurgy*, vol. 103, no. 9. pp.551–556.

Riedel, F. and Dehler, M. 2010. Recovery of unliberated diamonds by X-ray transmission sorting. *Proceedings of Diamonds - Source to Use 2017*, Gaborone, Botswana, 1–3 March 2010. Southern African Institute of Mining and Metallurgy, Johannesburg. pp. 193–199.

Tirmyaev, A., Kulikov, R., Potashnikov, A., and Sysoev, E. 2007. New methods and instruments in mining. *Journal of Mining Science*, vol. 43, no. 5. pp. 555–564.

Van der Westhuyzen, P., Bouwer, W., and Jakins, A. 2014. Current trends in the development of new or optimization of existing diamond processing plants, with focus on beneficiation. *Journal of the Southern African Institute of Mining and Metallurgy*, vol. 114. pp. 537–546.

Webb, M. 2014. DebTech develops new diamond sorters to fill gap. http://www.miningweekly.com/article/debtech-develops-new-diamond-sorters-to-fill-gap-2014-07-24 [Accessed 12 October 2015]. ◆

http://dx.doi.org/10.17159/2411-9717/2018/v118n1a2

A mine-to-mill economic analysis model and spectral imaging-based tracking system for a copper mine

by S.S. Nageshwaraniyer, K. Kim, and Y-J Son

Synopsis

An economic analysis model is proposed for estimating the cost savings incurred in all operations, from blasting to milling, in a copper mine using spectral imaging-based tracking. A conventional mid-sized copper mine in Arizona with two ore types is used as a case study. First, a combined regression and discrete event simulation model of the material-handling network of the mine, constructed in Arena™, is used mainly to obtain throughput information at pits, crusher, and mills as well as the stochastic power consumption at each operation from mine to mill. The two ore types are assumed to be distinguished using a spectral imaging-based tracking method. The main components of the spectral imaging-based tracking method are a multispectral camera and a regression model consisting of partial least-squares, principal component, or logistic regression methods. Partial least-squares, principal component, and logistic regression methods are then compared to select the best method to distinguish various ore types sampled from the mine. Finally, an economic analysis model based on tracking results fed to the simulation model is used to demonstrate the cost savings for each ore type as a function of the specific explosive's energies. This is a preliminary study of the economic analysis of overall cost savings before testing in an actual copper mine.

Keywords

mine-to-mill optimization, copper mine, ore tracking, hyperspectral imaging, multispectral, discrete event simulation.

Introduction

In a copper mining operation, the copper recovery in the mineral processing circuit is affected by upstream operations. The upstream operations in a conventional copper mine include blasting, excavation, crushing, transportation, stockpile storage, as well as milling in semi-autogenous grinding (SAG) and ball mills. Varying the specific explosive energy may have a significant impact on the downstream comminution processes, and can maximize the cost savings between blasting and ball milling while achieving a sufficiently small P_{80} at the ball mill (Chung and Katsabanis, 2000; Nielson and Lownds, 1997; Nielsen and Malvik, 1999; Scott, 1996). P_{80} is the 80% passing size in the cumulative size distribution (both post-blast and post-mill fragmentation), and it is generally used as a representative size of the fragmentation in the hard-rock mining industry. However, for a mine with two or more ore types, these savings are difficult to estimate in absence of an ore-tracking method that can detect ore type as well as estimate fragment sizes (Kim and Kemeny, 2011). There are challenges to ore-tracking methods as well, resulting from thorough mixing of ore, for example at the stockpiles. Dissimilarities between ore types in terms of their blastability, crushability, and grindability add to the complexity of estimating the energy expenditure required to achieve a target P_{80} during milling. In summary, although it may be difficult, it is important for mine operators to distinguish between ore types so as to be able to calibrate the total explosives energy accordingly in order to maximize the total cost savings over a period of time.

Tracking systems have been used in mines for other purposes in the past. A system based on a radio frequency identification (RFID) tracer in a plastic shell has been developed (Jansen *et al.*, 2009). Although this tracer does not provide continuous tracking of all ore types in a mine, it could be used to track ore transported between stockpiles and bins. Similarly, RFID tracers have been used to track blast movements (La Rosa and Thornton, 2011). Continuous tracking already exists for all ore transported from pits to crushers (Modular Mining, 2014). This tracking is based on global positioning system (GPS) devices attached to the trucks hauling ore from shovel sites to the primary crushers. However, the tracking process does not continue through the comminution circuit and stockpiles. Thus, tracking ore movement from blast sites to the ball mills requires prediction and tagging of ore type of each individual fragment transported on trucks and conveyors. Tagging and prediction is useful in mines where the majority of fragments are over 1 inch

* *University of Arizona, USA.*

 ISSN 2225-6253. Paper received Mar. 2017; revised paper received May 2017.

(2.54 cm) in size, which, in the authors' experience, is the typical cut-off size for feasible prediction of ore type. Where fragment sizes are smaller, bulk tagging and prediction can be more useful than individual tagging and prediction. X-ray fluorescence, X-ray diffraction, and imaging spectrometry are possible technologies that can be used to remotely sense the mineral content in fragments (Klug and Alexander, 1954). Imaging spectrometry relies on obtaining electromagnetic spectra from the minerals of interest. It has been used in the past to detect minerals having spectral reflectance characteristics (SRC) in the visible and invisible parts of the electromagnetic spectrum. Some of its applications include mineral mapping (Tangestani *et al.*, 2011), vegetation species identification (Bechtel, Ribard, and Sánchez-Azofeifa, 2002), and rock discrimination (Sgavetti *et al.*, 2007; Combs *et al.*, 2011) among others. The works cited have shown that wavelengths between 400 nm and 2500 nm, comprising both visible and near-infrared (VNIR) and short-wave infrared (SWIR) spectra, are the most useful for discrimination. Statistical analysis methods such as partial least-squares regression (PLSR) can be used for discriminating between mineral types based on a hyperspectral image (Haaland and Thomas, 1988; Blanco and Peguero, 2011). Principal component regression (PCR) is a method similar to PLSR that uses principal component analysis (PCA) to determine the unknown regression coefficients. Logistic regression (LR) is another competitive method for discriminant analysis, where the output specifies a particular fragment explicitly and categorically as belonging to an ore type.

To solve the tracking problem, we developed a spectral imaging-based automated tracking method for ore types and fragmentation. We demonstrate cost savings from applying the proposed system using a simulated conventional copper mine. A generic small-sized copper mine with two different types of ore – hard and soft rock (names of ore aligned with those used in the case study) – is considered. In general, mathematical programming and computer simulation can be applied to model mining operations in order to obtain various performance measures such as production and equipment utilization. When used as a standalone tool, stochastic programming is best suited for instances where the goal is to maximize a performance measure such as production under constraints with stochastic model parameters (Kataoka, 1963; Kall, Wallace, and Kall, 1994; Sahinidis, 2004; Santelices *et al.*, 2017). But when combined with simulation, in addition to maximization of a measure, the combined tool can be used to evaluate system performance measures as well as keep track of detailed system statuses over time, such as locations of trucks and movement of ore on conveyors. Simulation models of most processes in mines can be constructed through a combination of discrete event simulation and process simulation. The need to use process simulation arises when environmental factors underlying crushing and grinding processes vary significantly enough to impact performance measures such as quality of throughput. There are several recent applications of process simulation to model the underlying dynamics in crushers (Asbjörnsson, Hulthén, and Evertsson, 2012, 2013; da Cunha, de Carvalho, and Tavares, 2013; Asbjörnsson *et al.*, 2016). Discrete event simulation has been applied to model truck-shovel haulage operations in surface coal mines, underground mines, and similar operations in construction such as earth movement (Zhang, 2008; Meng *et al.*, 2013; Nageshwaraniyer, Son, and Dessureault, 2013; Salama, Greberg, and Schunnesson, 2014; Torkamani, and Askari-Nasab, 2015; Park, Choi, and Park, 2016). Discrete event simulation software packages such as Arena™ and SIMIO™ have become popular because they offer easy-to-use graphical user interfaces and attractive animation capabilities. An early, but thorough, review of software used in mine system simulation in the USA is provided by Sturgul (1999). Since conducting experiments at all locations from mine to mill in a real mine in order to collect inputs and outputs for estimating cost savings is difficult, a regression model (using experimental data from one of many operations of the mine) and discrete event simulation model using Arena™ software are used to model all the mining operations in this study. The Monte Carlo technique is embedded in Arena™ and is used to estimate the confidence intervals in performance measures such as production, equipment utilization, and queue times caused by uncertainties from shovel loading times, truck haul, and dumping times.

In this work, the first objective is to model all operations from blasting to grinding using a combination of regression and discrete event simulation. Constructing very granular models for blasting requires an understanding of the underlying physics. However, models predicting aggregated blast particle-size distributions have been constructed in the past based on linear regression (Kim and Kemeny, 2011; Modular Mining, 2014). Hence, real data for blasting parameters such as explosives energy, burden, spacing, rock properties (tensile strength or mode I fracture toughness), and block size of the bench face is used to construct a blasting regression model to predict the resulting particle size distribution (Kim and Kemeny, 2011). A MS Excel® linear regression tool has been used to estimate the coefficients of the blasting regression model. The other operations, such as excavation and transportation of ore via trucks and conveyors to crushers and grinders, mimic supply chain systems, and are therefore modelled using discrete event simulation in Arena™. The data for blasting and other operations, as well as the structure of the simulated mine, is based on a mid-sized copper mine in Arizona. One of the main contributions of this paper is to specify the mean cost savings percentage, together with its confidence interval, as a function of specific explosives energy.

The spectral imaging-based tracking method proposed involves a combination of software and hardware. The software tools used are SPLIT Online 4.1 (image processing system) and a MATLAB-based regression model. SPLIT Online 4.1 is used to estimate fragment contours and volumes. At the core of SPLIT Online 4.1 technology are particle delineation algorithms used for marking outlines of fragments in truck dumps, muckpiles, and moving conveyor belts (Kemeny, Mofya, and Kaunda, 2002; Latham *et al.*, 2003; BoBo *et al.*, 2004). PLSR, PCR, and LR are compared for selecting the best prediction model for distinguishing samples from real mines, using the built-in functions in MATLAB. The main hardware components used in the method are multispectral cameras. The regression algorithms mentioned above are used to distinguish between ore types in each image delivered by the multispectral camera. The

VNIR camera costs less than the SWIR camera because the SWIR camera captures much higher wavelengths. A 3D full-motion video spectral imaging (FMV-SI) camera such as the one from Surface Optics (SOC, 2014) is better than line-scanner cameras in retaining spectral information, even at medium to high conveyor speeds (approx. 1 m/s in Figure 1). Since training and validation testing on real ore samples is necessary for comparisons between different regression algorithms, the second objective of this work is to collect and perform laboratory tests on ore samples from different mines. The tests were conducted on both a static surface (wood) as well as a moving conveyor. The third objective is to determine the combination of multispectral camera and regression model for prediction that can most accurately detect and distinguish different ore types. To the best knowledge of the authors, this is one of the first investigations in which VNIR, SWIR, and FMV-SI cameras have been studied for distinguishing between ore types on moving conveyors in a laboratory setting.

A brief description of the blasting regression model, as well as the simulation model of the mine used as a case study, is provided. This is followed by a discussion of results from testing different regression models on different ore samples using VNIR and SWIR cameras. A technique for integrating the detected ore type information with delineation information for implementation in the real mine is explained. The economic analysis of the overall cost savings achieved through the proposed spectral imaging-based tracking is discussed, and finally, the conclusions are presented.

Simulation model of a copper mine

Three simulation sub-models were developed in Arena™ for the mid-sized copper mine: (1) forward blasting model, (2) reverse blasting model, and (3) comminution model (see Figure 2). The forward blasting model simulates the blasting process using site-specific blasting models at the pits (Kim and Kemeny, 2011). Two main assumptions are made for the simulation modelling: (1) a specific number of truckloads per day per pit along with cycle times is assumed, and (2) errors in blasting parameters – burden and spacing – are assumed to be induced by drill error and the mismatch between drill pattern and blast direction. The actual value of the error in blasting parameters can be obtained from operational blast data. In the experiments conducted, the errors are assumed to follow a uniform distribution. For example, if the error in burden is 5%, then the actual burden in a blast can vary between –5% and +5% of its mean value. Two ore types are considered in this model, and one shot per day is made at each of the pits. This sub-model is used to determine the coefficients of the site-specific blasting model when there is only limited data availablefor blasting parameters, such as burden, spacing, and particle size distribution of ore in truck beds.

For constructing our site-specific blasting model, data from visible range cameras at a real copper mine in Arizona was used. F_{80} of shots – the bench face block size (80% passing size) before blasting – and particle size distributions of blasted ore dumped into trucks were provided. F_{80}, bench height, and tensile strength (T_0), are taken to be deterministic variables. During the simulation run, for each

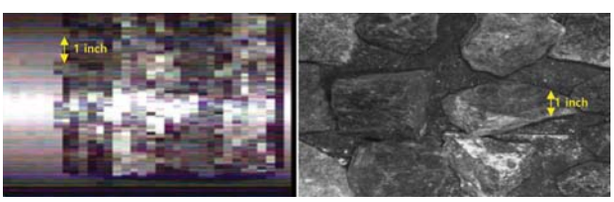

Figure 1—VNIR line-scanner camera image (left) and VNIR FMV-SI image (right)

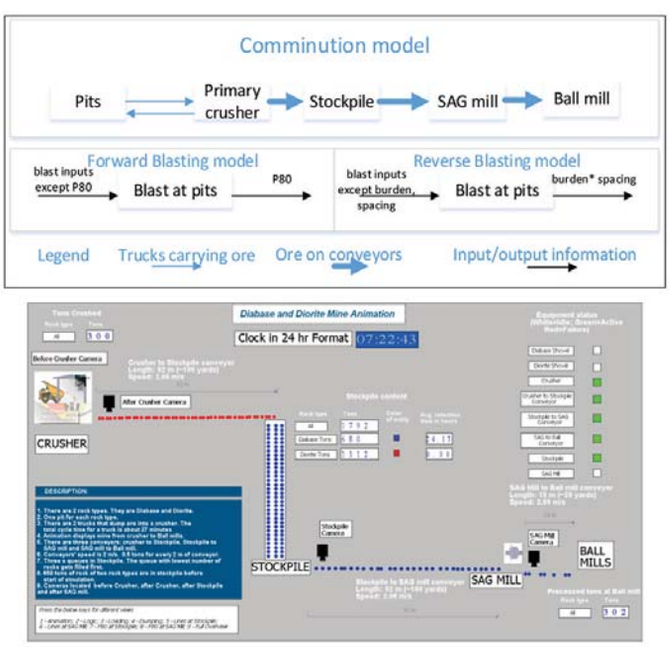

Figure 2—Overview of blasting and comminution simulation models (top); sample mine animation from crusher to ball mill (bottom) (Nageshwaraniyer, Kim, and Son, 2015)

pit, the values of burden, spacing, bench height, T_0, F_{80}, and P_{80} from each truckload were recorded into an MS Access database. The site-specific blasting model taken from Kim and Kemeny (2011) and its logarithmic form used in regression analysis are given in Equations [1] and [2], respectively. Although additional efforts are needed to validate this model for many mines around the world, the results presented by Kim and Kemeny (2011) applying this blasting model on data from a real copper mine are promising. E_{SE} is the specific explosives energy, whereas F_{80} and P_{80} are the 80% passing sizes before and after the shot respectively. $\ln(A)$ is the intercept, and B, C, and D are the coefficients in the regression model.

$$E_{SE} = A\,(F_{80})^B(P_{80})^C(T_0)^D \quad [1]$$

$$\ln(E_{SE}) = \ln(A)+B\ln(F_{80})+C\ln(P_{80})+D\ln(T_0) \quad [2]$$

The above model was also applied by Nageshwaraniyer, Kim, and Son (2015) using an MS Excel regression analysis tool on same sample data as in this paper, and the best model coefficients were chosen using the R^2 value (which is the proportion of variation in E_{SE} as explained by variation in T_0, P_{80}, and F_{80}). Values of R^2 above 0.9 were obtained, which implied that the regression model had a good fit between dependent (E_{SE}) and independent variables (T_0, P_{80}, and F_{80}). Thus, E_{SE} values could be explained by our sample data using the site-specific blasting model. The estimated regression coefficients were then provided as input to the reverse blasting model in order to determine the product of burden and spacing for a desired P_{80} for each ore type, given the F_{80}, bench height, explosives energy, tensile strength, and specific gravity for the corresponding pit. After many simulation replicas, the mean of product of burden and spacing along with the confidence intervals were recorded. If there is a known relationship between burden and spacing, the burden and spacing values can be deduced separately from this product of burden and spacing. If such a relationship is unavailable, different combinations of burden and spacing yielding the abovementioned product can be reviewed, and the best combination among these can be chosen by blast engineers for application at the real mine.

The P_{80} of each blast from the forward blasting model serves as input to the comminution model, which in turn is used to simulate truck haulage, crushing, stockpiling, and grinding operations. Using the forward blasting model, plus the F_{80}, power setting (with uncertainty) and the associated Bond work indices for each comminution process, we can estimate throughput as well as the P_{80} for each of these comminution processes. Thus, the forward blasting model is used to construct a model to predict blast fragmentation, the reverse blasting model is used to determine burden and spacing (for a desired P_{80}) when needed, and the comminution model is used to estimate throughput and P_{80} values for crushing and grinding operations.

Multispectral imaging and statistical prediction

Regression results using multispectral images

In this work, three types of regression techniques were applied for prediction of ore types from images of ore fragments: PLSR, PCR, and LR. Fragments of different sizes were present in each sample image. This was done in order to analyse the effect of varying fragment sizes on accuracy of prediction of rock types based on statistical regression techniques. The fragments, collected from a mid-sized copper mine in southern Arizona, were not cleaned before imaging, so as to mimic a real-world situation. In some cases, fines were added. Spectral imaging-based prediction involves calibration of the image, training and validation of regression model, and prediction. Calibration mainly involves correcting and recalculating the intensities, in raw multispectral images, of fragments on moving conveyors, based on the extreme values of intensities obtained from images taken at the same site on a static conveyor. Thereafter, for each pixel, the intensity values across all wavelengths are converted into absorbance values. As an example, in Figure 3, PLSR was used for distinguishing between QMP (quartz monzonite porphyry) and diorite, using the corresponding multispectral image as input. The image of a conveyor moving at 1 m/s was captured by a multispectral five-band camera with 1024×1360 pixel resolution; the spectral wavelength range was 400–1000 nm. For training, 11 pixels covering QMP (bright fragments; assigned '1'), diorite (other fragments; assigned '0'), and background (tray; assigned '0') were chosen. PLSR in this case was trained to predict the pixel-wise likelihood that there is QMP in an image. When the trained PLSR was validated, it produced the image depicted in Figure 3, where pixels that are more likely to be QMP exhibit red or yellow colours and other pixels blue or green colours. The bright red fragments are QMP and the others are diorite. The sets of scenarios that were considered are as follows: (1) QMP and diorite, (2) QMP and andesite, and (3) diorite and andesite. In each of these images, training was performed

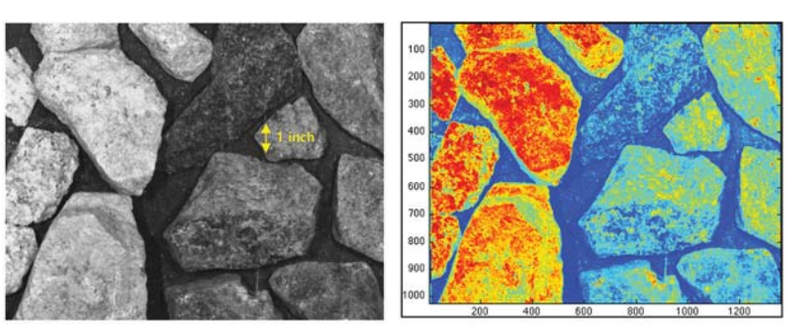

Figure 3—Results for QMP (red/yellow in right figure) and diorite fragments (blue/green in right figure) using PLSR in MATLAB

using spectral information from all types of materials available that could be visually identified. A summary of conveyor tests performed using this camera for ore type prediction in a laboratory setting is provided in Table I.

A summary of tests performed on a static surface with the SWIR and VNIR cameras is provided in Table II. These cameras generally have a large number of bands, and hence they are called hyperspectral cameras. However, due to their 'push-broom' mode of operation, these cameras can lose spectral information at high speeds (Figure 1). So, even though the results are impressive, they are not suited for prediction on conveyors at high speeds in real mines. The effect of the presence of dust and fines on ore type prediction is demonstrated in Figure 4. As illustrated in the left image of Figure 4, the presence of dust was simulated in a laboratory setting. Here, dust was simply blown when the image was being captured to imitate a real mine. The pixels covering the fines on top of andesite were not chosen for training. From Figure 4 (right), it can be observed that the presence of dust does not affect prediction using either the PLSR, PCR, or LR method. However, the pixels covered by fines were not detected as andesite. Here, the more reddish the colour, the more likely it corresponds to andesite.

Proposed spectral imaging system

The VNIR camera is mounted four to six feet above the belt to provide a wide field of view of the passing product. A LED lighting array is positioned around the camera to provide even illumination of the target (Figure 5). The FMV-SI camera uses a micro lens array so that all spectral bands are

Table I

Summary of conveyor tests for ore type prediction in a laboratory setting

Multispectral camera	Tested rock samples	Wavelength region (nm)	Best classification method	Comments (no. of fragments/ total fragments)	Rating
VNIR (400-1000nm; 5 band/channel)	QMP and diorite QMP and andesite Andesite and diorite	400–1000 400–1000 400–1000	Partial least squares Partial least squares Partial least squares	Mostly correct (7/7 QMP, 6/7 diorite) All correct (8/8 QMP, 6/6 andesite) Some correct (4/6 Diorite, 5/6 andesite)	90% 100% 70%

Table II

Summary of static tests for ore type prediction in a laboratory setting

Hyperspectral camera	Tested rock samples	Wavelength region (nm)	Best classification method (analysis)	Comments (no. of fragments/ total fragments)	Rating
SWIR camera (1000-2500 nm; 256 band)	Hard granite, soft granite, aplite	1275–2380	Logistic regression model	Mostly correct - aplite and soft granite are hard to differentiate (3/6 Aplite rocks correct, 5/5 HG correct, 4/5 SG correct)	90%
		1000–2500	Logistic regression model	Hard granite predicts well, soft granite & aplite are sometimes predicted as each other	90%
VNIR (350-1100nm; 540 band)	Hard granite, soft granite, aplite	350–1100	Logistic regression model	Mostly correct - aplite and soft granite are hard to differentiate (4/4 aplite correct, 4/4 HG correct, 2/4 SG correct)	90%
		400–900	Logistic regression model	All 12 out of 12 rocks were correctly identified. (4/4 aplite correct, 4/4 HG correct, 4/4 SG correct)	100%
		425–800	Logistic regression model	Mostly correct - aplite and soft granite are hard to differentiate (2/2 Aplite correct, 4/4 HG correct, 4/4 soft granite correct)	90%

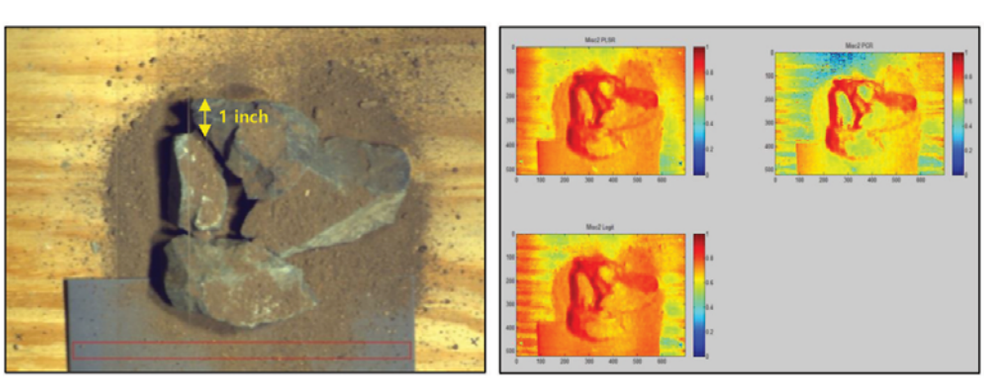

Figure 4—Andesite with dust and fines (left); training and prediction (right)

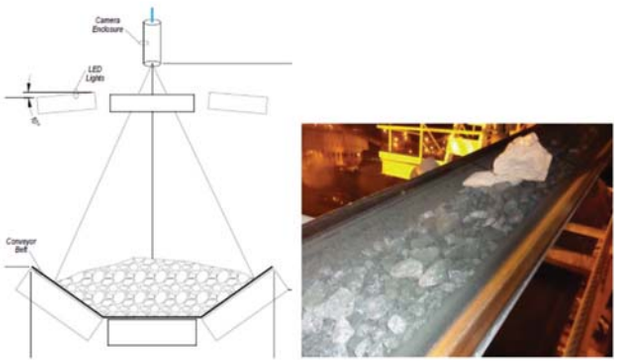

Figure 5—Imaging station layout (left) and typical product (right)

imaged with each captured frame. The camera has 16 narrow-band filters over a spectral range of 450–900 nm with each image size of 640×540 pixels while capturing at least 30 images per second.

The proposed hardware to be used for the spectral imaging-based tracking system (Figure 6) is as follows: (1) conveyor; (2) multispectral camera; (3) server for storing images; (4) computer for processing raw multispectral images and calibrated images using SPLIT Online and the PLSR regression model. The following software may be used: (1) dynamic process simulation using Arena™, (2) SPLIT Online, and (3) MATLAB. The sequence of steps involved in detection and prediction of ore type is as follows. At first, the raw feed from the cameras will be supplied to the server, which stores this information. SPLIT Online delineates the contours of each fragment from the feed images and also provides average volume information of each fragment. Then, MATLAB is used to run a PLSR code to distinguish between ore types. Subsequently, based on the delineations of the images provided by SPLIT Online, the PLSR outputs of fragment contours and shadows are ignored. The end results are the volume and tonnage by ore type that have passed the camera at a given time. This information will be written into a table in the server, which can be later used to run a dynamic process simulation as well as estimate the cost savings, as discussed later.

The integration technique for SPLIT (image processing system) and regression results distinguishing ore types are briefly discussed here using an example. Figure 7 (left) shows the delineations of a sample multispectral image (Figure 3, right) using SPLIT Online. For delineation, SPLIT Online first converts the RGB portion of the multispectral image to greyscale. Secondly, various image enhancement techniques, such as smoothing and sharpening, are applied. To identify rock fragments, SPLIT Online utilizes techniques such as texture analysis and threshold determination algorithms. Results obtained from image processing using SPLIT Online's particle detection algorithms are to be overlaid onto the PLSR code's colour maps (Figure 3, right for this example), as shown in Figure 7 (right). Here, pixels of very dark blue colour in Figure 7 (right) correspond to black pixels or non-fragment pixels in the delineated image in Figure 7 (left).

After ignoring non-fragment pixels, the remaining pixels are grouped into two clusters. A fragment's rock type is estimated after assigning it to an appropriate cluster, based on its average likelihood as determined by the PLSR code. Not all pixels of a fragment are homogenous, possibly because of variations in fracture or mineral content. In some cases, the detection of non-fragment pixels may not be a significant issue. For example, a real conveyor's background – such as in Figure 8 (left) and the delineated SPLIT image in Figure 8 (right) – will have no exposure since the fragments are very closely packed. In such cases, approximations can be made about the ore type and volume of the very small non-delineation dust-like fragments.

Economic analysis using simulation

The proposed tracking system can help estimate the power consumption for each ore type at blasting, crushing, and grinding stages. It follows that the four best camera locations for detecting ore fragment types and sizes leading to power consumption estimation are before the crusher, after the

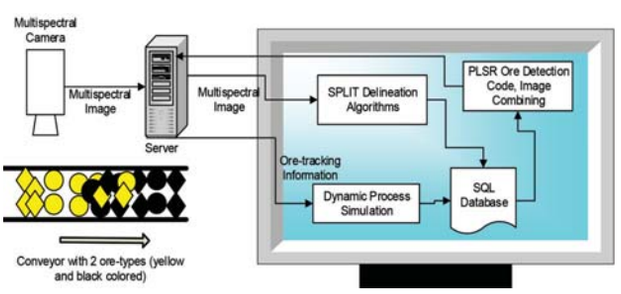

Figure 6—Processes involved in detection and prediction using the tracking system

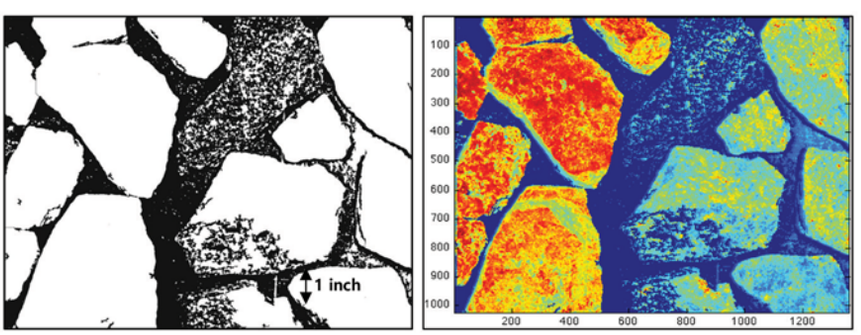

Figure 7—Delineation of multispectral image (left) and superimposed results (right)

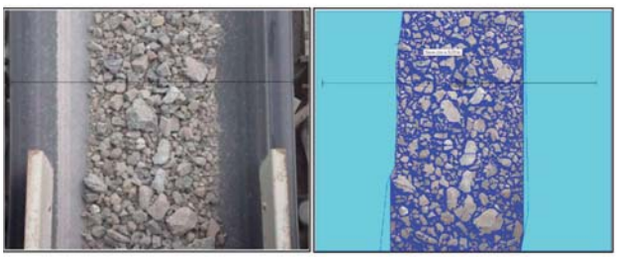

Figure 8—SPLIT Online conveyor sample (left) and its delineated image with sieve size (right)

crusher, after the stockpile, and after the SAG mill. Due to the non-availability of detailed P_{80} by ore type at each stage, the power consumptions have been calculated for an assumed reduction ratio (Kim, 2006, 2012; Kim, and Kemeny, 2011; Nageshwaraniyer, Kim, and Son, 2015) at each stage. The reduction ratio at a particular stage is defined in this work as ratio of F_{80} to P_{80}. The power consumption for blasting (using the camera before the crusher) is estimated using Equation [1]. The power consumptions for the crusher and grinding operations are estimated using the Bond work index formula with known Bond work indices.

The aim of this experiment is to demonstrate how spectral imaging-based tracking of classification into hard and soft rocks can be used to obtain their optimum E_{SE} values that maximize cost savings from mine to mill. The simulation model and the blasting parameter errors discussed earlier were considered (Nageshwaraniyer, Kim, and Son, 2015). In addition, a percentage error of uniform distribution UNIF (4, 5.5) was considered for each comminution power setting. To simplify calculations, it was assumed that the haulage costs are independent of specific explosives energy applied during blasting. Therefore, for the purposes of comparison of cost savings across different specific explosives energies, the total power consumption is the sum of power consumptions over the blasting and comminution processes (Kim, and Kemeny, 2011). It was also assumed that the mills are the primary bottlenecks in production (Nielsen and Lownds, 1997; Nielson and Malvik, 1999). Therefore, fixed relative power consumption cost percentages were assumed for the blasting, crushing, and milling processes, with the costs increasing as ore moves from blasting to milling (Kim, and Kemeny, 2011). The effects of reductions in Bond work indices due to micro-cracking were included as well. Ten replications were performed to determine the mean and confidence intervals of power consumptions at all the stages indicated in Table III. The cost savings shown in Figure 9 are compared to the base E_{SE} scenario of 175 kcal/t (732.2 kJ/t). It can also be seen that the cost savings for hard rocks are larger for a wider range of E_{SE} than those for soft rocks. Although this is a preliminary economic analysis based on some assumptions, the results show ore-tracking will provide the information necessary to choose the E_{SE} for each ore type in order to achieve the maximum cost savings.

Conclusions

The economic benefits of using a spectral imaging-based tracking method for ore type prediction in a mid-sized copper mine in Arizona with two ore types have been demonstrated. For the experiments, the ore types were assumed to have different hardnesses; hence, they were classified into hard and soft rocks (names of ore aligned with those used in the case study). A simulation model of the material-handling network from the blast sites to ball mills was constructed for the analysis. The determination of cost savings over ranges of E_{SE} (specific explosives energy) values for each ore type is made possible due to the tracking using a combination of

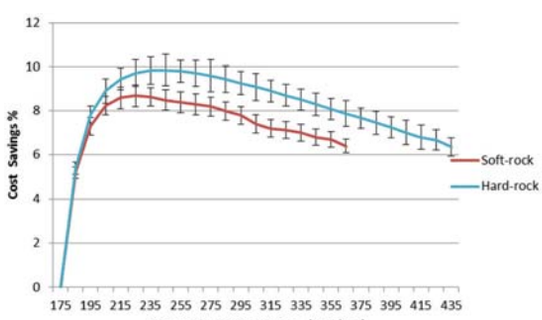

Figure 9—Cost savings percentages for hard and soft rocks

Table III

Feed and product sizes at different camera locations

Stage	Feed size: F_{80} (inches)	Product size: P_{80} (inches)	Mean power consumption (Kwh/t)
Blasting (before crusher)	6 (bench block size)	8.43	0.219
After crusher	8.43	5.51	20.782
After SAG mill	5.51	0.50	1211.632
After ball mill	0.50	0.100	774.858

multispectral camera, SPLIT Online fragment delineation algorithm, and an ore type regression model in MATLAB. After conducting tests using visible and near-infrared (VNIR) and short-wave infrared (SWIR) cameras with the number of bands ranging between 5 to 540, we concluded that:

(1) VNIR range cameras should be chosen, since they cost less while achieving similar effectiveness to SWIR cameras in ore type prediction
(2) Only up to five bands were needed for distinguishing the various samples we obtained from real mines
(3) A 3D full-motion video spectral imaging camera is better than line-scanner cameras in retaining spectral information at medium to high conveyor speeds.

It was observed that the cost savings as a function of E_{SE} do not behave the same way for the two ore types, which implies that the spectral imaging-based tracking is economically beneficial for the mine.

References

Asbjörnsson, G., Hulthén, E., and Evertsson, M. 2012. Modelling and dynamic simulation of gradual performance deterioration of a crushing circuit–Including time dependence and wear. *Minerals Engineering*, vol. 33. pp. 13–19.

Asbjörnsson, G., Hulthén, E., and Evertsson, M. 2013. Modelling and simulation of dynamic crushing plant behavior with MATLAB/Simulink. *Minerals Engineering*, vol. 43. pp. 112–120.

Asbjörnsson, G., Bengtsson, M., Hulthén, E., and Evertsson, M. 2016. Modelling of discrete downtime in continuous crushing operation. *Minerals Engineering*, vol. 98. pp. 22–29.

Bechtel, R., Rivard, B., and Sánchez-Azofeifa, A. 2002. Spectral properties of foliose and crustose lichens based on laboratory experiments. *Remote Sensing of Environment*, vol. 82, no. 2. pp. 389–396.

Blanco, M. and Peguero, A. 2011. A new and simple PLS calibration method for NIR spectroscopy. API determination in intact solid formulations. *Analytical Methods*, vol. 4, no. 6. pp. 1507–1512.

BoBo, T.W., Norton, B., Kemeny, J.M., and Taylor, M. 2004. Split-Online® digital image analysis system to quantify particle size for the industrial mineral industry. *2004 SME Annual Meeting Preprints*.

Chung, S.H. and Katsabanis, P.D. 2000. Fragmentation prediction using improved engineering formulae. *Fragblast*, vol. 4, no. 3-4. pp. 198–207.

Combs, J.H., Kudenov, M.W., Craven, J., and Kemeny, J.M. 2011. Evaluation of rock faces with hyperspectral imaging. *Proceedings of the 45th US Rock Mechanics/Geomechanics Symposium*. American Rock Mechanics Association, Alexandria, VA.

Da Cunha, E.R., de Carvalho, R.M., and Tavares, L.M. 2013. Simulation of solids flow and energy transfer in a vertical shaft impact crusher using DEM. *Minerals Engineering*, vol. 43. pp. 85–90.

Haaland, D.M. and Thomas, E.V. 1988. Partial least-squares methods for spectral analyses. 1. Relation to other quantitative calibration methods and the extraction of qualitative information. *Analytical Chemistry*, vol. 60, no. 11, pp. 1193–1202.

Jansen, W., Morrison, R., Wortley, M., and Rivett, T. 2009. Tracer-based mine-mill ore tracking via process hold-ups at Northparkes Mine. *Proceedings of the Tenth Mill Operators' Conference*, Adelaide, SA. Australasian Institute of Mining an Metallurgy, Melbourne. pp. 345–356.

Kall, P., Wallace, S.W., and Kall, P. 1994. Stochastic Programming. Wiley, Chichester, UK.

Kataoka, S. 1963. A stochastic programming model. *Econometrica*, vol. 31, no. 1–2. pp. 181–196.

Kemeny, J., Mofya, E., Kaunda, R., and Lever, P. 2002. Improvements in blast fragmentation models using digital image processing. *Fragblast,* vol. 6, no. 3–4. pp. 311–320.

Kim, K. 2006. Blasting design using fracture toughness and image analysis of the bench face and muckpile. Master's thesis, Virginia Tech.

Kim, K. and Kemeny, J.M. 2011. Site specific blasting model for mine-to-mill optimization. *Proceedings of the SME Annual Meeting and Exhibit and CMA 113th National Western Mining Conference 2011*. SME, Littleton, CO.

Kim, K. 2012. Rock fracturing and mine to mill optimization. Doctoral dissertation, University of Arizona.

Klug, H.P. and Alexander, L.E. 1954. *X-ray Diffraction Procedures*. Vol. 2. Wiley, New York.

La Rosa, D. and Thornton, D. 2011. Blast movement modelling and measurement. *Proceedings of the 35th International Symposium on the Applications of Computers and Mathematics in the Mineral Industries (APCOM 2011)*. Australasian Institute of Mining and Metallurgy, Melbourne. pp. 297–310.

Latham, J.P., Kemeny, J., Maerz, N., Noy, M., Schleifer, J., and Tose, S. 2003. A blind comparison between results of four image analysis systems using a photo-library of piles of sieved fragments. *Fragblast*, vol. 7, no. 2. pp. 105–132.

Meng, C., Nageshwaraniyer, S.S., Maghsoudi, A., Son, Y.J., and Dessureault, S. 2013. Data-driven modeling and simulation framework for material handling systems in coal mines. *Computers and Industrial Engineering*, vol. 64, no. 3. pp. 766–779.

Modular Mining. 2014. http://mmsi.com

Nageshwaraniyer, S.S., Kim, K.M., and Son, Y.J. 2015. Optimal blast design using a discrete event simulation model in a hard-rock mine. *Mining Engineering*, vol. 67, no. 11. pp. 47–53.

Nageshwaraniyer, S.S., Son, Y.J., and Dessureault, S. 2013. Simulation-based optimal planning for material handling networks in mining. *Simulation*, vol. 89, no. 3. pp. 330-345. https://doi.org/10.1177/0037549712464278

Nielsen, K., and Lownds, C.M. 1997. Enhancement of taconite crushing and grinding through primary blasting. *International Journal of Rock Mechanics and Mining Sciences*, vol. 34, no. 3. p. 226–e1.

Nielsen, K. and Malvik, T. 1999. Grindability enhancement by blast-induced microcracks. *Powder Technology*, vol. 105, no. 1. pp. 52–56.

Park, S., Choi, Y., and Park, H.S. 2016. Optimization of truck-loader haulage systems in an underground mine using simulation methods. *Geosystem Engineering*, vol. 19, no. 5. pp. 222–231.

Salama, A., Greberg, J., and Schunnesson, H. 2014. The use of discrete event simulation for underground haulage mining equipment selection. *International Journal of Mining and Mineral Engineering*, vol. 5, no. 3. pp. 256–271.

Sahinidis, N.V. 2004. Optimization under uncertainty: state-of-the-art and opportunities. *Computers and Chemical Engineering*, vol. 28, no. 6. pp. 971–983.

Santelices, G., Pascual, R., Lüer-Villagra, A., MacCawley, A., and Galar, D. 2017. Integrating mining loading and hauling equipment selection and replacement decisions using stochastic linear programming. *International Journal of Mining, Reclamation and Environment*, vol. 31, no. 1. pp. 52–65.

Scott, A. Ed. 1996. Open pit blast design: analysis and optimisation. *JKMRC Monograph Series in Mining and Mineral Processing*, no. 1. Julius Kruttschnitt Mineral Research Centre, University of Queensland.

Sgavetti, M., Pompilio, L., Carli, C., de Sanctis, M.C., Capaccioni, F., Cremonese, G., and Flamini, E. 2007. BepiColombo SIMBIO-SYS data: Preliminary evaluation for rock discrimination and recognition in both low and high resolution spectroscopic data in the visible and near infrared spectral intervals. *Planetary and Space Science*, vol. 55, no. 11. pp. 1596–1613.

SOC. 2014. Surface Optics Corp. www.surfaceoptics.com.

Sturgul, J.R. 1999. Discrete mine system simulation in the United States. *International Journal of Surface Mining, Reclamation and Environment*, vol. 13, no. 2. pp. 37–41.

Tangestani, M.H., Jaffari, L., Vincent, R.K., and Sridhar, B.M. 2011. Spectral characterization and ASTER-based lithological mapping of an ophiolite complex: A case study from Neyriz ophiolite, SW Iran. *Remote Sensing of Environment*, vol. 115, no. 9. pp. 2243–2254.

Torkamani, E. and Askari-Nasab, H. 2015. A linkage of truck-and-shovel operations to short-term mine plans using discrete-event simulation. *International Journal of Mining and Mineral Engineering*, vol. 6, no. 2. pp. 97–118.

Zhang, H. 2008. Multi-objective simulation-optimization for earth moving operations. *Automation in Construction*, vol. 18, no. 1. pp. 79–86. ◆

http://dx.doi.org/10.17159/2411-9717/2018/v118n1a3

Ground control in mining steeply dipping coal seams by backfilling with waste rock

by T. Zhao*, Z. Zhang†, Y. Yin*, Y. Tan*, and X. Liu†

Synopsis

The mining of steeply dipping coal seams involves significant safety risks because of instability caused by the weak nature of surrounding rocks and their movement after excavation. Physical and numerical models were developed to determine an optimum backfill approach to ground control in steeply dipping coal seams. Physical modelling showed that for mining without backfill, the thickness of the largest roof collapse was approximately twice that of the mined seam, the movement of roof strata tended to be asymmetrical, and there was a relatively large empty zone in the upper gob area. For mining with backfill, roof conditions were significantly improved; only slight roof separation appeared 1.5 m above the mined seam. The largest cumulative displacements occurred 5-15 m from the first cut of mining. With backfill, the levels of mining-induced stress release and concentration were significantly reduced, and the vertical range of mining disturbance was shortened by 18%. Numerical modelling showed that floor strata mainly undergo nearly horizontal displacements, while roof strata mainly undergo vertical subsidence, both with and without backfill. The integrity of roof strata improved as the extent of backfill increased, and the range of displacement direction increased. The conclusions are confirmed by results from a field trial.

Keywords

Steeply dipping coal seam, backfill, ground control, strata mechanics, waste rock.

Introduction

In the Chinese coal industry, a steep coal seam is defined as one that dips at an angle greater than 45° (Cao and Gou, 2011), as shown in Figure 1. In contrast to coal seams with little or no (flat) dip angle, mining production from steeply dipping seams is inherently low and the cost is relatively high. These factors hinder extraction from such seams in developed countries, such as the USA. In developing countries, however, mining of steeply dipping coal seams is rapidly growing because of high reserves available in such configurations, such as in western China and the Jharia coalfield in India. In China, steeply dipping coal seams comprise 15–20% of total coal reserves.

Underground mining of steep coal seams using current technologies presents significant safety risks: sliding movements cause instability in the working faces and the rock mass in and around such seams tends to be fragile due to impact of local geological structures such as faults and folds. Generally, fractures exist in the roof strata before mining; these fractures propagate and further coalesce with new fractures developed in the mining process, increasing the probability of roof collapse. Such roof failure can extend upwards as a consequence of the large inclination angle of the coal seam. To reduce deformation of the surrounding rock for ground control, backfill technology has been introduced in steep coal seam mining. In addition, backfill mining is also more environmentally friendly because less surface land is required to store mine tailings and dust or water contamination from surface storage of waste rock is reduced (Bian *et al.*, 2012; Sui *et al.*, 2015).

Wang *et al.* (2011) numerically determined that pillar strength increases with the extent of roadway backfill, regardless of the cohesive or non-cohesive nature of the backfill, especially for pillars of large height-to-width ratio. However, Kostecki and Spearing (2015) numerically found that use of a cohesive fill can improve the pillar strength by 10–40% with fill extent of 25% and 75%, while non-cohesive fill contributed little to pillar strength, indicating that the early bearing capacity of backfill should be considered in pillar design for weak roof conditions. Tesarik, Seymour, and Yanske (2009) investigated the long-term stability of a backfilled room-and-pillar test section in a metal mine (where the roof and floor strata usually consist of hard rocks) and found that backfill helps to maintain roof strata integrity and the pillar strength for long-term stability. All of these studies were, however, carried out in flat or gently inclined, rather than steep, strata. For steep coal seam mining, Kulakov (1995a, 1995b) argued that

* *State Key Laboratory of Mining Disaster Prevention and Control, Shandong University of Science and Technology,Shandong, China.*

‡ *State Key Laboratory of Coal Mine Disaster Dynamics and Control, Chongqing University, China.*

 ISSN 2225-6253. Paper received Dec. 2016; revised paper received May 2017.

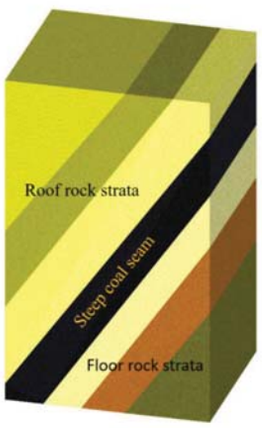

Figure 1—Schematic representation of a steep coal seam

the supporting pressure and roof deformation depend mainly on the mining depth, thickness of the seam, and roof parameters, such as roof span and thickness of the immediate roof; however, no ground control by backfilling was incorporated. More recently, Feng *et al.* (2017) developed a roof thin plate model to evaluate the effectiveness of solid-backfill in ground control. Mo *et al.* (2017) numerically investigated the effect of backfilling on coal pillar strength.

For backfilled mining, dry waste rock, cemented waste rock, hydraulic sand fill, and paste backfills have been used. This study focused on backfill with dry waste rock because the cost is relatively low and gravity-driven emplacement of the backfill material can be used for steeply dipping stopes. Extensive prior studies have been conducted on hydraulic and cement fills, either with respect to geotechnical evaluation of backfill or stress development in backfilled stopes (Klein and Simon, 2006; Sivakugan *et al.*, 2006). In a laboratory study, Klein and Simon (2006) reported that strength development of cemented paste backfill was closely related to its composition, noting that polycarboxylated acrylic acid-based polymer was especially favoured for its rapid stiffness development. Fall *et al.* (2010) and Walske *et al.* (2016) experimentally found that curing temperature had a significant influence on the mechanical properties of cement paste backfill; however, this influence changed with content of the components and curing time. Using an ultrasonic wave measurement technique, Galaa *et al.* (2011) investigated the effect of saturation on stiffness of cemented backfill and found that the binder content had a more significant impact on stiffness in submerged cemented paste backfill than in air-dried backfills. Fahey, Helinski, and Fourie (2011) confirmed that the strength of cemented backfill increased with applied effective stress during curing; this improvement became more pronounced if effective stress was applied at a higher rate during the early stages of hydration. This conclusion is consistent with the experimental study of Yilmaz, Belem, and Benzaazoua (2014). Mishra and Karanam (2006) used fly ash to replace widely used river sand and mill tailings as backfill material and found that its compressive strength increased significantly after 56 days of curing. Sivakugan *et al.* (2006) experimentally evaluated the geotechnical properties of a hydraulic fill that is widely used in Australia.

With respect to the stress developed in backfilled stopes, Li and Aubertin (2009) analysed the influence of stope geometry, backfill properties, and filling sequence on the stress state of inclined backfilled stopes using FLAC2D software, and found that the stope inclination angle had a significant impact on vertical stress but relatively little effect on horizontal stress. Fahey, Helinski, and Fourie (2009) numerically found that horizontal stress differed within a backfilled stope due to the arching effect. On a field scale, Helinski, Fahey, and Fourie (2011) monitored the vertical stress and pore pressure in a stope backfilled with cement paste and observed a significant arching effect on the vertical stress. Mkadmi, Aubertin, and Li (2013) numerically illustrated that drainage can effectively reduce pore pressure within backfill and hence increase the interactive frictional stress between the backfill and rock walls. Doherty *et al.* (2015) found that the filling and resting schedule was a dominant factor influencing total stress and pore pressure development in a stope with cemented paste backfill.

Regarding the barricade for the backfilling of mined-out gob (Figure 2), field measurement showed that the barricade tends to be stable in large stopes with a high binder content in cemented paste backfill, indicating the significance of the early development of bearing capacity in backfill (Thompson, Bawden, and Grabinsky, 2012). Hughes *et al.* (2010) introduced a novel destructive fill fence test to evaluate the ultimate capacity of a barricade. To ensure stability, an optimal position exists for a barricade to bear a low backfill load (Li and Aubertin, 2009, 2011). Fall and Nasir (2010) investigated the mechanical behaviour of the interface between cemented backfill and the retaining wall using a direct shear test, finding that it followed the Mohr–Coulomb criterion and its frictional angle increased with curing time.

Prior to extraction, steeply dipping coal seams generally experienced violent tectonic movements over geological time. As a result, the surrounding rock strata are usually weaker than in the case of flat coal seams. For this reason, the interaction between backfill and the surrounding rock mass can be complex compared to that of flat coal seams. It is therefore important to study the ground control mechanism of backfill in steeply dipping coal seam mining. This is also of great significance for promoting the utilization rate of coal mine waste rock in China.

To address the issues discussed above, physical and numerical simulations were employed to investigate the behaviour of rock strata and the ground control mechanism of backfill in steep coal seam mining. Physical modelling with

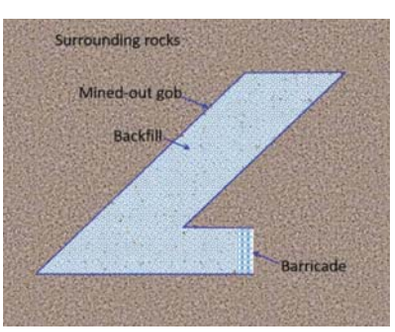

Figure 2—Schematic diagram of barricade for backfilling of mined-out gob

equivalent materials is usually used to investigate deformation and failure of engineering prototypes (Jeremic, 1985); however, its repeatability is poor. Therefore, a physical model was developed to elucidate the mechanism by which backfilled waste rock resists roof cave-in, while numerical modelling was introduced to study the effect of the extent of the backfill on ground control. A field trial was then conducted to examine ground control performance of backfill in a steeply dipping coal seam. Such a study is essential to the successful application of the backfill method in steep coal seam mining.

Experimental methods

Physical modelling with equivalent materials has been used in mining and geotechnical engineering to provide a basic understanding of the mechanical behaviour of engineering prototypes (Jeremic, 1985). A physical model was developed to simulate an engineering prototype according to the theory of similarity (Jeremic, 1985), where instrumentation can be mounted to monitor the deformation and stress variations and the characteristics of the prototype were inferred from the similarity ratio. Note that the concept of equivalent materials involves inherent limitations. For example, physical modelling in the case of stress analysis might encounter difficulties due to the differences in physical and strength properties of the model and prototype materials (Jeremic, 1985). Furthermore, even physical models developed with the same rule may yield results that indicate a greater or lesser difference in behaviour of strata mechanics due to the operational process during model preparation and implementation. Considering that the rock strata are invisible and mined-out gob is inaccessible in practical mining activities, field monitoring is usually costly. The physical modelling approach with the concept of equivalent materials, on the other hand, is relatively rapid to implement and of low cost.

Development of the physical model

The physical model addressed similarities of scale, geometry, loading, and physical and mechanical properties.

For geometric similarity, the prototype dimensions were shrunk to develop the physical model at the same ratio:

$$\alpha_L = \frac{L_P}{L_M} \quad [1]$$

where α_L is the similarity ratio of dimension L, and subscripts P and M denote the prototype and physical model, respectively.

With regard to the physical similarity, applied stress and specific mass were considered as:

$$\begin{cases} \alpha_\sigma = \dfrac{\sigma_P}{\sigma_M} \\ \alpha_\gamma = \dfrac{\gamma_P}{\gamma_M} \end{cases} \quad [2]$$

where α_σ and α_γ are the similarity ratios of stress σ and specific mass γ of the material, respectively. The subscript P represents the parameter of engineering prototype while the subscript M represents the parameter of physical model. The initial conditions of the physical model were similar to those of the prototype, including the strata distribution and mechanical properties. The boundary conditions of the physical model were consistent with the actual boundaries. To simplify, a plane model was considered with respect to how plane strain mode is accommodated in a field situation. Deformation normal to the model plane was restricted during experiments to ensure validity.

The prototype for the steeply dipping coal seam was the no. 5 coal seam in Datai mine, Beijing, China. The dip of this seam varies from 60° to 76°, with an average of 70°, and its thickness ranges from 1.23 m to 1.90 m, with an average of 1.70 m. The geometrical parameters of the roof, coal seam, and floor strata are listed in Table I.

The similarity ratio of dimension α_L was set to 50, and hence the corresponding thickness of the coal seam in the physical model was 3.40 cm according to Equation [1]. The similarity ratio for specific mass α_γ was set to 1.6, while the similarity ratio for stress α_σ was set to 80.

To compare the effects of mining a steeply dipping coal seam with and without backfill, two seams were established in the physical model, as schematically shown in Figure 3a, one of which was extracted and backfilled and the other extracted without backfill. The purpose of establishing these two seams in a single physical model was to reduce the experimental error introduced by the process of constructing a new model, and hence improve the reliability of the results. The interval between these two seams was designed as 60 cm, which represented 30 m in practice. According to the closed-form solution for a circular excavation, the impact zone of the excavation is around five times the excavation radius and the stresses recover to far-field stresses beyond this zone (Brady and Brown, 2004). It should be noted that this is only an estimation based on a circular excavation in an infinite half-plane. In this physical model, the thickness of two coal seams was 1.70 m and the vertical distance between them was set as 30 m to avoid any interactions. The dip

Table I

Physical and mechanical parameters of engineering prototype and physical model

Strata		Roof with backfill	Coal seam with backfill	Floor with backfill	Roof without backfill	Coal seam without backfill	Floor without backfill
Prototype	Thickness (m)	15	1.7	10	20	1.7	10
	Specific weight (kN/m³)	26.7	17.8	27.2	26.7	17.8	27.2
	UCS (MPa)	73.4	20.8	105	73.4	20.8	105
Model	Thickness (cm)	30	3.4	20	40	3.4	20
	Specific weight (kN/m³)	16.7	11.1	17.0	16.7	11.1	17.0
	UCS (MPa)	0.918	0.26	1.375	0.918	0.26	1.375

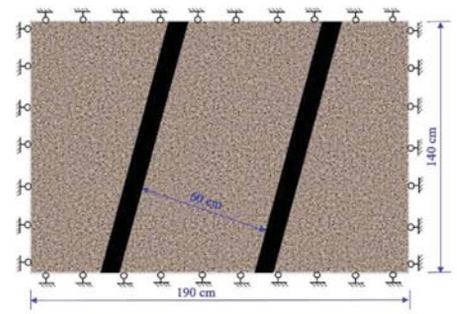

(a)

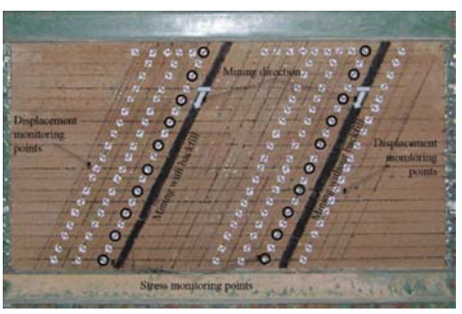

(b)

Figure 3—(a) Schematic diagram and (b) photograph of the physical model of mining a steeply dipping seam coal with and without backfill

angle of the two seams was set as 70°. The basic physical and mechanical parameters of the coal and rock mass were obtained by shrinking the engineering prototype according to the relevant similarity ratios, as summarized in Table I.

The composition of the equivalent materials is crucial for physical modelling in mining and geotechnical engineering. It should not only reflect similarity of physical and mechanical properties between the engineering prototype and the model, but also ensure stability of the physical model in case of experimental failure. In this study, fine sand grains (< 0.42 mm) were selected as the aggregate material, and gypsum and calcium carbonate were used as binders to simulate the roof and floor strata. For the coal seams, coal ground to less than 0.50 mm diameter was used as the aggregate material, and gypsum and calcium carbonate were again used as the binder material. These materials were selected because their failure mode tends to be brittle after construction. Tap water was used to mixed the aggregate and binder materials. The ratios of aggregate, binder, and water affect the mechanical parameters of the physical model. Following the calculated mechanical parameters shown in Table I, the ratio between aggregate and binder was determined for different rock strata, as summarized in Table II. The mass ratio of water to aggregate plus binder was kept strictly to 1:9, as extra water would increase the porosity of the physical model after curing.

The physical model, which was constructed on a laboratory test bench, had a length of 190 cm, a height of 140 cm, and a width of 22 cm. The physical model prior to any excavation is shown in Figure 3.

Instrumentation

Deformation and stress variation during the mining process were monitored. The plane surface of the physical model was first marked with two sets of parallel ink lines, one along the dip direction of the coal seam and the other along the horizontal direction. A mesh network with grid size of 5 cm × 5 cm was developed for convenience of instrumentation mounting, as shown in Figure 3b. Displacement calibration papers were pinned at some grid nodes to identify the positions at which deformation was monitored during mining (Figure 3).

For the case of mining without backfill, three displacement monitoring lines were set in the roof strata and one in the floor strata. The interval between two adjacent monitoring lines in the roof strata was 10 cm and the first displacement line was located 5 cm above the seam. Nineteen measurement points were set in each monitoring line at 5 cm intervals. In addition, a horizontal displacement monitoring line was set near the top boundary of the model, with nine monitoring points at 5 cm intervals. For the case of mining with backfill, three displacement monitoring lines were set in the roof strata and the detailed layout was the same as that without backfill. A horizontal displacement monitoring line was also set near the top boundary of the physical model, with six monitoring points at 5 cm intervals.

Pressure transducers were installed in the roof strata to monitor stress changes during mining. Stress monitoring lines, located 5 cm above the coal seam, were established for both cases. Each line consisted of eleven monitoring points at 10 cm intervals. The detailed layout of the stress monitoring points is shown in Figure 3b.

During an experiment, the mining sequence was from top to bottom and the initial excavation (first cut of mining) started 30 cm from the top boundary. The mining distance for each step along the vertical direction was 5 cm, representing 2.5 m in practice, and the time interval between subsequent

Table II

Ratio of aggregate to binder for rock strata in the developed physical model

Strata		Aggregate to binder	Binder (calcium carbonate to gypsum)
Mining with backfill	Roof	8:1	7:3
	Coal seam	9:1	7:3
	Floor	7:1	4:6
Mining without backfill	Roof	8:1	7:3
	Coal seam	9:1	7:3
	Floor	7:1	4:6

steps was 2 hours. In total, the mining excavation was conducted up to 80 cm along the vertical direction, representing 40 m in the real mining environment. In the case of mining without backfill, no treatment of the mined-out void (gob) after excavation was conducted, allowing for free roof collapse. In the case of backfilled mining, foam particles were used to backfill the gob after each mining step. Transparent plexiglass was used as a barrier to prevent loss of foam particles on the two lateral sides of the model.

Development of numerical model

The particulate discrete element modelling (DEM) method was chosen for two reasons. Firstly, with particulate DEM, the particle-scale mechanisms underlying the complex overall material response can be numerically analysed. Secondly, particulate DEM allows analysis of the mechanisms involved in large displacement problems, such as massive detachment of particles (O'Sullivan, 2011). These two issues cannot be solved with a continuum approach and traditional DEM methods, such as the commercial codes FLAC and UDEC. The numerical model, generated using PFC2D, was 40 m long and 50 m high, as shown in Figure 4.

In the numerical model, the thickness of the coal seam was 2 m with a dip angle of 70°. The roof strata consisted of siltstone and gritstone and the floor was fine sandstone. The geometrical parameters of the model are given in Table III. Roller conditions were applied on the lateral and bottom model boundaries; horizontal displacement was constrained by the lateral boundary, and vertical and horizontal displacements were constrained at the bottom boundary. A vertical compressive stress of 20 MPa was applied at the top boundary to simulate the overlying burden of rock strata. Note that the model geometrical dimensions, 40 m in length and 50 m in height, have a certain effect on the numerical results at the model boundary. However, this numerical study is mainly to investigate the effects of different backfill extents on the deformation of roof and floor strata, rather than at the model boundary. Therefore, such a limitation of the model dimension on the boundary result was not considered here.

The bonded-particle model (BPM) was used to simulate the rock strata and coal seam (Potyondy and Cundall, 2004). In a BPM model, the grain micro-properties are characterized by Young's modulus of the grains (E_c), the ratio of normal to shear stiffness of the grains (k_n/k_s), and the grain friction coefficient (μ); cement micro-properties are characterized by the radius multiplier used to set the parallel bond radii (λ), Young's modulus of the cement ($\bar{E}_c$), ratio of normal to shear stiffness of the cement ($\bar{k}_n/\bar{k}_s$), normal contact bond strength of the cement (σ_n), and the shear contact bond strength of the cement (σ_s). According to Potyondy and Cundall (2004), the grain and cement moduli are related to their normal stiffnesses:

$$\begin{cases} k_n = 2E_c \\ k_s = \dfrac{k_n}{k_n/k_s} \\ \bar{k}_n = \dfrac{\bar{E}_c}{2\bar{r}} \\ \bar{k}_s = \dfrac{\bar{k}_n}{\bar{k}_n/\bar{k}_s} \end{cases} \quad [3]$$

where $\bar{r}$ is the average radius of two contact grains. Considering the no-bonding characteristics of backfilled waste rock, its normal and shear contact bond strengths were set to zero to mimic the fact that there were no cohesive forces among the particles.

The Young's modulus of particle assembly, E_c, was taken from the laboratory test results. The normal contact bond strength of cement σ_n is derived according to the following relationship (Kulatilake *et al.*, 2001):

$$\sigma_n = 4r^2\sigma_t \quad [4]$$

where σ_t is tensile strength measured from the laboratory test. The shear contact bond strength σ_t was taken to be equal to the normal contact bond strength of cement σ_n.

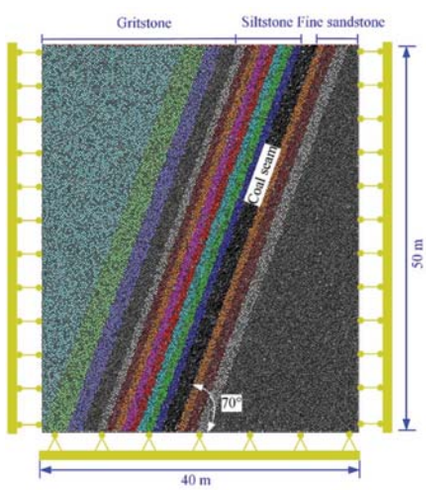

Figure 4—Numerical model for mining a steeply dipping seam coal with different backfill extents

Table III

Geometrical and mechanical parameters of the model

Rock	Gritstone	Siltstone	Coal seam	Fine sandstone	Waste rock
Particle radius r (m)	0.1-0.15	0.1-0.15	0.1-0.15	0.1-0.15	0.1-0.15
Young's modulus of grains E_c (GPa)	5	3	2	4	3
Young's modulus of cement (GPa)	5	3	2	4	0
Normal contact bond strength of cement σ_n (MPa)	50	20	10	30	0
Shear contact bond strength of cement σ_s (MPa)	50	20	10	30	0
Radius multiplier λ	1	1	1	1	0
Friction coefficient of grain μ	0.5	0.5	0.5	0.5	0.5

In BPM, the parameters of friction coefficient and spring stiffnesses are not directly linked to any physical measurement. Their sensitivity to the numerical modelling of particulate discrete element method is reviewed by O'Sullivan (2011). Referring to Kulatilake *et al.* (2001) and the PFC2D manual (Itasca, 2008), the ratios of normal to shear stiffness of the grains and cement were both taken as 2.5 and the radius multiplier of cement was set as unity. The mechanical parameters of the numerical model are given in Table III.

Mining was conducted from top to bottom with 2.5 m in each mining cut. Ten cuts were conducted in total. Mining processes without backfill and with 50%, 70%, and 90% backfill were simulated.

Results and discussion

Characteristics of strata mechanics

Failure of roof strata

During the entire mining process described above, there were four instances of major roof collapse for mining without backfill, while only slight separation occurred for mining with backfill.

Figure 5 shows the evolution of the state of the roof strata with advance of the face for both backfilled and non-backfilled mining. Without backfill, the first roof collapse occurred when the mining height was 17.5 m, and the thickness of collapsed roof strata was 1.5 m. Driven by gravity, the collapsed rock moved down to fill the lower part of the gob area. During the first roof collapse, damage to the upper part of the rock strata was caused by tensile fracturing, while that to the lower part was due to compressive bending. A beam structure developed in the roof strata was also bent downward, thereby supporting the overlying roof strata with the collapsed rock. With backfill, the waste rock played a positive role in supporting roof stability and inhibited roof collapse. The initially backfilled waste rock was, however, loose and could be compacted to a certain extent, and the roof strata were deflected by bending towards the gob area, leading to a slight roof separation at 1.5 m above the mined seam (Figure 5a).

The second roof collapse during mining without backfill occurred when the vertical mining height reached 20 m, and the thickness of the collapsed roof strata increased to 3.5 m, approximately twice the thickness of coal seam, as shown in Figure 5b. The second collapse occurred mainly in the strata above the first collapse. There was no roof collapse close the mining face, owing due to support of the collapsed rock and the beam structure formed in the first collapse. When mining with backfill, as shown in Figure 5b, the roof separation propagated slightly, but no new separation appeared.

Figure 5c shows the state of the roof strata when the vertical mining height was 27.5 m. For mining without backfill, the third roof collapse occurred and the roof beam structure formed during the first collapse failed unstably due to the roof overhang. The collapsed rock mass moved down along the gob and filled the lower area. In the upper area, collapsed rock blocks formed a self-supporting structure and downward movement was temporarily restricted, resulting in a wide empty void in the middle of the gob area, as shown in Figure. 5c. For mining with backfill, a relatively large separation occurred 3.5 m above the mined seam, owing to the movement of backfilled waste rock down to the lower mined-out area when mining to 25 m, thus weakening the support of the roof strata.

When the vertical mining height reached 35 m, the fourth roof collapse occurred for mining without backfill, as shown in Figure 5d. On this occasion, the arch structure formed during the third roof collapse broke and the rock block subsided to fill the gob area. When mining with backfill, the roof strata remained stable and the existing separation did not extend further due to the continued action of the backfill.

Figure 5e shows the deformation and failure modes of surrounding rock strata at a mining height of 40 m. Without backfill, the initial caving step distance was 17.5 m and the periodic caving step distance was 7.5 m. The collapsed roof strata covered 3.5 m in the vertical direction, approximately twice the thickness of the mined coal seam. The downward movement of collapsed rock caused a relatively large empty zone to form at the top of mined-out stope and the roof strata collapse tended to be asymmetrical in the stope. When the gob was backfilled after each mining cut, separation occurred only in the roof strata.

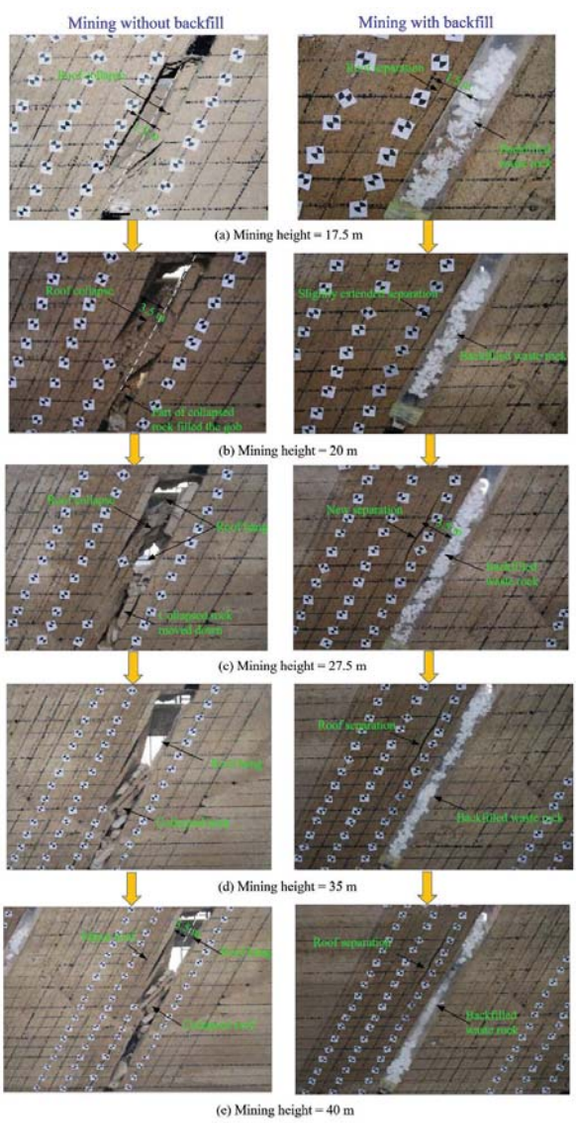

Figure 5—Evolution of roof strata state with mining face advance for the cases of backfill and no backfill

Displacement of roof strata

For the case of backfilled mining, Figures 6 and 7 show, respectively, the cumulative vertical and horizontal displacements of roof strata at 2.5 m above the seam at different stages of mining. The maximum cumulative vertical and horizontal displacements were only 0.05 m when the vertical mining height was 17.5 m, due to support of the roof strata by the backfilled waste rock; only a slightly amount of bending deformation occurred. However, when the vertical mining height reached 25 m, there was a sudden increase in roof deformation, with maximum vertical and horizontal displacements of 0.2 m and 0.3 m, respectively. A relatively large separation appeared, due to the delay in providing backfill during the normal process of cut and fill. In subsequent mining from vertical heights of 25 m to 40 m, the cumulative vertical and horizontal displacements increased gradually and the previously developed roof separation extended only slightly, but new roof separation did not occur.

Another important phenomenon illustrated in Figures 6 and 7 is that, at any mining stage, both the largest cumulative vertical and horizontal displacements occurred 5 to 15 m from the first cut of mining. This is attributed to a complex interactive mechanism between the rock strata and backfill. Generally speaking, subsidence of the roof strata initially compacted the backfill and a certain amount of roof deformation occurred due to the loose nature of backfill at the early stage. With advance of the mining face and subsequent backfilling, the top backfill tended to move downwards, further weakening the backfill support. Unmined coal blocks opposite to the mining direction also provided support and transferred a portion of the roof strata load to the floor. This helped to reduce deformation of the roof strata within 5 m from the first cut of mining.

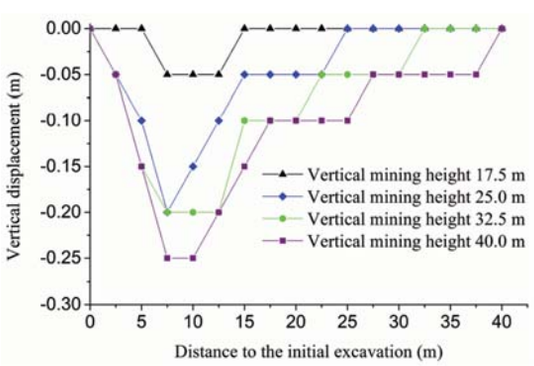

Figure 6—Vertical displacement of roof strata at 2.5 m away from the coal seam at different mining stages

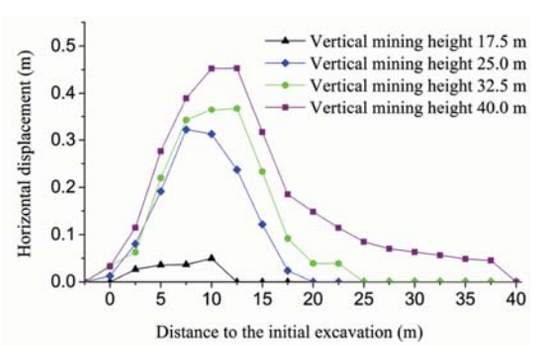

Figure 7—Horizontal displacement of roof strata at 2.5 m away from the coal seam at different mining stages

Pressure variation in roof strata

Figure 8 shows the pressure variation in the roof strata for mining a steep coal seam without backfill. At the start of mining, the pressure variation is very small because the hanging area of the roof strata is small and there is no obvious roof separation. The first cut of mining is marked as the reference point in Figure 3. When the face advanced vertically to 17.5 m, the first roof collapse occurred, reducing the stress in the roof strata 7.5 m below the first mining cut to zero. Before the first roof collapse, stress concentration in the roof strata occurred 2.5 m above and 20 m below the first cut; these stresses increased to 12.15 MPa and 11.67 MPa, corresponding to stress concentration coefficients of 1.35 and 1.30, respectively. However, following the first roof collapse, slight stress release occurred in roof strata 20 m below the initial excavation. With the second roof collapse, when the face advanced to 27.5 m, stress in roof strata 20 m below the initial excavation reduced to zero, while that 2.5 m above the initial excavation continued to increase to 14.82 MPa, corresponding to a stress concentration coefficient of 1.65. Such stress increases ceased when the mining face advanced to 27.5 m in the vertical direction, indicating that the roof strata at this position were no longer influenced by the mining face. Figure 8 also reveals that significant stress redistribution occurred with roof strata collapse within the disturbed zone.

Figure 9 shows the pressure variation in the roof strata with backfill. Mining with backfill in general significantly reduces the impact on rock strata, including stress release and stress concentration. Stress release occurred when the mining face passed the monitoring points; however, the stress finally stabilized at a level of approximately 5 MPa, rather than zero. The degree of stress concentration also reduced with backfill. Considering roof strata located 2.5 m above the first cut of mining as an example, the final stress concentration coefficient was only 1.33, compared with 1.65 for mining without backfill. A comparison of Figure 8 with Figure 9 also shows that the vertical disturbance due to mining was shortened to approximately 22.5 m, 18% less than that in mining without backfill.

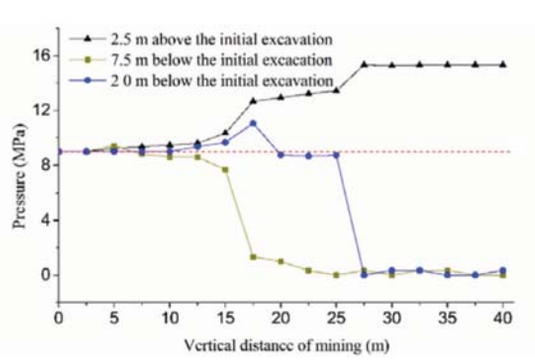

Figure 8—Variation in roof pressure for mining without backfill

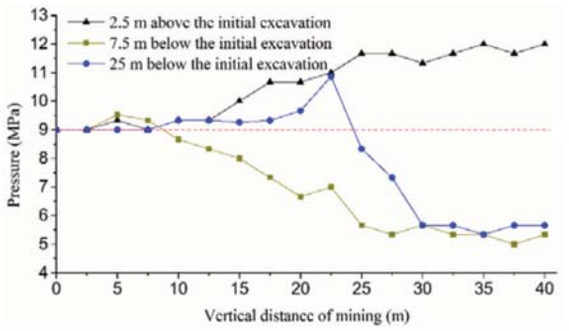

Figure 9—Variation in roof pressure for mining with backfill

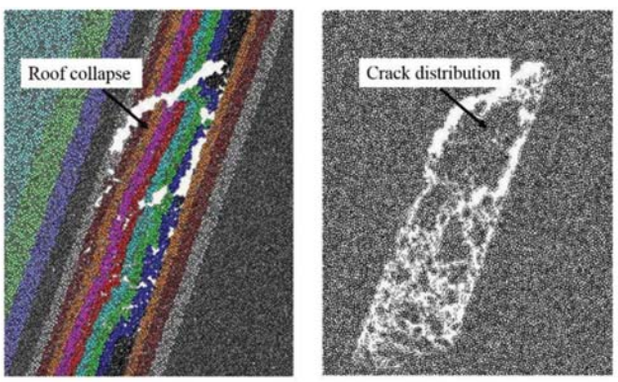

Figure 10—Roof collapse for mining without backfill

Effect of backfill extent on strata mechanics

Numerical modelling was used to investigate the effect of backfill extent on strata mechanics in steeply dipping seam coal mining.

Failure mode and crack development

Figure 10 shows the roof collapse for mining without backfill. A wide range of roof strata were damaged and the 8 m thick siltstone (which has relatively low strength) above the gob area caved in. The collapsed material moved down and filled the lower part of gob area, providing support for the roof strata and hence restricting the propagation of roof cave-in. Figure 10 also demonstrates that collapse of roof strata was distributed asymmetrically.

Figure 11 shows the failure modes and crack distribution in the roof strata for mining with 50%, 70%, and 90% backfill. In comparison with Figure 10, roof conditions were significantly improved by backfill mining. With 50% backfill only the roof strata 1 m above the gob collapsed; however, mining-induced cracks were still widely distributed across the entire siltstone layer. When the backfill increased to 70%, the space left for roof activity was reduced and support contributed by the backfill increased; as a consequence, roof conditions improved and only local collapse occurred in the strata located at the top part of gob area, as shown in Figure 11. With a further increase of backfill to 90%, roof collapse was almost eliminated; simultaneously, the range of mining-induced cracking was markedly reduced, occurring only in the immediate roof of the coal seam.

Displacement distribution and direction

The displacement of rock strata after mining using different backfill plans is shown in Figure 12. The largest displacement was asymmetrically distributed and obliquely biased upwards for mining without backfill; with backfill, the magnitude and range of the largest displacement were significantly reduced. Such displacement reduction continued with increasing extent of backfill.

The direction of the displacement angle of rock strata particles was investigated statistically using the built-in programming language *FISH* and is shown in Figure 13. The displacement direction angles of rock particles fell into two ranges: 160°–180° and 260°–320°. Particles of floor strata fell mainly in the former range, while roof strata fell mainly in the latter range, indicating that floor and roof strata mainly undergo nearly horizontal and nearly vertical displacements towards the mined-out void, respectively.

Figure 13 also shows that the backfill and extent of fill influence the displacement angle of the rock strata, particularly the roof strata. Without backfill, the displacement direction angle of roof strata varied between 260° and 290°; as the extent of backfill increased, the range of displacement direction angles became larger: 260–300° at 50%, 260–310° at 70%, and 260–320° at 90% backfill. The range of displacement direction angle also increased with increasing backfill, tending to become evenly distributed and indicating good integrity of the roof strata. The variation of displacement angle in the floor strata was smaller. This indicates that, with an increase in backfill, the integrity of roof strata was maintained and they deformed as a whole with an evenly distributed direction angle of displacement.

Implications for steep-seam coal mining

For mining without backfill, three types of strata movement can be categorized. The first is bending deformation towards the gob area, which occurs during the early stage of mining, starting from the immediate roof and extending along the vertical direction of roof strata. This type of deformation is continuous until roof separation occurs.

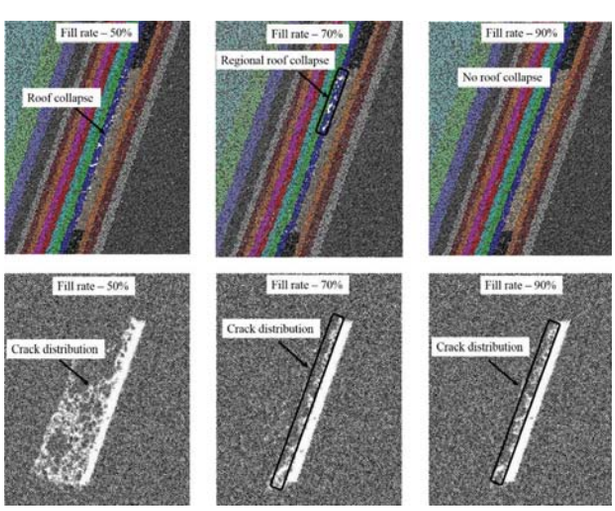

Figure 11—Failure modes and crack distribution in roof strata for mining with 50%, 70%, and 90% backfill

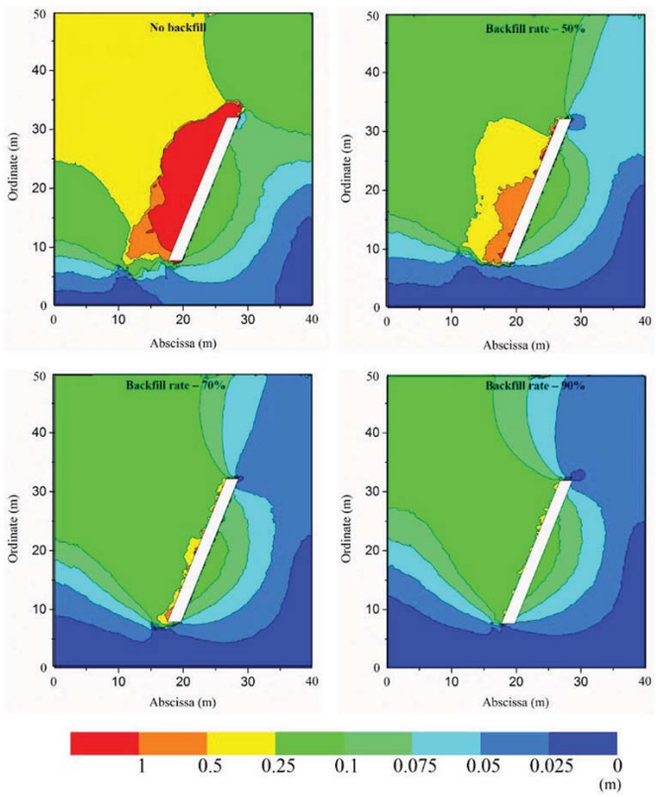

Figure 12—Strata displacement distribution for steep seam mining with different backfill plans

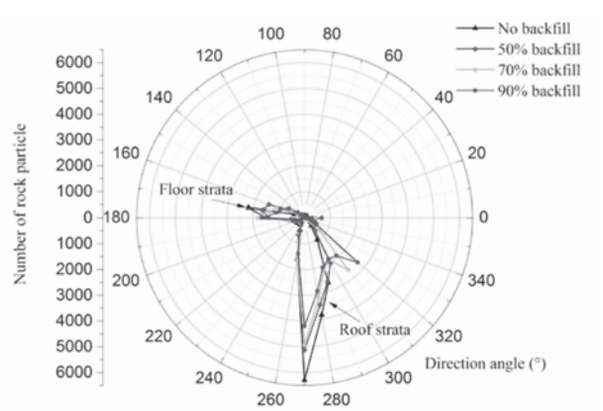

Figure 13—Strata displacement angles for steep seam mining with different backfill plans

The second type of movement is collapse of the roof strata. As mining advances, the cumulative bending deformation of roof strata becomes large and the developed stress exceeds the threshold of the strata. Cracks then initiate, propagate, and coalesce in the immediate roof strata, finally leading to roof collapse. The collapsed rock blocks move down along the dip direction of the seam and fill the lower part of the gob area. With cave-in of the immediate roof, major roof strata gradually subside, and a new round of roof separation starts. During this process, stress in released in roof strata above the top part of gob, while stress continues to concentrate in unmined coal blocks, creating a high abutment pressure. At the lower part of gob area, the collapsed rock blocks move downwards and support the roof strata to some extent, reducing subsidence. Roof collapse in steeply dipping coal seam mining without backfill therefore tends to be asymmetric; the movement and damage experienced by roof strata at the upper part of gob area are far larger than those at the low part.

The third type of movement is slip along the weak plane. For steeply dipping coal seam mining, the gravitational direction is not normal to the roof strata; hence, roof strata not only undergo bending deformation towards the gob, but also tend to slip down along the bedding plane. This is distinctly different from strata movement in flat coal seams. The upper roof strata are therefore in a tensile state, while the lower roof strata are in a compressive state. This is schematically shown in Figure 14.

Waste rock used to backfill the mined-out void after each cut tends to move downwards under the influence of gravity. Because the initial backfill is relatively loose and compressible during the early stage, roof strata incur a certain amount of subsidence. Once the subsided roof strata contact the backfill, the subsidence rate gradually decreases. The load-bearing capacity of the backfill increases during this process. The gradually compacted backfill resists subsidence of the roof strata and transfers the burden to the floor strata. As a result, the size of the stress release zone in the overlying rock strata and the stress concentration in the unmined coal seam block are reduced. The characteristics of strata movement in steep coal seam mining with backfill are schematically presented in Figure 15.

The extent of backfill has a significant impact on strata movement in steep-seam coal mining. Roof conditions can be

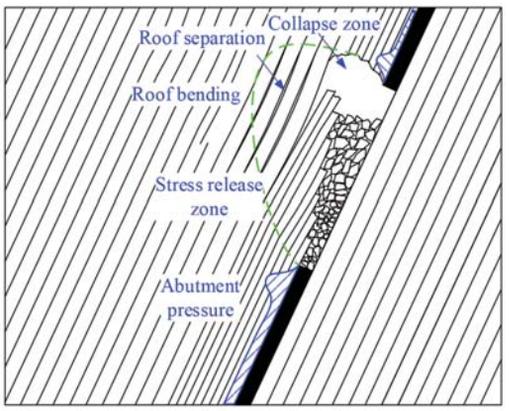

Figure 14—Strata movement characteristics of steep-seam coal mining without backfill

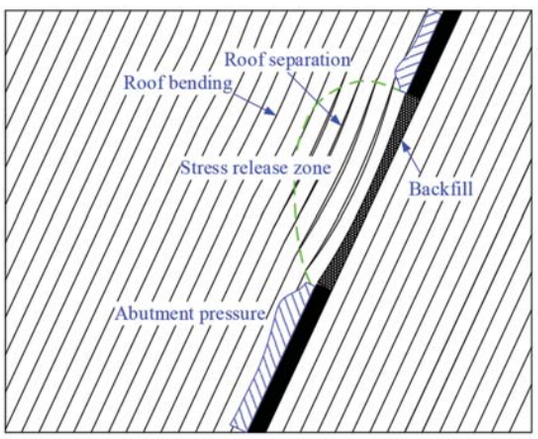

Figure 15—Strata movement characteristics of steep-seam coal mining with backfill

improved by increasing the amount of backfill and roof collapse can be completely eliminated when the extent of fill reaches a threshold value. With backfill, the variation in displacement direction angle of the floor strata is less than that of the roof strata, indicating that deformation control by backfilled rock is more effective in roof strata than in floor strata. As the extent of backfill increases, the integrity of the roof strata is maintained and they deform as a whole, with an evenly distributed direction of displacement.

Field trial

A field trial was conducted in no. 5 coal seam of Datai mine, China. The tailgate was enlarged, as shown in Figure 16, to meet the requirements of normal production and backfill equipment layout.

Mining sections 2 and 3 were co-extracted, as shown in Figure 17. Backfilling was carried out simultaneously with extraction. When the mining face advanced to 96 m, the mining void was 3115 m^2. Figure 17 shows that the backfilling was well conducted (except for the existence of an unfilled triangular void in the vicinity of the first cut of mining section 2); the fill ratio was 67.7–82.4%. Timely backfill helped to maintain the rock surrounding the backfill tailgate in very good condition.

As the mining face advanced, a fault was encountered, as shown in Figures 17 and 18. Dislocation and slip occurred in the surrounding rock strata when the face passed the fault, and severe deformation led to cessation of the backfill operation. As the face advanced from 99 m to 166 m, as shown in Figure 18, the extent of fill dropped significantly, with minimum and maximum backfill extents of 13.3% and 34.2%, respectively.

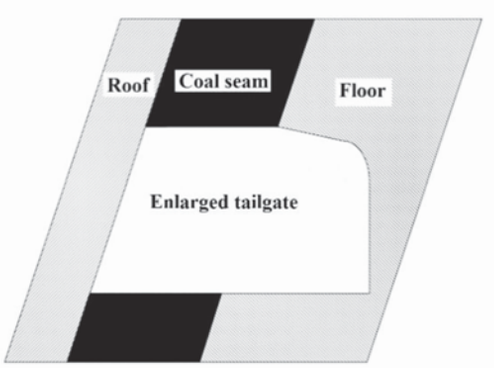

Figure 16—Schematic diagram of tailgate used for backfilling

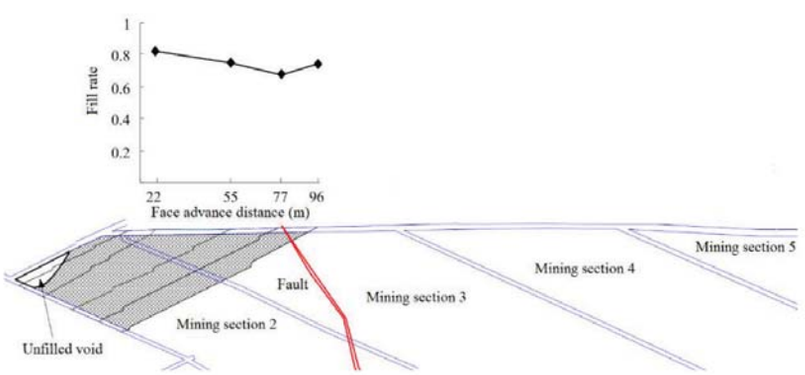

Figure 17—Backfill rate when the 845 face advanced normally

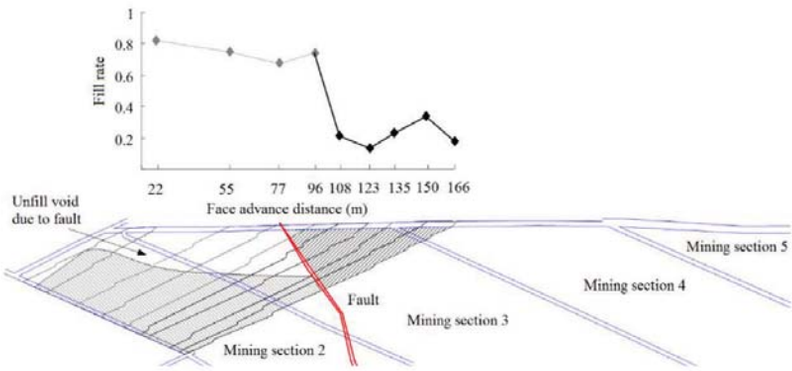

Figure 18—Backfill rate when the 845 face passed the fault zone

Deformation of roof strata of the backfill tailgate as the mining face advanced from the first cut of mining to 166 m is shown in Figure 19. During the early stage, starting from the first cut of mining, mining was conducted normally and the void was backfilled timeously with a high backfill extent. Roof deformation was effectively controlled and only slight roof bending occurred, as shown in Figure 19a. However, when the mining face passed the fault, the void in front of the fault could not be effectively backfilled due the dislocation and slip of the fault zone and so cracking occurred in the roof strata, as shown in Figure 19b. The opening height of the crack was approximately 0.5 m, and it extended the entire thickness of the immediate roof. As the mining face advanced, overhang of the roof strata increased, leading to roof collapse, as shown in Figure 19c. The lower part of the roof strata underwent downwards slip after the roof collapse due to the steep dip angle of the coal seam and deadweight of rock strata, as shown in Figure 19d. This is a specific characteristic of steeply dipping coal seam mining, which is distinctly different from flat coal seam mining. Breaking of roof strata started from the fault and extended to 170 m along the axial direction of the backfill tailgate, confirming the significance of using a high amount of backfill in ground control in steeply dipping coal seam mining. It should be noted that the fault also weakened the regional rock strata prior to backfilled mining. Such weak rock condition near the fault, combined with insufficient backfill extent, led to strata failure when the mining face advanced over the fault zone.

Conclusions

The deformation of rock strata in steep coal seam mining and its ground control with backfill were investigated by physical and numerical modelling, using the no. 5 coal seam of Datai coal mine, China, as the engineering prototype.

Without backfill, the initial roof collapse step distance was 17.5 m along the vertical direction and the step distance of periodic collapses was 7.5 m, was approximately twice the coal seam thickness. The collapsed rock mass moved down and filled the lower gob area, reducing roof subsidence in this area. There was a relative large empty zone in the upper part of stope due to the downward movement of collapsed rock, and the movement of roof strata tended to be asymmetrical.

With backfilling after each mining cut, the waste rock supported the roof strata and inhibited roof collapse. Initially backfilled waste rock was loose and of low stiffness, so bending deflection towards the gob area occurred, finally

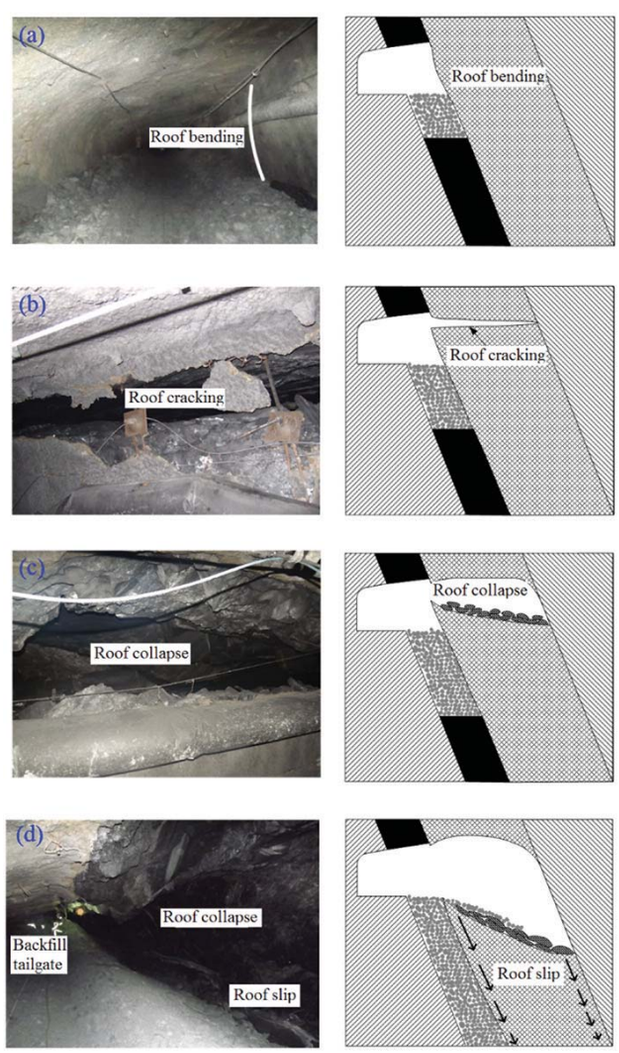

Figure 19—Deformation of roof strata when the mining face advanced from first cut of mining to 166 m away

leading to a slight separation of the roof strata at 1.5 m above the mined seam. The largest cumulative vertical and horizontal displacements occurred 5–15 m away from the initial excavation, which is attributabed to a complex interactive mechanism between the rock strata and backfill. Physical modelling with full backfill extent revealed that the backfill improved the roof strata conditions. The stress finally stabilized at a level of approximately 5 MPa in the release zone and the stress concentration coefficient reduced to 1.33 in the concentration zone. The vertical range of mining-induced disturbance was reduced by 18% compared with that without backfill. With an increase in the extent of backfill, roof conditions improved significantly. Roof collapse can be prevented at a threshold backfill rate value. The integrity of the roof strata was improved with increasing extent of backfill and the concentration range of displacement direction angle was reduced.

Acknowledgments

The study is financially supported by National Natural Science Foundation of China (No. 51304256, No. 51604165 and No. 51404168) and Fundamental Research Funds for the Central Universities (No.106112015CDJXY240005). Special thanks go to Dr. Jan Nemcik, University of Wollongong, for suggestions during the manuscript preparation.

References

Bian, Z., Miao, X., Lei, S., Chen, S.E., Wang, W., and Struthers, S. 2012. The challenges of reusing mining and mineral processing wastes. *Science*, vol. 337. pp. 702–703.

Brady, B.H.G. and Brown, E.T. 2004. Rock Mechanics for Underground Mining. Kluwer, Dordrecht.

Cao, S. and Gou, P. 2011. Coal Mining (Underground Mining section). China Coal Industry Publishing House, Beijing. (In Chinese).

Doherty, J.P., Hasan, A., Suazo, G.H., and Fourie, A. 2015. Investigation of some controllable factors that impact the stress state in cemented paste backfill. *Canadian Geotechnical Journal*, vol. 52. pp. 1901–1912.

Fahey, M., Helinski, M., and Fourie, A. 2009. Some aspects of the mechanics of arching in backfilled stopes. *Canadian Geotechnical Journal*, vol. 46. pp. 1322-–336.

Fahey, M., Helinski, M., and Fourie, A. 2011. Development of specimen curing procedures that account for the influence of effective stress during curing on the strength of cemented mine backfill. *Geotechnical and Geological Engineering*, vol. 29. pp. 709–723.

Fall, M., Célestin, J.C., Pokharel, M., and Touré, M. 2010. A contribution to understanding the effects of curing temperature on the mechanical properties of mine cemented tailings backfill. *Engineering Geology*, vol. 114. pp. 397–413.

Fall, M. and Nasir, O. 2010. Mechanical behavior of the interface between cemented tailings backfill and retaining structures under shear loads. *Geotechnical and Geological Engineering*, vol. 28. pp. 779–790.

Galaa, A.M., Thompson, B.D., Grabinsky, M.W., and Bawden, W.F. 2011. Characterizing stiffness development in hydrating mine backfill using ultrasonic wave measurements. *Canadian Geotechnical Journal*, vol. 48. pp. 1174–1187.

Helinski, M., Fahey, M., and Fourie, A. 2011. Behavior of cemented paste backfill in two mine stopes: measurements and modeling. *Journal of Geotechnical and Geoenvironmental Engineering*, vol. 137. pp. 171–182.

Hughes, P.B., Pakalnis, R., Hitch, M., and Corey, G. 2010. Composite paste barricade performance at Goldcorp Inc. Red Lake Mine, Ontario, Canada. *International Journal of Mining, Reclamation and Environment*, vol. 24. pp. 138–150.

Itasca. 2008. PFC2D-Particle flow code in 2 dimensions, version 4.0 user's manual, Itasca Consulting Group Inc., Minneapolis.

Jeremic, M. 1985. Strata Mechanics in Coal Mining, CRC Press.

Ju, F., Huang, P., Guo, S., Xiao, M. and Lan, L. 2017. A roof model and its application in solid backfilling mining. *International Journal of Mining Science and Technology*, vol. 27. pp. 139–143. doi: https://doi.org/10.1016/j.ijmst.2016.11.001

Klein, K. and Simon, D. 2006. Effect of specimen composition on the strength development in cemented paste backfill. *Canadian Geotechnical Journal*, vol. 43. pp. 310–324.

Kostecki, T. and Spearing, A.J.S. 2015. Influence of backfill on coal pillar strength and floor bearing capacity in weak floor conditions in the Illinois Basin. *International Journal of Rock Mechanics and Mining Sciences*, vol. 76. pp. 55–67.

Kulakov, V.N. 1995. Geomechanical conditions of mining steep coal beds. *Journal of Mining Science*, vol. 31. pp. 136–143.

Kulakov, V.N. 1995. Stress state in the face region of a steep coal bed. *Journal of Mining Science*, vol. 31. pp. 161–168.

Li, L. and Aubertin, M. 2009a. Horizontal pressure on barricades for backfilled stopes. Part I: Fully drained conditions. *Canadian Geotechnical Journal*, vol. 46. pp. 37–46.

Li, L. and Aubertin, M. 2009b. Numerical investigation of the stress state in inclined backfilled stopes. *International Journal of Geomechanics*, vol. 9. pp. 52–62.

Li, L. and Aubertin, M. 2011. Limit equilibrium analysis for the design of backfilled stope barricades made of waste rock. *Canadian Geotechnical Journal*, vol. 48. pp. 1713–1728.

Mishra, M. and Karanam, U.M.R. 2006. Geotechnical characterization of fly ash composites for backfilling mine voids. *Geotechnical and Geological Engineering*, vol. 24. pp. 1749–1765.

Mkadmi, N.E., Aubertin, M., and LI, L. 2013. Effect of drainage and sequential filling on the behavior of backfill in mine stopes. *Canadian Geotechnical Journal*, vol. 51. pp. 1–15.

Mo, S., Canbulat, I., Zhang, C., Oh, J., Shen, B., and Hagan, P. 2017. Numerical investigation into the effect of backfilling on coal pillar strength in highwall mining. *International Journal of Mining Science and Technology*. https://doi.org/10.1016/j.ijmst.2017.07.003

O'Sullivan C. 2011. Particulate Discrete Element Modelling: A Geomechanics Perspective. Spon Press.

Potyondy, D.O. and Cundall, P.A. 2004. A bonded-particle model for rock. *International Journal of Rock Mechanics and Mining Sciences*, vol. 41. pp. 1329–1364.

Sivakugan, N., Rankine, R.M., Rankine, K.J., and Rankine, K.S. 2006. Geotechnical considerations in mine backfilling in Australia. *Journal of Cleaner Production*, vol. 14. pp. 1168–1175.

Sui, W., Zhang, D., Cui, Z.C., Wu, Z., and Zhao, Q. 2015. Environmental implications of mitigating overburden failure and subsidences using paste-like backfill mining: a case study. *International Journal of Mining, Reclamation and Environment*, vol. 29. pp. 521–543.

Tesarik, D.R., Seymour, J. B., and Yanske, T.R. 2009. Long-term stability of a backfilled room-and-pillar test section at the Buick Mine, Missouri, USA. *International Journal of Rock Mechanics and Mining Sciences*, vol. 46. pp. 1182–1196.

Thompson, B.D., Bawden, W.F. and Grabinsky, M.W. 2012. In situ measurements of cemented paste backfill at the Cayeli Mine. *Canadian Geotechnical Journal*, vol. 49. pp. 755–772.

Walske, M.L., McWilliam, H., Doherty, J., and Fourie, A. 2016. Influence of curing temperature and stress conditions on mechanical properties of cementing paste backfill. C*anadian Geotechnical Journal*, vol. 53, no. 1. pp. 148–161.

Wang, H., Poulsen, B.A., Shen, B., Xue, S., and Jiang, Y. 2011. The influence of roadway backfill on the coal pillar strength by numericalinvestigation. *International Journal of Rock Mechanics and Mining Sciences*, vol. 48. pp. 443–450.

Yilmaz, E., Belem, T., and Benzaazoua, M. 2014. Effects of curing and stress conditions on hydromechanical, geotechnical and geochemical properties of cemented paste backfill. *Engineering Geology*, vol. 168. pp. 23–37. ◆

http://dx.doi.org/10.17159/2411-9717/2018/v118n1a4

Engineering education: an integrated problem-solving framework for discipline-specific professional development in mining engineering

by G. Haupt and R.C.W. Webber-Youngman

Synopsis

This article is based on the premise that the purpose of engineering education, in general, is to deliver engineering practitioners who are intellectually capable of identifying, structuring, and solving complex problems, and that solving engineering problems is systemic. The solutions to problems are viewed as objects, tools, processes, and systems. The purpose of this article is, however, to specifically explore some of the aspects of the intangible world of mining engineering from a generic problem-solving perspective, which would also be applicable to any other engineering discipline. This is done by focusing on higher order intellectual processes when processing information in the problem-structuring and problem-solving space. As such, this article builds on a previous study in which the intangible world of the mining engineer was identified as worth investing in. We begin by briefly reviewing the complexity of the mining engineering problem-solving space and the background and role of a generic cognitive approach to problem solving in the mining engineering curriculum at the University of Pretoria (UP). Several dimensions of extended cognitive processing are then detailed, explaining why the early phases of problem solving are difficult to learn, and more difficult still to teach. An outline is given of the classification of types of mining engineering problems, and its determinant role in the dynamics of information processing. Conceiving, designing, implementing, and operating (CDIO) as an overarching engineering methodology is discussed, together with the subsequent mapping of cognitive phases onto CDIO stages. Finally, we pose an open research question that seems important to answer in order to identify the best pedagogical practices for improving problem-solving capabilities not only in mining engineering but also in other engineering disciplines.

Keywords
extended cognition, information processing, problem solving, systems thinking.

Introduction

Mining is an essential activity for meeting people's needs for commodities and services. This is done through mining (mineral extraction) and beneficiation to produce end-products in sustainable ways that contribute to economic development and the provision of services to society. Mining engineering involves the application of the relevant knowledge and understanding of mathematical and natural sciences, and a body of mining engineering knowledge, technology, and methodologies. Mining engineering furthermore aims to deliver solutions, the effects of which can be projected even in mostly uncertain contexts. Streamlining mining engineering education therefore requires mastering of the necessary knowledge, and the teaching and learning of skills in ill-structured, non-routine, real-world problem-solving contexts (Jonassen, Strobel, and Lee, 2006).

In the mining environment, these problems vary from well-structured repair-type problems (including repair and replacement of faulty equipment), to semi- and entirely ill-structured problems. The latter can include the upgrading of safety infrastructure, optimizing the application and use of existing mining and mining-related equipment, processes, systems and procedures, as well as the design of innovative tools and systems to operate effectively and adapt to changing physical mining conditions. In all of this, occupational health and safety (OH&S)-related hazards and risks need to be considered and addressed so as to ensure a safe, healthy, productive, and profitable working environment.

The certified level of engineering education outcome and level of experience of the mining engineering practitioner (ECSA, 2015) together determine the nature and complexity of the problems a particular practitioner might be entrusted to solve. For this reason, when mining engineering learners at the University of Pretoria (UP) embark on their final year real-world mining projects, they are usually given relatively well-structured problems to solve. This, however, does not preclude introducing them to semi- and ill-structured problems as part of a larger research project or team effort. Establishing a sound problem-solving development process will serve them well in dealing with the semi- and ill-structured problems that they will encounter in their future careers.

One of the reasons for the difficulties in mining engineering education is that the mining environment is complex. Complexity

* *University of Pretoria, South Africa.*
 ISSN 2225-6253. Paper received Jan. 2017; revised paper received June 2017.

here refers to mining engineering being embedded in a country's social, technical, and economic systems (van der Merwe, 2011). In this environment, mining and other engineering practitioners are often faced with having to choose the best approach to solving the various types of problems encountered in a mining environment (Kluge and Malan, 2011). These problems are all context-bound, and require sensitivity to the type of information, methodologies, and tools required to make appropriate decisions. A sustained effort is needed to constantly improve OH&S at mines, and continued research is necessary on changing physical mining conditions to secure revenue from the sale of coal, platinum, gold, and other minerals. In addition, there seems to be a need to streamline the transfer of knowledge to future mining engineering practitioners (van der Merwe, 2011). The complexity of this field is compounded by rapid changing technology, intense national and international competition in the marketplace, rising employee and customer expectations, the demand for improved accountability for the natural environment, strict OH&S-related legislation, and the necessity of working in large, multidisciplinary project teams.

Healthy, safe, and profitable sustainable mineral production techniques are essential to support economic growth. This is ensured through exports in return for much-needed revenue, as well as exchange of knowledge. In turn, changing external mining environments require novel mining methodologies supported by new and appropriate technologies. The debate around the importance of preparing mining engineers to eventually become leaders and managers is ongoing. Opposing the emphasis on leadership is the argument that the need for specialized technical skills, such as mine planning and design (MP&D), strata control/rock engineering, mine ventilation, (mine environmental control) (MEC), mineral resource evaluation, and mineral asset valuation is more pressing (Musingwini, Cruise, and Phillips, 2012).

The complexity of mining engineering and the difficulty of teaching and learning in this diverse field are well known. The Engineering Council of South Africa (ECSA, 2015) acknowledges this in their *Standards and Procedures System* documents, which stipulate a two-phased approach to teaching and learning engineering competence encompassing all areas of specialization at various competency levels. In accordance with ECSA's standards and outcomes of engineering education, the first phase entails acquisition of knowledge through formal tertiary programmes. The second phase entails acquiring practical workplace experience and the application of knowledge to deal with mining-related challenges, including the solving of engineering and related problems. In a report on the status of the education of mining engineering learners internationally, McDivitt (2002, p. 14) confirms that mining engineering learners believe that they need to know more than what they are being taught at university in order to cope with mining engineering-related challenges.

One of the areas in which engineering learners typically need support is that of problem-solving in general, and specifically, the early planning phases, namely, problem structuring (Mingers and Rosenhead, 2004) and problem-solving entailing decision-making (Kluge and Malan, 2011). To assist them in solving given problems more easily, and to produce the best products in the shortest time and at the lowest cost (Wallace and Burgess, 1995, p. 429), engineering learners use tools and methods to alleviate their cognitive load (Goel, 1995). In the same manner, educators develop and use tools to guide their teaching and to facilitate the learning process that mirror the way experienced and competent engineers work and think (Haupt, 2015).

The purpose of this article is therefore to explore the possibilities of a novel, generic, yet integrated framework for problem-solving within discipline-specific learner education and development modules at the Department of Mining Engineering at UP. This would serve as an educational tool to guide learners in considering the psychology of extended cognition behind solving mining engineering problems, especially within the context of the CDIO problem-solving methodology. This framework represents the intangible world of extended cognition of the typical mining engineer (Webber-Youngman and Calaghan, 2011) and is a response to the need for streamlining the transfer of knowledge (van der Merwe, 2011).

Background to problem-solving

Transferring the latest knowledge and thinking skills to new learners, as well as to an older generation of experienced mining engineering practitioners, is one of the pursuits of mining engineering education. The general approach of tertiary institutions offering mining engineering degrees is, in the first two years of the academic engineering programme, to engage learners in knowledge and understanding of content and science-related tasks. These are related to disciplines including mathematics, chemistry, geosciences, and physics. In accordance with the convention in engineering courses over the past six decades, the first two years are thus devoted to 'engineering sciences' (McDivitt, 2002). The Washington Accord internationally agreed educational pathways for qualifying engineers require that the first two years of study include relevant science-related courses as applied in particular specialization fields (IEA, 2009). These serve as a foundation for analytical thinking, where learners are required to apply scientific principles to technological problems (Dym *et al.*, 2005). Engineering education literature (Jonassen, Strobel, and Lee, 2006; Dym *et al.*, 2005) overwhelmingly indicates that traditional curricula propagate linear thinking, which is not conducive to fostering the kinds of thinking needed when working in environments with complex systems.

The ensuing limitation on nonlinear processing of information leaves mining engineering graduates entering the workplace ill-equipped to contemplate the variety of problems that they are given to solve, and to connecting them consciously to a theory-based cognitive process. The aftermath of this limitation is a ripple effect where engineering practitioners who do not clearly identify the type of problems they are dealing with have little chance of effectively analysing and researching given problems by consciously integrating internalized and externally emerging information. Furthermore, their opportunities to intentionally find and unexpectedly discover new information, and interpret it as relevant to the problem or its potential solution, subsequently tend to be less focused. Therefore, there is a real danger of making unfounded assumptions before

investigating all possible sources of information. Ultimately this might lead to a limited set of professional and personal judgmental skills. In order to address restrictive information processing opportunities when teaching and learning ways to solve mining engineering problems, a new approach seems necessary.

Since 2011, the mining engineering department at UP has purposefully engaged in improving its entire offer of discipline-specific knowledge to learners enrolled for the four-year degree in pursuit of contributing to the developing learners' professional skills set. Several measures were taken specifically in the areas of content of MP&D, development of the discipline-specific profile, academic support, communication, and teaching. In the area of content, the unknown physical and intellectual world of the mining engineering practitioner has been addressed by developing simulations through instructional design and virtual reality (Webber-Youngman and Calaghan, 2011).

To improve the development of the discipline-specific profile of mining engineering learners, various psychological instruments have been implemented in the fourth year of the programme at the exit level. These include the Myers Briggs tool; DISC analysis (dominance, influence, compliance, and steadiness), measuring personality and group tendency relationships; Herman's Brain Dominance Instrument tool, determining thinking preferences; and the Shadowmatch tool, establishing dominant thinking habits. In addition, the emotional intelligence of final-year learners is tested to provide them with a better understanding of their ability to deal with difficult emotional situations and decisions in their careers.

There is evidence (Webber-Youngman and Calaghan, 2011) that learners have benefited from these various interventions and tools. However, when evaluating the fourth-year mining MP&D projects, mentors identified a prevailing limitation in the ability of learners to efficiently identify and understand the nature of the mining problems they are required to solve. In part, this might be attributed to learners' lack of appropriate exposure to real mining processes and problems. In addition, it might also be ascribed to the fragmentation of cognitive strategies and support focusing on the individual differences amongst learners within groups. There is also fragmentation in solving linear problems without accounting for generic and unseen nonlinear problem-solving skills that encompass content knowledge and process methodologies. This seems to be a problem with other engineering disciplines as well.

Further research is needed to establish how the cognitive measures that are currently implemented contribute to generic, nonlinear thinking. The ability of learners to integrate their internalized linear thinking tendencies with unexpected information that is typically encountered when involved in the early phases of the problem-solving process also requires research. Early phases here refer to understanding and structuring a given problem through conception, and incrementally solving it in stages through a critical thinking process (Haupt, 2015), which is discussed later in more detail.

The literature on engineering education research, in general, tends to focus on the problem-solving phase, which emphasizes the quality of the end products or solutions and disregards the importance of the problem structuring phase (Eastman, 2001). The same is true of the methodologies and problem-solving models available to learners and competent engineering practitioners.

Well-known problem-solving models, which include the Russian model *Teoriya Resheniya Izobretatelshkikh Zadatch* (TRIZ) translated as 'Theory of Inventive Problem Solving' (Barrie, Domb, and Slocum, 2010), are seen as being one-sidedly focused on finding the solution without sufficient attention to the research-driven process of identifying the problem. It is this limitation that this article attempts to address at a theoretical level, aiming to understand how to further improve the Mining Engineering module *Introduction to Project* in the third year of mining engineering studies.

Another well-known approach to solving engineering problems, suggested by Kepner and Tregoe (1981), involves finding the root causes, using cause-and-effect analysis of a particular problem. However, they do not differentiate between different types of problems. Literature exploring the nature of a problem and its effect on the dynamics of the problem-solving process, introduced by Simon (1973), provides important insights into the importance of the problem structuring phase.

There is a general need to guide learners in their discipline-specific development modules to a generic problem-solving methodology that is suitable for the multiple and diverse contexts of mining engineering practice. Based on this need, the authors developed an integrated problem-solving framework that serves as a teaching and learning tool. For this purpose, the most recent addition to the empowering tools in the third and fourth year learners' discipline-specific cognitive toolbox is the inception of the Theory of CDIO (Platanitis and Pop-Iliev, 2012) methodology. This provides a structured methodological context within which problem solving might be taught and learnt. The conceptualization of CDIO is based on the philosophy of 'design thinking', where 'design' implies a generic approach to 'problem solving' in a mine planning and design thinking environment, irrespective of the engineering discipline or specialization.

As such, CDIO is meant to guide learners in solving technical, systemic, and business-related problems that are typical of the mining context. However, as CDIO is a broad model, encompassing multiple aspects in a transdisciplinary manner, curriculum designers need to continuously update a careful and detailed mapping of the entire four-year mining engineering programme to ensure a well-balanced implementation of the model.

The authors suggest an integrated cognitive approach to problem solving in mining engineering education where the CDIO methodology is used as a context for teaching and learning particular cognitive skills. However, despite the value of the CDIO methodology as a context in engineering and business learning environments (Alarcon *et al.*, 2013), the authors argue that learners applying the suggested stages is, in itself, not sufficient. It does not provide satisfactory guidance for lecturers and learners to become sensitive to the microscopic complexities involved in the extended nature of the underlying early cognitive phases of problem solving. By understanding some aspects of the psychology of extended cognition as a backdrop, the authors aim to strengthen the professional capabilities of senior (exit-level) mining engineering learners.

Theoretical foundation – a psychological perspective

In order to guide the development of suitable curricula and teaching methodologies that might effectively foster information processing, two theoretical underpinnings seem to play an important role. The first set of theories concerns the ontological issues around microscopic information processing, known as design cognition. This is also, as mentioned earlier, known as the intangible world of mining engineering. The second set of theories concerns the methodological issues around the structuring of activities towards the effective solving of engineering problems. This is also known as the visible outer world of activities of the mining engineering practitioner.

The concept of design cognition is derived from the notion of design thinking as a form of problem solving which has planning at its core. As such, 'designing' is considered as an intentional mental activity precluding the early planning and does not refer to the production of the end product. Therefore, MP&D and 'problem solving' here are used interchangeably. The Theory of Human Problem Solving was conceptualized by Newell and Simon (1972) as a generic psychological process that could be scientifically studied and recorded by understanding the processing of information by humans. This theory focused on the internal computational processing of information, which became known as an abstract problem-solving space theory. In response to its one-sided emphasis on the unseen, intangible processes involved, Gibson (1986) introduced the notion of perception as a form of external information processing, which assumes that external objects afford useful information.

A theory that supports the combination of internal and external information processing as the underlying principle of problem solving is known as Extended Cognitive Theory (ECT). It is also termed Situated Design Cognition (SDC) (Gero and Kannengieser, 2006). An extended approach accounts for the complex dynamics involved in making connections between perceivable information about the material characteristics of objects, people, and contexts, and theoretical knowledge in order to make sound scientific, technical, and professional judgements and decisions when solving problems. This dynamic is the ontological basis of problem-solving methodology (Haupt, 2017). However, although this concept has been explored in various design-related environments, such as architecture (Suwa and Tversky, 1997), industrial design (Haupt, 2015), and mechanical engineering (Goel, 1995), it has not been articulated explicitly in a mining engineering context.

This thinking regarding engineering methodology as an intellectual activity originated in the 1960s (Cross, 1986). Researchers became interested in the intangible world of engineering practice and studied the cognitive processes involved in their problem-solving activities. The primary approach to such research was to study the ways in which engineering practitioners intentionally process information in the early phases of understanding a particular problem, and planning how to solve it. Two opposing psychological approaches ensued from this interest. On the one hand are the computational theorists, such as Simon (1969), who considered information processing as an internal process using internal sources of knowledge. On the other hand are the ecological psychologists, who advocated the use of external information sources and processes that form part of an engineering practitioner's physical environment when solving a given problem. A third view was developed in the late 1990s that attempts to combine these two opposing views and integrate these into an extended cognition paradigm. The authors subscribe to the assumptions of the latter to explain problem-solving and develop discipline-specific learning curricula for mining engineering learners.

However, despite the differences between these approaches, a common pool of assumptions that conceive the engineering or specifically MP&D process prevails. Irrespective of the particulars of the specialization knowledge and skills involved, and the complexity of the particular problem that competent engineering practitioners and learners are given to solve, the process involve a common sequence of steps through which engineers move. These steps can be summarized as follows:

- Identification, exploration, decomposition, and analysis of the problem
- Identification of the connections between the components
- The solution of the sub-problems in isolation
- Finally, the synergistic combination (taking into account the interconnections) of the partial solutions into the problem solution (Goel and Pirolli, 1989).

Based on these observations, engineering theorists (Simon, 1996) concluded that the act of thinking in an engineering manner is largely independent of the objects or systems that are involved.

The implication for engineering education, irrespective of the particular discipline, is that although sourcing and obtaining information *per se* is not considered as the solution to a given engineering problem, it is an essential sub-process of both cognitive phases at issue here, *i.e.* problem structuring and problem solving (Simon, 1973). In the case of the problem-structuring phase, engineers are often provided with insufficient information to clearly identify or define the engineering problem at hand, as is the case in ill-structured (mining) engineering problems. In the case of the problem-solving phase, engineers incrementally detect gaps in their information, especially in complex problems where multidisciplinary fields of specialized knowledge are required to develop a suitable solution or sub-solutions (Wiltschnig and Christensen, 2013). Sourcing and obtaining such information therefore forms in integral part of the problem-solving phase of the design process.

An extended cognition approach was adopted in this article. The implication thereof for mining engineering education is that learners require guidance in deliberate problem-solving strategies. This is needed to extend their intangible internal world of mining, science and mathematics, and applied engineering knowledge and information stored in their long-term memories to include their outer, physical, socio-economic world. They need to interact with the real, physical world surrounding the problem in order to identify the problem, its root cause, and search for information that might help them to find a solution.

Observations from empirical protocol studies over the past twenty years (Goel, 1995; Haupt, 2015) where the micro-processes of experts, experienced and competent planners, and designers solving problems have convincingly

shown a stable pattern of information processing distributed over two distinct cognitive phases, irrespective of the methodology that the participants were trained to use. The two early cognitive phases can be summarized as follows.

- Problem structuring through a process of observation, inquiry, research, analysis and interpretation, redefining, and explicit making of the real engineering problem or desired outcome to be achieved
- Problem solving through a three-pronged sub-process:
  a. Conceptualizing a solution through preliminary ideas
  b. Developing suitable ideas
  c. Refining ideas and producing blueprints and preferred plan(s) to be implemented and operationalized.

These early phases subsequently result in the 'late cognitive phases' during which the refinement of ideas and commitment to a particular conceptual solution is ultimately explicitly formulated and visualized in formats ready for construction and implementation. For educational purposes, it is important to emphasize that cognitive phases overarch the seeming linear approach listed above. The latter serve as a useful way of separating cognitive activities.

However, much research has shown that the mental processes of engineers during the problem-structuring and problem-solving phases cannot be described as a linear process. The cognitive phases, as well as the implied engineering activities, often overlap in what Goel (1995) terms a 'leaky phase', which is implied in the application of 'limited control' indicated in Table I, item 4. Table I is a summary of the typical psychological characteristics of the intangible information processes during the early phases of the design process identified by Goel and Pirolli (1992) in protocol studies on a variety of designers, including engineers.

The concept 'early phases', which is the focus of this article, entails the understanding of the problem by interpreting the given brief, and restructuring and redefining it until the desired outcome of problem-solving processes is mentally clear and represented in the form of sketches, diagrams, and models. Intertwined with structuring and defining the problem, is the coincidence of the 'later phases', entailing the generation of an appropriate solution and its subsequent incremental development and refinement. Finally the generated solution to which engineers commit themselves (Table I, item 5), and in which they state/define the problem or desired outcome of the problem in the particular project during the problem-structuring phase, is mentally and visually developed and refined into a useful blueprint specifying the construction and implementation of an envisaged artefact, process, or system during the final

Table I

Typical psychological characteristics of the intangible information processes during the early phases of the design process (adapted from Goel and Pirolli, 1992)

Psychological characteristic	Information processing
1. Extensive problem structuring.	Identification, exploration, and analysis of the given problem. Establishing the scope of the problem.
2. Extensive performance modelling – problem-solving.	Incremental process of conceptualizing functionality and subsequent physical components making efficiency, sufficiency, and desired performance of an artefact or system possible.
3. Personal and institutional evaluation and application of standards.	Personal and institutional knowledge of domain-specific knowledge of standards and norms. Determination of institutional and personal value system to be considered.
4. Limited control mode strategy with nested evaluation cycles.	Deliberate control of cycles of exploration, evaluating information, and generation of ideas. Controlling delay as well as acceleration of decision-making and commitment to both problem identification and solution development.
5. Making and propagating of commitments.	Idea generation, decision-making, testing and developing implementation plans. Committing to decisions implied and explicated in redefinition of the problem or desired outcome of the solution.
6. Solution decomposition into leaky modules.	Analysis of solution, evaluation, searching for more information, integrating suitable information, discarding irrelevant information and unsuitable ideas, developing solution further.
7. Hierarchical considering abstract theories and principles.	Transforming generalized abstractions such as intended goals and aims, including philosophy and functionality, into practical and tangible object and system specifications. Use of multidisciplinary knowledge. Use of domain-specific knowledge.
8. Use of visual modes of knowledge and decision-making representations.	2D and 3D modeling of ideas, processes, and decisions.
9. Extensive interaction with external sources of information emerging from the physical environment.	Reliance on perception, detecting sensorial information afforded by basic primitives including sound, smells, visual, tactile, and taste.

refinement phase of the design process. The basis for this theory of the early phases of the design process can be found in the numerous descriptive and explanatory protocol studies conducted over the years on engineering practitioners (Goel and Pirolli, 1992; Haupt, 2015; Cross and Clayburn, 1998), and specifically mechanical engineers, industrial designers and architects.

During their third year of study, the learners in the UP Mining Engineering Department in their discipline-specific development modules are introduced to the early cognitive phases through non-mining problem-solving case studies where they need to identify the two cognitive phases, namely problem structuring and problem solving. These case studies are carefully selected from business management or service design contexts involving a variety of types of problems. The focus is thus on the subsequent deliberate search for missing information and its appropriate application. Engaging analytically with the case studies serves to familiarize learners with the generic theoretical background of the process that they are expected to encounter during their fourth (final) year of study.

Learners are also required to deconstruct these case studies in terms of the types of problems (Table II), the search for information, and the identification of relevant information-processing activities (Table I). Abstract Cognition Theory is concretized through a team teaching strategy where the authors, a mining engineering practitioner, and a cognition specialist collaborate in the contextualization of the theory. The focus of such an intervention is on the intangible psychological characteristics typical of the search for information in each particular cognitive phase of the problem-solving process. Two assumptions are important here. The first is that the particular type of problem given determines the specificity of information available to understand its scope and implications. The second assumption underlying the search for information is that problem-solvers do not have sufficient information when given particular problems, depending on their ill-structured or well-structured nature.

From a cognitive perspective, information processing is seen to take place in a system consisting of three stages. The first is the start stage, typified by the vagueness and/or incompleteness of input information. The second is the transformation stage, typified by the change from vagueness to concrete, specific, sufficient and accurate information. The third stage entails the solution, with detailed specifics of the decisions made (Goel, 1995). The difficulty for the mining engineering learners lies in understanding how the structure of a given problem influences their search for information. The learners in the final year of study typically find that the openness and relative ill-structured nature of some of their project tasks presents difficulties, as they are neither sufficiently educated nor trained in classifying these types of problems, and lack experience in identifying the relevant missing information.

As a result of the abovementioned factors, learners often follow an inappropriate cognitive approach to solve problems. Their linear and prescriptive education in respect of science and mathematics training contributes to their uncertainty in a mental space where the pathway to a specific solution has not been outlined. In order to familiarize them with some of the uncertainty that they should expect in their projects, the authors believe that, at most, a set of descriptive characteristics that are typical of those experienced by competent engineering practitioners and other designers can be introduced to the learners. These characteristics, in which uncertainty is embedded, are summarized in Table I. The determinant factor of this set of psychological characteristics is the absence of information concerning a particular problem presented for solution. This absence, in turn, is determined by the type of problem that competent engineering practitioners are given, ranging from relatively small-scale, well-structured technical problems to large-scale, complex, ill-structured planning and design problems with medium-scale semi-structured optimization problems.

The advantage for lecturers of understanding the cognitive characteristics summarized in Table I lies in its focus on the process and not on the final product. This might assist them in detecting the growing maturity of learners' ability to channel their uncertainty in a rational and systematic manner through their MP&D projects. As such, it is not meant as a prescriptive set of rules or steps for learners to follow. These are unseen, intangible processes that result in the decisions that they take. Only when learners are guided/coached to physically and sensorially integrate what they perceive on surface or underground, in shafts, in production areas, or transportation systems with the theoretical models that they learn at universities can they develop meaningful cognitive connections/alignments between real-life mining problems, the knowledge they have acquired, and the methodologies that they select to apply.

The role and types of problems

In terms of the Theory of Extended Cognition, the availability of information at the start of a given problem is determinant to the dynamics of the entire problem-solving process. Simon (1969), in his seminal work *Sciences of the Artificial*, began the important task of theorizing about different types of problems – namely, well-structured, semi-structured, and ill-structured problems. The role of these types of problems is directly connected to the amount of information typically known and accessible to engineering practitioners and the associated psychological characteristics summarized in Table I. Therefore, to deepen learners' understanding of the dynamics involved in solving real-world mining problems and the associated uncertainties, the authors devised a classification system (Table II) for the various types of typical of mining engineering problems. This is based on the theory of well-structured and ill-structured problems, posited by Simon (1972) and developed by Rittel and Webber (1984).

The quality, applicability, and in many cases volume and availability or lack of information at the start of any engineering project determines the extent of the learner's or engineering practitioner's uncertainty. This can range from relatively low levels of uncertainty to extensive uncertainty in all phases of the process. Entry-level mining engineering practitioners are typically given the first type of problem on the one extreme of the available range, here termed 'repair/replacement tasks' (Table II). These might be considered as 'well-structured problems' as the goal of the task is known to the engineering practitioner, as well as they process involved in solving it.

Table II

Types of mining engineering problems and its implications for information search

SEARCH FOR INFORMATION	TYPES OF MINING ENGINEERING PROBLEMS		
	Repair tasks **Well-structured problems**	**Optimization tasks** **Semi-structured problems**	**Design/innovate tasks** **Ill-structured problems**
Availability of information	'Well-structured'. Information available through existing knowledge regarding existing similar objects and systems.	'Semi-structured'. Some information is known through existing knowledge and can be adopted in objects, tools, and systems. Much room exists for novel ideas to be integrated and combined into existing objects and systems.	'Ill-structured'. No information about the solution or its pathway is known. Extensive uncertainty exists about the end product or process to achieve it.
Extent of uncertainty	Relatively little uncertainty.	Some uncertainty exists about some of the aspects of the process and end product.	Extensive uncertainty about most aspects of the process and end product exists.
Starting point of search	Identify the faulty component presenting symptoms.	Problem contemplation: Mission contemplation, Existing objects, processes, tools/system/ technology. Search for areas in need of improvement.	Problem contemplation: Mission, need (new objects, processes, tools, systems), Intentions (functionality), Required behaviour, impact, brief, community, and environment.
Focal point of search	Identify the real causes of deficiency. Constraints are well defined and known.	Modification to artefact/system, interaction with people, and context, subject to constraints and restrains.	Constraints, restraints, required structure/system, behaviour, interaction with people, and context.
Core reasoning process	Determine corrective measures: Application of known domain-specific knowledge and experience.	Analysis, evaluation and improvement/refinement Application of known domain specific knowledge.	Planning and design: discover and refine/rework unknown and known information.
Sources of information	Recall internal domain-specific knowledge recalled from memory. Access external information accessed through visual perception of current problem situation.	Recall internal domain-specific knowledge recalled from memory. Access external information accessed through visual perception of current problem situation.	Recall internal domain-specific knowledge recalled from memory. Recall internal knowledge from personal experience of similar and different problem situations. Access external information through multiple direct perceptions of current problem situation and its constraints.
End goal of search	Restore the things back the way they were.	Improve physical and procedural characteristics of existing systems/objects.	Create something new that does not exist yet. Innovative. Apply basics Potential for multiple unknown constraints.
Scope of the system involved	Contained in one artefact or component thereof.	Singe component within a complex system, or more than one component in a range of artefacts, which form part of the system. A single change might optimize the entire system.	Large, complex, new artefacts or systems operating on the basis of novel principles/technology, supported by basic science and applied engineering knowledge.

The second type of problem is an optimization task, which entails some uncertainty as the aim is typically to improve elements, functionality, and effectivness of an existing object, tool, or system. At the other extreme is the third type, 'design' or 'innovation' tasks, which usually pose extensive uncertainty as to most aspects of the desired outcome and the process by which it is achieved. These types of problems are known as 'ill-structured' because of the extensive lack of sufficient and appropriate information at the start of the task (Rittel and Webber, 1984). They also usually lack specific and relevant information about the nature of the object, tool, or system that is being designed as they aim to create something that does not yet exist using basic scientific and applied engineering knowledge. Until it has been tested, the functionality and efficacy of the new object, tool or system – although it might be predicted – is largely unknown (Goel, 1995).

Only when learners/engineering practitioners are experienced and considered competent should they be charged with solving MP&D and innovation problems. In order to guide the third-year mining engineering learners through the 'search for information' process and its subsequent movement from low to high/acceptable levels of certainty, the different types of problems that learners are likely to encounter as they progress through their professional careers are summarized in Table II. Developing their theoretical grasp of what they might expect in their final-year projects, the learners are then introduced to a stage-based model of the MP&D processes, namely, CDIO.

CDIO – a problem-solving methodology

CDIO as design or problem-solving methodology was conceived at the Massachusetts Institute of Technology (MIT) in the late 1990s. In collaboration with the Swedish universities Chalmers University of Technology, Linkoping University, and the Royal Institute of Technology, the CDIO initiative was formally founded in 2000 (CDIO™ Initiative, 2003) as an audacious undertaking that would transform engineering education in the USA and Europe. With the participation of academics, industry, engineering practitioners, and learners, a stage-based framework was developed for engineering fundamentals that serves as a context in which particular descriptive cognition activities occur. The CDIO stages have been distilled from well-known models, including those of Pahl and Beitz (1996) and French (1999):

- Conceiving: this entails defining a particular need, describing the problem or desired outcomes, and connecting it with an appropriate technology that could fulfill it, while considering the strategies and regulations embedded in the company involved. This early phase leads to the development of a concept, and structural and business decisions to be made
- Designing: this involves drawing up the plans, models, algorithms, or formulae that provide blueprints of what will be implemented in the later stages of the process
- Implementing: this late phase comprises transforming the plans into the solution, which could be a product, system, or intervention
- Operating: this is also a late phase, which entails the use of the implemented product to deliver the intended function/desired outcome, inclusive of its entire life-cycle.

The advantage of this methodological framework is that it is universally adaptable and lends itself to multiple contextual applications. The CDIO framework has the further advantage that it does not restrict engineering practitioners to a linear step-by-step process, but allows for iteration and movement between the early and later stages. It furthermore allows for the translation of stages and sub-stages into cognitive activity concepts, making the theoretical and practical integration of isolated early phases with early D&P cognition phases and consequential educational implications possible. For the purpose of this article, the focus is on the first two stages, conceiving and designing, which translates to the two early cognitive phases, problem structuring and problem solving, at issue here.

An integrated problem-solving framework

The purpose of the proposed descriptive problem-solving framework in this article is to guide the facilitation of mining engineering education projects undertaken by learners in their final year of study. As such, as seen from Figure 1 and Figure 2, it integrates elements of the CDIO methodology and activities (Table I) from the Theory of Extended Cognition. The first step in the integration process is to map the two early cognitive phases, problem structuring and problem solving, onto the stages of the CDIO model, namely Conceive, D&P, Implement, and Operate, as seen in Figure 1. The second step is to populate the overlaps with cognitive activities that are relevant to each of the overlaps, as visualized in Figures 2a (Conceive) and 2b (D&P).

Each of the overlapping areas between CDIO phases and cognitive activities, as represented by the blank triangles in Figure 1, are amplified in Figures 2a (Conceive) and 2b (D&P). Each of the overlapping areas between CDIO phases and cognitive activities, as represented by the grey triangles in Figure 1, are amplified in Figures 2a (Conceive) and 2b (D&P). For purpose of economy, in the 'Conceive' (C) triangle in Figure 2a, the cognitive phase, mission and conceptual D&P activities have been presented in a linear manner. The 'D&P' triangle received the same linear treatment in Figure 2. However, not only do the individual items treated in this way interact with one another; they also depend on each other. Furthermore, the two triangles also interact with each other in a co-evolutionary manner, indicated by the crisscrossing connection between the two triangles at the centre. Co-evolution is an acknowledged (Cross and Dorst, 1998) cognitive phenomenon in the methodology of engineers. This implies that, when solving engineering problems, engineers concurrently and simultaneously move between seeking to understand a given problem or aspects thereof and developing potential solutions. It is therefore necessary that training in problem solving should not enforce linearity, but allows engineering learners to iteratively and dynamically move between problem structuring and problem solving.

Figure 1—Model of an integrative framework, cognitive phases onto CDIO stages

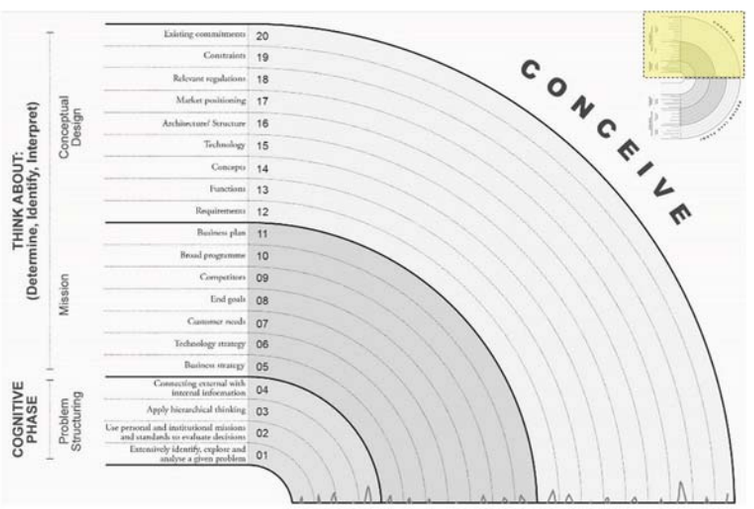

Figure 2a—Mapping early cognitive activities onto early CDIO stages (Conceive)

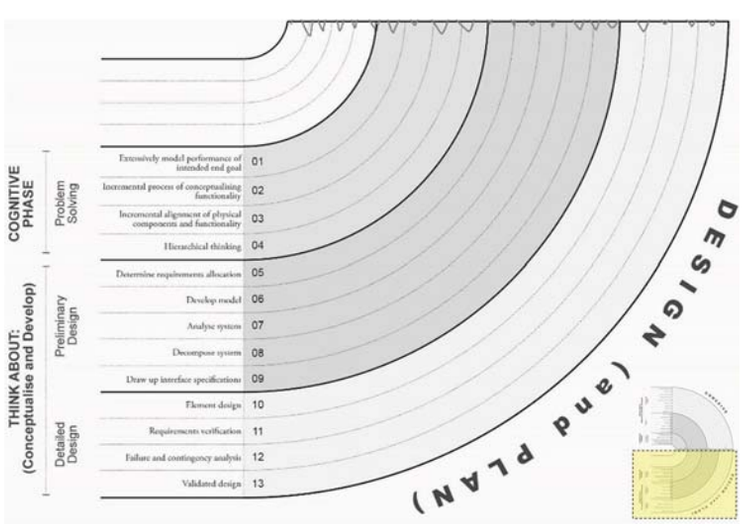

Figure 2b—Mapping early cognitive activities onto early CDIO stages (D&P)

Conclusion

The descriptive integrative framework introduced in this article is strongly focused on the technical aspects of problem-solving methodology, describing the early cognitive phases, problem structuring, and problem solving. It described the activities thought necessary to progress from understanding the problem to solving it. It further described how this overlaps with the CDIO stage of conceiving the nature of a problem or need, and connecting it through integrating relevant internal knowledge and external information. The use of appropriate technical concepts that could fulfill the need or solve a particular problem was also discussed, as this takes place within the confines of a given structural and business context.

The problem-structuring phase is followed by the problem-solving phase, which is divided into sub-phases. The first sub-phase, preliminary design, overlaps with the Conceive stage and the D&P stage. Conceiving of a suitable solution, however, implies a clearly defined problem with a transparent description. This sub-phase includes cognitive activities that allow engineering practitioners to move simultaneously and seamlessly between searching for more information about the nature of the problem and its components, and conceptualizing initial ideas for a suitable solution. Progressing to the next cognitive sub-phase, Developing, seems to coincide with the CDIO stage of designing. The cognitive activities involved here allow engineers to visualize their ideas by drawing up plans, algorithms, formulae, or layouts. This entails the addition of details and multiple iterations as a result of the critical evaluation of decisions and ideas. The refinement sub-phase of the cognitive theory overlaps with the CDIO stage of designing. This involves the refinement and finalization of planning, including implementation instructions and plans for the blueprints.

In educational practice, the value of the integrated model is limited by its product-focused perspective. This implies that the crucial difficulty in facilitating design thinking in mining engineering problem-solving projects lies in finding solutions to technical problems. This is contrary to what happens in reality, where even the most well-structured technical problem-solving process is a highly complex socio-technical and socio-economic responsible cognitive activity, requiring a combination of both microscopic, internal-external information processing skills and a much broader range of skills, ranging from teamwork to human resource management to business management.

In this article it has also been shown that for mining engineering practitioners to become intimately familiar with new trends, new mining methodologies, technology, and practice by generating new knowledge at universities is no simple task. At the UP Mining Engineering Department, the decision to adopt an integrated framework that encompasses technical, managerial, and entrepreneurial problem-solving needs further testing and evaluation. A careful alignment between various components of the discipline-specific education and development module and integrative MP&D project is necessary. In general, the suggested framework requires further research regarding the way in which it can contribute to the generation and transfer of knowledge. This specifically applies to the synergistic integration of technical knowledge and skills into the development of learners' cognitive profiles in the areas of sustainable information processing skills that are suitable for the 21st century. This emphasizes the need for an approach to mining engineering education that encompasses discipline-specific knowledge.

The changing context of mining engineering furthermore implies the reconsideration of mining engineering education and its research agenda in the following aspects, as adapted from the CDIO approach (Crawley *et al.*, 2014, p. 28), to current problem-solving contexts:

- Environmental sustainability: a change from mastery of the mining practice area to stewardship of the mining engineering practice area
- Globalization: competitiveness, collaboration, and cooperation, and distribution of engineering activities without the depletion of local expertise through permanent emigration
- Innovation: an emphasis on the delivery of new mining methodology, technology, and goods and services
- Leadership: a new emphasis on engineering practitioners as leaders, not only as managers of enterprises, but also of mining specialization areas and transfer of new knowledge and skills from experienced, competent engineering practitioners
- Entrepreneurship: the creation of new enterprises and the positive economic impact that this has on local communities
- Research: new knowledge about mining engineering practice for a changing environment.

Together, these diverse knowledge and skill focal areas point to a complex world where mining engineering learners need to be able to process information from a variety of sources, and of diverse types, if they want to contribute to solving some of the complex problems that they will inevitably encounter once they enter the world of real work.

Suggestion for further work

Immersive education through the use of the related technology such as virtual reality, augmented reality, holograms, and 3D printing, to mention but a few, will in future make significant contributions towards understanding and visualizing specific problems and the subsequent enhancement of the development and/or design of related solutions. The cognitive impact of the inclusion of related technology in education, with specific reference to teaching and learning enhancement in the complex problem-solving space, needs to be pursued.

References

Alarcon, E., Bou, E., Camps, A., Bragos, R., Oliveras, A., Pegueroles, J., Sayrol, E., and Marques, F. 2013. Designing CDIO capstone projects: a systems thinking approach. *Proceedings of the 9th International CDIO Conference*, Massachusetts Intitute of Technology, Cambridge. Massachusetts Intitute of Technology and Harvard University.

Barrie, K., Domb, E., and Slocum, M.S. 2010. Triz - What is Triz. *The Triz Journal*. Real Innovation Network. https://triz-journal.com/triz-what-is-triz/ [accessed 17 January 2017].

CDIO™ Initiative. 2003. Wallenberg CDIO Documents. http://www.cdio.org/Wallenberg_docs/wallenberg_docs.html [Accessed October 2016].

Crawley, E.F., Malmqvist, J., Östlund, S., Brodeur, D., and Edström, K. 2014. Rethinking Engineering Education. The CDIO Approach. Springer, Dordrecht.

Cross, N. 1986. Understanding design: the lessons of design methodology. *Design Methods and Theories*, vol. 20. pp. 409–438.

Cross, N. and Clayburn, A. 1998. Expertise in engineering design. *Research in Engineering Design*, vol. 10. pp. 141–149.

Cross, N. and Dorst, K. 1998. Co-evolution of problem and solution spaces in creative design: observations from an empirical study. *Computational Models of Creative Design IV*. Gero, J. and Maher, M.L. (eds). University of Sydney.

Dym, C L., Agogino, A.M., Eris, O., Frey, D.D., and Leifer, L.J. 2005. Engineering design thinking, teaching, and learning. *Journal of Engineering Education*, January. pp. 103–120.

Eastman, C.M. 2001. New directions in design cognition: studies on representation and recall. *Design Knowing and Learning: Cognition in Design Education*. Eastman, C.M., McCracken, W.M., and Newsletter, W.C. (eds). Elsevier, Amsterdam.

Engineering Council of South Africa. (2015). Standards and Procedures System. Process for training engineering candidates towards professional registration under a Commitment and Undertaking. pp. 1–18. https://www.ecsa.co.za/register/Professional%20Engineers/R-11-P_CnU.pdf

French, M.J. 1999. Conceptual Design for Engineers. Springer, Dortdrecht.

Gero J.S. and Kannengieser, U. 2006. A framework for situated design optimization. DDSS. http://mason.gmu.edu/~jgero/publications/2006/06GeroAscona.pdf

Gibson, J.J. 1986. The Ecological Approach to Perception. Lawrence Erlbaum Associates, Hillside, NJ.

Goel, V. 1995. Sketches of Thought. MIT Press, Cambridge, MA.

Goel, V. and Pirolli, P. 1989. Motivating the notion of generic design within information-processing theory: the design problem space. *AI Magazine*, vol. 10, no. 1. https://doi.org/10.1609/aimag.v10i1.726

Goel, V. and Pirolli, P. 1992. The structure of design problem spaces. *Cognitive Science*, vol. 16. pp. 395–429.

Haupt, G. 2015. Learning from experts: Fostering extended thinking in the early phases of the design process. *International Journal of Technology and Design Education*, vol. 254, no. 4. pp. 483–520. http://www.springer.com/journal/10798 [Accessed December 2014].

Haupt, G. 2017. Design in technology education: current state of affairs. *International Handbook of Technology Education*. De Vries, M.J. (ed.). Springer, Dortdrecht.

IEA. (2009). Graduate attributes and professional competencies. International Engineering Alliance.

Jonassen, D., Strobel, J. and Lee, C.B. 2006. Everyday problem solving in engineering: lessons for engineering educators. *Journal of Engineering Education*, vol. 95. pp. 139-151. doi:10.1002/j.2168-9830.2006.tb00885.x

Kepner, C.H. and Tregoe, B.J. 1981. The New Rational Manager. Princeton Research Press and John Martin, London.

Kluge, P. and Malan, D.F. 2011. The application of the analytical hierarchical process in complex mining engineering design problems. *Journal of the Southern African Institute of Mining and Metallurgy,* vol. 111. pp. 847–855.

McDivitt, J. 2002. Status of education of mining industry professionals. International Institute for Environment and Development and World Business Council for Sustainable Development.

Mingers, J. and Rosenhead, J. 2004. Problem structuring methods in action. *European Journal of Operational Research*, vol. 152. pp. 530–554.

Musingwini, C., Cruise, J.A., and Phillips, H.R. 2012. A perspective on the supply and utilization of mining graduates in the South African context. *Proceedings of the Fifth International Platinum Conference*, Sun City, South Africa, 17-21 September 2012. Southern African Institute of Mining and Metallurgy, Johannesburg. pp. 937–952.

Newell, A. and Simon, H.A. 1972. Human Problem Solving. Prentice-Hall, Englewood Cliffs, NJ.

Pahl, G. and Beitz, W. 1996. Engineering Design. A Systematic Approach. Springer, London.

Platanitis, G. and Pop-Iliev, R. 2012. Self evaluation for compliance with the 12 CDIO Standards. *Proceedings of the Canadian Engineering Education Association*, June 2011. https://ojs.library.queensu.ca/index.php/PCEEA/article/view/3652/3666

PCEEA. Proceedings of the Canadian Engineering Education Association. file:///C:/Users/user/Downloads/3652-6470-1-PB%20(3).pdf [Accessed March 2016].

Rittel, H.W.J. and Webber, M.M. 1984. Planning problems are wicked problems. *Developments in Design Methodology*. Cross, N. (ed.). Wiley, Chichester, UK

Simon, H.A. 1969. The Sciences of the Artificial. MIT Press, Cambridge, MA.

Simon, H.A. 1973. The structure of ill-structured problems. *Artificial Intelligence*, vol. 4. pp. 181–201.

Simon, H.A. 1996. The Sciences of the Artificial. MIT Press, Cambridge, MA.

Suwa, M. and Tversky, B. 1997. What do architects and learners perceive in their design sketches? *Design Studies*, vol. 18. pp. 385–403.

Van der Merwe, J.N. 2011. Future of the South African mining industry and the roles of the SAIMM and the universities. *Journal of the Southern African Institute of Mining and Metallurgy*, vol. 111, no. 9. pp. 581–592.

Wallace, K. and Burgess, S. 1995. Methods and tools for decision making in engineering design. *Design Studies*, vol. 16. pp. 429–446.

Webber-Youngman, R. and Calaghan, R. 2011. Educating the future mining engineering practitioner. *Journal of the Southern African Institute of Mining and Metallurgy*, December. pp. 815–820.

Wiltschnig, S., and Christensen, B. T. 2013. Collaborative problem-solution co-evolution in creative design. *Design Studies*, vol. 34. pp. 515–542. ◆

Acronyms

CDIO: Conceiving, Designing, Implementing, Operating

D&P triangle: Figure 2: Design and Plan

DISC: Dominance, Influence, Compliance and Steadiness (analysis)

ECSA: Engineering Council of South Africa

ECT: Extended Cognition Theory

IEA: International Engineering Alliance

MIT: Massachusetts Institute of Technology

MP&D: Mining Planning and Designing

OH&S: Occupational Health and Safety

SDC: Situated Design Cognition

TRIZ: Teoriya Resheniya Izobretatelshkikh Zadatch (Russian for 'Theory of Inventive Problem Solving')

UP: University of Pretoria

SAIMM
THE SOUTHERN AFRICAN INSTITUTE OF MINING AND METALLURGY

Application of Multiple Point Statistics to Mineral Resource Estimation—School

OBJECTIVES

The course is aimed at providing geostatistics practitioners and mineral resource evaluators with newly developed skills, knowledge and competency for application in the evaluation and classification of Mineral Resources. The development of these skills is seen as being of strategic importance.

To increase the knowledge and competency amongst technical staff of the application of Multiple Point Statistics in Mineral Resourses estimation and evaluation.

23–26 April 2018

School of Mining Engineering at the University of the Witwatersrand

Lecturers:

Prof. Philippe Renard and Prof. Julian Straubhaar

Philippe Renard, Prof. Dr. Eng., (born 1967), Professor of Hydrogeology at the University of Neuchatel, Switzerland (2006-present), PhD from École des Mines de Paris in 1996 (honours), Lecturer in hydrogeology at the Swiss Federal Institute of Technology Zurich (ETHZ) from1997 to 2001. Water supply engineer in Kankan,Guinea for the French ministry of Cooperation from 1992 to 1993. His research focuses on groundwater hydraulics in porous and fractured rocks, upscaling techniques, and innovative geostatistical methods for uncertainty quantification. He has been working on the regional modeling of saltwater intrusions in Cyprus and Tunisia. He has participated to numerous international projects such as the evaluation of the groundwater resources in the north-west of the Sahara (Mauritania) for the world bank. He was editor of Hydrogeology Journal, president of the geoENVia association and is currently a member of the leadership team of the Groundwater Committee of the International Association of Hydraulic Research (IAHR). He is the author of more than 100 scientific articles in international journals and covering a wide range of topics. His current research is focused on the development of multiple-point statistics methods as well as pseudo genetic approaches for heterogeneity modeling, uncertainty quantification and inverse groundwater modeling.

Julien Straubhaar, Dr, born in 1979, senior researcher in the stochastic hydrogeology group of the University of Neuchâtel. He holds a PhD in applied mathematics (University of Neuchâtel, 2007), with a focus on numerical methods for partial differential equations and in particular preconditioners for linear equations. His current research mainly deals with geostatistics and inverse methods. He is author of more than 20 scientific papers published in international journals and he has been a reviewer for several scientific journals. Over the last ten years, he has been heavily involved in the development of parallel multiple-point statistics algorithms, in particular Impala and Deesse softwares, which are available in professional products.

WHO SHOULD ATTEND

The course content will be of interest to:

- Geostaticians
- Geologists
- Surveyors
- Samplers
- MRM practitioners
- Mineral resource technicians.

For further information contact:
Head of Conferencing: Camielah Jardine, SAIMM · P O Box 61127, Marshalltown 2107
Tel: (011) 834-1273/7 · Fax: (011) 833-8156 or (011) 838-5923
E-mail: camielah@saimm.co.za · Website: http://www.saimm.co.za

http://dx.doi.org/10.17159/2411-9717/2018/v118n1a5

Resource and Reserve estimation for a marble quarry using quality indicators

by I. Kapageridis* and C. Albanopoulos†

Synopsis

The use of standard estimation and modelling software tools in estimating marble quarry reserves poses a number of challenges. Marble quarry reserves are based on marble quality categories, which are unique for each quarry/deposit considered. These categories represent visual and physical aspects of marble such as colour, texture, and fractures. Classification of marble in one of the categories is performed by experienced personnel and is based on samples much smaller in area than the slabs of marble that would be produced. Furthermore, the available information is mostly qualitative, leading to further complications in the application of geomathematical estimation methods. The method of estimating marble reserves described in this paper is based on interpolating quality indicator values from drill-hole and quarry face samples to blocks in three dimensions. The procedure is applied in all working quarries of Iktinos Hellas SA and is based on Maptek Vulcan Quarry Modeller, a mine planning package adapted for quarrying. Its application and results are demonstrated using a case study from a quarry in northeastern Greece.

Keywords

inverse distance weighting, quality indicators, Reserve estimation, marble quarrying.

Introduction

The reserve estimation procedure discussed in this paper concerns the Platanotopos quarry of Iktinos Hellas SA (Figure 1) – similar procedures are applied to the other quarries of the company. Specialized mine planning software (Maptek Vulcan Quarry Modeller) was used in all estimation and reporting stages. Data was provided by Iktinos Hellas SA personnel, including sample quality characterization. A technical report was issued on behalf of Iktinos Hellas SA (Kapageridis, 2015). Similar computerized estimation efforts are reported by Forlani and Pinto (2000), Careddu, Siotto, and Tuveri (2010), and Abdollahisharif *et al.* (2012).

Location

The quarry area is located in the Municipal District of Platanotopos of the Piereon Municipality of Kavala Prefecture, approximately 1.5 km NNE of Platanotopos village and 2 km SW of Mesoropi village (Figure 1). The quarry area under exploration is 88 649 m^2. The quarry area is in public forest land covered by bushes, between 380 and 540 m elevation and administered by Kavala Prefecture Authorities and Kavala Forest Inspection Authorities.

Figure 1—Location of Platanotopos quarry near Platanotopos village

Geological background and production history

The area is part of the Rodopi metamorphic massif, which extends from Thrace to part of Central Macedonia, with characteristic metamorphic geological formations and in particular marble horizons (metamorphosed limestones) in gneissic country rocks. Generally, the wider area is characterized by horizons and outcrops of white to semi-white and grey marbles, which are quarried locally. The quarry area contains calcitic and dolomitic marbles, gneiss, and gneissic schists. The calcitic marbles, gneiss, and gneissic schists have no commercial value and are not exploited.

Interest is focused on the dolomitic marbles, which occur as lenses enclosed by alternating gneissic schist layers and calcitic marbles. The marble-bearing horizon has a regular strike of NNW-SSE and dips between 25° and 30°° ESE. The lensoid white dolomitic

* *Technological Educational Institute of Western Macedonia, Department of Environmental and Pollution Control Engineering, Koila, 50100, Kozani, Greece.*

‡ *Iktinos Hellas SA, Aeshilou 11, 66100, Drama, Greece.*

 ISSN 2225-6253. Paper received Apr. 2016; revised paper received Mar. 2017.

Figure 2—Appearance of 'Golden Spider' marble from Platanotopos quarry

microcrystalline marbles are massive, white, fine-grained, and traversed by red-yellow 'spider-web' fractures filled with iron oxides and hydroxides.

This rare combination of white fine-grained fractured marble and fractures filled with secondary material results in a massive, cohesive rock mass with an interesting appearance (Figure 2). Because the marbles are massive, large slabs can be recovered with minimal production of waste material. The top 1–2 m of the marble deposit consist of a weathered layer which has a low recovery factor for marketable marble.

Production from the quarry is scheduled for 7 000–10 000 m3 per annum and at this rate, the life of the operation is estimated at 15 years. The marble, which is known as 'Golden Spider', has very good physical and mechanical properties and can take a very high polish (Table I).

Table I

Physical and chemical properties of marble from Platanotopos quarry

Specific gravity (g/cm^3)	2.850	Flexural strength (dry condition) MPa** DIN 52112	11.31
Open porosity factor wt% DIN 52102	0.60	Flexural strength MPa** (wet condition) DIN 52112	8.25
Absorption factor wt% DIN 52103	0.21	Compressive strength after freeze and thaw cycles N/mm^{2**} DIN 52104 and 52105	81.25
Elasticity GPa ASTM C-170	42	Abrasion wearing mm DIN 52108	2.06
Compressive strength N/mm^2** (dry condition) DIN 52105	120.6	Impact strength cm UNI-U 32.07.248.0	29
Compressive strength N/mm^2** (wet condition) DIN 52105	146.3		

**1 MPa = 1 N/mm^2 = 10.2 kp/cm^2

Table II

Production history of Platanotopos quarry between 2010–2014

	2014		2013		2012		2011		2010	
	m^3	%	m^3	%	m^3	%	m^3	%	m^3	%
Extraction*	77 617		92 668		89 929		73 533		34 618	
A1	353	3	915	5	1 014	5	1 367	6	1 290	10
A2	1 835	14	2 136	10						
AB	3 423	25	3 981	19	4 684	24	5 135	24	4 100	31
B	7 246	54	11 509	56	10 011	50	8 833	42	5 630	42
BB	636	5	2 116	10	4 196	21	5 816	27	2 390	18
Total production	13 494	17	20 657	22	19 905	22	21 151	29	13 409	39

*Extraction refers to total quantities mined (including waste), while total production refers to final marble products extracted (the sum of A1, A2, AB, B, and BB).

Table III

Texture categories of Platanotopos marbles

1	Classic spider, even net, clear background (classic type)
2	Relatively even spider with local strong concentrations (logs), or unclearly constructed net (fuzzy spider) or uneven zones of dense/coarse net, (standard type)
3	Dense spider, or many continuous brown lines, (heavy type)
4	Absence of spider, many white parts or with minimum net, (white type)

Table IV

Marble categories based on defects

1	Solid slab with no evident defects or less than 10% defects, which is handled with a 3% or 6% discount
2	One or two defects up to 20–25% of each slab
3	Defects up to 30–35% of each slab
4	Defects up to 50% of each slab

Table V

Platanotopos marble quality based on defects and texture/colour categories

Rectangular (length >180 cm, height > 120 cm)	**1** - No defects	**2** - Defects 25–35% of each slab	**3** - Defects 25–35% of each slab	**4** - Defects 35–50% of each slab
Classic type 1	1-1=A1	1-2=A2	1-3=AB	1-4=B
Standard type 2	2-1=A2	2-2=AB	2-3=B	2-4=BB
Heavy type 3	3-1=AB	3-2=B	3-3=BB	3-4=BB
White type 4	4-1=B	4-2=BB	4-3=BB	4-3=BB

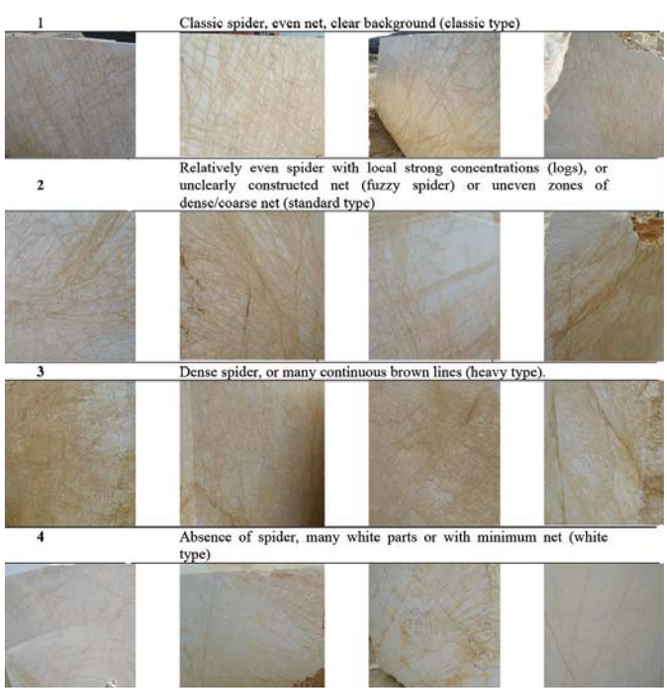

Figure 3—Colour and texture categories of Platanotopos marbles

Historical production from the quarry is given in Table II – the marble quality categories are explained in the following section.

Marble quality characterization

Colour and texture

Quality grading of Golden Spider marble is initially based on colour according to the following categories: G - golden, Y - yellow, R - red. Grading based on the spider-web texture is in one of four categories as described in Table III. Colour and texture combinations are presented in Figure 3.

Defects

Based on defects (fractures, dendrite zones, brown lines, discolourings or marks *etc.*) each slab is classified using the four categories in Table IV, and the final quality is assigned according to Table V. The slabs produced from the Platanotopos quarry are 6 × 2.8 × 7 m (width, depth, height).

Reserve estimation data

Data used in the reserve estimation for each quarry includes the original as well as the current topography of the quarry area based on the quarrying activities up to the date of the study, as well as diamond drill-hole samples and sections on quarry faces, which are analysed every metre as to the marble quality. A separate data folder was created for each quarry with a separate database for the topographical/vector data and one for the drill-hole/section data. An effort was made to maintain a systematic naming scheme for all files of databases and models created during modelling and estimation. Topographical data was provided in AutoCAD™ (DWG, DXF) file format and imported to Maptek Vulcan Quarry Modeller software and stored in appropriate layers. Drill-hole data was provided in Microsoft Excel™ file format and imported to the specialized sample databases in Maptek Vulcan Quarry Modeller. In the following paragraphs, we discuss briefly the data provided for each quarry.

Topographical data

For the Platanotopos quarry, two layers were provided with the minor and major contours every 4 m and 20 m respectively. The exploitation limits were depicted on a separate layer as shown in Figure 4. The contours covered an area much larger than the quarry area and contained very good detail, suitable for reserve estimation. The current morphology of the quarry was also provided in two separate layers for crests and toes.

Drill-holes and quarry face sections

A total of 92 drill-holes and sections were provided for the Platanotopos quarry (47 sections and 45 drill-holes), giving a total of 1684 one-metre samples for use in reserve estimation. This data sufficiently covers the extent of the estimated final pit as show in Figure 5. The data was validated using the software for collar location and overlapping intervals.

Quarry volumetric model

The estimated volume of the final excavation was designed per bench (level) starting from the existing quarry morphology. The design of each of the 16 benches was modelled as a solid triangulation which was used in reserve estimation (Figure 6). These solids were visually checked and validated using triangulation topology checks (self-crossing, opening, inconsistencies) to ensure that they can be used for valid volumetric calculations.

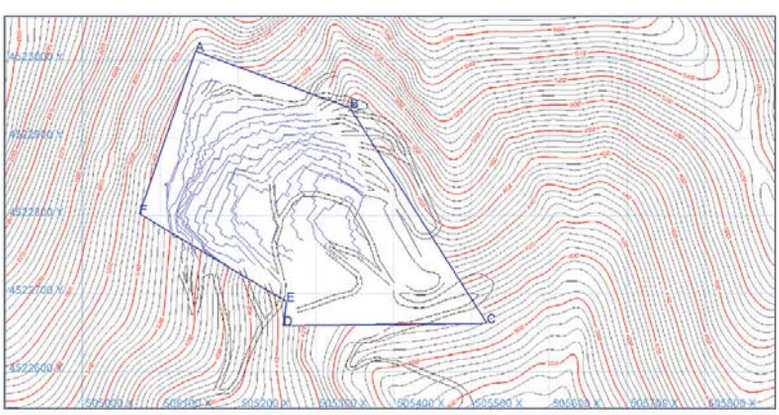

Figure 4—Original topography contours, current pit, and exploitation limits of the Platanotopos quarry

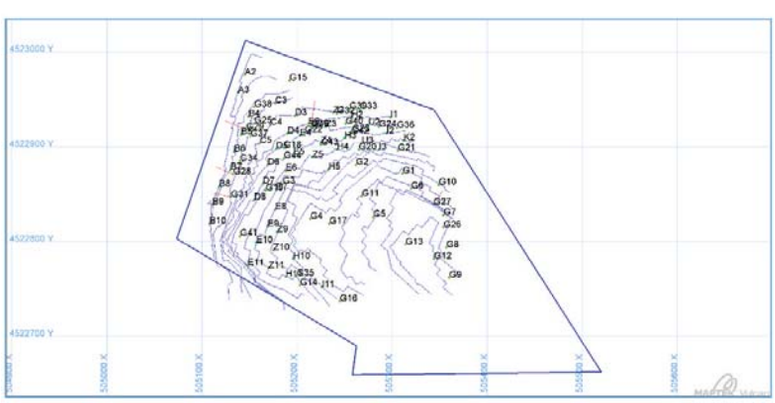

Figure 5 – Plan view of drill-hole and face section locations

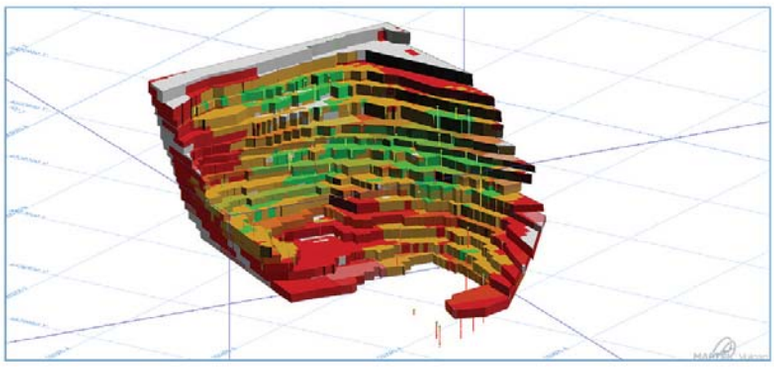

Figure 6—Solid triangulation models of the final excavation benches of the Platanotopos quarry coloured by reserves classification (green = Proved Reserves, orange = Probable Reserves, red = In-pit Inferred Resources)

Methodology

Sample database processing

The drill-hole and section sample database was configured with extra fields to allow the interpolation of arithmetic values in space. Specifically, fields were added which represent the different marble qualities based on original colour, texture, fracture, and tectonism fields. These fields take only two values, 0 or 1, based on whether the specific sample belongs to or does not belong to the particular quality category, which is based on criteria that are specific for each quarry. As shown in Figure 7, at the Platanotopos quarry, if a sample has lithology value LITHO = 'SPIDER' and spider type SPTYP = 1 and fractures BACKRO = 1 then it belongs to quality 1. This logic leaves out of the definition of initial quality due to the large-scale tectonism (represented by a solidity field called SYNOXH), which affect the final quality after it is estimated separately, with its own class fields. Thus different tectonism categories are defined for evaluation as for the different initial quality classes (1, 2, *etc.*). The reason for handling tectonism separately is the different orientations of large-scale tectonism, which requires a different search ellipsoid orientation (see Table VII). It is combined with initial qualities to derive the final ones with downgrading wherever necessary based on the estimated value of this field.

In other words, if the original field SYNOXH (solidity) has a value of 1, then the indicator field SN1_PR receives the value of 1; if it has a value of 2, then indicator field SN2_PR receives the value of 1 and so on up to SN5_PR. Only one indicator field can have the value of 1 in any case, while the others would be 0. The initial qualities are downgraded based on the SN*x*_PR fields. For example, if the initial quality is A1 and SN1_PR is 1 then the final quality is again A1 – no downgrading occurs. If the initial quality is A1 and SN3_PR is 1 then the final quality is AB – downgrading to two qualities lower.

After calculation of initial quality class fields and tectonism categories, a second procedure is carried out on the database by which the location of each sample (XYZ coordinates at the centre of each sample) is calculated and a weighting factor is assigned to the samples. This factor takes the value of 1 if the sample is from a section on the face of the quarry, and 0.5 if the sample comes from a drill-hole. Essentially, more weight is given to face sections as quality assessment is performed on a surface larger than the drill core and therefore better approaches the actual quality of the marble in that specific location. These weighting factors are used to further assess samples during interpolation.

Quality estimation

Quality class field values were interpolated using the inverse distance squared method as implemented by Maptek Vulcan Quarry Modeller software on the basis of a block model. The estimated volume is divided into blocks of the same size. For Platanotopos quarry, a block model with rotation around the Z axis was constructed that covered the entire quarry volume and current sampling. The model specifications are given in Table VI. Block dimensions were configured based on the marble volumes that are extracted separately at the Platanotopos quarry (slab dimensions). In each block, the percentage of each marble quality was estimated using the method analysed earlier using neighbouring samples. These samples are selected around each block using search ellipsoids that are oriented according to the geological features of the particular deposit. Ellipsoid parameters are given in Table VII.

Condition	Field	Equation
LITHO == "SPIDER" AND SPTYP == 1 AND BACKRO == 1	A1_PR	1
LITHO == "SPIDER" AND ((SPTYP + BACKRO) == 3) AND A1_PR == 0	A2_PR	1
LITHO == "SPIDER" AND SPTYP == 2 AND BACKRO == 2 AND (A1_PR + A2_PR == 0)	AB_PR	1
LITHO == "SPIDER" AND (SPTYP == 3 OR SPTYP == 4) AND BACKRO == 1 AND (A1_PR + A2_PR + AB_PR == 0)	B_PR	1
LITHO == "SPIDER" AND BACKRO < 4 AND SPTYP < 5 AND (A1_PR + A2_PR + AB_PR + B_PR == 0)	BB_PR	1
	W_PR	1 - A1_PR - A2_PR - AB_PR - B_PR - BB_PR

Figure 7—Quality class fields calculation based on original colour, texture, and fracture fields for Platanotopos marble

Table VI

Block model specifications of the Platanotopos quarry

Origin	X	505 460
	Y	4 522 340
	Z	290.5
Model dimensions	X	582 m
	Y	728 m
	Z	350 m
Block dimensions	X	6 m
	Y	2.8 m
	Z	7 m
Orientation	X-axis azimuth	28[c]
	X-axis rotation around Y-axis	0°
	Y-axis rotation around X-axis	0°
Block count		1 261 000

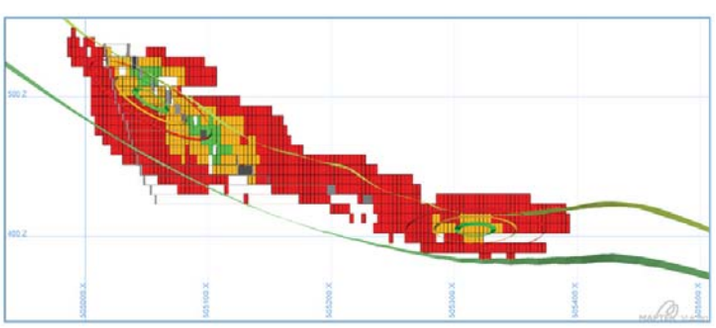

Figure 8—Cross-section through block model and resource classification ellipsoids following the folding of the deposit in the Platanotopos quarry (smaller to larger – Measured, Indicated, Inferred)

Table VII

Plantanotopos quarry estimation parameters

	Measured Resources	Indicated Resources	Inferred Resources	SYNOXH parameter
Major axis (m)	15	30	50	50
Semi-major axis (m)	15	30	50	50
Minor axis (m)	5	10	15	10
Azimuth	Variable	Variable	Variable	330
Plunge	Variable	Variable	Variable	0
Dip	Variable	Variable	Variable	70
Minimum number of samples	8	8	4	4
Maximum number of samples	20	20	20	20
Maximum samples per drill-hole	4	4	4	4
Blocks estimated	1 342	9 754	26 259	37 355

Table VIII

Reserves estimation results for the Platanotopos quarry

		Proved Reserves (m^3)			Probable Reserves (m^3)			Inferred In-Pit Resources (m^3)				
Bench	**Elevation**	**A**	**AB**	**B**	**A**	**AB**	**B**	**A**	**AB**	**B**	**Waste**	**Total**
P11	423	296	227	242	2 753	8 229	14 236	4 443	18 843	27 146	130 896	207 312
P10	430	140	128	337	3 942	7 863	12 088	7 094	19 414	41 562	92 659	185 228
P09	437	43	68	51	3 402	11 166	16 313	5 460	21 649	39 272	68 859	166 283
P08	444	28	156	708	2 078	13 171	25 174	4 088	16 381	34 392	59 047	155 222
P07	451	204	1 993	4 101	2 590	12 393	36 991	4 506	11 370	32 786	59 560	166 494
P06	459	336	1 548	4 253	2 444	7 987	24 850	2 485	5 618	12 518	31 392	93 432
P05	464	600	1 718	5 871	2 405	7 263	25 625	2 194	5 335	12 740	26 246	89 998
P04	469	722	2 351	9 020	2 116	7 906	30 162	2 530	6 826	18 035	30 793	110 460
P03	476	771	2 019	8 445	1 059	5 642	28 002	1 554	7 095	20 281	26 147	101 015
P02	483	398	1 031	4 824	465	2 732	18 544	573	5 367	16 006	18 327	68 267
P01	488	227	644	5 839	443	2 927	22 082	277	5 568	23 672	25 995	87 676
P00	495	1	826	5 230	358	2 691	28 704	177	5 356	29 298	38 795	111 435
P-01	505	165	818	3 063	343	2 376	20 618	104	3 624	18 147	22 949	72 207
P-02	513	118	253	2 536	298	2 012	11 791	134	2 634	17 007	14 016	50 801
P-03	520	17	19	192	198	1 022	14 530	82	1 034	10 987	20 008	48 090
P-04	529				-	22	1 240	89	139	8 449	18 125	28 063
Total		**4 068**	**13 801**	**54 713**	**24 894**	**95 402**	**330 951**	**35 790**	**136 251**	**362 299**	**683 814**	**1 741 983**

Block estimation in Platanotopos quarry was different to that for the other quarries as the ellipsoids had a different orientation in each block due to the folding of the deposit. Thus, a special function of the software was used before estimation that calculates the appropriate ellipsoid orientation for each block, taking in to account reference surfaces that define folding (Figure 8).

In the case of Iktinos Hellas SA quarries, the modifying factors for converting marble Resources to Reserves include the limitation of Resources inside a technically feasible excavation as designed by the company's personnel (mining and legal factors), inside the exploitation license limits (legal, environmental, and governmental factors). Classification based on the three categories of Mineral Resources was performed during three stages of block estimation, using ellipsoids of different dimensions and different sample count requirements (Table VI).

Results and conclusions

Reserve estimates

Table VIII gives the results of the reserve estimation. For each reserve category, three generalized qualities are reported. Generalizing of qualities was considered necessary as the limited sampling does not allow for a more detailed analysis of reserves to the original A1, A2, AB, B, and BB quality categories produced by the particular quarry. Therefore, reported quality A corresponds to quantities A1 and A2, AB is reported on its own, while B quality contains both B and BB. Reported waste quantities are the remaining bench volume, which cannot be estimated using the available sampling and the limitations set by the reserve categories with reference ellipsoid dimensions and minimum sample count. As a result, a considerable part of the waste and the Inferred Resources can potentially be upgraded in the future with additional drilling, which will provide a clearer and more detailed picture in areas where there are currently no samples.

Conclusions and future work

A Resource and Reserve estimation procedure applied at the Platanotopos marble quarry of Iktinos Hellas SA was performed using specialized software. Original sample quality values were converted to indicator values to allow interpolation to a block model using inverse distance weighting. This procedure provides Iktinos Hellas SA and potentially other marble quarrying companies with a method of producing reliable results according to international standards of Resources/Reserves reporting.

Future work will include integration of historical production data with the quality estimation process and implementation of an appropriate production quality control system that will produce the necessary data to improve the current quality models and reserve classification. As is evident in Figure 6, there is room to improve the Resource and Reserve classification of exposed marble – most of the exposed quarry face blocks are not classified as Proved. Standardization of quality assignment to drill core samples and production marble slabs is also an area where significant improvement is required.

References

Abdollahisharif, J., Bakhtavar, E., Alipour, A., and Mokhtarian, M. 2012. Geological modeling and short-term production planning of dimension stone quarries based on market demand. *Journal of the Geological Society of India*, vol. 80, September 2012. pp. 420–428.

Careddu, N., Siotto, G., and Tuveri, A. 2010. Evolution of a marble quarry: from open cast to underground exploitation. *Proceedings of Global Stone Congress 2010*, Alicante, Spain, 2–5 March 2010.

Forlani, G. and Pinto, L. 2000. Monitoring marble extraction in open cast quarries. *International Archives of Photogrammetry and Remote Sensing*, vol. XXXIII, part B4. pp. 283-289. *Proceedings of the XIX ISPRS Congress*, Amsterdam, The Netherlands, 16-23 July 2000. *Technical Commission IV: Mapping and Geographic Information Systems.* Fritsch, D. and Molenaar, M. (eds). http://www.isprs.org/proceedings/XXXIII/congress/part4/283_XXXIII-part4.pdf

Kapageridis, I. 2015. Iktinos Hellas SA quarries – marble reserves estimation. Technical report, September 2015. Maptek Pty Ltd. ◆

Digitalization in Mining Conference 2018

'Mining business make-over –Exploiting the digital revolution'

>> 6–7 June 2018

>> Johanneburg, South Africa

Call for papers/presentations

>> Submission of abstracts	28 February 2018
>> Submission of papers/presentations	9 April 2018

Whatever terminology you wish to use, it is obvious is that the world of work is changing rapidly.

The Mining Industry, along the Mining Value Chain, has to be a part of this in order to remain competitive, and to reach its ambition of Zero Harm.

Mining businesses in Africa need to join this journey, to stay alive, or be left behind. This event is a showcase and learning experience for everyone people associated with the Mining Industry, to learn about Global Best Practices, to network with global leaders in mining and other businesses, and to do so in an exciting and interactive format that we have never used before.

Be prepared to be BLOWN AWAY and to come away excited, informed and modernized!

SAIMM
THE SOUTHERN AFRICAN INSTITUTE OF MINING AND METALLURGY

Contact: Conference Co-ordinator, Gugu Charlie · Tel: +27 11 834-1273/7
Fax: +27 11 833-8156 or +27 11 838-5923 · E-mail: gugu@saimm.co.za · Website: http://www.saimm.co.za

Conference Announcement

http://dx.doi.org/10.17159/2411-9717/2018/v118n1a6

Governing risk elements through open pit slope optimization

by M. Golestanifar*, K. Ahangari*, K. Goshtasbi†, A. Akbari Dehkharghani‡, and P. Terbrugge§

Synopsis

With the increasing competition in global mineral markets, designers are attempting to drive down overall mining costs. The demands for steeper pit slopes have triggered developments in the field of modern and comprehensive slope design. Risk-based optimization techniques are one of the most challenging state-of-the-art solutions for enhancing conventional procedures. Recognizing risk aspects has a fundamental role in updating the methods. Considering geotechnical and mine planning issues, this study describes the consequences of varying slope angles on final pit walls. Twenty-three risk elements are introduced and discussed in four groups: economic, technical, strategic, and regulatory compliance. Related examples are given on the state of the elements, and possible ways to achieve them from overall slope optimization studies of the Sungun copper mine in Iran. The circumstances indicate that decisions on optimized slopes do not relate only to geotechnical studies, but that relevant consequences depend on the four groups. Evaluation of the elements can promote slope optimization based on the concepts of risk.

Keywords

pit slope design, risk evaluation, slope stability, mine planning, Sungun copper mine.

Introduction

Optimum slope design plays a significant role in the economics and safety of open pit mines, with one important aspect being the selection of appropriate overall slope angles. The impact of slope steepening will vary depending on the mine but, for example, it has been shown that an increase in slope angle of 1° in a 50° wall 500 m high results in a reduction of approximately 9000 t of stripping per metre of face length (Stacey, 2009). One of the main differences in slope design for open pit mines in comparison with civil engineering projects such as road cuts and excavations is that the design does not completely depend on geotechnical factors. Limitations such as the requirement for production and economics of the operation will affect the plan in each mining period. These differences cause conflicts in concepts, goals, and required techniques for conventional slope design derived from civil and geotechnical engineering, with the variations in design factor of safety (FoS) for civil engineering applications being quite different from those for open pit mines, as shown in Figure 1.

Similarly, there are complicating criteria for probability of failure (PoF) in probabilistic design methods, which vary in the range from 0.003 to 0.3 (Wesseloo and Read, 2009). In addition to the uncertain nature of materials in slopes, different governing conditions around mining slopes are the main causes of variability.

In general, consequences of failure drive the evaluation of overall slope design, with the importance of equipment, personnel in the high-risk areas, related structures, loss of ore and production having a direct effect on the risk evaluation. Therefore, in order to achieve optimum slope angles, a robust system using multidimensional risk concepts is required. By considering the governing factors, trade-off models such as cost-benefit analyses are developed to assess the shortcomings of FoS and PoF analyses (SRK Consulting, 2006; Tapia *et al.*, 2007). Furthermore, risk models can assist stakeholders in making the important decisions required for optimum slope design.

The probability of slope failure, P, and its consequences, C, are defined using risk assessment methods. Then, by comparing the calculated risk for various consequences with threshold limits, decisions are made on the desirability of design slope angles (Contreras, Le Sueur, and Maran, 2006). Since the steepest possible slopes are required, decisions are taken in the ALARP (as low as reasonably practical) zone. If the values of calculated risk fall above the threshold limit, various risk management decisions are required prior to

* *Department of Mining Engineering, Science and Research Branch, Islamic Azad University, Tehran, Iran.*

† *Faculty of Mining Engineering, Tarbiat Modares University, Tehran, Iran.*

‡ *Department of Mining Engineering, Islamic Azad University, Central Tehran Branch, Tehran, Iran.*

§ *SRK Consulting, South Africa.*

 ISSN 2225-6253. Paper received Oct. 2012; revised paper received Jun. 2017.

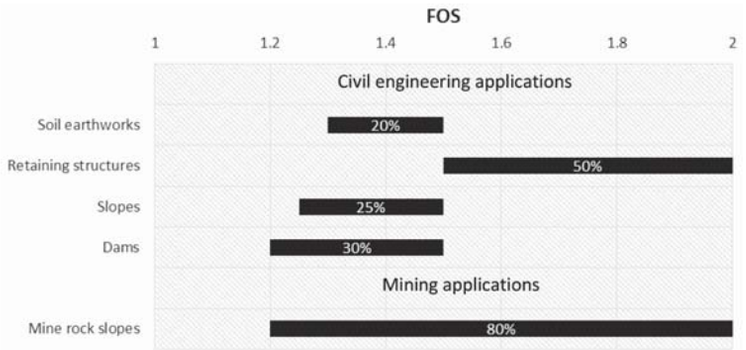

Figure 1—Range of the FoS for various applications of slope (Priest and Brown, 1983)

the slope designs being implemented. A flow chart of the risk evaluation method for slope design of open pits is included as Figure 2.

The objectivity of a risk assessment method is based on its recognized risk aspects, and in practice, risk elements are derived from reviewing events in a similar system and/or failure analysis, using fault trees or influence diagrams, in conceptual models. Since failure analyses require knowledge of real-world system responses, gathering data on global events in pit slope instability is a vital step for anticipating various elements in the multi-factor risk model. Unfortunately, comprehensive published reporting of the consequences of pit slope failures is limited. Current reports do include specific concerns on elements such as fatalities and injuries to personnel, but seldom divulge appropriate information on other consequences of failure, including the economic consequences. The current research is dedicated to defining the categorized effective risk elements in optimization of pit slope through several practical cases from the Sungun copper mine, Iran.

A literature review on risk analysis procedures and embedded risk elements is included in the next section, followed by an overview of the Sungun mine as a case study. New risk elements are classified into economic, technical, strategic, and regulatory categories and discussed in conjunction with related examples for the Sungun mine.

Literature review

Contreras, Le Sueur, and Maran (2006) used a bow-tie diagram for evaluating the variability in slope design parameters at the Cerrejon coal mine, Columbia, with the probability of slope failure under normal conditions being assessed. By considering specific slope configurations, variability in parameters introduced and the PoF of the slopes calculated. The risk was calculated for each slope scenario by determining the various consequences of failure. Finally, a decision on appropriate slope angles was made by comparing the risk values with the defined thresholds.

Ideally, the optimum overall angle, followed by the inter-ramp angle, should be selected by comparing the benefits gained (less stripping, more ore) with the potential costs (failure cleanup, downtime, ore losses, equipment damage, *etc.*) by steepening the slope, and followed by determining the angle providing the optimum economic slope (Ryan and Pryor, 2000). This approach is generally referred to as a cost-benefit analysis (Call and Kim, 1978), and has been used successfully at several large porphyry copper mines to assist the mine planners in maximizing economic recoveries (Ryan and Pryor, 2000). Two general cost-benefit analyses have been used over the years: a long form and a short form, with the short form being used more frequently. The long form is a detailed process requiring significant work by the mine planners prior to the stability modelling process. The short form analysis addresses only the final wall and therefore requires much less work (Ryan and Pryor, 2000).

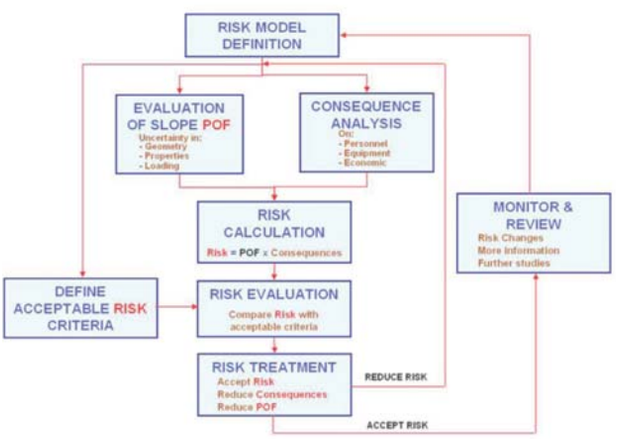

Figure 2—Slope design flow chart based on failure risk (Contreras, Le Sueur, and Maran. 2006)

Generally, using cost-benefit methods in open pit mine design requires a large amount of data and calculations with accurate economic information, defined ramp locations, open pit NPVs, economic value of the last blocks on each mining level, unit cost of cleanup, cost of lost production, and cost of backfilling for ramp re-establishment. Moreover, there are a number of possible costs for specific cases such as the requirements for slope drainage, repair cost of installations, cost of railroad track recovery, repair cost of in-pit crushers and conveyor belts, and the requirements for access roads for underground structures (Dinis da Gama, 1994).

Appropriate numerical forecasting of the consequences of failure will be more complicated when various alternatives are available for the remediation of failures.

Contreras, Le Sueur, and Maran (2006) and Terbrugge *et al.* (2006) cover the major consequences of slope failure in a bow-tie diagram, including injury to personnel, damage to

equipment, economic impact on production, *force majeure* (a major economic impact), industrial action, and public relations, such as stakeholder resistance and environmental impact. They also consider that three of the six consequences are economic-related, although on different scales regarding the acceptable risk that would apply to each case.

In addition, Terbrugge *et al.* (2006) suggested more items to define economic consequence, being cleanup cost, slope remediation, haul road repair, equipment re-deployment, loss of ore, damage to equipment and infrastructure, cost associated with fatalities and injuries, and disruption of production.

Stacey (2009) categorized the main considerations in slope design of open pit mines into three groups:

- Safety/social factors, including loss of lives or injury, loss of worker's income, loss of workers' confidence, and loss of corporate credibility, both externally and among shareholders
- Economic factors, including disruption of the operations, loss of ore, loss of equipment, increased stripping, cost of cleanup, and loss of market share
- Environmental/regulatory factors, including environmental impacts, increased regulation, and closure considerations.

Sungun mine case study

A case study of the Sungun mine in the northwest of Iran is used in order to illustrate the various risk elements that exist. The Sungun copper mine, containing more than 388 Mt of copper ore with the average grade of 0.63%, is one of the deepest open pit mines in Iran, with the final pit planned to a depth of approximately 700 m (Abbaszadeh *et al.*, 2011). The location of the mine is shown in Figure 3.

As details on the risk assessment study for the mine comprise a large database, this paper considers only the RS02 section of the southwestern wall. In this section the maximum height of the planned wall is 615 m with an overall slope angle of 29° (32° for a drained condition), an inter-ramp slope angle of 37° (42° for a drained condition), and bench slope angles (BSAs) of 65°. The width of the catch berms is 38 m (30 m for drained condition), and the width of the geotechnical berm is 50 m (SRK Consulting, 2008). The geotechnical section of the RS02 section is presented in Figure 3.

Risk inventory

In order to assess the overall risk, 23 risk elements for the Sungun case study have been recognized. The elements are classified into four groups: economic (*E*), technical (*T*), strategic (*S*), and regulatory (*R*). Table I summarizes the risk elements in these groups and the source of each element. Despite the previous studies considering only failure consequences, overall slope variations have been investigated from a design and mine planning viewpoint.

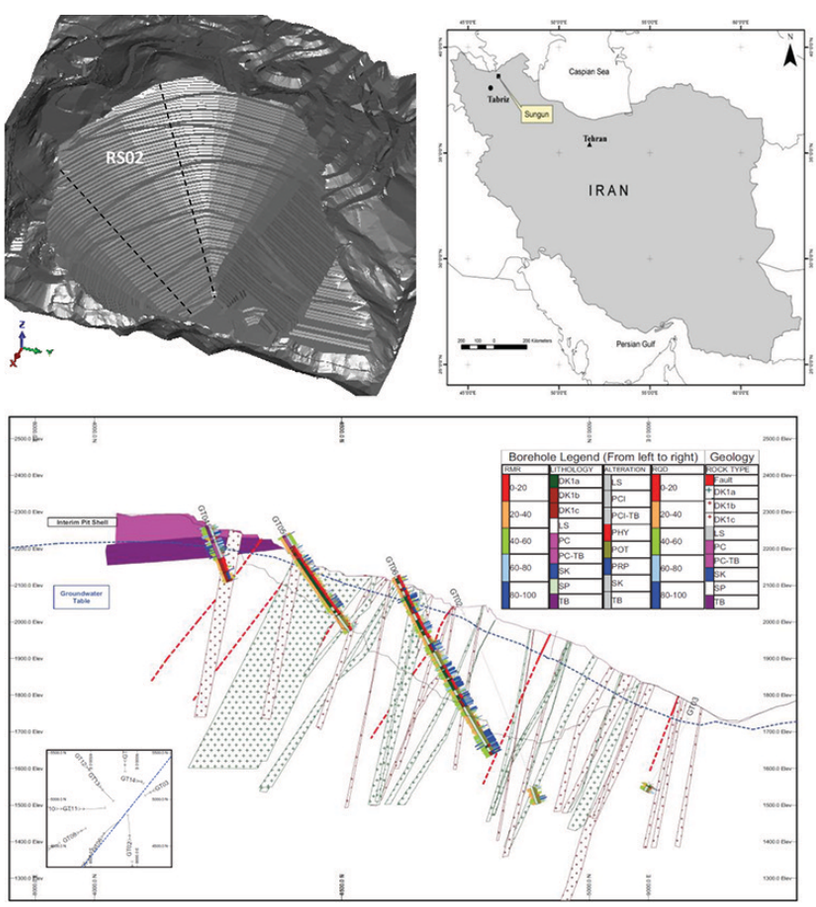

Figure 3—Location of the Sungun mine and details of the RS02 wall

Table I

Developed risk elements for an overall slope study in open pit mines

Category	Element	Source	Definition
Economic (*E*)	E_1	Design	Variation in pre-stripping tonnage
	E_2	Failure	Loss of or damage to equipment
	E_3	Failure	Ore loss due to dilution
	E_4	Failure	Requirement to re-establish drainage systems
	E_5	Failure	Backfill and ramp re-construction
	E_6	Failure	Clean-up volume or preparation for mine closure
	E_7	Design	Variations in stripping ratio
	E_8	Failure	Loss of profit due to production delays
	E_9	Failure	The cost of cutback and/or support of the failed slope
Technical (*T*)	T_1	Design	Narrow ramps
	T_2	Failure	Incompatibility of mine fleet for clean-up
	T_3	Design	Increase in problems due to mining below the water table
	T_4	Failure	Effect of ramp loss
Strategic (*S*)	S_1	Failure	Loss of market share
	S_2	Failure	Contractual penalties
	S_3	Failure	Stakeholder confidence
	S_4	Failure	Political response
Regulatory (security – social – environmental) (*R*)	R_1	Failure	Fatalities within the workforce
	R_2	Failure	Injuries within the workforce
	R_3	Failure	Workforce confidence
	R_4	Failure	Increase of legislation
	R_5	Failure	Employment opportunity
	R_6	Design and Failure	Environmental impact (mine waste and failed material)

Economic risks (E)

Economic consequences could be generally defined as those that have a direct effect on the economics of the mine. These are categorized as follows.

Variation in pre-stripping tonnage (E_1)

The overall slope angle of a pit has an inverse relationship with the stripping ratio (W/O), with the amount of stripping divided into overburden (pre-stripping) and mining waste. Pre-stripping has a direct relationship with capital costs, and is investigated in the study as a separate element.

Based on the Sungun block model, with overburden of 150 m from the 2375 m level to the 2225 m level, by increasing the overall slope angle of the RS02 section from 29°, the design case, to 37°, pre-strip tonnage decreases, while the total waste and ore tonnages increase. However, the stripping ratio decreases from 1.86 to 1.75, as shown in Figure 4.

As a general rule, an increase in overall slope angle (OSA) leads to lower stripping ratios. However, this does not always result in a reduction in the waste tonnage. Indeed, it permits the mine planner in certain cases to expand the pit limits or the total pit size with similar waste to ore ratios. In such a situation the total mineable volume increases, which leads to more ore and more waste tonnage, while the stripping ratio decreases or at least remains the same. A valid case is the porphyry deposit at Sungun, where the orebody extends to depth. The phenomenon is based on an improvement in the financials of the pit by steepening the OSA, where possible, which leads to the extraction of 'sterilized ore' not included in the original life of mine plans.

Loss of, or damage to, equipment (E_2)

The consequence of a failure for the mine fleet can be related to the magnitude of the failure, reliability of the monitoring system, and the pit evacuation procedures. An assessment of the proportion of the total investment in fleet which is divided between each section of the mine is required to evaluate this consequence. Techniques such as O'Hara's cost estimating model (O'Hara, 2008), and detailed cost calculations (Hustrulid and Kuchta, 1995) have been developed to evaluate the fleet capital investment. Since a complete and constant inventory of the mine fleet is not found in the case study, O'Hara's model is implemented to forecast approximate capital costs, first for the entire mine, and then specifically for the RS02 section. Since a fifth of the

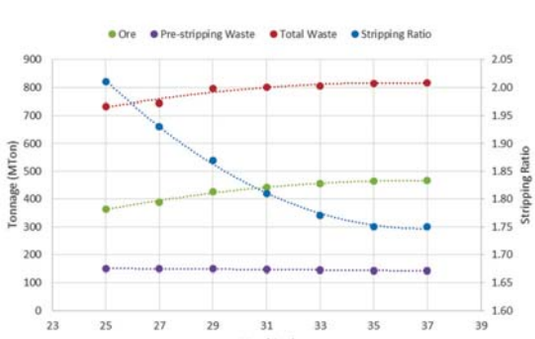

Figure 4—Variations of pre-stripping, strip ratio, and overall slope angle in the RS02 sector

rock tonnage is located in RS02 section, it is expected that the same proportion of personnel and equipment will be concentrated in RS02. Using an updated O'Hara model (Akbari and Osanloo, 2005), the capital cost for the RS02 section is estimated at US$44 million, and the workforce is estimated at 42 persons.

The likelihood of losing equipment is dependent on the effectiveness of the monitoring system and the evacuation procedures, which are obtained from an event tree as shown in Figure 5.

Ore loss due to dilution (E_3)

The dilution could be more than the permitted limit, depending on the failure mechanism, and generally, because of the conditions of the failed mass, it is not possible to separate ore from waste.

Requirement to re-establish drainage systems (E_4)

If a drainage system installed in the pit is at risk of being lost or damaged, this should be considered in the risk model. The damage to the drainage system is dependent on the volume and shape of the failure. If deep drainage systems such as long horizontal drains are used, the shape, and especially the depth, of failure are important. Damage resulting from movement of the failed zone is low when considering an ex-pit dewatering system. Since the water table at Sungun mine is in the upper levels of the pit (1850 m level), the ex-pit dewatering system should be more robust. Therefore loss of the dewatering system is excluded from the analysis.

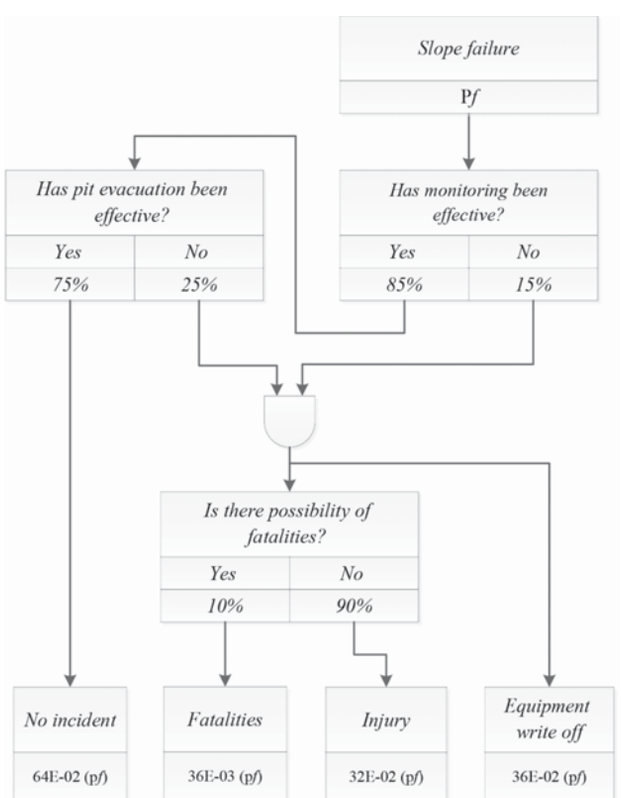

Figure 5—Consequences of failure for personnel and equipment (event tree method)

Backfill and ramp reconstruction (E_5)

If the slope failure includes main ramps, generally there are two solutions for restoring them, which may be applied individually or in combination. The first solution would be flattening the upper parts of the pit if possible and reconstructing the ramps. However, cutting back could exceed the optimum pit limit, although the stability of new ramps constructed in an undisturbed rock mass constitutes a major advantage. The second method includes backfilling and creating new ramps. This is mostly used when the volume of the required materials is low and requirements for stabilization are economically available. The economic risk of reconstructing ramps can be forecast by assessing the costs of the remedial measures.

Cleanup volume or preparation for mine closure (E_6)

Depending on the age of the mine, the severity of the failure, and other conditions, when a failure occurs the mine is faced with two alternatives. Firstly, cleanup in order to continue the mining operations, and secondly, leaving the remaining ore *in situ* and moving to the closure plan. Golestanifar (2011) developed a new concept of *slope transmission* level to solve this problem: for a given overall slope, when the mine reaches a specified level, failure could lead to mine closure. Based on decisions made after failure, item E_6 could be estimated according to cleanup costs and compared to mine closure costs.

Variations in stripping ratio (E_7)

Assuming that the failure can be mined at a lower level in the pit, a cutback may be required to stabilize the slope, which will have an impact on the stripping ratio. By steepening the overall slope, the total mineable tonnage, both ore and waste, will be increased. However, at first glance, the increase in waste could signify reduced profits, due to the increased rate of exploitation of mineable ore and decreased stripping ratio (Figure 4). Thus for a unit of ore, a lower waste tonnage needs to be mined. It should be noted that this relationship is true when the ore deposit extends deeper than the pit.

Loss of profit due to production delays (E_8)

If a failure occurs in a critical area, production will probably be delayed due to the time required for cleanup, with the mine life being prolonged artificially. The duration of cleanup tasks depends on volumes and available equipment, and therefore, the current present value of profit, P_p, could be reduced by using a lump sum value, as in Equation [1] (Hustrulid and Kuchta, 1995).

$$P_p = P_F\left[\frac{1}{(1+i)^n}\right] \quad [1]$$

where P_F is the future profit of postponed production, i is the annual discount rate, and n is the delay in years. Therefore, a decrease in profit value, *Loss*, could be estimated by multiplying the loss factor, L (Equation [2])by P_F as in Equation [3].

$$L = 1-\left(\frac{1}{(1+i)^n}\right) \quad [2]$$

$$Loss = L \times P_F \quad [3]$$

This forecasting is valid when no stockpile exists in the mine, although issues such as blending might be raised.

Cost of cutback and/or support of the failed slope (E_9)

Following a failure, decisions on whether to cut back the slope, or consider the potential for supporting the failed slope, must be taken. This will largely be dictated by logistics, equipment availability, and costing. The geometry of the failure, volume of the failed mass, and *in situ* ground conditions would also be included in the evaluation.

Technical risks (T)

Narrow ramps (T_1)

By steepening the OSA, the horizontal projection of the pit decreases, resulting in a reduction of berm and ramp widths, steeper BSAs, or a combination thereof, each having its own consequences. The reduction in berm widths intensifies rockfall problems, and will also increase instability problems on a bench and inter-ramp scale. Decrease in the ramp widths will cause safety problems for trucks on the ramps, which can lead to a requirement for smaller units (Bozorgebrahimi, Hall, and Morin, 2005). Finally, an increase in the BSA could increase safety concerns for the operation.

The relationship between overall slope elements, as shown in Figure 6, is given in Equations [4] and [5] (Bozorgebrahimi, Hall, and Morin, 2005).

$$Tan\alpha = \frac{H}{X} \quad [4]$$

$$X = \sum_{1}^{n_1} W_b + \sum_{1}^{n_2} W_R + \sum_{1}^{(n_1+n_2)} \frac{h_b}{Tan\beta} \quad [5]$$

where α is the overall slope angle, H is slope height, X the slope horizontal projection, W_b the berm width, W_R the ramp width, h_b the bench height, β the bench slope angle, and n_1 and n_2 the number of berms and ramps, respectively. With an increase in any one of the elements, problems in the others develop accumulatively.

In the Sungun case it is assumed that slope variation occurs in all three elements, with the portion of their projection. By increasing the overall slope angle, the width of the ramps is limited and smaller trucks should be used. This negative effect is a function of the maximum width of the trucks. A 30 m ramp width is suggested for the design sector at Sungun, assuming a 29° overall slope (recommended slope in design) and 25 m bench heights on the pit limit (double benching). Based on the evaluation, the sum of the ramp widths is 16% of the horizontal projection of the overall slope angle and accommodates the inclusion of six ramps in the profile with inter-ramp heights of 100 m. Thus, for decreasing and/or increasing the slope angle and its horizontal projection, the width of new ramps can be calculated. The allowable width for the largest trucks has been considered as being one quarter of the ramp width (Bozorgebrahimi, Hall, and Morin, 2005). The capacities and models of the haul trucks, mostly Komatsu, are shown in Figure 7, from which it can be seen that the steeper the overall slope angle, the narrower the ramp width in the design, and hence the requirement for smaller capacity trucks. However, with the requirement for increased production, this presents a conflict in terms of required production rate and economic slope angle.

Unsuitability of mine fleet for cleanup (T_2)

The projected failed mass will have different characteristics in comparison with initial *in situ* conditions, and may therefore require a different type of operation and equipment from the conventional, depending on the muckpile geometry, characteristics of the failed mass, and tonnage to be moved.

Problems due to mining below the water table (T_3)

Steeper overall slope angles can result in an increase in pit depth and the area of the lower levels, with the possible requirement for operating below the water table. The ensuing problems can include loss of access to the mining area due to flooding, increased use of explosives, increased explosive failures due to wet blast-holes, requirement for the use of special explosives, increased wear to equipment and tyres, inefficient loading and hauling, and unsafe working conditions (Morton and van Niekerk, 1993).

In order to evaluate the effect of 'wet' ground to be mined, cumulative tonnage variations below the water table have been considered in the study. With the average water level in the pit at the 1850 m level, the cumulative tonnage to be mined below this level for various slope angles is shown in Figure 8.

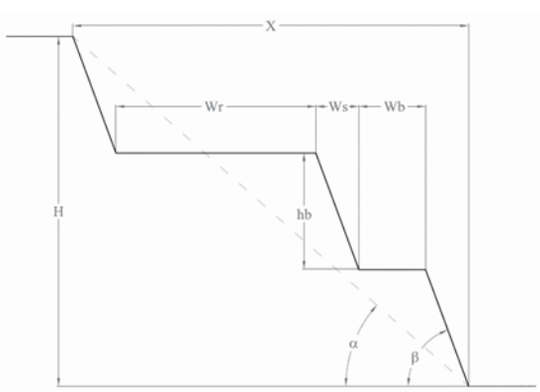

Figure 6—Components of the overall slope

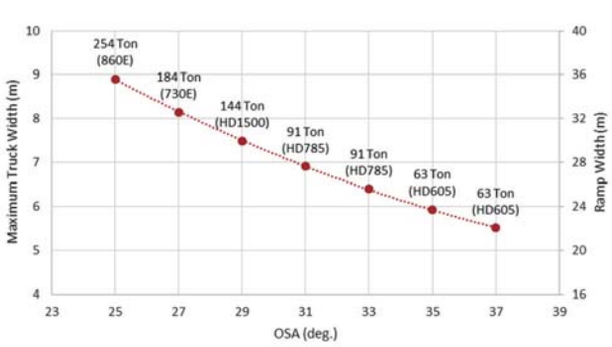

Figure 7—OSA of RS02, ramp width, truck capacity, and recommended model in Sungun

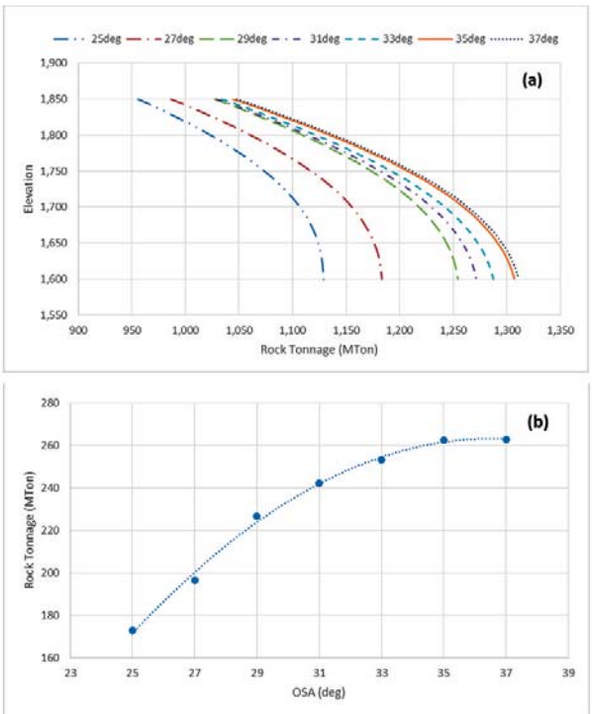

Figure 8—Wet tonnages for various slope alternatives in RS02 mining sector. (a) Cumulative rock tonnage per level, (b) total wet tonnage for varying slope angle

Effect of ramp loss (T4)

Different situations will occur in comparison with routine pit operations when the wall fails, for example the loss of a ramp. This can result in restricted access to the failed mass, as well as to operations not impacted by the wall failure, with the magnitude of the problem depending on the volume of the failure.

In the case study, with a failure in the RS02 domain, material handling will be possible from the northern and northwestern sectors of the pit (Figure 3), with the consequence of failure being relatively insignificant in this regard.

Strategic risks (S)

Loss of market share (S_1)

In the event of a failure resulting in an ore gap developing, the mine may be unable to fulfil contractual obligations. This can result in the cancellation of such contracts, with serious implications for the operation. Depending on the size of the failure and cleanup rate, the amount of production downtime can vary significantly.

The production rate at Sungun is 40 Mt/a, one-fifth of which is expected to be from RS02 according to the mineable ore resource in the section. Assuming that resumption of the operation interrupted by a failure in the section requires cleanup of at least half of the failure volume, the downtime is calculated for each case of the OSA provided that all of the dedicated workforce and equipment in RS02, *i.e.* one-fifth of the entire mine, were implemented. The effect of the OSA on downtime for cleanup is represented in Figure 9. Alternatively, when the cleanup operation is accelerated by implementing half of the available operational capacity in the pit, which might also be supplied by appointing an additional contractor, the downtime on production can be more than halved, as illustrated in Figure 9.

Contractual penalties (S_2)

Once the failure occurs, the inability to fulfil corporate obligations constitutes an essential risk. If re-establishment of normal operations is time-consuming, or deferred due to unexpected problems, then depending on the contract, the mine will be subject to various consequences, depending on the failure volume, including lost or damaged equipment, and the requirement for replacing sources such as stockpiles and reserves.

Stakeholder confidence (S_3)

Although slope failure is common in open pit mines, such events decrease the company's credibility both internally and among decision-makers, as well as external stakeholders. The magnitude of the consequences would be defined by not fulfilling contracts, implications of fatalities and the effect on the workforce, as well as the implications of lost equipment that would need to be replaced.

Political response (S_4)

The political response to large failures is a significant factor, and therefore consideration must be given to this factor in the long-term programme. Some of the factors that affect the political consequences are damage to other industrial sectors due to lost production, market disturbance, as well as domestic and international pressures in the event of fatalities.

Regulatory risks (R)

Injuries and fatalities among the workforce (R_1 and R_2)

According to Sullivan (2006), if pit slopes are covered by a reliable monitoring system and the slopes are managed by a competent geotechnical team, pit slope failure should not result in injuries or fatalities . Therefore, this issue is not normally considered in the final design, although the consequences of injuries and fatalities should be considered if the risk model is being used to justify monitoring systems.

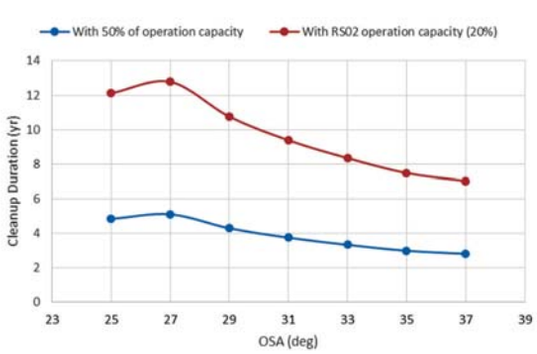

Figure 9—Downtime on production due to failure for different OSA in the RS02 domain in Sungun copper mine

Workforce confidence (R_3)

Unlike the economic benefits of well-managed steeper slopes, which only some of the project experts are aware of, the news of failures is widely broadcast,. In order to increase workforce confidence, it is important that the workforce is made aware of stability issues and convinced by management that monitoring and management of the slope is being carried out, and that sufficient warning will be available in the event of a failure developing.

Increased legislation (R_4)

A review of the history of legislation for open pit design shows that large-scale failures have resulted in more stingent legislation, and will in all likelihood continue to do so. Integrating this element in the analysis could benefit sustainable development in the optimization of pit slope design.

Employment opportunities (R_5)

When a mine is developed in an area, employment opportunities are created and workforce migration will occur. If the mine is closed and workers lose their jobs, adverse consequences such as social and even political disturbances can take place. It should be noted that private companies usually have less ability than governmental organizations to guarantee workforce income, and this should be considered in the risk analysis.

Environmental impact (mine waste and failed material) (R_6)

By steepening the pit slope, the volume of mineable rock (waste and ore) may be increased due to the economic viability of deeper ore, and this can lead to problems related to waste management of both dumps and tailings dams.

Impact matrix

Guidelines were provided in the previous section for making the 23 risk elements measurable. Since some of the elements are qualitative in nature, a qualitative assessment must be made in these cases. Finally all of the quantitative and qualitative performances should be assembled into an impact matrix, which would be processed by risk analysis techniques. Table II depicts the impact matrix containing the performance of the overall slope of section RS02 in the Sungun case study. In order to study the OSA, evaluations have been made on alternatives in the range of 31±6°.

Golestanifar (2011) developed a soft-computing method that processes both quantitative and qualitative measures to find an optimum OSA solution. This model has been successfully implemented in the Sungun case study. The formulation of the model, as well as the details of the Sungun case study, will be covered in future publications.

Table II

Impact matrix of RS02 section in Sungun case study (Golestanifar, 2011)

Category	Element	Unit	OSA alternatives (deg.)						
			25	27	29	31	33	35	37
Economic (*E*)	E_1	W/O	0.41	0.386	0.347	0.33	0.317	0.306	0.301
	E_2	million$	12.904	12.904	12.904	12.904	12.904	12.904	12.904
	E_3	kt	76.72	78.75	63.77	53.87	46.23	39.07	35.48
	E_4	-	VL	VL	VL	VL	VL	VL	VL
	E_5	-	H	H	H-M	M	M	M-L	L
	E_6	Mt	197	207	175	152	136	122	114
	E_7*	W/O	1.603	1.54	1.519	1.476	1.455	1.444	1.436
	E_8	see Eq. [3]	0.37	0.39	0.34	0.3	0.27	0.25	0.24
	E_9	-	VL	VL	L	M-L	H	VH-H	VH
Technical (*T*)	T_1	m	8.9	8.15	7.49	6.91	6.39	5.93	5.51
	T_2	-	H	H	M	M-L	M-L	L	L
	T_3	Mt	172.85	196.46	226.84	242.32	253.17	262.45	262.91
	T_4	-	M	M	M-L	M-L	M-L	L	L
Strategic (*S*)	S_1	year	4.8	5.1	4.3	3.8	3.3	3.0	2.8
	S_2	-	M	M	L	L	L-VL	L-VL	VL
	S_3	-	H	H	M	M	M-L	L	L
	S_4	-	H-M	M	M	L	L	L	VL
Regulatory (security – social – environmental) (*R*)	R_1	Person	42	42	42	42	42	42	42
	R_2	Person	42	42	42	42	42	42	42
	R_3	-	L	L	M	H-M	VH	VH	VH
	R_4	-	L	L	M	H-M	VH	VH	VH
	R_5	-	M-L	M-L	L	L	L	L-VL	L-VL
	R_6†	Mt	197	207	175	152	136	122	114
	R_6‡	Mt	733	745	796	800	806	815	816

VL: very low; L: low; M: medium; H: high; VH: very high
* Excluding pre-stripping waste, *i.e.* E_1.
† Cleanup residuals.
‡ Mining waste.

Conclusions

Currently, open pit slopes are designed based on geotechnical programmes that include extensive drilling and laboratory testing campaigns, but also calling on the designers' experience. With the competition in global ore markets, designers are attempting to drive down the overall mining costs in all sectors. It appears, however, that advances in pit slope design are largely confined to a conventional analysis approach, with interpretation of the slope designs resulting in conservative results guided by factor of safety or probability of failure results. The latest developments using risk models are, however, faced with practical limitations that make it difficult to define a robust system with clear and valid numerical results. One of the major difficulties in developing risk models for optimum pit slope design is a lack of definition of the risk elements to the required levels for input to an analysis. When risk elements are well defined, accurate analysis can be carried out with reliable input, with logical results representing optimum pit slope angles. The result will also identify critical elements which are required as further input to the study or treated by risk management efforts.

This study is concerned with investigating developed models and classification of risk elements, and detecting their ambiguities, deficiencies, and shortcomings in order to introduce a comprehensive classification of risk elements for pit slope optimization.

A wide range of slope parameters and circumferential conditions are to be considered in the multidimensional concept of risk optimization. The 23 elements included here have been classed into four groups – economic (E), technical (T), strategic (S), and regulatory (R). The economic group consists of elements that have direct effect on pit economics, while the elements in the other groups can have indirect economic outcomes. Although certain elements have a threshold and are controlled by local regulations, others can be traded off against each other.

Depending on the governing strategy in the mine, the elements can have a variable weighting. In developing countries, various objectives such as enhancing infrastructure, updating technology, welfare of local inhabitants, or increasing skills levels can be included in the motivations for opening a mine. In this case, the range of the elements could be wide, with different validities. The elements introduced in this study are appropriate for general conditions, with specific elements considered in certain circumstances.

References

Abbaszadeh, M., Shahriar, K., Sharifzadeh, M., and Heydari, M. 2011. Uncertainty and reliability analysis applied to slope stability - a case study from Sungun copper mine. *Geotechnical and Geological Engineering*, vol. 29, no. 4. pp. 581–596.

Akbari, A. and Osanloo, M. 2005. An updated and modified O'Hara cost estimating model based on world and Iran economic conditions. *APCOM 2005. Proceedings of the 32nd International Symposium on Computer Applications in the Minerals Industry Conference*, Tucson, Arizona, 30 March - 1 April 2005. CRC Press, Boca Raton, Florida. pp. 3–18.

Bozorgebrahimi, A., Hall, R.A., and Morin, M.A. 2005. Equipment size effects on open pit mining performance. *International Journal of Surface Mining, Reclamation and Environment*, vol. 19, no. 1. pp. 41–56.

Call. R.D. and Kim. Y.C. 1978. Composite probability of instability for optimizing pit slope design. *Proceedings of 19th US Symposium on Rock Mechanics*, Reno, Nevada, 1–3 May 1978. Kim, Y.S. (ed.). American Rock Mechanics Association, Alexandria, Virginia.

Contreras, L.F., Le Sueur, R., and Maran, J. 2006. A case study of risk evaluation at Cerrejon mine. *Proceedings of the International Symposium of Rock Slope Stability in Open Pit Mining and Civil Engineering*, Cape Town, South Africa, 3-6 April 2006. *Symposium Series* S44. Southern African Institute of Mining and Metallurgy, Johannesburg. pp. 181–210.

Dinis da Gama, C.D. 1994. Variability and uncertainty evaluations for rock slope design. *Proceedings of the 1st North American Rock Mechanics Symposium*, Austin, Texas. American Rock Mechanics Association, Alexandria, Virginia. pp. 547-555.

Golestanifar, M. 2011. Introducing a new model to pit slope optimization based on multiple risk attributes approach. MSc thesis, Tehran Science and Research Branch, Islamic Azad University, Tehran (in Persian).

Hustrulid, W. and Kuchta, M. 1995. *Open Pit Mine Planning and Design*, vol. I – Fundamentals. AA Balkema, Rotterdam.

Morton, K.L. and van Niekerk, F.A. 1993. A phased approach to mine dewatering. *Mine Water and the Environment*, vol. 12. pp. 27–33.

O'Hara, T.A. 1980. Quick guides to the evaluation of orebodies, *CIM Bulletin*, vol. 73. pp. 87–99.

Priest, S.D. and Brown, E.T. 1983. Probabilistic stability analysis of variable rock slopes. *Transactions of the Institution of Mining and Metallurgy Section A - Mining Technology*, vol. 92. pp. A1–12.

Ryan, T.M. and Pryor, P.R. 2000. Designing catch benches and inter ramp slopes. *Slope Stability in Surface Mining*. Hustrulid, W., McCarter, M.K., and van Zyl, D.J.A. (eds.). SME, Littleton, Colorado. pp. 27-38.

SRK Consulting. 2006. The stability of rock slopes in large open pit mines design manual. *Project no*. 2004-ha62. CSIRO, Melbourne.

SRK Consulting. 2008. Mining geotechnics and slope design studies for Sungun copper mine project. NICICO, Tehran.

Stacey, P.F. 2009. Fundamentals of slope design. *Guidelines for Open Pit Slope Design*. Read. J.R.L. and Stacey. P.F. (eds.). CSIRO Publishing, Melbourne. pp. 1-14.

Sullivan, T.D. 2006. Pit slope design and risk – a view of the current state of the art. *Proceedings of the International Symposium of Rock Slope Stability in Open Pit Mining and Civil Engineering*, Cape Town, South Africa, 3-6 April 2006. *Symposium Series* S44. Southern African Institute of Mining and Metallurgy, Johannesburg. pp. 51–80.

Tapia, A., Contreras, L.F., Jefferies, M.G., and Steffen, O.K.H. 2007. Risk evaluation of slope failure at Chuquicamata mine. *Proceedings of the International Symposium of Rock Slope Stability in Open Pit Mining and Civil Engineering*. Potvin, Y. (ed.). Australian Centre for Geomechanics, Perth. pp. 477–485.

Terbrugge, P.J., Wesseloo, J., Venter, J., and Steffen, O.K.H. 2006. A risk consequence approach to open pit slope design. *Journal of the South African Institute of Mining and Metallurgy*, vol. 106. pp. 503–511.

Wesseloo, J. and Read, J. 2009. Acceptance criteria. *Guidelines for Open Pit Slope Design*. Read, J.R.L., and Stacey, P.F. (eds.). CSIRO Publishing, Melbourne. pp. 221–235. ◆

SAIMM: Diamonds — Source to Use 2018 Conference

'Thriving in Changing Times'

11 June 2018 — Workshop: SAMREC/SAMVAL Reporting – Diamond Projects
12–13 June 2018 — Conference • 14 June 2018 — Technical Visits
Birchwood Conference Centre (Jet Park, Johannesburg)

BACKGROUND

Being the seventh conference in the series, the ***Diamonds – Source to Use*** conferences target the full spectrum of the diamond pipeline from exploration through to sales and marketing. The last conference in this series (***Diamonds – Still Sparkling***) was held in Botswana in 2016 and it is now returning to Johannesburg, where it was last held in 2013

Keynote Speakers

The State of the Diamond Market
E. Blom, *Blom Diamonds (Pty) Ltd*

Financing Diamond Projects
J. Campbell, *Botswana Diamonds PLC*

OBJECTIVE

The objective of the conference is to provide a forum for the dissemination of information relating to the latest tools and techniques applicable to all stages of the diamond industry; from exploration, through mine design, processing, to cutting, marketing and sales.

WHO SHOULD ATTEND

- Geologists
- Mineral (Diamond) Resource Managers
- Mining Engineers
- Process Engineers
- Consultants
- Suppliers
- Sales/marketing
- Diamantaires
- Mine Managers
- Mining Companies
- Students.

TOPICS

- Geology and exploration
- Mine expansion projects
- Mining, metallurgy and processing technology
- Rough diamond sales and marketing
- Cutting, polishing and retail
- Financial services and industry analysis
- Industry governance, beneficiation and legislation
- Mine-specific case-studies
- Value optimization.

Sponsors

De Beers Group of Companies
DEBTECH
GEO-EXPLORE STORE (PTY) LTD
Imexsar DMS Ferrosilicon
MSA THE MSA GROUP

SAIMM THE SOUTHERN AFRICAN INSTITUTE OF MINING AND METALLURGY

For further information contact:
Camielah Jardine • Head of Conferencing · SAIMM
P O Box 61127 • Marshalltown 2107
Tel: (011) 834-1273/7• Fax: (011) 833-8156 or (011) 838-5923
E-mail: camielah@saimm.co.za • Website: http://www.saimm.co.za

Conference Announcement

http://dx.doi.org/10.17159/2411-9717/2018/v118n1a7

Particle segregation associated with sub-sampling of flotation feed at a UG2 concentrator

by N. Naicker and V. Sibanda

Synopsis

A concentrator treating an Upper Group 2 (UG2) reef ore has been historically under-accounting in terms of 4T (platinum, palladium, rhodium, and gold) content. The 4T content declared after sampling the flotation feed (or mill product) has always been more than that accounted for when concentrates and tailings exiting the flotation plant are analysed. This suggests that the sample head grade of the concentrator feed is possibly overstated. A plant audit indicated no reason to believe that the built-up head grades were the likely contributor to the under-accounting trend. The debate on the source of under-accounting pointed towards possible non-representative and/or biased sampling occurring in the concentrator feed vezin-vezin sampling system.

This work investigates the possibility that the bias is due to particle segregation occurring in the intermediate hopper that stores the primary increment sample before sub-sampling.

Vezin credibility and chronological sub-sampling tests were done on the current sampling arrangement. A consistent bias was observed between the reject and official samples, with the official samples having finer particles and analysing higher in 4T grade than the reject samples, confirming the hypothesis of particle segregation in the intermediate hopper. An alternative hopper discharge nozzle was then designed and replicate tests performed. The results with the new nozzle showed much improvement in the bias using particle size as the analyte, indicating that particle segregation has been significantly reduced.

Keywords

sampling, vezin sampler, metal accounting, intermediate hopper, particle segregation, bias.

Introduction

The importance of sampling in the mining industry, whether in exploration, in mining, or in mineral processing, cannot be over-emphasized (Bartlett, 2005). Conventional wisdom suggests that when the rules for representative sampling are followed and the sampling equipment is in good order, and procedures used by the operators are well defined and followed, unbiased samples will be obtained. The measured parameter or analyte is considered to be biased if the mean of its distribution is not equal to the true value of the parameter. Thus the bias can be positive when the measured value is more than the true value or negative when the measured value is less than the true value. In sampling, there are two major areas where bias can arise, namely sampling and sample preparation. Sampling bias generally occur when increments coincide with cyclic events, where only a portion of the stream is being sampled, where cutter specifications are not adhered to, and when sample containers are overfilled (Kruger and Millar, 2002). Therefore the best defense against any sampling bias is the correct sampling protocol, correct mechanical design of the sampling rig, and adequate control and maintenance during its operation (Bartlett, 2005; Kruger and van Tonder, 2014).

An Anglo American Platinum concentrator plant treating Upper Group 2 (UG2) ore in South Africa has been historically under-accounting in terms of 4T (platinum, palladium, rhodium, and gold) content. The debate on the source of under-accounting pointed towards possible non-representative sampling and/or biased sampling in the concentrator feed sampling system. The feed grades were believed to be overstated, and when compared to the built-up head grade, resulted in the under-accounting trend. A plant audit indicated no reason to believe that the built-up head grades were the likely contributor to the under-accounting trend. The current practice at this plant is that crushed run-of-mine UG2 ore is milled in a semi-autogenous (SAG) mill and the mill product is classified by screening into undersize and oversize streams. The oversize is returned to the SAG mill for further grinding. The undersize is gravity-fed to a surge tank and then pumped to the primary rougher flotation circuit. Prior to being fed to the primary rougher flotation circuit, the material is sampled by an automatic vezin-vezin sampler. The position of the sampler in the production process is shown in Figure 1.

* *University of the Witwatersrand, South Africa.*

 ISSN 2225-6253. Paper received Apr. 2017; revised paper received June 2017.

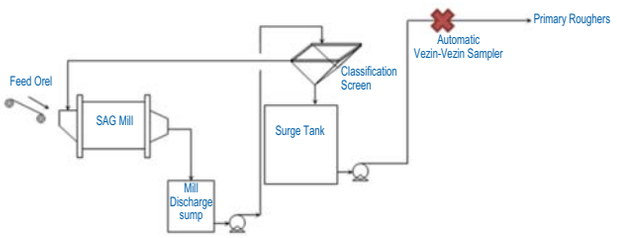

Figure 1—Basic process flow sheet

Vezin-vezin sampler arrangement

A vezin sampler is a multipurpose device that collects samples from materials that are free-falling from pipes, chutes, or hoppers. A schematic of the vezin-vezin sampler combination used at the concentrator and in which tests were performed is shown in Figure 2. This device operates by one or more cutters, revolving on a central shaft, that pass through the sample stream and collect a fixed percentage of the total material (Trottier and Dhodapkar, 2012). This sampling system comprises a primary sampler and a secondary sampler. The bulk stream that is sampled is generally large and thus the primary increment is often too large to be further processed or prepared. A secondary sampler is thus incorporated as part of the overall sampling system to reduce the primary sample to a more manageable sized sub-sample. The secondary sampler is generally in the form of a vezin sampler or rotary splitter. Kruger and van Tonder (2014) explain in detail the mechanical design of a typical vezin sampler and its mode of operation.

It was believed that particle segregation may be playing a more significant role in the intermediate hopper/holding tank of the UG2 feed sampling system than originally assumed. Intermediate hoppers typically have a design capacity to hold a single primary sample increment for a certain retention time until the entire primary sample increment is sub-sampled by a secondary sampler. It has been hypothesized that the main reason for the consistent under-accounting may be due to over-sub-sampling of finer material into the official samples, and consequently under-sub-sampling of the coarser material present in the feed slurry streams. UG2 feed material assays by size fraction indicated that higher platinum and palladium grades are associated with the sub-75 µm size fractions as opposed to the coarser size fractions above 75 µm (Ntlhabane, 2014). Indications are that because of the under-sub-sampling of coarse material, the head grade of the feed to the plant is overstated, leading to an under-accountability of metal content. For metallurgical accounting, it is vital that there is unbiased sampling of input and output streams (Bartlett, 2005).

Experimental methodology

The automatic vezin-vezin feed sampler as illustrated in Figure 3 was used to perform all experimental work.

Dual primary vezin samplers as depicted in Figure 3 were available on site. Under normal operating conditions, only one primary vezin sampler is meant to operate at a time. The primary sampler has a single vezin cutter arrangement and the secondary sampler has a four-cutter vezin arrangement. The primary sampler produces a primary sample which is then discharged from the primary cutter outlet through a flexible pipe (‘7’ in Figure 3) into a Y-feed pipe (‘4’ in Figure 3) and then into the intermediate hopper (‘3’ in Figure 3) of volume capacity 20 L. The primary sample increment is then discharged from the intermediate hopper through a nozzle via gravity, at which point sub-sampling begins. The intermediate hopper is fitted with a regulated compressed air supply (approx. 2–4 bar pressure).

Principal bias testing relating to segregation of particles in the intermediate hopper was conducted using the vezin credibility technique (Kruger and Millar, 2002). The primary and secondary sampling stages as depicted in Figure 2 were used to collect samples.

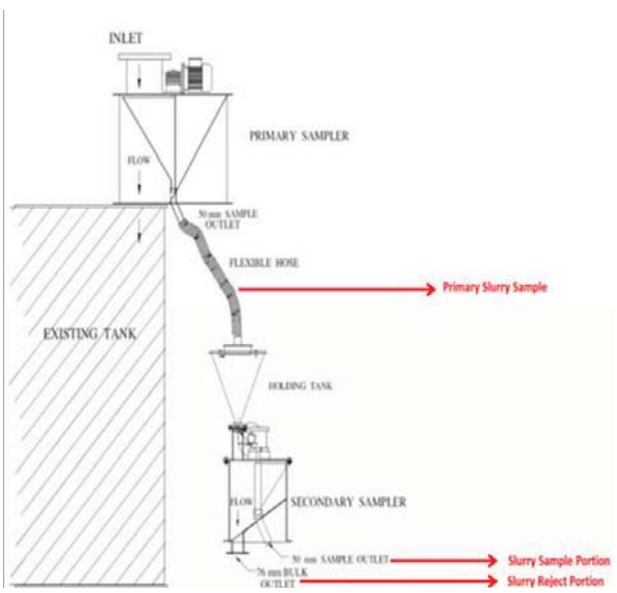

Figure 2—Schematic of vezin-vezin sampler

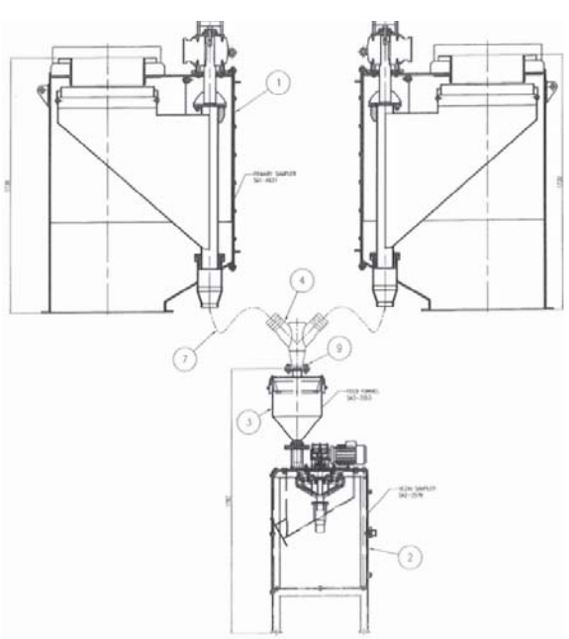

Figure 3—Schematic of dual primary vezin samplers

Experimental programme

The experimental work reported in this paper was conducted in two stages. Stage 1 involved experimental baseline test work on the existing sampling equipment. Stage 2 involved test work using a re-designed intermediate hopper nozzle.

Twin stream analyses were done for all samples sent to the analytical laboratory in order to determine the analytical variance. The analytical laboratory that conducted the assaying is ISO 17025 accredited. A certified reference material (CRM) matching the samples was used for quality control purposes. The CRM samples were randomly placed in each batch of samples that were analysed. All samples were analysed in triplicate and the relative standard deviation used to eliminate outliers. If there were no outliers, the average value of the three results was then reported. Backup samples were reserved (where possible) for repeat analysis.

The first objective was to investigate whether particle segregation occurs in the intermediate hopper of the UG2 feed sampling system. Two different tests were performed, namely the vezin credibility test and a chronological sub-sampling test. The purpose of a vezin credibility test is to verify whether the vezin sampler produces sound, repeatable, and unbiased results. If a vezin sampler is credible then the characteristic/analyte under consideration should be almost identical for both the official sample and reject sample. A total of five test runs were performed for repeatability purposes. For each test run, five individual samples were generated.

The vezin credibility test work involved the following steps:

- The plant control room personnel were notified of the test work plan
- A pre-work risk assessment was performed by all personnel involved in the test work. The equipment was inspected for leaks and physical damage. The secondary vezin speed was also determined
- The main feed stream was sampled by the primary vezin on a pre-determined time interval basis. The primary vezin sampler was operated in manual mode for this purpose
- A clean and empty 20 L plastic bucket was placed at the secondary vezin reject sample pipe discharge, and a clean and empty 5 L container was placed at the official sample pipe discharge
- With the primary vezin sampler in manual mode, the manual 'cut' button was pressed once. This resulted in a single cut of the main stream. Two more manual cuts were taken at intervals of approximately 30 seconds Each primary sample increment resulting from the primary vezin operation was then sub-sampled by the secondary vezin sampler to produce an official sample and reject slurry portion. The hopper retention time was measured in order to calculate the number of secondary cuts per primary increment
- The two buckets containing the official and reject samples were then removed from the sampling points. The containers were closed securely with the provided lids to ensure that no moisture evaporated and no sample was spilled. Each sample was accompanied by a sample identification tag
- The flexible hose connecting the discharge point of the primary vezin cutter to the Y-bend feed inlet of the intermediate hopper was then detached
- A single manual primary cut was then taken. An empty and clean 20 L bucket was used to collect this primary sample increment. The sample container with the primary slurry sample was then removed from the sampling point and secured as for the others
- The flexible hose was then re-attached to the inlet of the intermediate hopper.

The above steps were repeated five times for repeatability purposes. The time between each test run was minimized (less than 15 minutes) to reduce the risk of introducing unpredicted process variability into the test work. Once the required number of samples had been collected, *i.e.* five primary slurry sample increments and ten pairs of official sample and reject slurry samples, the sampler was immediately switched back to automatic operation. The collected samples were taken to a central storage area for further preparation, analyses, and data recording.

A schematic of the sampling and sample preparation methodology for the vezin credibility test work is shown in Figure 4.

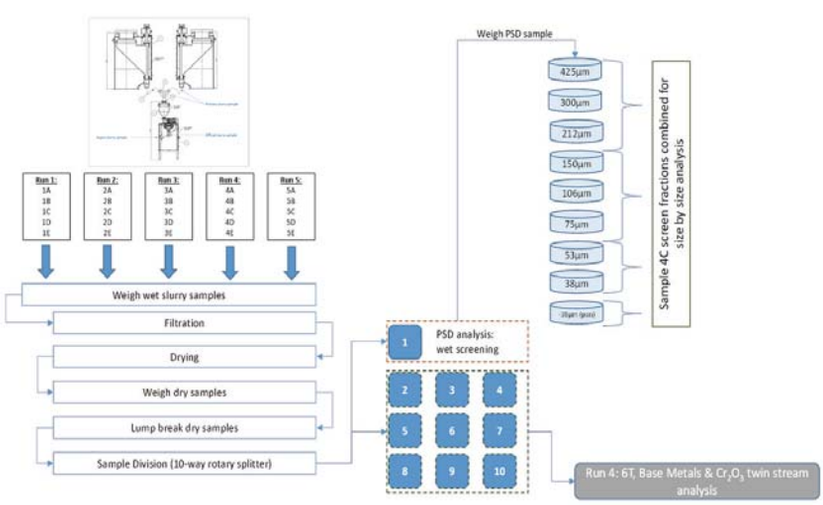

Figure 4—Sampling and sample preparation methodology for stage 1, test 1

The chronological sub-sampling test work was designed to determine the presence of particle segregation. The intermediate hopper discharge was sampled intermittently over a predetermined period of time in order to examine the constitution of the samples with respect to particle size. If coarse particles settle faster in the intermediate hopper, as intuition and Stokes Law (McCabe, Smith, and Harriott, 1993) suggest, they should exit the hopper first and more quickly on sub-sampling and are therefore not sub-sampled for the entire duration of the sampling campaign.

The chronological sub-sampling test work was carried out as follows:

- A primary increment was collected into the intermediate hopper by sampling the primary feed
- For every primary increment sub-sampled from the intermediate hopper by the secondary vezin, an official sample portion was collected every 6 seconds in separate containers until the intermediate hopper emptied out
- Seven primary increments were taken and the above steps repeated until enough sample mass was cumulatively collected in this chronological sequence
- Each of the chronological sub-samples was accompanied by a sample identification tag
- The sub-samples were then wet-screened independently over a 38 µm screen to produce a +38 µm fraction and –38 µm fraction
- The + 38 µm fraction was dried and weighed
- The –38 µm fraction was filtered, dried, and weighed
- The two fractions were then combined and weighed
- The % + 38 µm was then calculated
- The combined sample was then sent for 6T, base metals, and Cr_2O_3 twin-stream analysis.

A schematic of the sampling and sample preparation methodology for the chronological sub-sampling test work is shown in Figure 5.

Results and discussion

Stage 1 baseline test work results

Figure 6 shows the cumulative particle size distributions of the primary, official, and reject samples for all five of the test

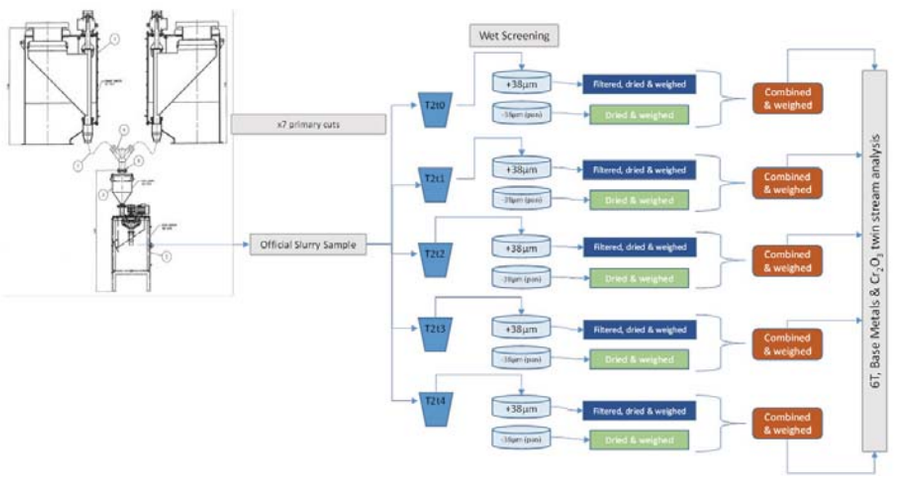

Figure 5—Sampling and sample preparation methodology for stage 1, test 2

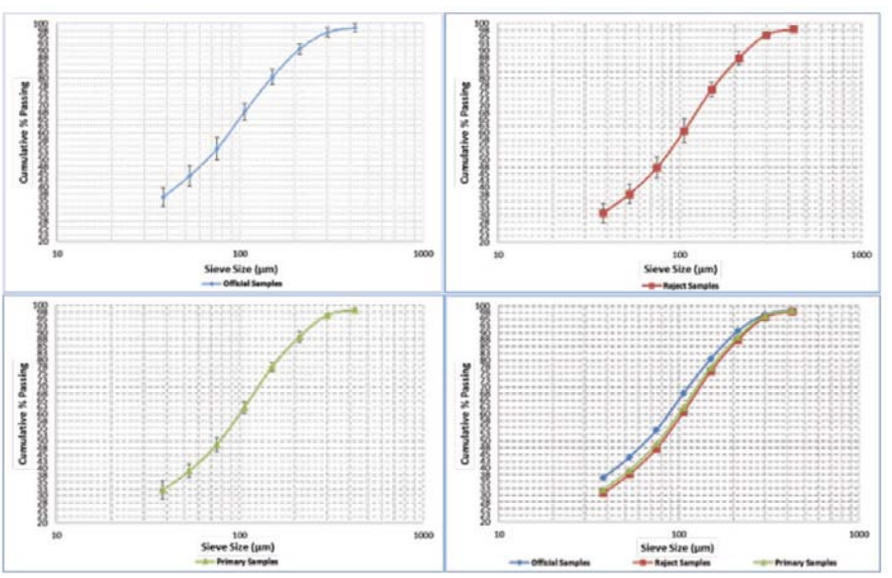

Figure 6—Stage 1: cumulative percentage passing comparison

runs. It is clear from Figure 6 that the reject sample is coarser than both the official and the primary 'feed' sample and that the primary sample PSD lies between the PSDs of the official sample and reject sample.

This demonstrates that the sampling system has a tendency to sample more of the finer particles than the coarser fraction. Figure 7 shows that bias exists between the reject and official samples. The official samples consistently have a higher cumulative percentage passing than that of the reject samples across all screen sizes.

The percentage bias between the reject and official samples wase calculated per size fraction and is shown in Figure 8.

Figure 8 shows the bias between official and reject samples across the spectrum of particle sizes. The official samples are consistently finer than the reject samples and the bias increases as the particles size decreases. The largest bias of 18.5% is observed for the –38 µm fraction. Considering the previous suggestion that sub-75 µm particles normally have higher PGM grades, such biases would therefore have an effect on the overall grades of the primary, reject, and official samples, resulting in the declaration of an incorrect feed grade for metal accounting purposes.

A size by assay analysis was performed and the results are shown in Figure 9. It can be observed that there is an almost exponential increase in the PGM grade with decreasing in particle size.

This again emphasizes that if sampling has a bias towards the finer fraction (below 75 µm), which has a much higher PGM grade, then the overall grade of the official sample will be much higher than that of the primary or reject samples. From Figure 10, the official samples (4B and 4E) clearly have the highest PGM grades, followed by the primary sample (4C) and reject samples (4A and 4D).

The results of the chronological sub-sampling of the official sample are shown in Figure 11. For the initial 12

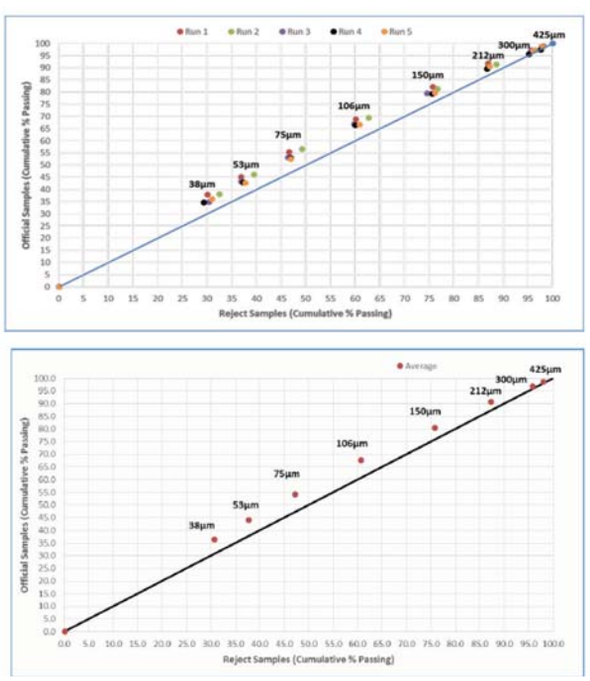

Figure 7—Stage 1: cumulative percentage passing comparison (official and reject samples)

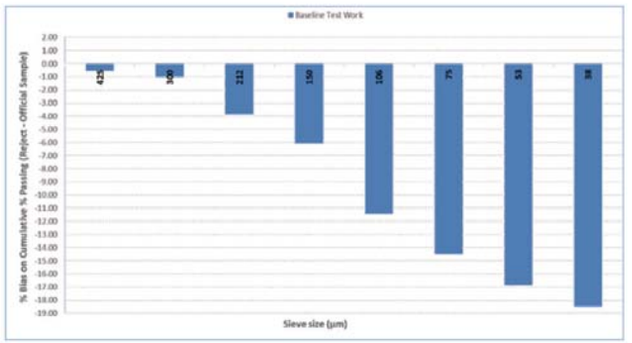

Figure 8—Stage 1: percentage bias between reject and official samples passing each sieve size

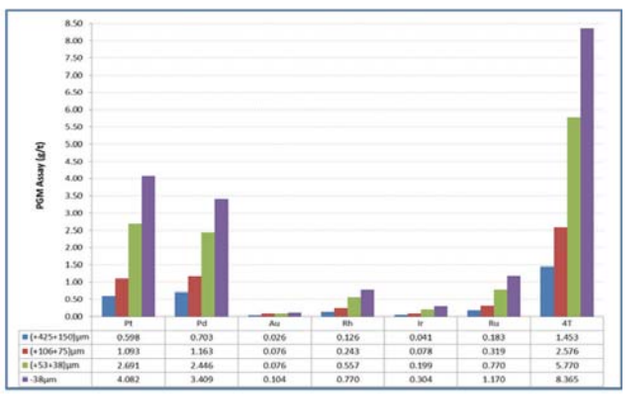

Figure 9—Relationship between PGM grade and particle size

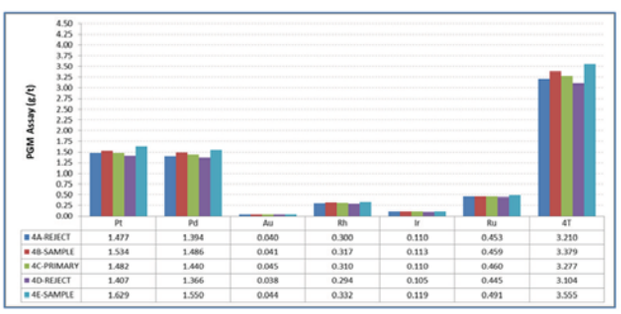

*Assay data has been factorized for confidentiality purposes

Figure 10—Stage 1: PGM assays for run 4

seconds of secondary sampling (T1t0 to T1t1) the 4T grade remains fairly constant, thereafter increasing as the percentage +38 µm fraction decreases. This proves that coarser particles have a tendency to exit the intermediate hopper faster than finer particles. The base metal (BM) composition remains fairly constant as time progresses, suggesting that deportment of base metals does not change across the particle sizes as much as the deportment of PGMs. This has been proved by historical mineralogical investigations. Cr_2O_3 composition, however, follows the percentage +38 µm trend.

Changes in the intermediate hopper discharge nozzle design

The second objective of this research project was to determine how particle segregation could be minimized by optimization

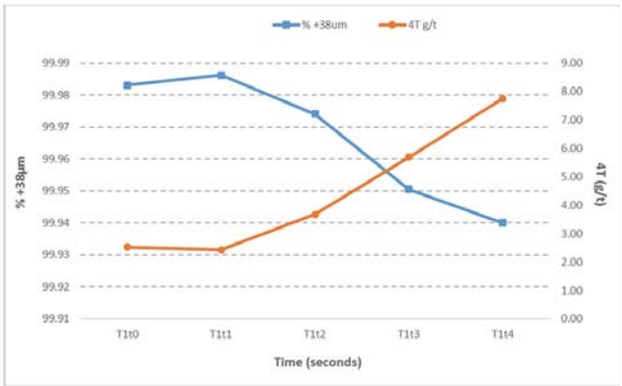

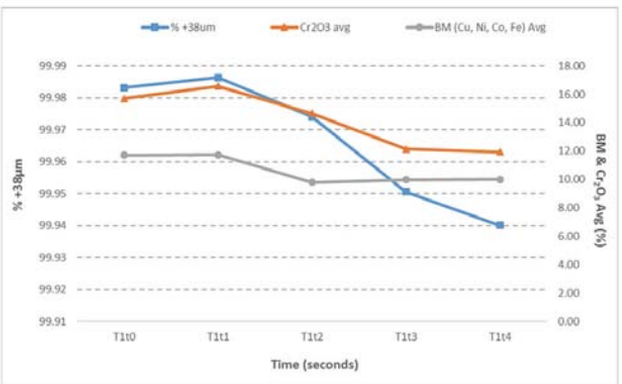

*Assay data has been factorized for confidentiality purposes

Figure 11—Stage 1: variation of grade with percentage +38 µm retained over time

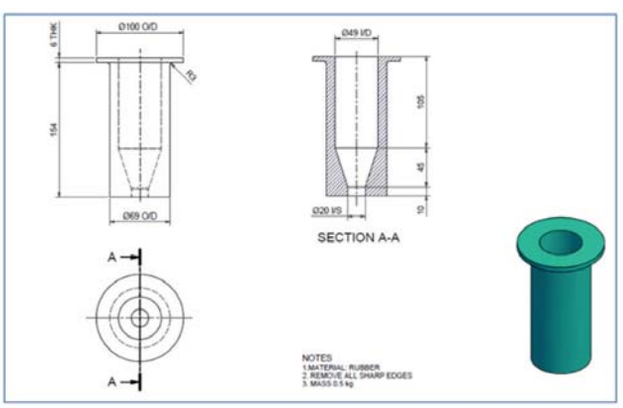

Figure 12—Engineering schematic of original nozzle design

of the existing sampling equipment. A re-design of the intermediate hopper nozzle was considered. The original nozzle design is depicted in Figure 12.

It was considered that the geometry of the nozzle could be the main contributor to the possible particle segregation, since compressed air at the inlet of the nozzle probably mixes the particles as they leave the intermediate hopper. The original nozzle design tapers off to an exit diameter after 105 mm of straight length. This promoted the argument that segregation could occur in the straight wider section. Under normal operation, the primary slurry sample would enter the intermediate hopper and be air-agitated at the base of the hopper before entering the nozzle. The particles in the slurry material would then have an opportunity to settle out over the length of the nozzle. The nozzle discharges into the secondary vezin sampler, which is used for sub-sampling until the intermediate hopper is emptied out. The idea of a new nozzle design was then suggested. The new nozzle design tapers off much earlier and has a narrower discharge length, as depicted in Figure 13.

Test work was then conducted to compare both nozzle designs in terms of their effect on particle segregation in the intermediate hopper of the UG2 feed sampling system. The same test work protocol as per stage 1, test 1 and stage 1, test 2 was followed).

Stage 2: optimization of existing sampling equipment

Figure 14 shows the cumulative particle size distribution of the feed slurry, official and reject samples for all five test runs performed. There is generally a closer agreement between the reject, official, and primary samples on the cumulative percentage passing.

It is clear from Figure 15 that the reject and official samples are not identical at each respective size fraction, as the data is generally scattered around the 45° line; however, an averaged cumulative percentage passing comparison shows no net segregation. This indicates that over an entire sampling campaign, the random bias observed for individual increments would mostly likely average out and not result in a consistent bias in terms of particle size and hence overall grade of the reject and official samples.

The percentage bias between the reject and official samples was calculated per size fraction and is plotted in Figure 16, which also compares the new bias values with those obtained from the test work with the old nozzle. These results show that there is a consistent bias in the finer fractions and that the quantum of the bias per size class is much less than recorded with the old nozzle.

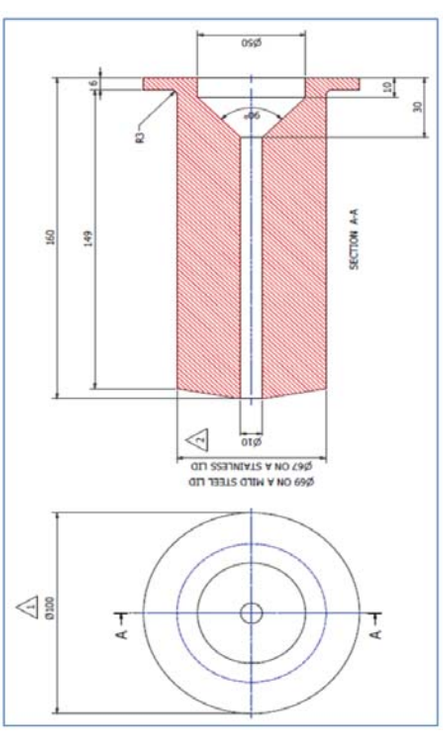

Figure 13—Engineering schematic of alternative nozzle design

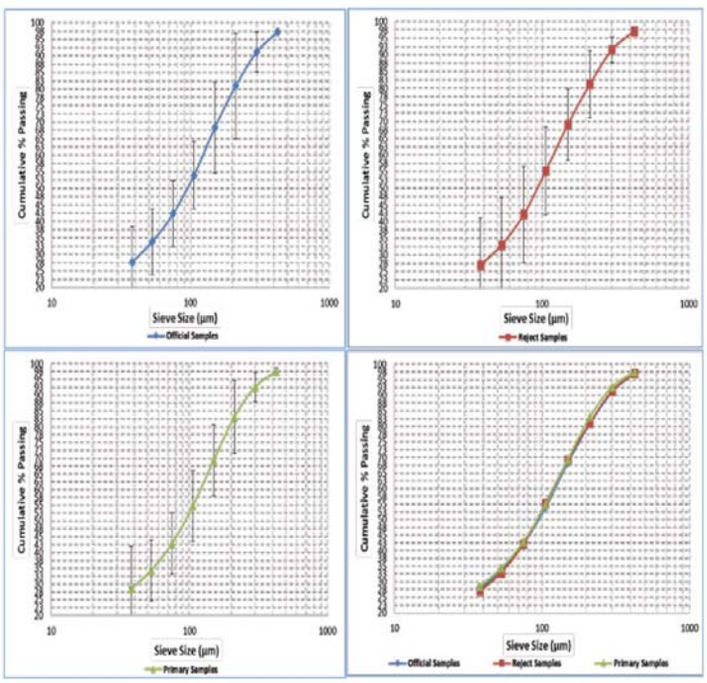

Figure 14—Stage 2: cumulative percentage passing comparison

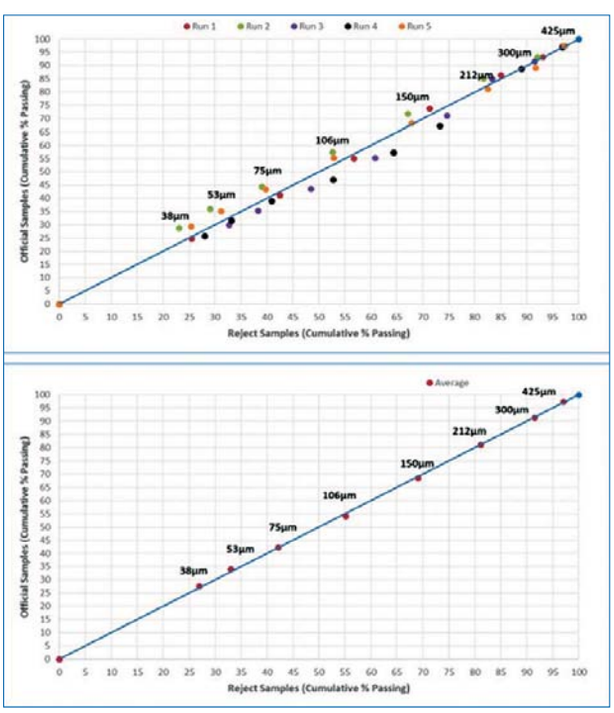

Figure 15—Stage 2: cumulative percentage passing comparison (official and reject samples)

The chronological sub-sampling results for the tests with the new nozzle are shown in Figure 17. They indicate that for the initial 18 seconds of secondary sampling (T2*t*0 to T2*t*2) the 4T grade remains fairly constant. The 4T grade thereafter increases as the percentage +38 µm fraction decreases, but to a lesser degree than with the old nozzle. The BM composition remains fairly constant as time progresses, with the Cr_2O_3 composition again following the percentage +38 µm trend.

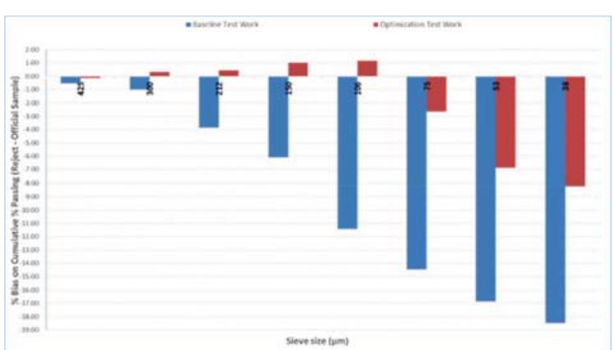

Figure 16—Stage 1 and 2: percentage bias between reject and official samples passing each sieve size

Figure 18 shows a comparison of the percentage +38 µm fraction for the tests with the old and the new nozzle tests. The results indicate that segregation is reduced to some extent with the new nozzle design.

The paired t-test method was applied in order to confirm whether there is a consistent bias between the reject and official samples that are correlated (*i.e.* it is expected that these measures would change with the change in the feed conditions) and are significantly different from zero. The differences in percentage mass retained for each pair of reject and official samples arising from an independent feed condition was compared in the statistical analysis. Table I indicates the confidence levels for the significance in the bias between reject and official samples. Red, yellow, and green cells indicate greater than 95% confidence, between 90% and 94.9% confidence, and less than 89.9% confidence respectively.

For Stage 1 test work, there is generally a greater than 95% confidence that a bias exists and that the bias is significant between the reject and official sample. The statistical confidence level for Stage 2 test work indicates that

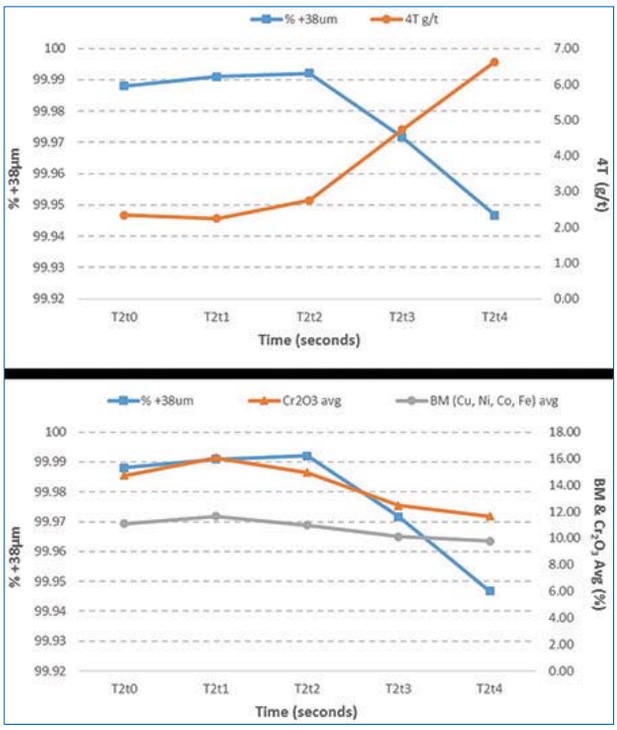

Figure 17—Stage 2: variation of grade with percentage +38 µm retained over time

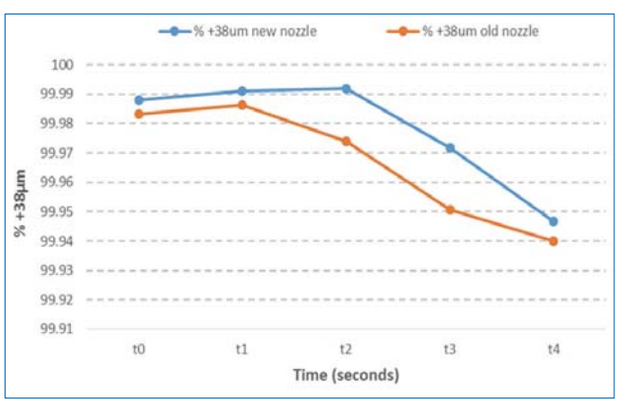

Figure 18—Stage 1 and 2: variation of grade with percentage +38 µm retained over time

bias is not significant, and confirms that modifying the hopper discharge nozzle design effectively reduced particle segregation in the intermediate hopper of the sampling system.

Conclusions

The hypothesis that particle segregation is present in the intermediate hopper of a typical UG2 feed sampling system was confirmed by the vezin credibility and chronological sub-sampling test work on the original sampling system. A consistent bias was observed between the reject and official samples, with the official samples being depleted of coarse particles and higher in 4T grade than the reject samples. By means of a paired t-test, the calculated bias for percentage mass retained was deemed significant at the 95% confidence level. This outcome, together with the size by assay analysis, indicated that an under-accounting scenario would result.

Table I

Paired t-tests between reject and official samples

	Summary of Statistical Confidence in the Differences of % Retained between Reject and Official Samples			
	Stage 1		Stage 2	
	(Reject Sample A - Official Sample B)	(Reject Sample D - Official Sample E)	(Reject Sample A - Official Sample B)	(Reject Sample D - Official Sample E)
+425µm	99.8	42.7	58.9	32.8
+300µm	96.3	95.7	85.0	97.1
+212µm	98.0	100.0	51.6	24.5
+150µm	93.3	98.7	1.8	57.5
+106µm	99.1	99.9	51.8	69.3
+75µm	53.7	67.7	82.6	94.5
+53µm	29.4	99.2	80.0	12.1
+38µm	80.1	90.2	26.2	36.0
-38µm	99.8	99.8	8.4	31.4

Stage 2 test work indicated that optimization of the existing sampling system by modifying the design of the intermediate discharge hopper nozzle changed the dynamics at the base of the hopper and resulted in a random distribution of fine and coarse particles in both the reject and official samples. The PSDs for reject and official samples were similar across all test runs. The statistical confidence level for test work with the new nozzle indicates that bias is not significant and confirms that modifying the hopper discharge nozzle design reduced to some extent the particle segregation in the intermediate hopper of the sampling system.

In general, it is has been proven that particle segregation, which was so evident in the baseline test, was reduced with the incorporation of the alternative nozzle design.

Acknowledgements

The authors would like to thank Anglo American Platinum for the opportunity to conduct test work at one of their concentrator plants and for providing various resources throughout the research. The authors also wish to express appreciation to the technical services department of the concentrator plant where the experiments were sanctioned and carried out.

References

BARTLETT, H.E. 2005. Confidences in metallurgical balances estimated from the errors in mass measurement, sampling and analytical determinations. *Proceedings of the Conference on Exploration, Mine, Met and Environmental Sampling (EMMES 2005)*, Eskom Conference Centre, South Africa, 3-4 November 2005. South African Institute of Mining and Metallurgy, Geological Society of South Africa, and Geostatistical Association of Southern Africa.

KRUGER, C.J. and MILLAR, N.C. 2002. Evaluation manual. Group evaluation metal accounting. Anglo American Platinum, South Africa.

KRUGER, C. and VAN TONDER, E. 2014. Pitfalls in vezin sampling for finely crushed materials. *Journal of the Southern African Institute of Mining and Metallurgy*, vol. 114. pp. 47–52

MCCABE, W.L., SMITH, J.C., and HARRIOTT, P. 1993. Unit Operations of Chemical Engineering. 5th edn. McGraw-Hill, Singapore.

NTLHABANE, S. 2014. Benchmark mineralogical investigation of UG-2 concentrator. *Research report.* no. MPR/14/183. Anglo Research, Crown Mines Campus, Johannesburg, South Africa.

TROTTIER, R. and DHODAPKAR, S. 2012. Sampling particulate materials the right way. *Chemical Engineering,* vol. 119, no. 4. pp. 42–49. ◆

http://dx.doi.org/10.17159/2411-9717/2018/v118n1a8

Effect of frother and depressant interaction on flotation of Great Dyke PGM ore

by T. Mberi*, L.L. Mguni*, and F. Ntuli†

Synopsis

In the optimization of platinum group metal flotation plants, various parameters are considered in order to achieve the desired recovery and grade of the precious metals. There should be a balance in the operating parameters so as to produce a high-grade valuable mineral concentrate without compromising recovery. This project seeks to investigate the individual and interactive effect of flotation reagents at different dosages, using a full factorial experimental design approach with two factors at six levels. Laboratory tests were conducted to illustrate the effect of frother and depressant on flotation. The results were analysed using SPSS and MiniTab. Based on the F-test at 95% confidence level, the frother had no significant effect on the concentrate grade but had a significant effect on 4E recovery, mass pull, and water recovery. The depressant had a significant effect on concentrate grade, water recovery, and mass pull. The interactive effect of frother and depressant had significant negative effect on all responses except concentrate grade. The optimum levels for recovery and grade were analysed assuming equal importance of grade and recovery as well as double importance for grade.

Keywords

froth flotation, PGMs, flotation reagents, frother, depressant, interactive effect.

Introduction

Platinum group metals (PGMs) in Zimbabwe are mined along a 550 km long geological feature known as the Great Dyke. The major PGM mining and concentrator operators are Zimplats, Mimosa, and Unki mine. The platinum group element (PGE), nickel (Ni), and copper (Cu) mineralization is restricted to the Main Sulphide Zone (MSZ) (Oberthur, Muller, and Lodziak, 1999). The Great Dyke is divided into two magma chambers: the North and South chambers. The magma chambers are further divided into the Musengezi and Hartley complexes, and these are divided into the Dwarendale and Sebakwe sub-chambers and Selukwe and Wedza complexes, respectively (Prendergast, 1988). The Great Dyke is generally said to be comprised of a lower ultramafic sequence (chromite, dunites, pyroxenites, and related cumulates) and an upper mafic sequence consisting of plagioclase-rich rocks (mainly gabbros, norites, gabbronorites, and olivine gabbros) (Prendergast, 1990).

The primary collector used in ore flotation is xanthate. A depressant is added to suppress naturally floating gangue minerals. Optimization of reagents has been traditionally performed by varying one while keeping the others fixed. This method ignores interaction effects among reagents. Changes in reagent dosage to achieve a particular outcome may have secondary effects that override the desired effect, hence interactions have to be well understood if optimization is to be achieved. Little work has been reported on the flotation performance of Great Dyke ore. Nashwa (2008) reported on the effect on SIBIX and SIBIX-TTCs blends, but most of the work that has been reported is based on Bushveld Complex ore. Interaction effects between aeration rate and froth have been reported by Venkatesan and Harris (2014). The work showed that interaction effects were significant at conditions of high air flow rate (40 m/s) and cell level (max. 95 % cell level). In other work based on UG2 ore, McFadzean and Pani (2015) reported on interactive effects between depressant, frother, froth height, and superficial air velocity. They reported that among the process parameters, superficial air velocity had the dominant effect on chromite and PGM recovery, while depressant had a dominant effect only on chromite grade.

In this research, the interactive effects of depressant and frother were investigated while collector dosage was held constant. A two-factor analysis with six levels was done so as to observe the individual and interactive effects of frother and depressant on 4E (platinum, palladium rhodium, plus gold) recovery, grade, mass pull, and water recovery using PGM-bearing ore from the Great Dyke.

* *National University of Science and Technology, Bulawayo, Zimbabwe.*

‡ *University of Johannesburg, South Africa.*

 ISSN 2225-6253. Paper received Sept. 2016; revised paper received June 2017.

Effect of frother and depressant interaction on flotation of Great Dyke PGM ore

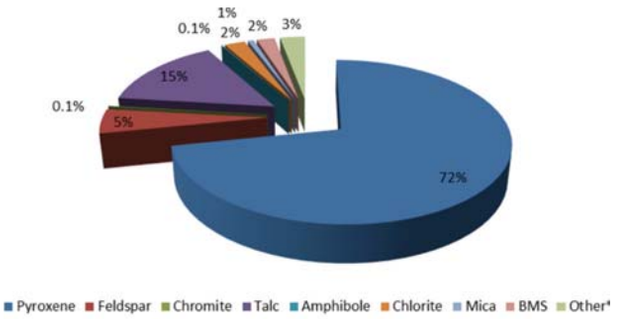

Figure 1—Bulk mineralogical composition (by mass) of the ore

Materials and methods

Sample preparation

Freshly ground underground ore was used for the experiments. A 4 m belt cut bulk sample was taken from the run-of-mine silo conveyor belt under normal plant operating conditions. The bulk sample weighed approximately 180 kg. Rocks larger than 50 mm were crushed using a laboratory jaw crusher. The ore was further crushed using a Boyd crusher to a top size of 4 mm and the crushed ore was blended using a Y-blender. A ten-way rotating splitter was used to split the ore into 1.3 kg sub-samples, which were ground in a laboratory rod mill with a grind time of 12 minutes used in order to achieve a grind of 40% passing 75 µm, which matches the product of the primary grinding circuit (primary rougher feed; MF1) at the operations. The rod mill discharge was wet-screened to produce a grind curve. The bulk mineralogical composition of the ore used is shown in Figure 1. It consisted mainly of pyroxene (72%) and talc (15%), which is a naturally floating gangue mineral.

Table I shows the base metal sulphide (BMS) distribution of the ore. Pyrrhotite, chalcopyrite, and pentlandite are generally associated with the economic PGMs (Lee, 1996). Of these three major sulphide minerals, chalcopyrite has been shown to be the most rapidly floating, followed by pentlandite, and the least floatable being pyrrhotite. Studies indicate that about 80% of the chalcopyrite can be recovered without any collector (Wiese and Harris, 2007).

Flotation

A Denver flotation cell was used at a rotor speed maintained at 1200 r/min for all batch flotation tests. The collector, sodium isobutyl xanthate (SIBX), was maintained at 300 g/t for all batch tests while frother (SAS FROTH) and depressant (DLM), which is a mixture of natural and modified polysaccharides) dosages were varied. The froth was scraped from the cell every 15 seconds, using paddles which were custom-made to scrape just above the froth-pulp interface, for a total time of 25 minutes. The concentrates were collected and the solids and water masses recorded. Water was added to the cell after every scrape to maintain the pulp level in the cell. The initial and final spray water bottle masses were recorded and the difference calculated in order to obtain the amount of water added during scraping.

Table I

BMS distribution

Composition	%
Pentlandite	25.5
Pyrrhotite	39.1
Pyrite	7.1
Chalcopyrite	28.3
Total	100.0

Experimental full factorial design

A full factorial experimental design approach was used to identify individual and interactive effects of frother and depressant. Full factorial experimental design is a useful tool for the study of the effect of the various process parameters. In the factorial design approach the interdependency of process variables can be studied with respect to targeted responses (Araujo and Brereton, 1996; Cochran and Co., 1999). The responses used were concentrate grade, 4E recovery, mass pull, and water recovery. The responses were tested for significance by the F-test. The confidence level was set at 95%. The experiments were carried out using two factors at six levels as given in Table II. Samples were analysed using fire assay.

Results and discussion

Effect of frother and depressant on mass pull

Based on the established hypothesis, the frother and depressant have a significant effect on mass pull, as shown in Table III. These results are consistent with the main effects plots in Figure 2. The plots were observed to be steeper at low dosages; 20–60 and 180–420 g/t for frother and depressant respectively (Figure 2). These results suggest that the effects of these reagents on mass pull are more pronounced at low dosage. An increase in frother dosage at low concentrations was observed to have a positive effect on mass pull. This is as expected since it has been generally accepted that increasing frother concentration stabilizes the froth, resulting in poor drainage of entrained gangue and recovery of both valuable and gangue minerals, hence the higher mass pull (Valenta and Harris, 1999). This also agrees with the work by Langevin (2000), which supports the contention that froth stability is increased with increasing frother concentration. On the other hand, increasing depressant dosage resulted in a decrease in mass pull due to destabilization of the froth and lowered entrainment (Wiese, Harris, and Bradshaw, 2009). It was also observed at high

Table II

Two-factorial by six-level experimental design for frother and depressant

Factors ↓	Varying dosages (levels) g/t →					
Frother	20	40	60	80	100	120
Depressant	180	260	340	420	500	580
Collector	300	300	300	300	300	300

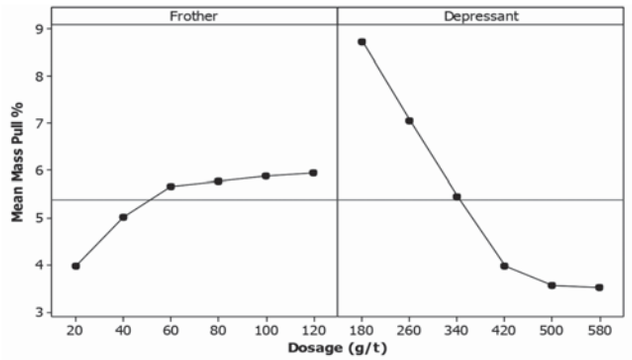

Figure 2—Main effect plots for mass pull

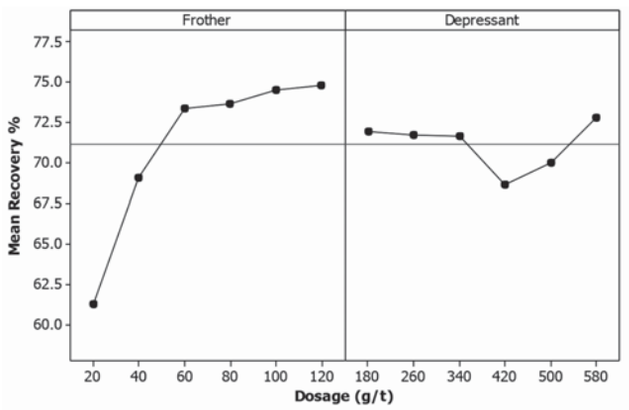

Figure 3 – Recovery main effect plots

depressant concentration (420–580 g/t) that mass pull varied very little, suggesting that most material that is amenable to suppression has been suppressed.

The interaction of frother and depressant had a negative effect on mass pull. High dosages of both these reagents have an adverse effect on mass pull, hence dosage of these reagents should be monitored if the desired mass pull is to be maintained.

Effect of frother and depressant on 4E recovery

From Figure 3 it can be observed that recovery increased with increasing frother concentration for low frother concentrations (20–60) g/t and thereafter almost levelled off. The initial increase in recovery with increase in frother quantity is expected as discussed earlier, due to entrainment. Changes in depressant concentration had no significant effect on recovery, which only fluctuated between 69% and 72%. The insignificant effect of depressant on recovery could be due to a very low response of PGE-bearing minerals to an increase in depressant, *e.g.* chalcopyrite recovery is reported not to be affected by depressants while pentlandite is affected only at high dosages (Wiese and Harris, 2007). According to Corin and Reddy (2011), who used nickel and copper as indicators of the response of PGE-bearing minerals, only a high depressant dosage of 500 g/t had an influence on maximum recovery. However, in this work depressant concentration had no effect on recovery, suggesting that the depressant at the investigated dosages (up to 580 g/t) did not suppress PGMs significantly and that the gangue material was mainly suppressed (McFadzean and Pani, 2015). This results in a continual increase in grade at the expense of the gangue material, as depicted in Figure 4.

The probability (P) values in Table III indicate that depressant-frother interactions had a significant negative effect on the recovery of valuable minerals, similarly to mass pull.

Table III

Summary of major effects of variables and interactions on responses at 95% confidence level

Response	Term	P value	Effect on response
Mass pull	Frother dosage	0.000	Significant (+)
	Depressant dosage	0.000	Significant (–)
	Frother*depressant	0.000	Significant (–)
4E PGE recovery	Frother dosage	0.000	Significant (+)
	Depressant dosage	0.552	Insignificant
	Frother*depressant	0.030	Significant (–)
4E concentrate grade	Frother dosage	0.264	Insignificant
	Depressant dosage	0.000	Significant (+)
	Frother*depressant	0.240	Insignificant
Water recovery	Frother dosage	0.000	Significant (+)
	Depressant dosage	0.000	Significant (–)
	Frother*depressant	0.000	Significant (–)

Effect of frother and depressant on concentrate grade

Figure 4 indicates the effect of increasing both frother and depressant on the concentrate grade. The concentrate grade increased with an increase in depressant dosage while the frother was observed to have insignificant effect on the grade. These results support the earlier assumption that depressant significantly suppressed only gangue minerals, and hence decreased the mass pull and increased the concentrate grade but had no effect on recovery. A slight drop in grade from 41 to 35 g/t was observed with increasing frother concentration (Table III), possibly as a result of the increase in mass pull due to entrainment, shown in Figure 2. These results suggest that the minimum amount of frother should be added that produces a sufficiently stable froth and

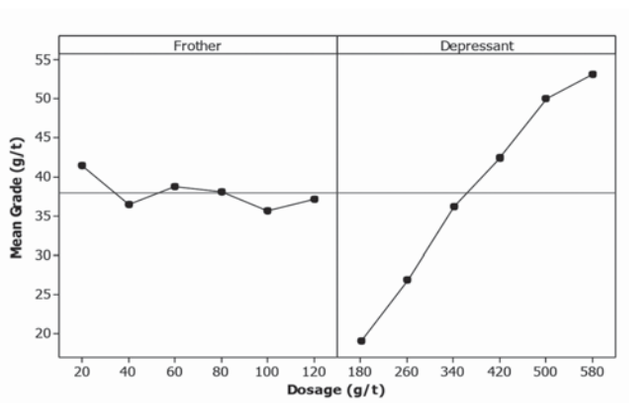

Figure 4 – Concentrate grade *versus* frother and depressant dosage

an acceptable mass pull. It was also observed that frother-depressant interactions were insignificant. The absence of interactions means that concentrate grade can be optimized by fixing one variable and varying another.

Effect of frother and depressant on water recovery

As shown in Figure 5, water recovery increased with increasing frother quantity between 20 and 60 g/t. This is a similar trend to that observed for mass pull and recovery, suggesting the increase in mass pull and recovery is due to entrainment (Wiese and Harris, 2007). Increasing frother dosages increase solid recovery due to the stable froth which reduces selectivity and leads to non-selective entrainment (Yoon and Luterell, 1989). Water recovery was also observed to decline with increasing depressant quantities above 340 g/t. This suggests that froth stability is affected by depressant and frother-depressant interactions at high depressant concentrations (above 340 g/t), hence a decrease in water recovery. These results are consistent with observations that bubble formation was poor at depressant concentrations from 420–580 g/t. Similar findings were obtained by Ekmeckci and Bradshaw (2003) at high depressant dosages. Wiese (2011) stated that depressants have a significant effect on water recovery

From Table III it can be seen that frother had a positive effect on water recovery, while depressant had negative effect, in agreement with Figure 5. However, a closer look at Figure 5 shows that the negative effect of depressant was more pronounced at high dosages (420–580g/t).

Optimization

The main effects graphs do not enable process optimization but enable the effect of various process parameters to be investigated. For the purposes of optimization, only results based on low depressant dosages (180–340 g/t) were analysed. High dosage were not considered because of the poor froth stability observed, as discussed earlier, hence they will be of no practical use at a plant scale. Figure 6 was produced by assuming equal importance for both recovery and grade (Venkatesan and Harris, 2014). From Figure 6 it can be seen that the areas that give best values for the normalized product are towards high depressant and low frother concentration. Taking the first region or contour with a depression dosage range of 280–340 g/t and frother dosage range of 20–80 g/t as the optimum region, regardless of other values not included in test work (280, 300, 320 g/t), the

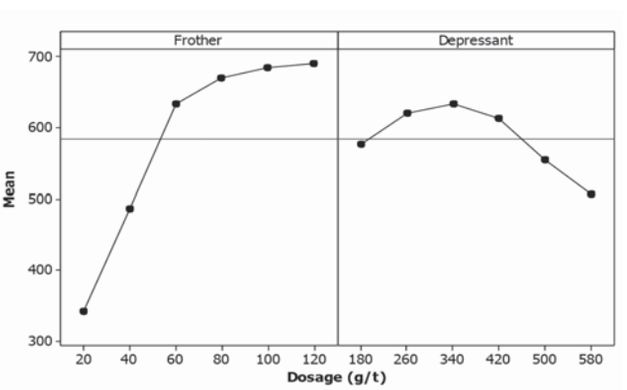

Figure 5 – Water recovery main effect plot

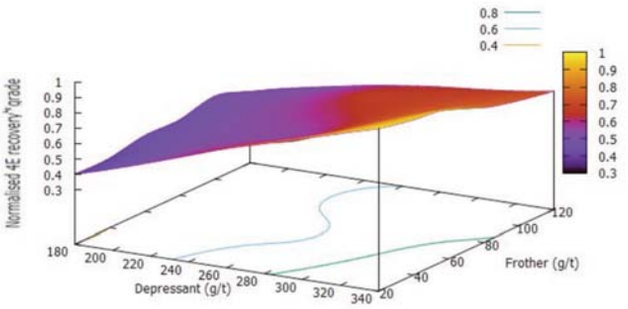

Figure 6—Surface plot for normalized 4E recovery*grade

range of recovery and grade in this region is 61–74% 4E recovery and 31–44 g/t concentrate grade. Further investigations of reagent combinations in this region are recommended to verify the suggested values.

When grade is considered more important than recovery, the index of recovery* grade^2 is used. From Figure 7, it can be seen that the number of regions marked by contours increased from the previous three to five. This results in small regions, meaning that if the importance of grade is doubled there is a need for stricter reagent control and optimization. Figure 7 agrees with earlier findings that frother had minimal effect on grade compared to depressant. The contour line shifts from 280 g/t to approximately 330 g/t depressant if the importance of grade is doubled compared to the frother, which only declined to approximately 70 g/t from 80 g/t (Figure 6).

Analysis of interdependence of responses

Figure 8 shows 4E recovery and mass pull as a function of water recovery. There is a reasonable good linear relationship for both 4E recovery and mass pull *versus* water recovery for varying frother dosage. A good correlation with water recovery suggests that the variables mass pull and recovery are dependent solely on entrainment (Valenta and Harris, 1999).

When the depressant concentration was varied no correlation was observed between water recovery, mass pull, and 4E recovery. This suggests the depressant is selective, as opposed to the frother, which increases entrainment with increased dosage.

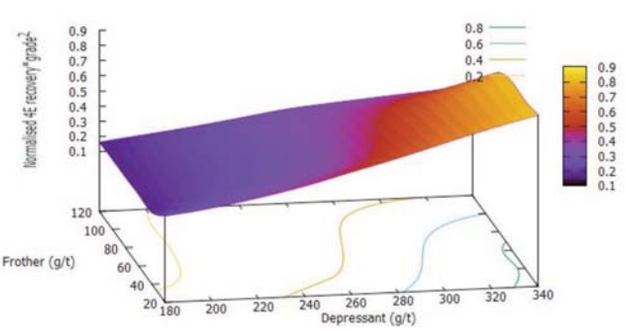

Figure 7—Surface plot for normalized 4E recovery*grade^2

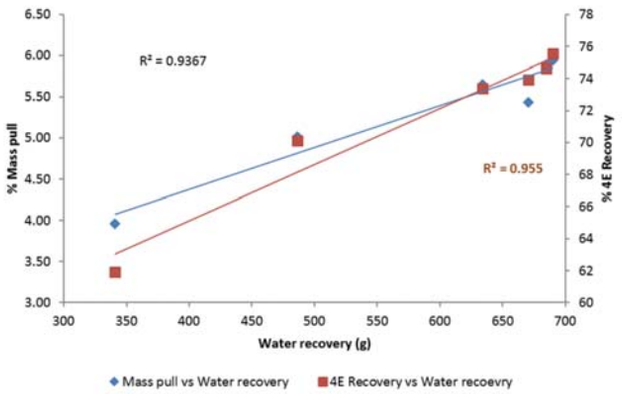

Figure 8—Water recovery *versus* recovery and mass pull

Table IV

Summary of results

Reagent	Effect on			
	Grade	Recovery	Mass pull	Water recovery
Frother	No	Yes	Yes	Yes
Depressant	Yes	No	Yes	Yes
Frother*Depressant	No	Yes	Yes	Yes

Conclusion

Based on the F-test at 95% confidence level, the results can be summarized as in Table IV.

Increase in frother dosage resulted in an increase in recovery and mass pull due to entrainment, as corroborated by an increase in water recovery. A slight drop in grade was observed, hence frother dosage can be manipulated to achieve a desired PGE recovery without significantly affecting grade.

An increase in depressant resulted in an increase in grade and a decrease in mass pull. Depressant had an insignificant effect on recovery, suggesting that there was selective suppression of gangue minerals in the range investigated. Frother-depressant interactions had a negative effect on mass pull, 4E recovery, and water recovery, but an insignificant effect on concentrate grade. Assuming equal importance of 4E recovery and concentrate grade, the optimum reagent dosage range was 280–340 g/t depressant and 20–80 g/t frother.

Recommendations

As stated above, assuming equal importance of 4E recovery and concentrate grade the optimum reagent dosage range is 280–340 g/t depressant and 20–80 g/t frother. Further test work is therefore recommended to narrow this range. Furthermore, this range may be investigated using three-factorial experimental design to incorporate the effect of collector. The reagents used and the ranges should be representative of the plant-scale flotation circuit.

References

Araujo, P.W. and Brereton, R.G. 1996. Experimental design II. Optimisation. *TaAC Trends in Analytical Chemistry*, vol. 15, no. 2. pp. 63–70.

Cochran, W.G. and Cox, G .M. 1990. Disefios Experimentales, 2nd edn. Trillas, Mexico.

Corin, K., and Reddy, A.M.L. 2011. The effect of ionic strength of plant water on valuable mineral and gangue recovery in a platinum bearing ore from the Merensky reef. *Minerals Engineering*, vol. 24, no. 2. pp. 131–137.

Ekmeckci, Z. and Bradshaw, D.A. 2003. Effects of frother type and froth height on the flotation behaviour of chromite in UG2 ore. *Minerals Engineering*, vol. 16, no. 10. pp. 941–949.

Langevin, D. 2000. Influence of interfacial rheology on foam and emulsion properties. *Advances in Colloid and Interface Science*, vol. 88, no. 1-2. pp. 209–222.

Lee, C. 1996. A review of mineralisation in the Bushveld Complex and some other layered intrusions. *Developments in Petrology*, vol. 15. pp.103-145.

McFadzean, B. and Pani, S.W. 2015. The interactive effects of chemical and process parameters on the flotation performance of a UG2 ore. *Minerals Engineering*, vol. 70. pp. 92–98.

Nashwa, V.M. 2008. The flotation of high talc containing ore from the Great Dyke. MSc thesis, University of Pretoria.

Oberthur, T., Muller, P., and Lodziak, J. 1999. Mobility of PGE and PGM in the supergene environment at the Hartley Mine, Great Dyke. A case study. *Mineral Deposits - Processes to Processing. Proceedings of the Fifth Biennial SGA Meeting and the Tenth Quadrennial IAGOD Symposium*, London, UK, 22-25 August. Balkema. pp. 763–766.

Prendergast, M. 1988. The geology and economic potential of the PGE-rich Main Sulphide Zone of the Great Dyke, Zimbabwe. *Proceedings of Geo-platinum 87*, Open University, UK. Prendergast, M. (ed.). Springer, Dordrecht. pp. 281–302.

Prendergast, M. 1990 Platinum-group minerals and hydrosilicate 'alteration' in Wedza-Mimosa platinum deposit, Great-Dyke, Zimbabwe, Genetic and metallurgical implication. *Transactions of the Institution of Mining and Metallurgy Section B: Applied Earth Science*, vol. 99. pp. B91–B105.

Valenta, M. and Harris, P.J. 1999. The contribution of entrainment to the UG2 ore. *Proceedings of the Mineral Processing Conference*, Cape Town.

Venkatesan, L. and Harris A.G.M. 2014. Optimisation of air rate and froth depth in flotation using a CCRD factorial design - PGM case study. *Minerals Engineering*, vol. 60-68. pp. 221–229.

Wiese, J., Harrris, P.J., and Bradshaw, D. 2009. The effect of increased frother dosage on froth stability at high depressant dosages. *Flotation 09. Proceedings of: 4th International Flotation Conference,* Cape Town, 9–12 November 2009. Bradshaw, J., Franzidis, J.-P., and Wills, B.A. (eds). pp. 1010–1017. doi:10.1016/j.mineng.2010.04.011

Wiese, J. and Harris, P.B. 2007. The response of sulphide and gangue minerals in selected Merensky ores to increased depressant dosages. *Minerals Engineering*, vol. 20, no. 10. pp. 986–995.

Wiese, J. (2011). The effect of the reagent suite on froth stability in laboratory scale batch flotation tests. *Minerals Engineering*, vol. 24. pp. 995-1003.

Yoon, R.H. and Luttrell, G.H. 1989. The effect of bubble size on fine particle flotation, *Mineral Processing and Extractive Metallurgy Review*, vol. 5, no. 1-4. pp. 101–122. ◆

BM
BASE METALS
2018

Copper Cobalt Africa

In Association with

The 9TH Southern African Base Metals Conference

9–12 July 2018

Avani Victoria Falls Resort, Livingstone, Zambia

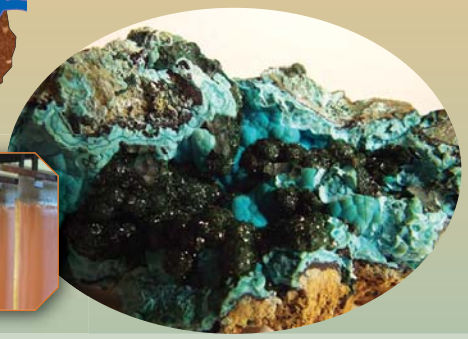

SAIMM is proud to host the Second Copper Cobalt Africa Conference in the heart of Africa

To be held in Livingstone, Zambia, this anticipated and prestigious event provides a unique forum for discussion, sharing of experience and knowledge, and networking for all those interested in the processing of copper and cobalt in an African context, in one of the world's most spectacular settings - the Victoria Falls.

The African Copper Belt is again experiencing a resurgence of activity following the commodity downturn of recent years. A significant proportion of capital spending, project development, operational expansions, and metal value production in the Southern African mining industry take place in this region. The geology and mineralogy of the ores are significantly different to those in other major copper-producing regions of the world, often having very high grades as well as the presence of cobalt. Both mining and metallurgy present some unique challenges, not only in the technical arena, but also with respect to logistics and supply chain, human capital, community engagement, and legislative issues. This conference provides a platform for discussion of a range of topics, spanning the value chain from exploration, projects, through mining and processing, to recycling and secondary value addition.

For international participants, this conference offers an ideal opportunity to gain in-depth knowledge of and exposure to the African copper and cobalt industries, and to better understand the various facets of mining and processing in this part of the world.

Jointly hosted by the Mining and Metallurgy Technical Programme Committees of the Southern African Institute of Mining and Metallurgy (SAIMM), this conference aims to:

- Promote dialogue between the mining and metallurgical disciplines on common challenges facing the industry
- Enhance understanding of new and existing technologies that can lead to safe and optimal resource utilization
- Encourage participation and build capacity amongst young and emerging professionals from the Copper Belt region.

The organizing committee looks forward to your participation.

Conference Topics

- Mineralogy
- Exploration and new projects
- Open-cast mining
- Underground mining
- Rock engineering
- Mine planning
- Mineral resource management
- Geometallurgy
- Minerals processing
- Pyrometallurgy
- Hydrometallurgy
- Current operational practices and improvements
- Project development and execution
- Novel technologies for this industry
- Socio-economic challenges
- Recycling
- Waste treatment and minimization
- Environmental issues

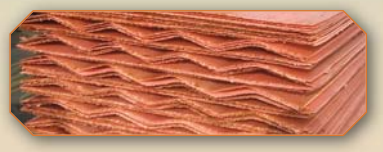

To add your name to the mailing list and to receive further information, please e-mail your contact details to: Gugu Charlie: Conference Co-ordinator
SAIMM, P O Box 61127, Marshalltown 2107, Tel: +27 (0) 11 834-1273/7
E-mail: gugu@saimm.co.za, Website: http://www.saimm.co.za

SAIMM
THE SOUTHERN AFRICAN INSTITUTE OF MINING AND METALLURGY

http://dx.doi.org/10.17159/2411-9717/2018/v118n1a9

A yielding bolt – grouting support design for a soft-rock roadway under high stress: a case study of the Yuandian No. 2 coal mine in China

by X. Sun*, L. Wang*, Y. Lu*, B. Jiang*, Z. Li*, and J. Zhang†

Synopsis

The stabilization of roadways in soft rock under high stress has always been a major concern for deep underground coal mines. This paper describes a case study focusing on the stability of a soft-rock roadway in Yuandian coal mine in Anhui Province, China. The Beiyi main return roadway in this mine was primarily supported by U-steel support; however, considerable deformation and severe failures occurred. Therefore, a new support design, the yielding bolt – grouting support design, was proposed based on the physical and mechanical parameters, *in situ* stress measurements, and the failure characteristics of the roadway. The mechanics of the yielding bolt – grouting support was analysed and compared to the normal bolt – grouting support. A field experiment was conducted in a 100 m long section of the roadway. The monitoring results showed that compared with the old support, the new support design reduced the deformations of roof, floor, and rib by 41.4%, 56.1%, and 64.7% respectively, and the maximum deformation rate decreased from 15.12 mm/d to 9.28 mm/d. This case study indicates that the yielding bolt – grouting support design is an effective method to support roadways in soft rock under high stress.

Keywords
stabilization, soft roadway, yielding bolt, grouting, U-steel support.

Introduction

The stabilization of roadways in soft rock under high stress has been a major concern in deep underground coal mines (He, 2014; Li *et al.*, 2015). Especially after absorbing underground water or water vapour, the rock surrounding these roadways undergoes considerable weakening and swelling (Erguler and Ulusay, 2009; Wasantha and Ranjith, 2014). Under high overburden and tectonic stresses, the roadway and the surrounding rock commonly display the following characteristics: (a) large displacements, (b) high deformation rates, and (c) long deformation time (Lu *et al.*, 2010; Kang, Liu, and Xi, 2014). The conventional support structure cannot adapt to the excessive deformation, which leads to damage of the support structure (loosening or breaking of the bolts, twisting of the U-steel legs). The instability of the roadway not only reduces its functionality, but also constitutes a safety hazard.

Numerous studies have investigated the deformation and failure mechanisms in deeply buried soft-rock roadways (He, 2014; Guo, Qian, and Wang, 2009; Gao *et al.*, 2010; Shen, 2014; Jiang *et al.*, 2015; Wang *et al.*, 2016). The deformation and failure mechanisms can be summarized as follows:

(1) Low strength of the surrounding rock, with development of fractures
(2) Weakening of the surrounding rock by absorption of water
(3) Swelling of the clay minerals after absorbing water
(4) Complicated stress environment
(5) Inappropriate support parameters and design.

Many support systems have been proposed to control the deformation and failure of soft-rock roadways. He (2006, 2014) developed a new type of anchor bolt with constant resistance and large deformation; Guo, Qian, and Wang (2009) suggested a coupled bolt-mesh-anchor-truss support technology; Gao *et al.* (2010) developed the concrete-filled steel tube support; Lu, Wang, and Zhang (2011) proposed a yielding support system with yielding bolts, anchor cables, and metal mesh; Wang *et al.* (2016) proposed a coupled bolting – grouting support technology with a grouting anchor and a grouting bolt.

Taking a soft-rock roadway as engineering background, and based on the deformation and failure mechanisms, we propose a new support technology, the yielding bolt – grouting support. The support mechanisms and mechanical characteristics of the yielding bolt – grouting support are analysed and compared with the bolt – grouting support

* *State Key Laboratory for Geomechanics and Deep Underground Engineering, China University of Mining and Technology, China.*
‡ *Faculty of Architecture and Civil Engineering, Huaiyin Institute of Technology, China.*
 ISSN 2225-6253. Paper received Jul. 2016; revised paper received Aug. 2017.

method. A field experiment has been carried out, and the monitoring data indicates that the deformation of the Beiyi main return way has been controlled by the new support technology. This case provides a useful reference for the design of roadway support in soft rock.

Geology and engineering background

The Yuandian No. 2 coal mine in Anhui Province, China, has a mining area of 41.60 km² (10.9–13.3 km from east to west and 1.3–5.3 km from south to north) with an estimated production capacity of 1.5 Mt/a. The depth of the Beiyi main return way is approximately 600 m. The tunnelling direction of the roadway is 31° north by east. The cross-section of the roadway is a semicircular arch. The walls are 1.5 m high, the arch is 2.7 m high, and the net width of the roadway is 5.4 m. The dip angle of the rock strata is 15–25°; the roadway passes through weak strata, such as mudstone, siltstone, and sandy mudstone (Figure 1). The lithology of the roof and floor is mudstone with a thickness of 7.5 m and 3.0 m respectively; the lithology of the two ribs is mudstone and siltstone. The strength and bearing capacity of the surrounding rock is very low.

There are many faults in the Yuandian No. 2 coal mine, most of which strike northeast. In total, 107 geological sites were drilled to explore the characteristics and locations of the faults, and a total of 44 (39%) boreholes encountered faults. There are two faults in the area near the Beiyi main return way that affect the surrounding bedrock (Figure 2), creating fractures and secondary faults. The main parameters of the two faults are listed in Table I. Since the working face of the Beiyi main return way had to pass through fault WF107 (Figure 2), the effect on excavation was very marked. The other fault also had some effect on the excavation, but it was not as serious as that of fault WF107.

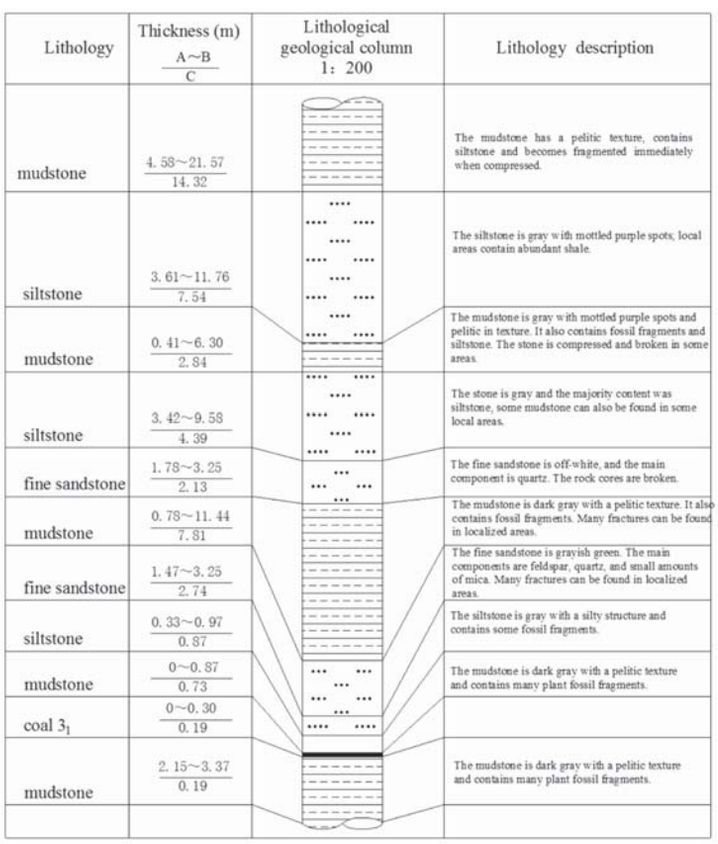

Figure 1—Stratigraphic column of the Beiyi main return way. *A* represents the minimum thickness of the rock stratum, *B* represents the maximum thickness of the rock stratum, and *C* represents the average thickness of the rock stratum

Table I

Main parameters of the two faults

Fault	Strike (°)	Inclination (°)	Inclination angle (°)	Fault throw (m)	Effect on excavation
WF107	20	110	70	0–5	Strong
WF49	90	180	60–70	0–120	Weak

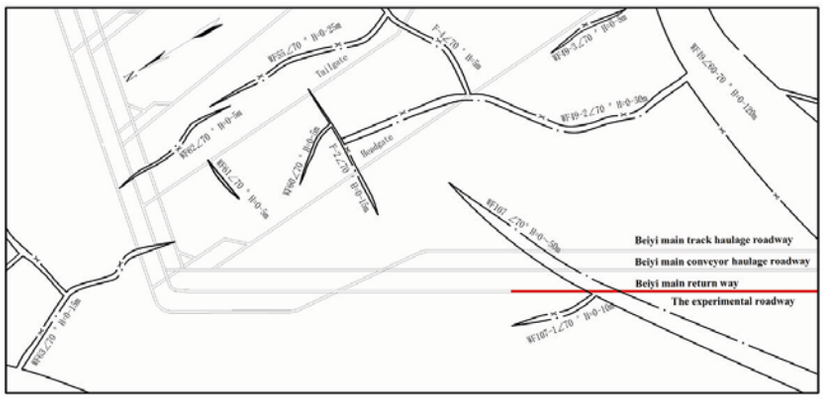

Figure 2—The distribution of faults in the No. 104 mining area. The roadway highlighted red is the experimental roadway

Primarily, U-steel support was used as the permanent support to maintain the roadway stability. A cross-section of the roadway and the supporting structure is shown in Figure 3. The support parameters are as follows (listed in Table II): U-steel lapped length 500 mm, and U-steel interval 600 mm. A layer of metal mesh is installed to fill the interval between the surrounding rock and the U-type steel, with a mesh specification of ø8×800 × ø12×650 and a mesh size of 80 × 80 mm. The thickness of the shotcrete between the U-steel supports is 150 mm, and the strength of the sprayed concrete is 20 MPa. Locked lag bolts (Figure 3) with a diameter of 22 mm and a length of 2800 mm were installed in the two ribs approximately 1200 mm above the floor. They were used to apply a pre-tightening force to keep the U-steel support in close contact with the surrounding rock.

Although the load-bearing capacity of the support was very high, macroscopic deformation and failure of the main roadway occurred within a week, especially in the two ribs and floor. In the two ribs, some locked lag bolts were pulled out or broken within two weeks after excavation (Figure 4a), and severe distortion of the U-steel support (Figure 4b) and falling of the sprayed concrete were prevalent in the roadway after one month. Timber props with a diameter of approximately 300 mm were set up to help mitigate the substantial deformation of the roadway (Figure 4d). The roadway floor heave (Figure 4c) was so serious that the concrete ditch was broken several times and was replaced with a steel tank. The results suggest that the traditional U-steel support design could not control the deformation of the roadway effectively under high stress. The roadway with this support required repair and the daily procedures of transport, ventilation, and safe production could not be guaranteed, therefore the costs of the production increased significantly.

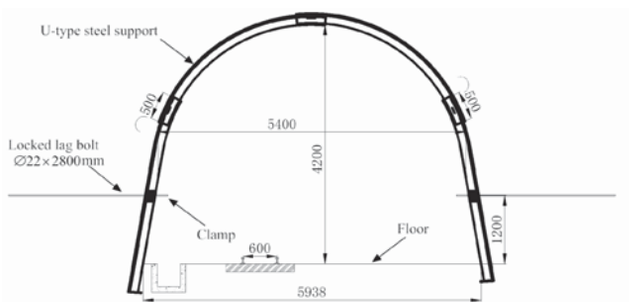

Figure 3—The design of the old roadway support

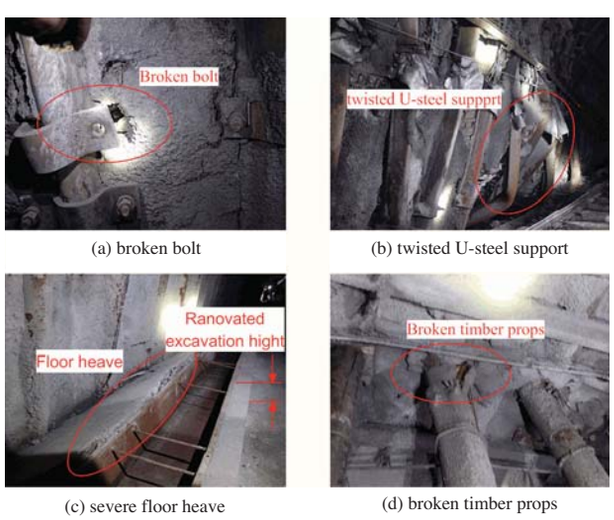

(a) broken bolt (b) twisted U-steel support

(c) severe floor heave (d) broken timber props

Figure 4—The deformation and failure characteristics of the Beiyi main return way with the old support design

Table II

Support parameters of the roadway with the old support design

U-steel		Locked lag bolt			Metal mesh	
Interval (mm)	Lapped length (mm)	Diameter (mm)	Length (mm)	Pre-tightening force (N·m)	Specification (mm)	Mesh size (mm)
600	500	22	2800	300	Φ8×80 0× Φ12×650	80×80

Failure mechanics of the main return way

Physical and mechanical characteristics of surrounding rock

The surrounding rock is primarily mudstone, sandy mudstone, and siltstone. The roof and the two ribs consist of mudstone and siltstone with localized fine sandstone, while the floor is mainly siltstone and mudstone. Most of the surrounding strata are soft rock affected by faults and high tectonic stresses. With widespread development of fractures and fissures in the surrounding rock, the rock mass strength is very low. Lithological samples were collected from the surrounding rock of the Beiyi main return way, and conventional physical and mechanical tests (uniaxial compression testing, triaxial compression experiments, and Brazil disk split test) were conducted with an MTS 815.02 rock servohydraulic machine. The test results are shown in Table III. The mudstone and the sandy mudstone were typical soft rock, with a uniaxial compressive strength of 25.8 MPa and 28.7 MPa, respectively. The uniaxial compressive strength of the siltstone was about 52.4 MPa. Absorption of water reduced the strength of the rocks significantly, especially the mudstone. Uniaxial compression testing of the saturated mudstone indicated (Figure 5) that the UCS and modulus were reduced by 72.4% and 76% respectively, compared with the original samples.

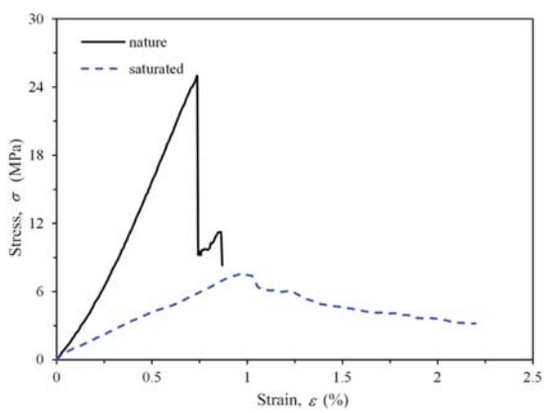

Figure 5—The stress-strain curve of the mudstone. The mudstone samples were immersed in water for 72 hours to saturate them with water

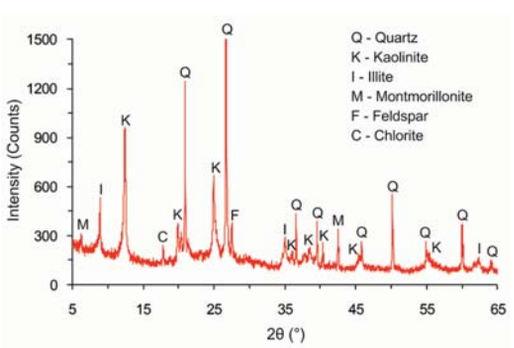

Figure 6—X-ray diffraction pattern of the tested mudstone

During excavation, the mudstone exhibited obvious weakening and swelling after contact with water. Zhou and He (2008) pointed out that montmorillonite is extremely sensitive to water, especially Na-montmorillonite, which can undergo a volume expansion of 600–1000%. Li *et al.* (2007, 2010) investigated the deformation characteristic of mudstone from the Guhanshan mine, and the results indicated that the strain of the saturated mudstone was 7–8 times larger than that of the original sample. Erguler and Ulusay (2009) also concluded that the clay-rich rocks can expand, undergoing a dramatic reduction of the UCS, average modulus, and tensile strength (more than 90%) after absorbing water.

The mudstone collected from the Beiyi main return way was analysed using X-ray diffraction. The analysis (Figure 6) indicated that the mudstone is composed of quartz, feldspar, and clay minerals (including kaoline, illite, and montmorillonite). The content of clay minerals, which are very sensitive to environmental factors, is greater than 39%. Using scanning electron microscopy (SEM) techniques to observe the micromorphology and composition of the roof mudstone, we found that the mudstone is relatively unconsolidated and has a well-developed porosity. The hard skeleton grains, such as quartz and feldspar, are enclosed in the clay minerals. The single flaky crystals of minerals are distributed in a non-uniform, honeycomb-like pattern (Figure 7). This porous and loose microstructure could allow the mudstone to absorb water from the air, fractures in the rock mass, and construction process more easily, which would have an adverse effect on the long-term stability of the surrounding rock of the roadway. The Beiyi main return way was exposed to air after excavation, and this accelerated deformation and fracturing.

In situ stresses

Three stress test stations are situated according to the geological and engineering conditions, but only the no. 3 station is close to the Beiyi main return way. A schematic diagram of the location of the no. 3 test site is shown in

Table III

Rock mechanics parameters

Strata	Properties of the surrounding rock			
	Young's modulus (GPa)	Poisson's ratio	UCS (MPa)	Tensile strength (MPa)
Mudstone	3.10	0.3	25.8	2.7
Sandy mudstone	4.6	0.24	28.7	3.6
Siltstone	9.1	0.2	52.4	4.5

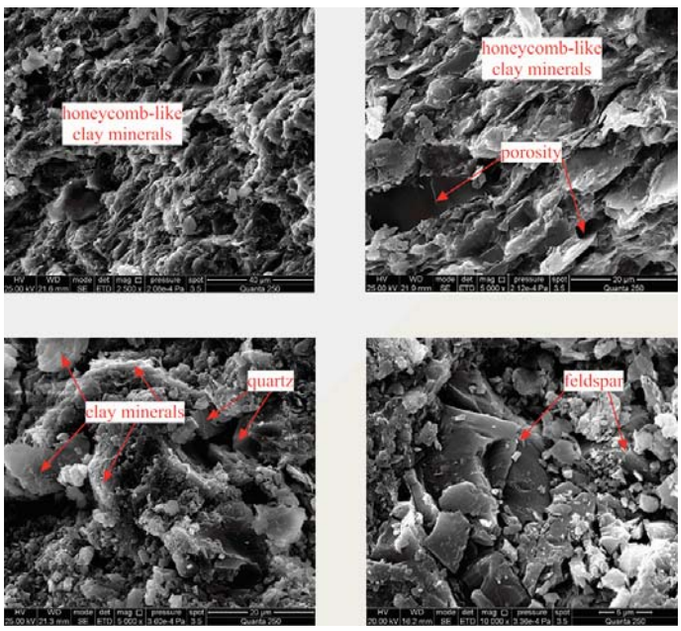

Figure 7—SEM photomicrographs of the tested mudstone

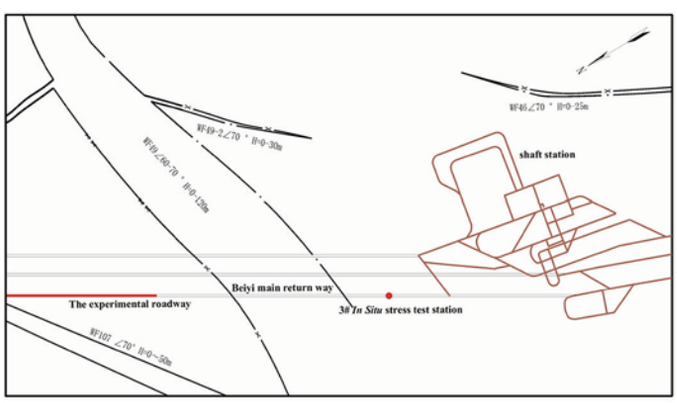

Figure 8—Schematic diagram of the *in situ* stress test station in Yuandian No. 2 Coal Mine

Figure 8. The principal stresses and their directions were determined, and are listed in Table IV. The test results showed that the maximum principal stress was approximately 21 MPa, the direction horizontal, and the azimuth angle between 83° and 86°. The tunnelling direction of the Beiyi main return way is 31° NE, resulting in an angle of approximately 52° between the tunnelling direction and the maximum principal stress direction. The current theoretical research and practical results (Zhao *et al.*, 2015) show that the roadway stability would be affected by the tectonic stress, the influence being greater if the angle between the tunnelling and tectonic stress directions exceeds 45°. The minimum principal stress was approximately 10 MPa, with a dip angle and azimuth of approximately 7° and 184°, respectively. The vertical principal stress was approximately 14 MPa. The ratio between the maximum principal stress and vertical principal stress was 1.51, which indicated that the mining activities of the Yuandian no. 2 coal mine were affected by the tectonic stress.

Fracture characteristics of the surrounding rock

The fracture development characteristics of the surrounding rock have an important effect on the stability of the roadway. The failure characteristics of the surrounding rock were investigated with an intelligent drill-hole optical imager. The rock surrounding the main roadway can be classified into intact, initial fissure, mining-induced fracture, and rupture zones based on the development of the fractures. After the old support system was damaged, two monitoring sections were arranged in the Beiyi main return way to detect fracture development. Each cross-section included six observation drill-holes (Figure 9) – two in the roof, two in the floor, and two in the ribs. The observation drill-holes were 28 mm in diameter, and the maximum depth was 6.0–8.0 m. The observation results are shown in Figure 10.

As can be seen from Figure 10, the rocks surrounding the roadway consist of mudstone, sandy mudstone, and siltstone. The rupture zones are all found in the shallow

Table IV

Summary of *in situ* stress measurement results

Station no.	Burial depth (m)	Principal stress				Vertical stress (MPa)
		Principle stress	Value (MPa)	Azimuth angle (°)	Dip angle (°)	
1	558.6	σ_1 σ_2 σ_3	21.09 13.95 11.94	83.40 89.97 186.01	10.80 82.41 7.29	13.97
2	556.5	σ_1 σ_2 σ_3	20.91 13.57 9.91	86.39 3.77 183.98	5.86 85.95 7.31	13.91
3	581	σ_1 σ_2 σ_3	21.31 14.61 9.31	85.55 21.99 184.46	8.21 76.84 6.53	14.52

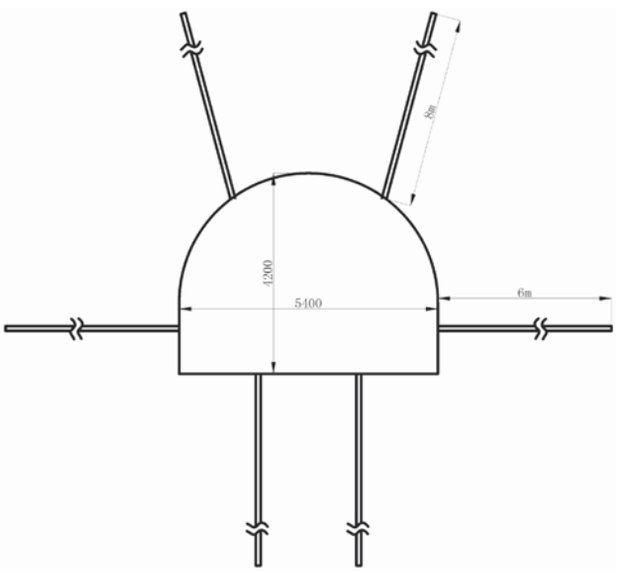

Figure 9—Cross-section of the arrangement of the observation drill-holes

section of the roadway; the fracture depths of the rupture zone for roof, rib, and floor are 3.0 m, 1.7 m, and 1.0 m respectively. Between 2.0 and 4.0 m, there is a soft intercalated layer with a thickness of 1.2 m, consisting of mudstone containing abundant clay minerals. After absorbing water, the mudstone softened and expanded. Because of the wide range and short distance to the roof, the soft intercalated layer would seriously affect the long-term stability of the roadway. Many mining-induced fractures were generated after excavation, with maximum depths of 1.2 m in the roof, 1.6 m in the ribs, and 2.2 m in the floor. There were some initial fissures in deep surrounding rock, but they had little influence on the stability of the roadway.

The design of yielding bolt – grouting support

The yielding grouting bolt and its mechanical characteristics

The main support material used in this yielding bolt – grouting design is the yielding grouting bolt. comprising a rod, pallet, metal gasket, plastic gasket, nut, and yielding tube (Figure 11b). There are many air-holes distributed on the hollow rod for the grout permeating into the rock

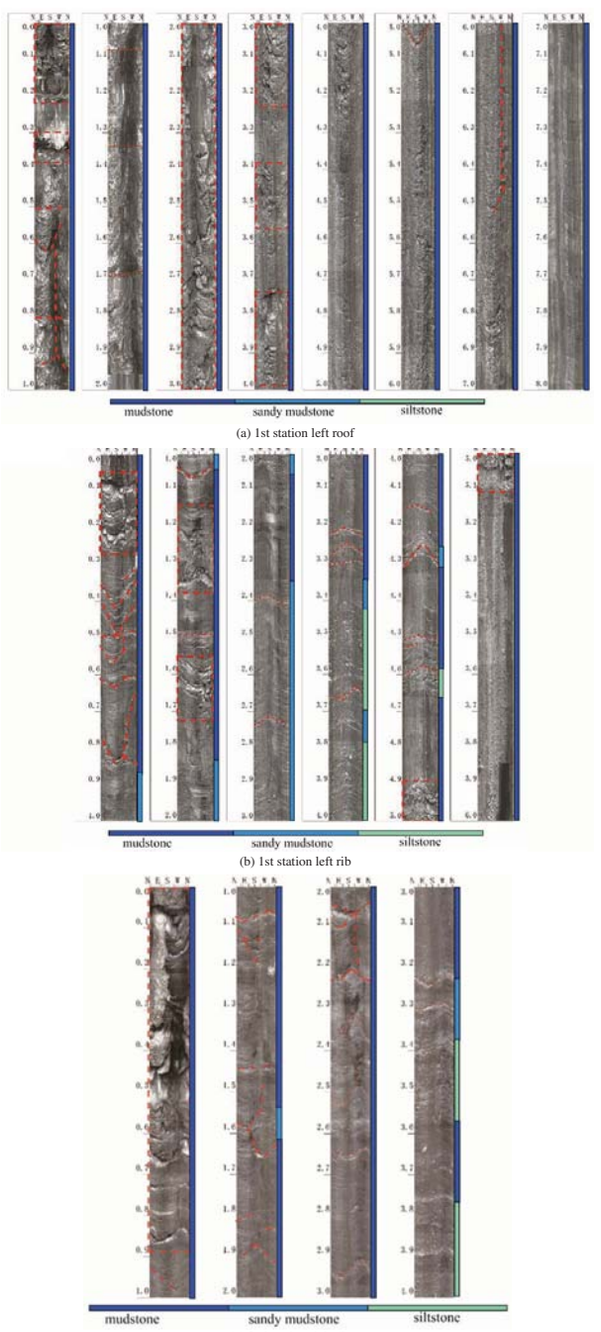

Figure 10—Fractures in the surrounding rock from the drill hole optical imager. Rupture zone ⁚⁚ Mining-induced fracture – – Initial fissure ·····

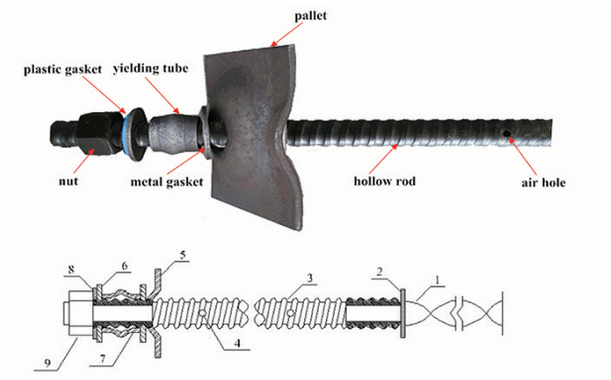

1—Twist anchor head; 2—Resin cartridge damper; 3—Rod; 4—Air hole; 5—Pallet; 6—Metal gasket; 7—Yielding tube; 8—Plastic gasket; 9—Nut

(a) The yielding grouting bolt

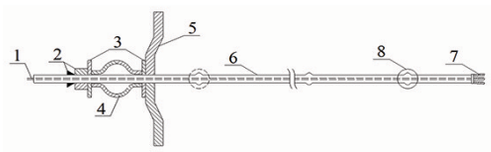

1—Rubber grouting pipe; 2—Anchor cable locks; 3—Metal gasket; 4—Yielding tube; 5—Pallet; 6—Anchor cable rope body; 7—Twist anchor head; 8—grout output section

(b) Schematic diagram of the yielding grouting bolt

Figure 11—The main support elements of the yielding bolt-grouting support

fractures. Bolt pull-out tests were conducted and the results are shown in Figure 12. The load-displacement curve of the grouting bolt (Figure 12a) can be divided into three stages: (a) elastic stage, (b) yield stage, and (c) broken stage. The length of the yield stage accounts for 86.4% of the total deformation. After installation, the working condition of the grouting bolt was generally in this stage until the grout permeated into the surrounding rock. However, in high stress conditions, the deformation rate was high and the working condition of the grouting bolt always proceeded to the broken stage before grouting. Compared with the grouting bolt, a new yield stage was added to the load-displacement curve of the yielding grouting bolt before the rod yielded (Figure 12b). The length of the first yield stage can be varied by changing the structural features of the yielding tube. The existence of the first yield stage ensures that the working condition of the yielding grouting bolt is in the second yield stage and protects the yielding bolt – grouting support system from damage. The yielding grouting cable anchor consists of a rubber grouting pipe, anchor cable locks, metal gasket, yielding tube, pallet, anchor cable rope body, and twist anchor head. Its mechanical characteristics are similar to those of the yielding grouting bolt.

Compared with the traditional grouting bolt, the most obvious characteristic of the yielding grouting bolt is that a yielding tube is added to the bolt tail. A typical load-displacement curve of a yielding tube is shown in Figure 13. The load-displacement curve can be divided into three stages (Lu, Wang, and Zhang, 2011): elastic stage, yield stage, and plastic stage. The mechanical characteristics of the yielding tube mainly refer to the yielding load and yielding length. The load at the beginning of the yield stage is called the yielding load, and the length of the yield stage represents the yielding length.

Mechanics of yielding bolt – grouting support

Because of the intense deformation and failure of the surrounding rock, the stability of the Beiyi main return way could not be ensured by traditional support technology. Therefore, the yielding bolt – grouting support technology, which combines yielding grouting bolts (cable anchors) with other supporting structures, was proposed to stabilize the roadway. The mechanics of yielding bolt – grouting support can be interpreted with reference to five aspects.

(1) Compared with the traditional support system, the yielding bolt-grouting support can extend the maximum deformation that the support structure can accommodate. A schematic diagram of the traditional bolt – grouting support and yielding bolt – grouting support is shown in Figure 14. With the addition of a new yield stage, the maximum deformation of the yielding bolt – grouting support is much larger than that of the traditional support. Under high overburden and tectonic stresses, the deformation is large and the deformation rate is high in the earlier stages of the excavation. In the process of construction, there is about two weeks before grouting is prepared. With increasing deformation of the surrounding rock, the grouting bolt in the traditional support breaks while the yielding grouting bolt is still at the second yields tage with a flattened yielding tube. The yielding bolt – grouting support prevents the support system from proceeding to the broken stage before grouting is prepared.

(2) By changing the yielding length of the yielding tube, we can optimize the grouting time to obtain a better grouting effect. Lu *et al.* (2012) considered that there are two disadvantages if the grout permeates into the rock mass too early. One is that the fracture aperture is not large enough for the grout grains to permeate

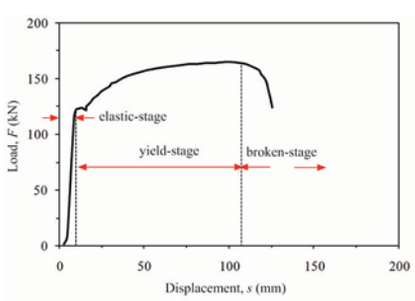

(a) The load-displacement curve of the grouting bolt.

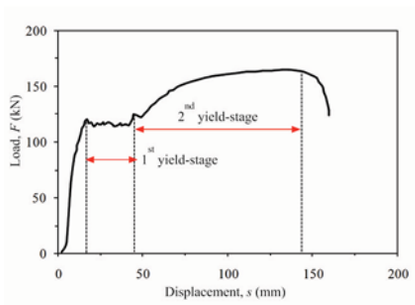

(b) The load-displacement curve of the yielding grouting bolt.

Figure 12—The load-displacement curves of the grouting-bolt and yielding-grouting-bolt

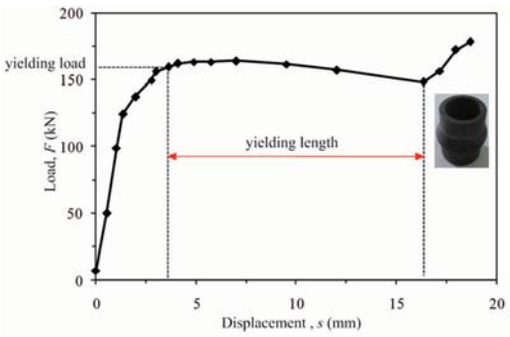

Figure 13—The yielding tube and its load displacement curve

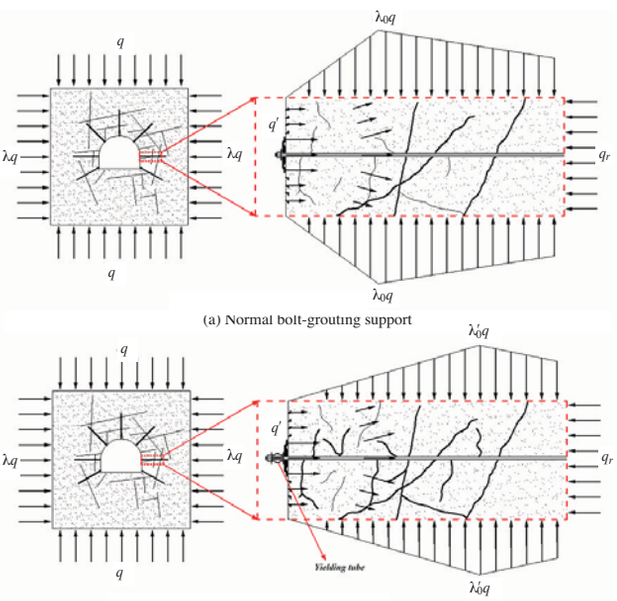

Figure 14—Schematic diagram of the mechanics of the yielding bolt-grouting support. q is the vertical stress; q' is the equivalent support resistance of the bolts; λ is the side pressure coefficient; λ_0 is the stress concentration coefficient under normal bolt-grouting support; λ_0' is the stress concentration coefficient under yielding bolt-grouting support; the bold lines represent the grouted fractures

into it. Eklund and Stille (2008) conducted extensive laboratory tests and concluded that the grain size of the grout should be at least 2–3 times smaller than the fracture aperture; otherwise, the channels in the fractures would be obstructed by clogging of the cement grains. The other disadvantage is that the grouted fractures are still propagating and new fractures are continually generated under high stress after grouting. As a consequence, the grouted factures are re-broken and the control of the rock surrounding the roadway fails.

With the traditional support system, there is not enough extra deformation available to adjust the grouting time according to the fracture development in the surrounding rock. However, with the yielding bolt – grouting support the yielding length of the yielding tube can be changed in order to control the grouting time. In this way, the grouting effect and roadway stabilization have been improved. Moreover, the deformation of the yielding tube acts as an indicator to remind the miner to permeate the grout into the surrounding rock.

(3) With more effective grouting, the yielding bolt – grouting support can more effectively prevent the clay minerals from absorbing water, and reduce the adverse effects of swelling and weakening. Grouting fills the fractures and dramatically reduces the permeability of the surrounding rock (Eriksson and Stille, 2000; Yang, He, and Chen, 2001). Due to propagation of the grouted fractures and newly generated fractures, the grouting effect of the traditional support is not good enough to prevent the clay-rich rock from absorbing water. With excellent grouting quality obtained with the yielding bolt – grouting support, the rock permeability is much lower, and the clay-rich rock has less opportunity to contact water. Therefore, the yielding bolt – grouting support can more effectively prevent the surrounding rock from weakening and swelling due to contact with water.

(4) Compared with the traditional support system, the concentrated stresses caused by the excavation are transferred to the deeper surrounding rock and the degree of stress concentration is much less. Previous studies showed that the concentrated stress will be generated in the shallow surrounding rock of the roadway after excavation, and will break the rock mass and reduce the bearing capacity. The concentrated stress will then move into the deeper surrounding rock (Fahimifar and Hedayat, 2010; Zhang, Zhao, and Meng, 2013). For the traditional bolt – grouting support, as the maximum deformation of the support system is limited, the degree of fracture development is low and the stress is concentrated in the shallow surrounding rock. Assuming that the concentrated stress is $\lambda_0 q$ (q is the *in situ* stress, λ_0 is the stress concentration coefficient), the stress distribution is simplified as in Figure 14a. Because the concentrated stress is still in the shallow surrounding rock, the secondary damage would occur in the grout-filled cracks under the high concentrated stress after grouting. However, compared with the traditional bolt – grouting support, the degree of fracture development is much higher in the shallow surrounding rock under the yielding bolt – grouting support before grouting. The bearing capacity of the shallow surrounding rock declines and the stress has to transfer into deeper surrounding rock. As a result, the concentrated stress declines to $\lambda_0' q$ ($1< \lambda_0' 0< \lambda'$) (Figure 14b) and its location moves into deeper surrounding rock.

(5) With the better grouting effect, the bearing capacity of the rock mass is much higher than under traditional support. As one of the main active support technologies, grouting can fill the cracks, improve the surrounding rock strength, and enhance the resistance to deformation (Kikuchi *et al.*, 1997; Varol and Dalgıç, 2006; Nikbakhtan and Osanloo, 2009). However, the grouting effect was not always

satisfactory with the traditional grouting support, which would directly affect the stability of the roadway after grouting. With better grouting quality, the fractures in the surrounding rock under yielding bolt grouting support are filled with grout. After grout consolidation, the broken rock is bonded and the strength and stiffness of are improved, thus the bearing capacity of the surrounding rock is greatly increased.

The new support design

After investigating the deformation and failure mechanics of the Beiyi main return way, we found that the reasons for the roadway instability could be summarized as follows:

(a) Soft and weak surrounding rock due to the widespread development of fractures
(b) Weakening and swelling due to the effects of water
(c) High tectonic and overburden stress
(d) Inappropriate support.

Bolt grouting support is an ideal choice, because grouting can seal fractures, bond the broken rock, improve the strength of the surrounding rock, and enhance the resistance to deformation (Kikuchi *et al.*, 1997; Varol and Dalgıç, 2006; Nikbakhtan and Osanloo, 2009). However, the deformation and deformation rate are very large during the early stage of excavation, the support system may be damaged before grouting can be completed, and the grouted fractures would be broken again. To solve this problem, the yielding bolt – grouting support method is proposed, with the new support design shown in Figure 15. The support parameters are as follows.

(1) Since the yielding grouting bolts (anchors) have been added to the yielding bolt-grouting support scheme, the density of U-steel supports can be reduced. The U-steel interval was extended from 600 mm to 700 mm to reduce the labour requirements and support costs.
(2) Yielding grouting bolt: according to the fracture characteristics analysis, the maximum development depth of the mining-induced fractures is 2.2 m, and the minimal bond-anchorage length is at least 0.3 m. Therefore, the length of the yielding grouting bolt is 2.6 m and the specification of the yielding bolt-grouting was ø25 × 2600 mm. Since the interval between the U-steel supports is extended to 700 mm, the bolts are added to supply the support load. The spacing between the bolts along the roadway axis is 1.4 m, and the spacing radially along the roadway is 1.5 m. Eleven yielding grouting bolts were installed on each cross-section, with five in the roof, four in the two ribs, and two in the floor. All the bolts should be under pre-tension. Considering the yielding load of the yielding grouting bolt and construction conditions, the pre-tension load is 70 kN.
(3) Yielding grouting cable anchor: the maximum development depth of the fractures is 6.5 m in the roof, and there is a soft intercalated layer between 4.9 and 5.1 m. To ensure that the cable anchors are bonded into the intact rock, the length of the cable anchors is chosen as 7.0 m. The spacing between the cable anchors along the roadway axis is 2.1 m, and the specification is ø31.5 mm × 7.0 m.
(4) Inverted arch: the floor of the roadway was broken under the tectonic stress, therefore the inverted arch was adopted to control the floor heave. The roadway floor was excavated 0.5 m deeper than necessary and then filled with waste rock and concrete. The grouting bolts, with a specification of ø25 mm × 2.6 m, were then installed. The spacing between the bolts along the roadway axis is 2.1 m, and 2.0 m radially along the roadway.
(5) Grouting reinforcement: the grout used in the support is no. 525 Portland cement with a little additive. The additive increases the stability, fluidity, and expansibility to improve the curing rate and the strength of the anchorage body. The water to cement ratio is between 0.7:1 and 1:1, the grouting pressure of the yielding grouting cable anchor is 4.0 to 6.0 MPa, and the grouting time is 600 to 800 seconds. The grouting pressure of the yielding grouting bolt was 2.0 to 3.0 MPa, and the grouting time was 250 to 400 seconds.

Field experiment and monitoring

A field experiment was conducted in the mine to test the effectiveness of the new ' 'yielding bolt – grouting' design and compare it to the old design. A 100 m long section of the Beiyi main return way was chosen to compare the two support designs. Half of the roadway was supported with the old design, and the other half by the new yielding bolt – grouting design. Four monitoring stations were arranged to measure the deformation of the roadway. Two stations

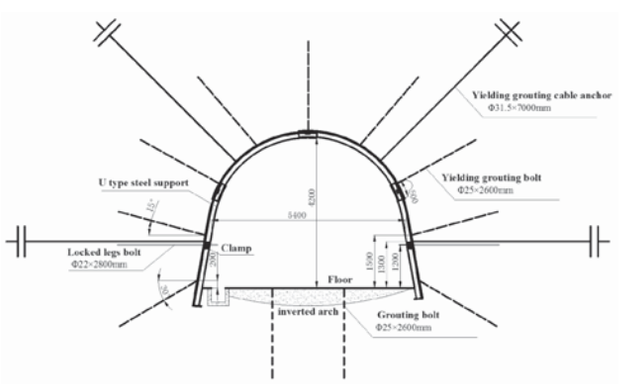

(a) Roadway support cross-section

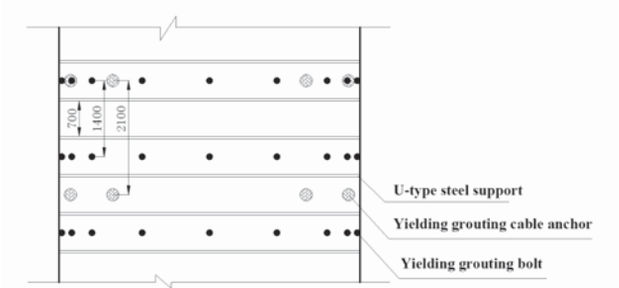

(b) Roadway support plan

Figure 15—The new support design of the roadway

(stations I and II) were in the experimental roadway with new support design, and the other two (stations III and IV) were in the section with old design. The monitoring locations in both the new and old designs were separated by 20 m as shown in Figure 16a. The deformation of the surrounding rock was monitored by two extensometers installed in each of the four monitoring sections. One extensometer was installed in the two ribs of the roadway between points B and C, and the other between points D and Point E as shown in Figure 16b. BC is the horizontal measuring line, and DE the vertical measuring line. 'A' is the intersection point of segments BC and DE. A decrease of segment BC indicates the inward displacement of the two ribs, while a decrease of segment AD represents displacement of the roof, and a decrease of AE indicates displacement of the floor. The technical specifications of the extensometers were: measurement range 0 to 1000 mm, and accuracy 0.2 mm.

The extensometers were installed immediately after the roadway support structure was completed, and the data from the extensometers was read every five days. All the data was collected and plotted to analyse the deformation of the roadway surrounding rock. The grout was injected approximately 20 days after completion of the roadway support. The deformation of the surrounding rock was monitored for 65 days, and the results are shown in Figure 17.

It is clear that the displacements of the roadway with the new support design are much smaller than with the old support design. In the first 20 days after excavation, the maximum displacements of roof, floor, and left rib with the yielding bolt – grouting were 92.4 mm, 109.2 mm, and 63.6 mm respectively, compared with 118.6 mm, 169.2 mm, and 119.1 mm with the old support design. Although the displacements for the yielding bolt – grouting support are smaller, there is no dramatic difference between the two support schemes before grouting. This is because the support load densities (the support load per square metre) of the two support schemes are almost the same. After grouting, this

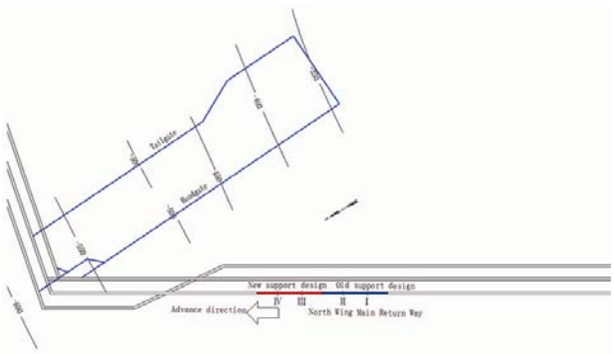

(a) Location of the monitoring stations

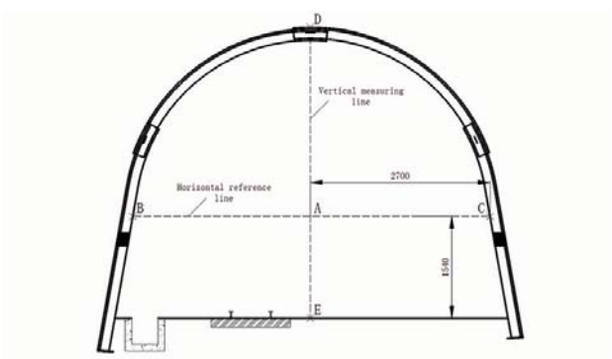

(b) Monitoring sites for the deformation of the roadway

Figure 16—The location of monitoring stations (a) and monitoring design (b)

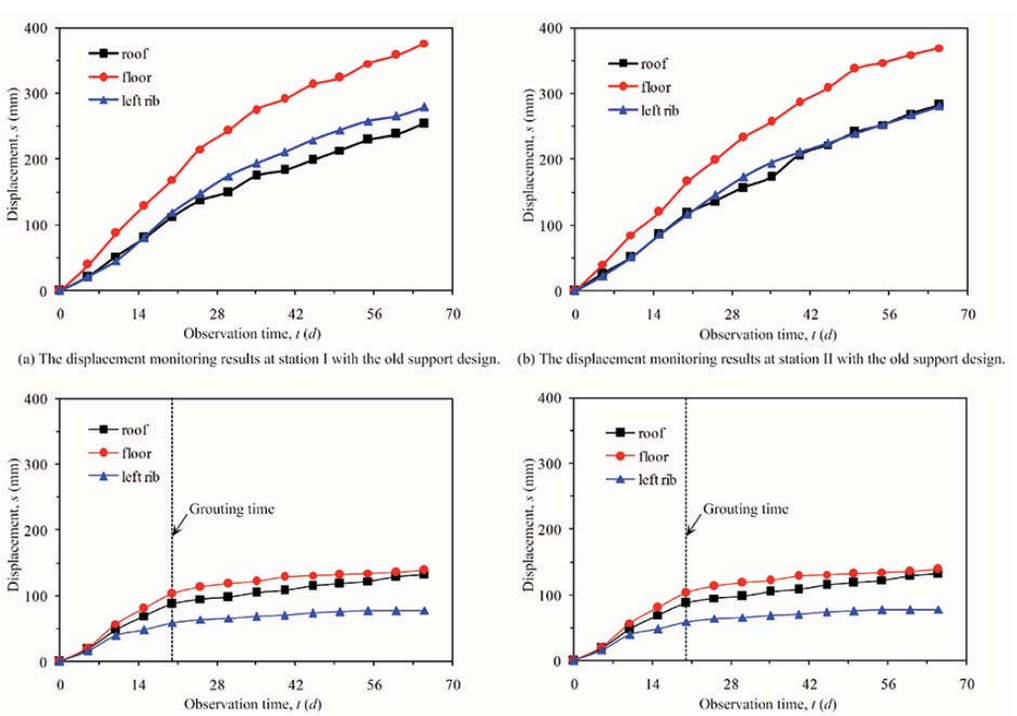

(a) The displacement monitoring results at station I with the old support design. (b) The displacement monitoring results at station II with the old support design.

(c) The displcement monitoring results at station III with the new support design. (d) The displacement monitoring results at station IV with the new support design.

Figure 17—Results of the displacement monitoring with different roadway support designs

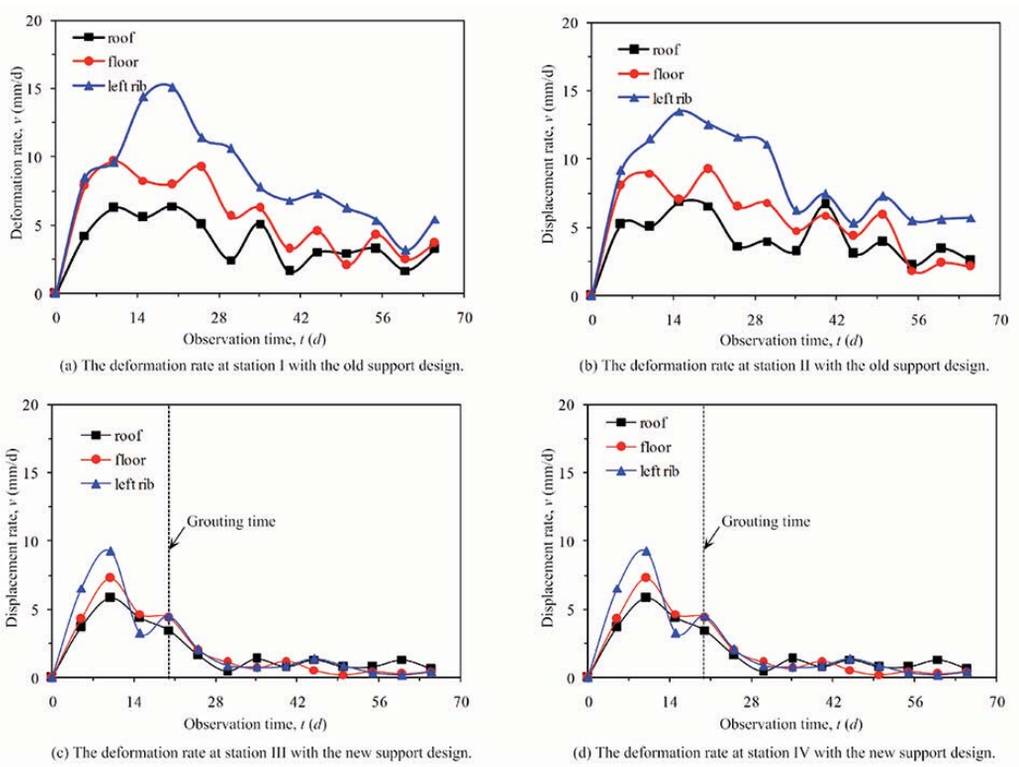

Figure 18—The deformation rate of the roadway with different support designs

situation changes. The displacements of the roof, floor, and rib at the monitoring station I (in the old support design section) were 254.4 mm, 376.8 mm, and 279.8 mm, respectively, after 65 days. Similar results can be seen at station II. The resulting instability of the roadway necessitated repair work to ensure safety and continued production. With the new support design, the maximum displacements of roof, floor and rib were 149 mm, 165.4 mm, and 98.8 mm, respectively. Compared with the old support design, the new support design reduced the deformations of roof, floor, and rib by 41.4%, 56.1%, and 64.7% respectively.

Since the support load density (the support load per square metre) of the yielding bolt – grouting support is only slightly larger than that of the old support design, the deformation rates of the surrounding rocks are very high for both designs before grouting (Figure 18). However, the displacement rates of the roadway with the yielding bolt – grouting support dropped sharply after grouting, while the deformation continued to increase rapidly in the old support design section. The deformation rate of the left rib in station II decreased by 29.6% (from 15.12 to 10.64 mm/d) in ten days after grouting, while the deformation rate in station IV decreased by 80.5% (from 4.52 to 0.88 mm/d) in the same period. After inspection of the support systems we found that some U-steel supports had been twisted and 17 bolts had broken in the old support design section, while no damage was found in the yielding bolt – grouting support system. After the support elements were damaged, the bearing capacity of the old support system would drop rapidly, and this is the most important reason why the old design could not control the deformation and failure of the Beiyi main return way. After 65 days, the maximum displacements of roof, floor, and rib were 3.24 mm/d, 3.68 mm/d, and 5.44 mm/d, respectively, which led to considerable deformation. With the new support design, all the deformation rates of the surrounding rock dropped to less than 1.0 mm/d. Therefore, the deformation of the Beiyi main return way was controlled efficiently by the yielding bolt – grouting support, as shown in Figure 19. This significantly reduces roadway maintenance and repair costs. Compared to the old support system, the yielding bolt-grouting support design could reduce support costs by 985.2 Yuan (US$159.60) per metre of roadway. The full length of the Beiyi main return way is 1285 m, so 1 265 982 Yuan US$205 089 would be saved by this design. The yielding bolt – grouting support therefore offers considerable economic and as well as technical benefits.

Figure 19—The supporting effect of the roadway with the yielding bolt-grouting support

Conclusions

A case study on the effect of the yielding bolt – grouting support design on the stability of a roadway in soft rock was conducted in an underground coal mine in Huaibei Province, China. The surrounding rock was very weak and contained an abundance of clay minerals, which were vulnerable to weathering. The roadway experienced substantial deformation with the old support design, therefore a new support design was proposed.

The deformation and failure of the Beiyi main return way can be attributed to four reasons: (1) abundant clay minerals in the surrounding rock, (2) high tectonic stress, (3) widespread development of fractures in the surrounding rock, (4) unscientific support design.

Compared with traditional support, the mechanics of the yielding bolt – grouting support system were analysed and interpreted from five aspects:

(1) With larger maximum deformation of the support structure being accommodated, the yielding bolt – grouting support can prevent the support system from proceeding to the broken stage before grouting
(2) Grouting time can be optimized to obtain a better grouting effect
(3) Clay minerals are prevented from absorbing water and the effects of swelling and weakening are reduced
(4) The degree of stress concentration is reduced and the concentrated stresses are transferred into deeper surrounding rock
(5) The bearing capacity and resistance to deformation of the surrounding rock are improved.

A field experiment was performed in the mine along a 100 m section of roadway. The monitoring results indicated that the new support design could significantly improve the stability of the Beiyi main return way. Compared to the old support system, the yielding bolt – grouting support design significantly reduces roadway maintenance and repair costs. The new support system has great prospects for broader application.

Acknowledgments

This work was supported by the National Natural Science Foundation of China (Project No. 51274191 and 51204159), the National Basic Research Program of China (Project No. 2014CB046905), the National Natural Science Foundation of China (Project No. 51708245), the Natural Science Foundation for Colleges, Universities in Jiangsu Province (Project No. 17KJB130003 and 17KJA560001), and the Doctoral Fund of the Ministry of Education of China (Project No. 20130095110018). The authors thank the anonymous referees for their careful reading of this paper and valuable suggestions.

The authors declare that there are no conflicts of interest regarding the publication of this paper.

References

Eklund, D. and Stille, H. 2008. Penetrability due to filtration tendency of cement-based grouts. *Tunnelling and Underground Space Technology*, vol. 23, no. 4. pp. 389–398.

Erguler, Z.A. and Ulusay, R. 2009. Water-induced variations in mechanical properties of clay-bearing rocks. *International Journal of Rock Mechanics and Mining Sciences*, vol. 46, no. 2. pp. 355–370.

Eriksson, M., Stille H., and Andersson, J. 2000. Numerical calculations for prediction of grout spread with account for filtration and varying aperture. *Tunnelling and Underground Space Technology*, vol. 15, no. 4. pp. 353–364.

Fahimifar, A. and Hedayat, A.R. 2010. Elastoplastic analysis in conventional tunnelling excavation. *Geotechnical Engineering*, vol. 163, no. 1. pp. 37–45.

Gao, Y., Wang, B., Wang, J., Li, B., Xing, F., Wang, Z., and Jin, T. 2010. Test on structural property and application of concrete-filled steel tube support of deep mine and soft rock roadway. *Chinese Journal of Rock Mechanics and Engineering*, vol. 29, no. 1. pp. 2604–2609.

Guo. Z., Qian. L., and Wang. J. 2009. Coupled bolt-mesh-anchor-truss supporting technology and its engineering application to deep soft rock roadway. *Chinese Journal of Rock Mechanics and Engineering*, vol. 28, no. 2. pp. 3914–3919.

He, M. 2006. Rock mechanics and hazard control in deep mining engineering in China. *Rock Mechanics In Underground Construction*. Leung, C.F. and Zhou, Y. X. (eds.). World Scientific, London. pp. 29-46.

He, M. 2014. Progress and challenges of soft rock engineering in depth. *Journal of China Coal Society*, vol. 39, no. 8. pp. 1409-–417.

Jiang, B., Wang, L., Lu, Y., Gu, S., and Sun, X. 2015. Failure mechanism analysis and support design for deep composite soft rock roadway: a case study of the Yangcheng coal mine in China. *Shock and Vibration*, vol. 2015. pp. 1-14.

Kang, Y., Liu, Q., and Xi, H. 2014. Numerical analysis of THM coupling of a deeply buried roadway passing through composite strata and dense faults in a coal mine. *Bulletin of Engineering Geology and the Environment*, vol. 73, no. 1. pp. 77–86.

Kikuchi, K., Igari, T., Mito, Y., and Utsuki, S. 1997. In situ experimental studies on improvement of rock masses by grouting treatment. International *Journal of Rock Mechanics and Mining Sciences*, vol. 34, no. 3–4. pp. 138.e1–138.e14.

Li, G., Dai, T., Lv, F., and Yang J. 2007. Deformation mechanism of swelling rock and its grouting reinforcement techniques. *Journal of Mining & Safety Engineering* , vol. 24, no. 4. pp. 44–4448.

Li, G., Li, Z., and Dai, T. 2010. Mechanical test of swelling rock and prediction of roadway support parameters. *Engineering Mechanics*, vol. 27, no. 2. pp. 96–101.

Li, W., Li, S., Xuan, C., Wang, Q., and Wang, X. 2015. Mechanism and control of failure of rock roadway support in highly stressed soft rock. *Chinese Journal of Rock Mechanics and Engineering*, vol. 34, no. 9. pp. 1836–1848.

Lu, Y., Wang, L., Yang, F., Li, Y., and Chen, H. 2010. Post-peak strain softening mechanical properties of weak rock. *Chinese Journal of Rock Mechanics and Engineering*, vol. 29, no. 3. pp. 640–648.

Lu, Y., Wang, L., and Zhang, B. 2011. An experimental study of a yielding support for roadways constructed in deep broken soft rock under high stress. *Mining Science and Technology* (China), vol. 21, no. 6. pp. 839–844.

Lu, Y., Wang, L., Zhang, B., and Li, Y. 2012. Optimization of bolt-grouting time for soft rock roadway. *Rock & Soil Mechanics,* vol. 33, no. 5. pp. 1395–1401.

Nikbakhtan. B. and Osanloo. M. 2009. Effect of grout pressure and grout flow on soil physical and mechanical properties in jet grouting operations. *International Journal of Rock Mechanics and Mining Sciences*, vol. 46, no. 3. pp. 498–505.

Shen, B. 2014. Coal mine roadway stability in soft rock: a case study. *Rock Mechanics and Rock Engineering*, vol. 47, no. 6. pp. 2225–2238.

Varol, A. and Dalgiç, S. 2006. Grouting applications in the Istanbul metro, Turkey. *Tunnelling and Underground Space Technology*, vol. 21, no. 6. pp. 602–612.

Wang, L., Lu, Y., Huang, Y., and Sun, H. 2016. Deep-shallow coupled bolt-grouting support technology for soft rock roadway in deep mine. *Journal of China University of Mining & Technology*, vol. 45, no. 1. pp. 11–18.

Wasantha, P.L.P. and Ranjith, P.G. 2014. Water-weakening behavior of Hawkesbury sandstone in brittle regime. *Engineering Geology*, vol. 178. pp. 91–101.

Yang, M., He, Y., and Chen, M. 2001. Law of grouting penetrating through fracture network of rock mass. *Journal of Hydraulic Engineering*, vol. 7. pp. 41–46.

Zhou, L. and He M. 2008. Study on mineralogical characteristics of high stress soft rock at depth of Nanshan Mine. *Metal Mine*, vol. 384, no. 6. pp. 73–76.

Zhang, X., Zhao, G., and Meng, X. 2013. Elastoplastic analysis of surrounding rock on circular roadway based on Drucker-Prager yield criterion. *Journal of the China Coal Society*, vol. 38, Supplement. pp. 30–37.

Zhao, W., Han, L., Zhang, Y., Zhao, Z., and Wang, G. 2015. Study on the influence of principal stress on the stability of surrounding rock in deep soft rock roadway. *Journal of Mining and Safety Engineering*, vol. 32, no. 3. pp. 504–510. ◆

http://dx.doi.org/10.17159/2411-9717/2018/v118n1a10

Manufacturing and testing of briquettes from inertinite-rich low-grade coal fines using various binders

by N.T. Leokaoke, J.R. Bunt, H.W.J.P. Neomagus, F.B. Waanders, C.A. Strydom, and T.S. Mthombo

Synopsis

Inertinite-rich, low-grade coal was used with 12 binders: clays (attapulgite and bentonite), biochar, cow dung, crystallized medium-tar pitch, coal tar sludge, flocculant, fly ash, lignosulphonates, polyester resin, and two South African coal tar pitches in order to produce mechanically strong and water-resistant briquettes. The binders were added in concentrations of 2.5, 5, 7.5, and 10 mass%, and the compressive strength, cohesiveness, and water resistance of the resultant briquettes were determined. The briquettes manufactured using lignosulphonate and resin as binders were the strongest, with compressive strengths of 16 and 12 MPa respectively at a 7.5 mass% binder. Cured and uncured, with and without binder addition, the briquettes all retained their shape and size during drop tests, but none proved to be water-resistant. Paraffin and wax were therefore used as waterproofing agents after pressing and curing. These briquettes showed sufficient strength, cohesiveness, and water resistance to be considered for industrial application.

Keywords
agglomeration, binders, coal fines, compressive strength, inertinite, waterproofing.

Introduction

Eleven per cent of South African run-of-mine (ROM) coal is classified as fine (–0.5 mm) and ultrafine (–0.1 mm), and continues to be discarded into slimes dams and old underground workings (England, 2000; SACRM, 2011). This material could be used locally by agglomerating it for applications which require lump coal, such as fixed-bed gasifiers. There are several techniques for agglomerating fine coal, which include pelletization, flocculation and briquetting (Sastry, 1991). This paper focuses on briquetting.

The suitability of coal briquettes for industrial use is determined by their mechanical strength, water resistance, and thermal stability (Waters, 1969; Richards, 1989). Richards (1989) established that fuel briquettes should have a minimum compressive strength of 375 kPa, which takes into account the pressure exerted during transportation on conveyor belts or during bin storage. In order for briquettes to endure everyday handling, including loading and offloading from trucks and dropping from conveyor belts, a minimum cohesiveness of 80% is required (Kaliyan and Morey, 2009). Water resistance is an important factor to be considered during stockpiling and transportation, and a maximum water absorption of 5 mass% is acceptable for fuel briquettes to be classified as water-resistant (Richards, 1989). Wet briquettes should also be able to withstand a minimum break pressure of 375 kPa, as stipulated by Richards (1989).

Binderless agglomeration of vitrinite-rich coal has shown great potential, producing mechanically stronger and more waterproof briquettes compared to inertinite-rich coal (Mangena *et al.*, 2003; Mangena and du Cann, 2006; Motaung, Mangena, and de Korte, 2007). According to Mangena *et al.* (2003), briquettes produced from vitrinite-rich coal could withstand compression pressures over 1000 kPa, while inertinite-rich briquettes produced at the same pressing conditions by Mangena and du Cann (2006) could only tolerate compression pressures up to 720 kPa. This was mainly attributed to the distortion and subsequent linking of the reactive macerals into joined masses at the surface of the briquette with pressure, thereby increasing its strength – a phenomenon observed to a lesser extent for inertinite-rich coals (Mangena and du Cann, 2006). Mangena *et al.* (2003), Mangena and du Cann (2006), and Motaung, Mangena, and de Korte (2007) found that binderless agglomeration of inertinite-rich coal resulted in briquettes with a reduced wet strength, mainly as a result of the kaolinite mineral matter in conjunction with high ash content (> 15 mass%). Water resistance tests of inertinite-rich, low-grade coals by Mangena *et al.* (2003) and Mangena and du Cann (2006) resulted either in the disintegration of the briquettes in water or reduced wet strengths compared to their vitrinite counterparts.

* *North-West University, Potchefstoom Campus, South Africa.*

 ISSN 2225-6253. Paper received Feb. 2016; revised paper received Dec. 2016.

Although binderless briquetting is the most economical form of briquetting, use of a binder becomes necessary when briquetting inertinite-rich, low-grade coals (England, 2000; Mangena, 2001; Woods *et al.*, 1963). A binder functions as a coherent or adhesive medium between the fine coal particles, and binding agents are desired for their ability to enhance agglomeration through various mechanisms, depending on their properties.

A suitable binder is required to produce mechanically strong, thermally stable, and water-resistant briquettes in a cost-effective manner (Mills, 1908; Waters, 1969). Coal tar pitch is known to produce mechanically strong and waterproof briquettes (Dehont, 2006; Waters, 1969). The pitch can be added to the coal fines in granular form or in a molten state. Due to the carcinogenic nature of coal tar pitch, it has generally been replaced with bitumen, which possesses similar binding characteristics but produces less harmful fumes (England, 2000). The more environmentally friendly binders, such as starches and molasses, produce good-quality, low-smoke briquettes, but require more intensive thermal post-treatment. The main disadvantage of these binders is the increased processing costs (Dehont, 2006; Waters, 1969). Lignosulphonate and kraft lignin, derived from lignin, which is the strengthening agent in plants and trees, have also been investigated for their binding properties (Boudet, 2000; Ekeberg *et al.*, 2006).

Inorganic compounds such as clays have also been investigated for their suitability as binders. These compounds produce stronger and more water-resistant briquettes at low concentrations and low initial moisture contents of the binder-coal mixture (Gul *et al.*, 2014; Mangena *et al.*, 2003). Materials such as cow manure and municipal solid waste have also been investigated for their binding abilities and were found to increase the reactivity of the resulting briquettes at specific binder concentrations (Massaro, Son, and Groven, 2013; Mishra, Sharma, and Agarwal, 1999). These binders, although affordable, require complex pre- and post-treatment, thereby increasing processing costs.

South African coal resources are mostly comprised of inertinite coal, and this study is therefore aimed at exploring methods of producing mechanically strong and waterproof briquettes from a South African inertinite-rich, low-grade coal. The effect of selected binders and waterproofing agents was determined by means of compressive strength, drop shatter, and water submersion tests.

Materials and methods

Coal

A South African, medium-rank C, low-grade, inertinite-rich discard coal (filter cake) from the Highveld area was used. The particle size distribution of the filter cake indicated that 80% of the sample is below 100 µm, and it can therefore be classified as ultra-fine. The chemical, mineralogical, and petrographic analyses of the coal fines are given in Table I. The proximate and X-ray diffraction (XRD) analysis indicated an ash content of 23 mass% with high levels of kaolinite. The inertinite content of the coal is 56 mass%, as seen from the petrographic analysis. Oven drying the sample at 105°C indicated a surface moisture of 20 mass% (as received) for the filter cake. For comparison, the run-of-mine (ROM) coal from the same colliery was obtained and analysed.

Table I

Coal properties

Proximate analysis (wt%, adb[a])	
Inherent moisture	4.9
Ash content	23.1
Volatile matter	26.3
Fixed carbon	45.7
Ultimate analysis (wt%, dafb[b])	
Carbon	79.2
Hydrogen	4.8
Nitrogen	2.2
Oxygen	12.6
Total sulphur	1.2
Petrographic analysis (vol%, mmb[c])	
Vitrinite	27.7
Liptinite	5.4
Inertinite	56.1
Visible minerals	10.8
Total Reactive macerals (vol%)	63.8
Reflectance properties (%)	
Mean vitrinite random reflectance (Rr)	0.65
Rank (Bituminous)	Medium Rank C
Mineralogical XRD analysis (wt%, graphite basis)	
Calcite	1.9
Dolomite	2.6
Graphite	59.8
Gypsum	2.8
Kaolinite	22.3
Muscovite	2.0
Pyrite	0.6
Quartz	8.0

[a]adb – air-dried basis,
[b]dafb – dry, ash-free basis
[c]mmb – mineral matter basis

Figure 1—Lloyd LRX press

Additives

The binders used are summarized in Table II. The clays, lignosulphonate, kraft lignosulphonate, pitches, as well as the crystallized medium-tar pitch (MTP) were milled using a

Table II

Origin, pre-treatment requirements, and costs of the binders and waterproofing agents utilized

Binder	Abbreviation	Origin/supplier	Pretreatment	*Cost (R/ton)
Clays (attapulgite and bentonite)	A/B	Yellowstone bentonite mine near Koppies, South Africa	Milling	195
Biochar	BC	Sunflower husks from a farm in the North West Province	None	-
Cow manure	CM	From a farm in the North West Province	Grating	-
Magnafloc (high molecular weight flocculant)	F	South African mining chemicals supplier	Pre-mix 24 hours prior to pressing	40 000
Lignosulphonate and kraft lignosulphonate	LS/KL	Paper mill byproduct from Mpumalanga	Milling	4 500
NCS polyester resin	R	NCS Resins	None	39 500
Coal tar pitch - (55/59)	CTP1	South African petrochemical industry	Milling	-
Coal tar pitch - (68/73)	CTP2			
Crystallized medium-tar pitch	MTP	South African petrochemical industry	Milling	-
Coal tar sludge	CT	South African petrochemical industry	None	-
Fly ash	FA	South African petrochemical industry	None	-
Paraffin	P	Hardware store in the North West Province	None	1 040
Wax	W	Low temperature Fischer-Tropsch process in South African petrochemical industry	None	-

*Supplier provided costs. Intellectual property restrictions applied to costs not disclosed.

ball mill to a particle size below 1 mm prior to blending with the coal sample. The cow manure was shredded prior to being added to the coal fines. The flocculant granules were added directly to the coal fines and left for 24 hours before pressing. Paraffin and wax, also listed in Table II, were used to improve the water resistance of the briquettes.

Briquetting process

The briquettes were produced by means of a 13 × 13 mm cylindrical die using a Lloyd LRX Plus press, which is shown in Figure 1. The binders were each added in mass concentrations of 2.5, 5.0, 7.5, and 10%, but due to the sticky nature of the coal-flocculant mixture, the flocculant was added only up to 4 mass%. Samples of 2.5 g were prepared and pressed with a force of 4.0 kN. The mechanical test results for the briquettes produced with the 12 binders were compared to those of the binderless briquettes, as well as to ROM coal ground and smoothed into 13 × 13 mm cylinders.

Curing

Binderless briquettes were cured at 100°C for 1, 2, 3, and 4 hours. The optimum curing time was determined as 3 hours by means of compressive strength tests. The binderless briquettes were subsequently cured at 100, 200, 300, and 400°C for 3 hours and an optimum curing temperature of 100°C was obtained. The binderless briquettes, as well as briquettes containing binder, were cured at these conditions and compared to the uncured briquettes.

Test procedures

The physical testing methods as detailed by Mangena *et al.* (2003), Richards (1989), and Kaliyan and Morey (2009) were used to evaluate the mechanical strength of the briquettes.

Compressive strength test

A briquette was placed between two flat plates, 50 mm in diameter. An increasing force was applied to the briquette until it cracked or broke, and this force was recorded as the maximum compressive strength of the briquette (Richards, 1989). Each experiment was repeated four times. The Lloyd LRX Plus press was used to compress the briquettes and the breaking force recorded was converted to a pressure by means of Equation [1] (Richards, 1989).

$$\sigma = \frac{F_{max}}{A_b} \quad [1]$$

where F_{max} is the force applied to fracture or break a briquette (N), and A_b is the cross-sectional area of the plane of fracture (m²).

Drop test

Each briquette was dropped twice from a height of 1.85 m onto a concrete floor and the largest remaining piece was weighed (Kaliyan and Morey, 2009). Drop shatter tests were repeated five times. The cohesiveness of the briquettes was then determined by means of Equation [2].

$$F = \frac{M_f\,(g)}{M_i\,(g)} \quad [2]$$

where M_i is the initial weight of a briquette (g), and M_f the weight of the largest piece after dropping (g).

Water resistance

In order to determine the water resistance, the briquettes were submerged in water for 2 hours, weighed, and then air-dried with periodic weighing until no further significant mass loss was observed (Mangena *et al.*, 2003). The wet strength of the briquettes was also determined by conducting compressive strength tests on the immersed briquettes.

Microscopic surface imaging

High-definition microscopic images of the surface of the briquettes were obtained and investigated using a Nikon SMZ-1 stereo light microscope.

Table III

Binder concentration and briquette cohesiveness at maximum compressive strength for cured and uncured briquettes

Binder	CMCS (mass%)		MCS (MPa)		θMCS (%)	
	Uncured	Cured	Uncured	Cured	Uncured	Cured
Binderless	-	-	0.9	4.9	97	99
Attapulgite	10.0	2.5	1.1	3.3	97	98
Bentonite	7.5	2.5	1.0	5.5	98	98
Biochar	7.5	2.5	0.9	3.5	56	93
Cow manure	7.5	2.5	0.9	2.4	47	90
Flocculant	1.0	1.0	4.1	1.4	50	64
Lignosulphonate	2.5	10.0	0.6	17.0	99	97
Kraft lignosulphonate	5.0	7.5	0.9	3.3	97	97
Polyester resin	2.5	10.0	0.9	12.3	98	100
(55/59) Coal tar pitch	10.0	7.5	1.1	5.6	97	98
(68/73) Coal tar pitch	10.0	10.0	1.1	6.4	99	98
Medium-tar pitch	10.0	7.5	1.0	7.1	100	100
CT sludge	5.0	2.5	0.9	5.8	98	100
Fly ash	2.5	5.0	0.9	3.9	98	97

Results and discussion

Binderless briquettes

Table III summarizes the compressive strength and cohesiveness results for the cured and uncured briquettes manufactured with the pre-selected binders. From Table III, the maximum compressive strength (MCS), binder concentration *(C_{MCS})*, and cohesiveness (θ_{MCS}) at maximum compressive strength can be seen. Uncured, the binderless briquettes met the minimum requirements set out by Richards (1989), reaching compressive strengths up to 0.9 MPa. Curing increased the mechanical strength, with the cured binderless briquettes yielding a maximum compressive strength of 4.9 MPa. This increase in compressive strength can be attributed to the uniformity in morphology as a result of curing, as also reported by Blesa (2002a). The binderless briquettes retained their shape and size, attaining a cohesiveness of 97% and 99% for the cured and uncured briquettes, respectively.

Briquettes with binder addition

Uncured

Table III shows the binder concentrations required to reach maximum compressive strengths. It can be seen that flocculant is the only binder that significantly enhanced the mechanical strength of the uncured binderless briquettes, with 1 mass% flocculant addition resulting in a compressive strength of 4.1 MPa. Further increases in flocculant weakened the briquettes, refuting the use of flocculant as a binder at high concentrations. The other binders did not increase the mechanical strength of the briquettes to any significant degree, yielding maximum compressive strengths between 0.9 and 1.1 MPa. The briquettes produced with biochar, cow manure, and flocculant were the most friable, with cow manure yielding cohesiveness as low as 47%. The low cohesiveness was attributed to internal fractures that occurred as a result of the addition of this binder.

Cured

Curing of the briquettes resulted in either no change or an increase in cohesiveness. The binderless briquettes showed a compressive strength increase of 4.0 MPa consequent to curing. This may be attributed to the activation of the binders at elevated temperatures, inducing interaction between the coal and the binders (Blesa *et al.*, 2002b).

The kraft lignosulphonate (at maximum concentration) did not increase the mechanical strength of the briquettes above that of the binderless, cured briquette. This binder left the briquettes brittle after curing, causing a reduction in compressive strength. The fly ash, attapulgite, biochar, cow manure, and flocculant all reduced the mechanical strength of the briquettes with increasing binder concentration.

Both coal tar pitches and MTP increased the compressive strength of the cured, binderless briquettes with every increase in binder concentration. These binders were well-dispersed within the briquettes at higher concentrations after heat treatment, which was observed upon breaking the briquettes. On the other hand, bentonite and CT sludge both reduced the strength of the briquettes at concentrations above 2.5 mass%. The CT sludge seeped out of the briquettes at concentrations above 2.5 mass%, creating cracks at the surface of the briquettes, thereby reducing their compressive strength.

The most significant increase in mechanical strength was observed for lignosulphonate- and resin-bound briquettes. The compressive strengths are given in Figure 2 as a function of the binder concentration. The compressive strength increased with every increase in binder concentration. Lignosulphonate-produced briquettes met the minimum requirements, even at the lowest concentration of 2.5 mass%. At concentrations above 5 mass%, the lignosulphonate briquettes could withstand pressures above 14 MPa, which is above the compressive strength of the ROM coal.

Lignin, the main naturally binding component in lignosulphonate, is an amorphous thermoplastic material which undergoes plastic deformation at low compaction pressures and temperatures within its glass transition temperature (Back and Salmen, 1982), which Irvine (1984) found to be in the range of 60–90°C. Curing the lignosulphonate-bound briquettes at 100°C provided the desired glass transition conditions wherein the cell content of the lignin was activated or 'softened'. The glass transition conditions may also have reduced the viscosity and thus increased the mobility of the binding components in the lignosulphonate (Finney, Sharifi, and Swithenbank 2009). This would result in the diffusion of polymer chains and

chain ends from one fibre into the proximity of an adjacent fibre, thereby increasing the bonding area. Upon cooling, these bonds are consolidated, resulting in the formation of hardened solid bridges (Kaliyan and Morey, 2010).

Another binder producing strong briquettes was the polyester resin, with briquette break strengths above the minimum requirement observed from 2.5 mass% binder addition. With every increase in resin concentration, an increase in compressive strength was observed, as illustrated in Figure 2. Although the resin is highly viscous at ambient temperature, its mobility was enhanced upon curing, as a result of the decrease in viscosity. This may have resulted in the formation of solid bridges upon cooling, thereby increasing the mechanical strength of the resulting briquettes (Kaliyan and Morey, 2010).

The lignosulphonate- and resin-bound briquettes were further investigated by light microscope imaging, which provided a better visualization of the surface morphology. The light microscopic images (Figure 3) show a significant difference between the binderless briquettes and the briquettes manufactured with the use of lignosulphonate and resin binders. The cracks visible in the binderless briquettes contribute largely to the low mechanical strength compared to the lignosulphonate and resin briquettes. The resin briquette exhibits less voids than the binderless briquette, which also becomes apparent in the mechanical strength differences between the two briquettes. The lignosulphonate briquette has a more uniform surface, exhibiting the least amount of voids; which explains the high compressive strengths attained by the lignosulphonate briquettes.

The costs of each binder as provided by the suppliers are specified in Table II. Zero costs were assumed for the fine discard coal. Addition of 5 mass% lignosulphonate results in binding costs of R225 per ton of coal. Binding agent costs associated with utilizing resin were determined as R2 963 per ton of coal. Sasol coal mining costs were estimated at R227 per ton for 2016, well comparable to the lignosulphonate binding costs (Sasol, 2016).

Water resistance tests

The binderless briquettes and briquettes manufactured with

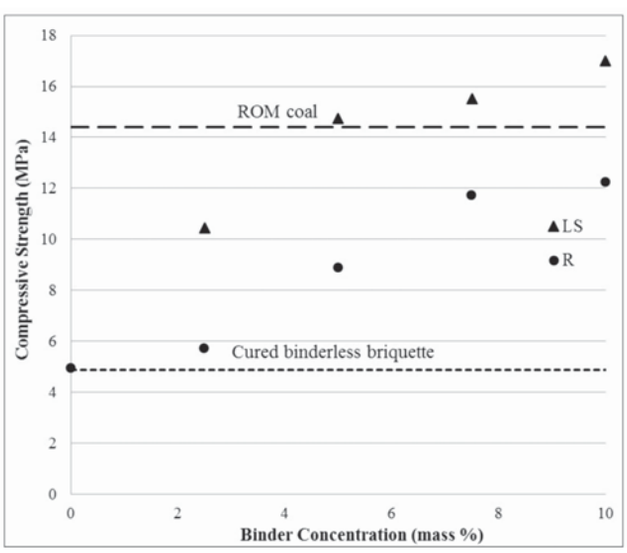

Figure 2—Compressive strengths of cured lignosulphonate- (LS) and resin- (R) bound briquettes as a function of binder concentration

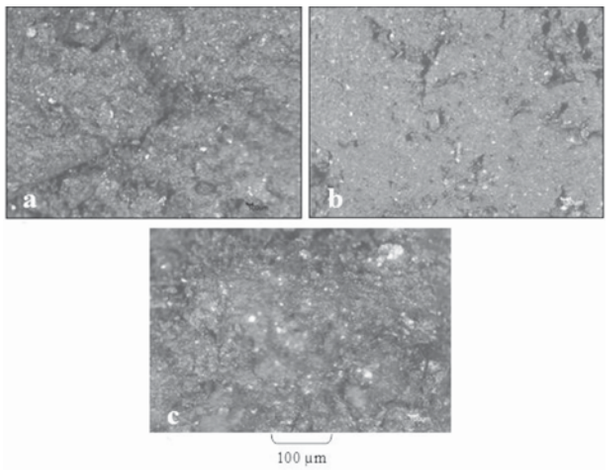

Figure 3—Light micrographs of the surfaces of briquettes containing (a) no binder, (b) lignosulphonate binder, and (c) resin binder

the selected binders all disintegrated within seconds in the presence of water, which was attributed to the high ash and kaolinite clay content (Table I). Mangena *et al.*, (2003) found that kaolinite significantly reduces the water resistance of binderless briquettes when the ash content of the parent coal is above 15 mass%. This is due to the softening and swelling of kaolinite in the presence of water.

To ensure that manufactured briquettes are comparable to their ROM coal counterparts during storage and utilization, the strongest two briquettes were selected for waterproofing. The only additives considered to improve the water resistance of the briquettes were paraffin and wax, due to their hydrophobic nature. Consequently, these additives were investigated for their use as waterproofing agents for the lignosulphonate and resin-bound briquettes, which yielded the highest compressive strength results.

The wet strength and moisture content of the lignosulphonate- and resin-bound briquettes after waterproofing, water submersion, and air-drying can be seen in Figure 4. Lignosulphonate briquettes yielded better resistance when submerged in molten wax, while the resin briquettes were more water resistant when submerged in paraffin immediately after curing. The lignosulphonate briquettes had an initial moisture intake of 2 mass%, which decreased with increasing air-drying time. Moisture absorption of 5 mass% and less was deemed acceptable by Richards (1989). Although the resin briquettes initially absorbed high amounts of moisture (9.3 mass%), both binders produced briquettes that displayed the minimum compressive strength of 375 kPa as suggested by Richards (1989) for industrial fuel briquettes. The lowest wet strengths attained by the lignosulphonate and resin briquettes were 1.6 and 2.2 MPa respectively, and these briquettes would therefore endure weathering during stockpiling and transportation.

Conclusion

Briquettes manufactured from inertinite-rich, ultrafine coal (23% ash content) and using suitable binding and waterproofing agents have suitable mechanical properties for industrial application. Lignosulphonate and resin proved to increase the dry strength of the briquettes to a larger extent, producing briquettes that meet the minimum dry strength requirements even at the lowest binder concentration of 2.5

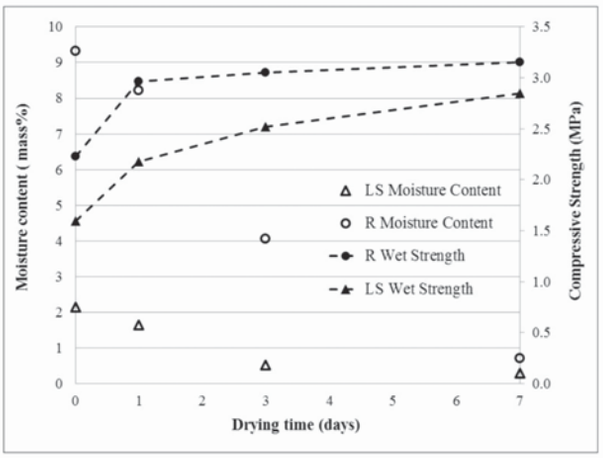

Figure 4—Moisture contents and wet compressive strengths of lignosulphonate (LS) and resin (R) briquettes as a function of air-drying time

mass%. Due to the high ash and kaolinite contents of the coal, waterproofing was essential. Coating the lignosulphonate briquettes with molten wax and the resin briquettes with paraffin immediately after curing resulted in water-resistant briquettes that met the minimum mechanical strength requirements. The binder costs for lignosulphonate, estimated at R225 per ton coal, were more acceptable compared to the resin (R2 963 per ton coal). An in-depth reactivity analysis of both lignosulphonate- and resin-bound briquettes will be carried out. Considering the mechanical, reactivity and economic results, a final briquette formulation will be selected for pilot-scale testing in a chain grate stoker.

Acknowledgements

The information presented in this paper is based on research financially supported by the South African Research Chairs Initiative (SARChI) of the Department of Science and Technology and National Research Foundation of South Africa (Coal Research Chair Grant No. 86880).

Any opinion, finding, or conclusion or recommendation expressed in this material is that of the author(s) and the NRF does not accept any liability in this regard.

Facets of the study have been presented at three conferences. A poster presentation was given at the *7th Annual Granulation Workshop Conference* that took place on 2 July 2015 in Sheffield, UK. A paper was presented at the Southern African Coal Processing Society 2015 conference, *Coal Processing: Unlocking Southern Africa's Coal Potential*, which took place on 27 August 2015 at Secunda in South Africa. The study was also presented at the Fossil Fuel Foundation 2015 conference, *Sustainable Energy Research*, in Potchefstroom, South Africa on 25 November 2015.

Nomenclature

A_b	Cross-sectional area of plane of fracture of the briquette (m²)
C_{MCS}	Binder concentration at maximum compressive strength (mass%)
F_{max}	Force applied to fracture or break a briquette (N)
MCS	Maximum compressive strength (MPa)
M_f	Weight of the largest piece after drop shatter test (g)
M_i	Initial weight of a briquette (g)
σ	Compressive strength (MPa)
θ	Cohesiveness (%)
θ_{MCS}	Cohesiveness at maximum compressive strength (%)

References

Back, E.L. 1987. The bonding mechanism in hardboard manufacture. *Holzforschung-International Journal of the Biology, Chemistry, Physics and Technology of Wood*, vol. 41, no. 4. pp. 247–258.

Back, E.L. and Salmen, N.L. 1982. Glass transitions of wood components hold implications for molding and pulping processes. *Tappi Journal*, vol. 65, no. 7. pp. 107–110.

Blesa, M.J., Miranda, J.L., Izquierdo, M.T., and Moliner, R. 2002a. Curing temperature effect on mechanical strength of smokeless fuel briquettes prepared with molasses. *Fuel*, vol. 82, no. 8. pp. 943–947.

Blesa, M.J., Miranda, J.L., Izquierdo, M.T., and Moliner, R. 2002b. Curing time effect on mechanical strength of smokeless fuel briquettes. *Fuel Processing Technology*, vol. 80, no. 2. pp. 155–167.

Boudet, A.M. 2000. Lignins and lignification: selected issues. *Plant Physiology and Biochemistry*, vol. 38, no. 1-2. pp. 81–96.

Dehont, F. 2006. Coal briquetting technology. http://www.sahutconreur.com [accessed 1 August 2013].

Ekeberg, D., Gretland, K.S., Gustafsson, J., Braton, S.M., and Fredheim, G.E. 2006. Characterisation of lignosulphonates and kraft lignin by hydrophobic interaction chromatography. *Analytica Chimica Acta*, vol. 565, no. 1. pp. 121–128.

England, T. 2000. The economic agglomeration of fine coal for industrial and commercial use. CoalTech 2020. Coaltech Research Association, South Africa.

Finney, K.N., Sharifi, V.N., and Swithenbank, J. 2009. Fuel pelletization with a binder: Part I - Identification of a suitable binder for spent mushroom compost - coal tailing pellets. *Energy and Fuels*, vol. 23, no. 6. pp. 3195–3202.

Gul, A.G., Sirkeci, A.A., Boylu, F., Guldan, G., and Burat, F. 2014. Improvement of mechanical strength of iron ore pellets using raw and activated bentonites as binders. *Physicochemical Problems of Mineral Processing*, vol. 51, no. 1. pp. 23–36.

Irvine, G.M. 1984. The glass transitions of lignin and hemicellulose and their measurement by differential thermal analysis. *Tappi Journal*, vol. 67, no. 5. pp. 118–121.

Kaliyan, N. and Morey, R.V. 2009. Factors affecting strength and durability of densified biomass products. *Biomass and Bio-energy,* vol. 33, no. 3. pp. 337–359.

Kaliyan, N. and Morey, R.V. 2010. Natural binders and solid bridge type binding mechanisms in briquettes and pellets made from corn stover and switch grass. *Bioresource Technology*, vol. 101, no. 3. pp. 1082–1090.

Mangena, S.J. 2001. The amenability of some South African bituminous coals to binderless briquetting. MTech dissertation, Technikon Pretoria, Pretoria.

Mangena, S.J., de Korte, G.J., McCrindle, R.I., and Morgan, D.L. 2003. The amenability of some Witbank bituminous ultra fine coals to binderless briquetting. *Fuel Processing Technology*, vol. 85, no. 15. pp. 1647–1662.

Mangena, S.J. and du Cann, V.M. 2006. Binderless briquetting of some selected South African prime coking, blend coking and weathered bituminous coals and the effect of coal properties on binderless briquetting. *International Journal of Coal Geology*, vol. 71, no. 2-3. pp. 303–312.

Massaro, M.M., Son, S.F., and Groven, L.J. 2013. Mechanical, pyrolysis and combustion characterization of briquetted coal fines with municipal solid waste plastic (MSW) binders. *Fuel*, vol. 115, no. 1. pp. 62–69.

Mills, J.E. 1908. Binders for coal briquettes. US Geological Survey, Washington.

Mishra, S.L., Sharma, S.K., and Agarwal, R. 1999. Briquetting of lignite for domestic fuel. *Science and Industrial Research*, vol. 59, no. 5. pp. 413–416.

Motaung, J.R., Mangena, S.J., and de Korte, G.J. 2007. Effect of coal composition and flotation reagents on the water resistance of binderless briquettes. *Coal Preparation*, vol. 27, no. 4. pp. 230–248.

Richards, S.R. 1989. Physical testing of fuel briquettes. *Fuel Processing Technology*, vol. 25, no. 2. pp. 89–100.

SACRM. 2011. South African coal roadmap. http://www.sanedi.org.za [accessed 31 August 2015].

Sasol. 2016. Additional Analyst Information for the year ended 30 June 2016. Sasol Limited, Johannesburg.

Sastry, V.S. 1991. Pelletization of fine coals. *Department of Energy Report* no. DE-FG-22-89PC89766. University of California, Berkeley, California.

Waters, P.L. 1969. Binders for fuel briquettes. *Technical Communication* no. 51. CSIRO, New South Wales, Australia.

Woods, M.F., Habberjam, G.M., Elsworth, K., and Bennett, S. 1963. The effect of maceral compostion on the binderless briquetting of hot char. National Coal Board, Cheltenham, England. ◆

http://dx.doi.org/10.17159/2411-9717/2018/v118n1a11

Effect of stirring time on oil agglomeration of fine coal

by W. Guan, J. Sha, P. Liu, Y. Peng, and G. Xie

Synopsis

Flotation is widely used to process fine coal. However, problems of concentrate contamination caused by slime coating, entrapment, and entrainment have severely impeded its performance. Oil agglomeration, another physicochemical separation method, works as a substitute to solve the contamination problems. Agglomerates were prepared from coal fines using different stirring times and the ash content and combustible recovery in four size fractions: +500, 500-250, 250-125, and -125 μm determined. The results showed that coal particles finer than 45 μm with low ash content transformed from scattered particles to solid agglomerates. With longer stirring times, the number of large and stabilized agglomerates increased and attained equilibrium. The agglomeration process can be separated into three stages according to the degree of agglomeration at different stirring times.

Keywords
oil agglomeration, stirring time, fine coal, kerosene.

Introduction

Modern mechanized mining techniques produce enormous quantities of coal fines. These coal fines are usually associated with gangue minerals and need to be cleaned at high cost (Mehrotra, Sastry, and Morey, 1983; Gürses, Doymu, and Bayrak Eken, 1997). Physicochemical separation methods including flotation, flocculation, and oil agglomeration are widely used in fine coal processing (Cebeci and Eroglu, 1998). With flotation, contamination of the concentrate by gangue minerals occurs by slime coating, entrapment, as well as entrainment of micro- and nano-sized particles (Wang *et al.*, 2015). Oil agglomeration is a suitable alternative to flotation because it can produce clean coal at higher recoveries and better qualities (Capes and Darcovich, 1984). As one of the major physicochemical separation methods (Capes and Darcovich, 1984; Duzyol, and Ozkan, 2014), oil agglomeration relies on the difference between the surface properties of the hydrophobic valuable minerals and the hydrophilic gangue minerals. In this process, non-polar oil droplets attach to the hydrophobic particles first. When such particles collide with each other, the oil droplets attached to the hydrophobic particles can merge and bridge the particles into larger agglomerates (Laskowski and Yu, 2000). The agglomerated hydrophobic particles can be separated from the hydrophilic materials by screening, or alternatively by flotation and skimming (Abakay, Ayhan, and Kahraman, 2004).

Extensive studies have been conducted to investigate the effects of oil dosage and type, agglomeration time, pH, electrolyte, and other factors like solid content of the slurry, amount of washing water, agitation speed, and surfactant on the upgrading of bituminous coal by oil agglomeration (Cebeci, Ulusoy, and Şimşek, 2002; Akta, 2002; Unal and Akta, 2001; Lin *et al.*, 2012). Some studies have shown that oil agglomeration effectively reduces the sulphur content of high-sulphur coal (Sahinoglu and Uslu, 2008, 2014. 2015; Chary and Dastidar, 2013; Ayhan, 2009). Low-rank and oxidized coals cannot be effectively concentrated by flotation, but oil agglomeration has obtained good results for these types of coal (Cebeci and Eroglu, 1998; Laskowski and Yu, 2000; Sahinoglu and Uslu, 2015; Unal and Gorgun Ersan, 2007; Temel, Bozkurt, and Majumder, 2009; Cebeci and Sonmez, 2002). The effect of pretreatment processes such as microwave and ultrasonic treatment on the oil agglomeration process have also been investigated (Unal and Ersan, 2005; Sahinoglu, and Uslu, 2013a, 2013b).

In this research, the effect of stirring time on the oil agglomeration of fine bituminous coal was investigated. In addition, the distribution of the ultra-fine coal (–45 μm) in different size fractions and the formation and growth of the large agglomerates (+500 μm) were analysed at different stirring times. Particular attention was paid to the role of ultra-fine coal particles in the oil agglomeration process.

* *China University of Mining and Technology, Xuzhou, China.*

 ISSN 2225-6253. Paper received Nov. 2016; revised paper received Oct. 2017.

Materials and methods

Materials

A fine coal sample of approximately 10 kg was obtained from Wanglou coal preparation plant in China. A large portion of the sample was below 0.25 mm. The small fraction that was over 0.25 mm was discarded. The sample was divided by repeated coning and quartering until one-fourth of initial sample (approx. 2.5 kg) was obtained. Samples of approximately 30 g were prepared for test work by combining small samples that were arranged in a chessboard fashion. A sample of 200 g was also obtained and sieved at 250, 125, 74 and 45 μm to obtain the particle size distribution, as shown in Table I. Table I shows that more than 64% of the sample was finer than 45 μm. The –45 m fraction also had the highest ash content.

A coal sample was ground to –0.045 mm for mineralogical investigations by XRD, using a Bruker D8 Advance instrument. The data processing (peak fitting) was performed with JADE software. The XRD work was carried out at room temperature. From the XRD analysis of the feed coal (Figure 1), it can be seen that the gangue minerals are kaolinite, calcite, and quartz.

Float-sink tests were carried out on the –45 μm size fraction. The results are shown in Table II. Four coal samples of 15 g were placed in the centrifuge tube with heavy fluid. After centrifuging, the floats and heavy fluid were poured into a beaker. Heavy fluid with a higher density was then added into the tube and was further centrifuged with the precipitate.

Industrial kerosene was used as the non-polar oil in the oil agglomeration experiments. Tap water was used in all the tests.

Table I

Particle size distribution of the coal sample finer than 250 μm

Size fraction (μm)	Mass (%)	Ash content (%)
250–125	11.90	21.82
125–74	14.96	26.80
74–45	8.76	30.35
–45	64.38	50.47
Total	100.00	41.76

Table II

Float-sink test results on –45 μm size fraction

Density range (g/cm³)	Floats		Cumulative floats		Cumulative sinks	
	Fraction (%)	Ash (%)	Mass (%)	Ash (%)	Mass (%)	Ash (%)
<1.40	3.38	8.85	3.38	8.85	100.00	50.16
1.40–1.50	5.61	16.18	8.99	13.42	96.62	51.61
1.50–1.60	6.81	22.88	15.80	17.50	91.01	53.79
1.60–1.80	11.41	32.38	27.21	23.74	84.20	56.29
1.80–2.00	45.29	51.35	72.50	40.99	72.79	60.04
>2.00	27.50	74.35	100.00	50.16	27.50	74.35

Oil agglomeration

Oil agglomeration experiments were undertaken in a 250 mL conical flask with agitation using a JJ-1B digital display constant-speed electric mixer as shown in Figure 2. First, a coal sample of 30 g was added into the conical flask with only a little water (50 mL) to wet the coal and the suspension was conditioned at 1000 r/min for 2 minutes. Water was then added to increase the total volume of the suspension to 200 mL and the suspension was further stirred for 3 minutes to achieve complete wetting of coal particles. Then the kerosene (7.5 mL) was added while stirring for different predetermined periods, namely 5, 10, 15, 20, 25, 30, 35, and 40 minutes.

After agglomeration, the suspension was transferred to a series of sieves with apertures of 500, 250, and 125 μm. The agglomerates retained on the sieve cloth were collected by washing slowly and carefully with an appropriate amount of water, and the products of different size fractions were filtered and dried in an oven at 105 ± 5°C. These products were then immersed in a beaker filled with acetone for about 2 minutes until they were completely loose, and these de-oiled products were wet screened at an aperture of 45 μm to investigate the behaviour of coal particles finer than 45 μm in the whole oil agglomeration process. The masses of the different products were recorded.

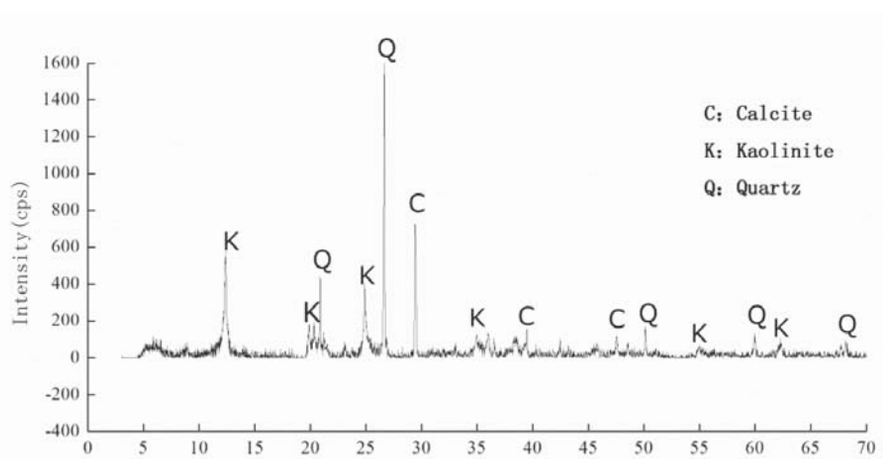

Figure 1—XRD analysis of feed coal

Effect of stirring time on oil agglomeration of fine coal

Figure 2—Oil agglomeration system

The optimum conditions for the oil agglomeration test work were established in a series of preliminary tests. Kerosene concentrations of 9.1, 16.7, and 23.1 wt.% were adopted and the suspension was stirred at 1200 r/min for 20 minutes to determine the optimum value. Then, using a kerosene concentration of 9.1 wt.%, the suspension was stirred at different stirring speeds (1200, 1450, and 1700 r/min) for 20 minutes. A kerosene concentration of 16.7 wt.% and 1450 r/min stirring speed were finally chosen. Eight sets of agglomeration experiments were repeated to obtain enough samples for further analysis. A schematic of the experimental procedure is shown in Figure 3.

Results and discussion

Effect of stirring time on oil agglomeration performance

The effect of stirring time on the combustible recovery and ash content of the agglomerate is shown in Figure 4. The combustible recovery was calculated by means of the following equation:

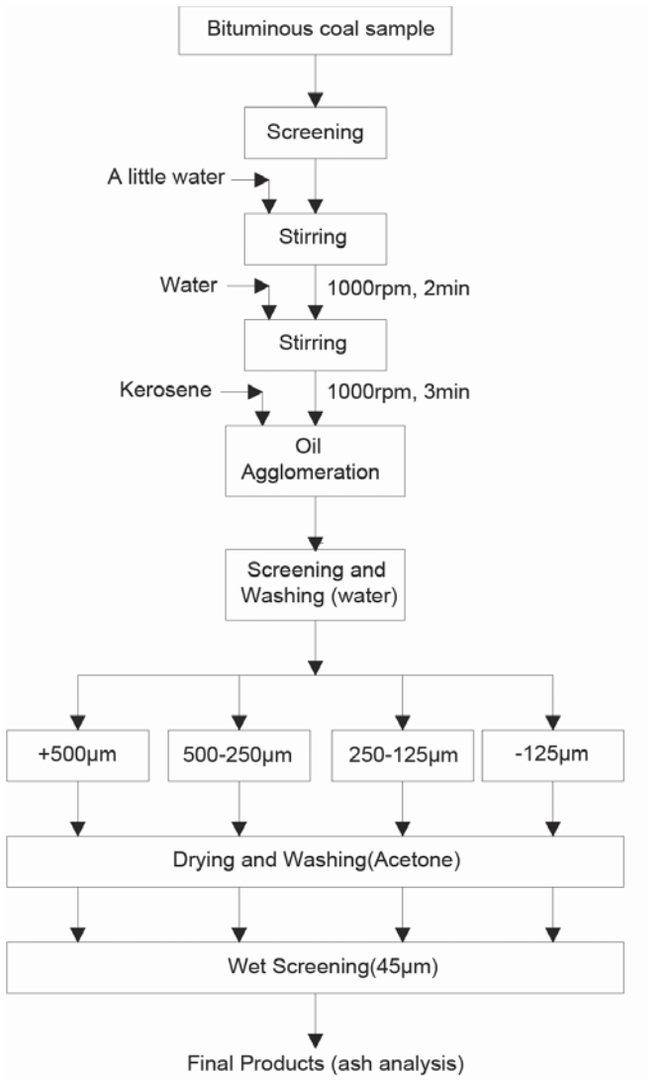

Figure 3—Schematic of the experimental procedure

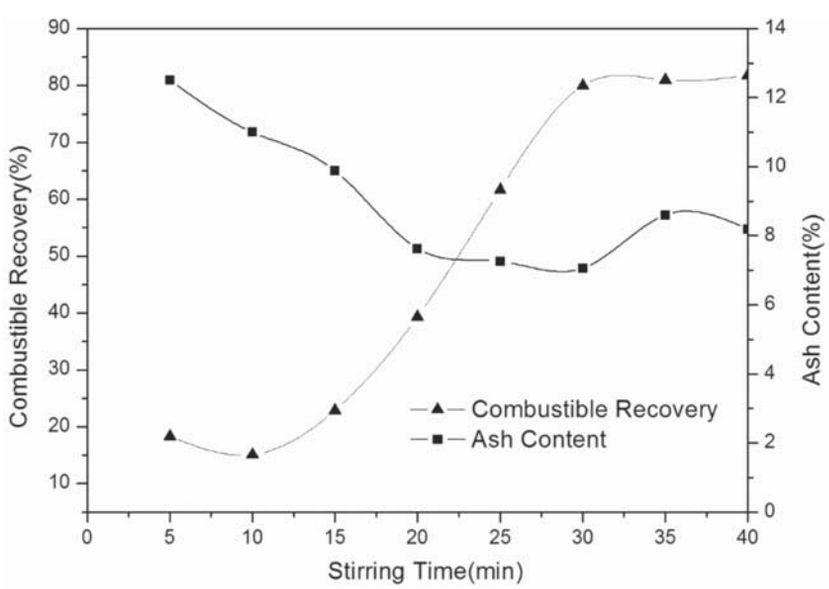

Figure 4—Effect of stirring time on the combustible recovery and ash content (kerosene concentration 16.7 wt.%, stirring speed: 1450 r/min)

Combustible recovery (%) = $[(M_P/M_F) \times ((100–A_P)/(100–A_F))] \times 100$

where, M_p is the mass of dry and oil-free product (g), M_F the mass of dry feed (g), A_F the ash content of the dry feed (wt.%), and A_P the ash content of the dry and oil-free product (wt.%).

It should be noted that the +250 m fraction was chosen to be the concentrate combined with the requirement for ash content of agglomerates as a general representation of the total result. This is consistent with the opinion of Sahinoglu and Uslu (2015) that the recovery sieve size should be the same as the top feed size.

As seen from Figure 4, the combustible recovery generally increased with increasing stirring time. This can be attributed to the enhancement of collisions between particles and micro-agglomerates, and thus the agglomerates consolidate and become spherical (Abakay, Ayhan, and Kahraman, 2004).

Figure 4 also shows that the ash content of the agglomerates decreased with increasing stirring time up to 30 minutes. This behaviour was due to the formation of more compact-structured agglomerates and the decrease in the amount of water phase entrapped in the agglomerates. After 30 minutes, while the stirring time was gradually increased up to 35 minutes, the ash content of the concentrates increased. This may be due to the increased possibility of entrapment of particles with high ash content. Cebeci, Ulusoy, and Şimşek (2002) also noted that the ash content of agglomerated product increased after a certain agglomeration time. After that, the ash content did not change much because the structure of the agglomerates remained relatively unchanged.

In Figure 5, it can be seen that the yields and ash contents of products of different size fractions displayed different trends with increasing stirring time. In this study, the whole oil agglomeration process can be divided into three stages: the initial formation of micro-agglomerates, the growth of agglomerates, and stabilization, as shown in Figure 6. In the first stage, from 0 to 10 minutes, preferential wetting of hydrophobic particles by oil formed the fundamental basis for the separation (Mehrotra, Sastry, and Morey, 1983). Initially, the yield of –125 μm fraction decreased with increased stirring time up to 5 minutes while yields of the other three fractions increased to form loose agglomerates. From 5 to 10 minutes the yields of –125 and +500 μm fractions increased slightly while the other two fractions showed opposite tendencies. This is perhaps because the agglomerate structure of the 500–250 and 250–

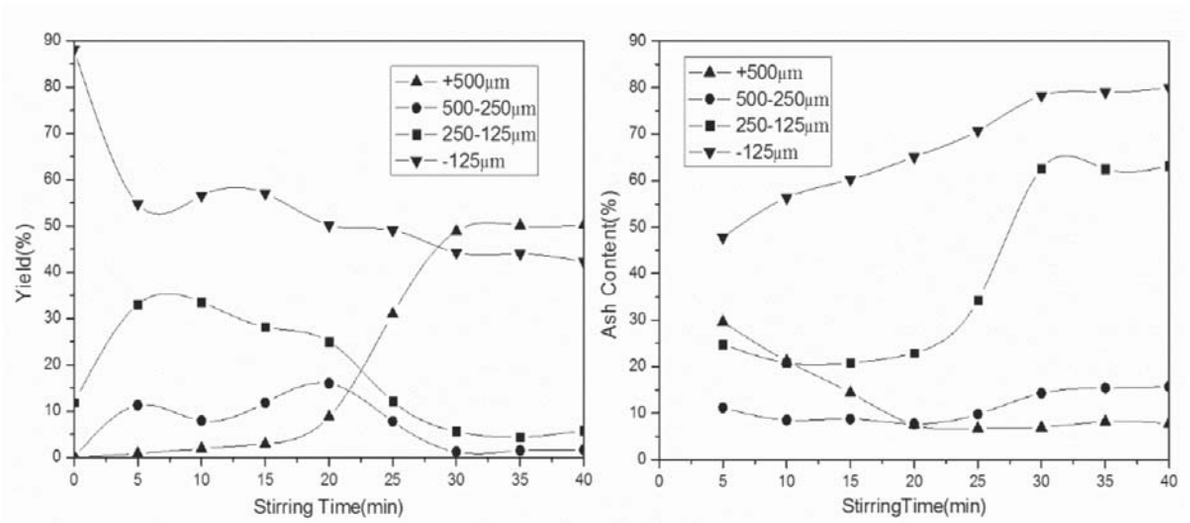

Figure 5—Yields (left) and ash contents (right) of products of four different size fractions (kerosene concentration 16.7 wt.%, stirring speed 1450 r/min)

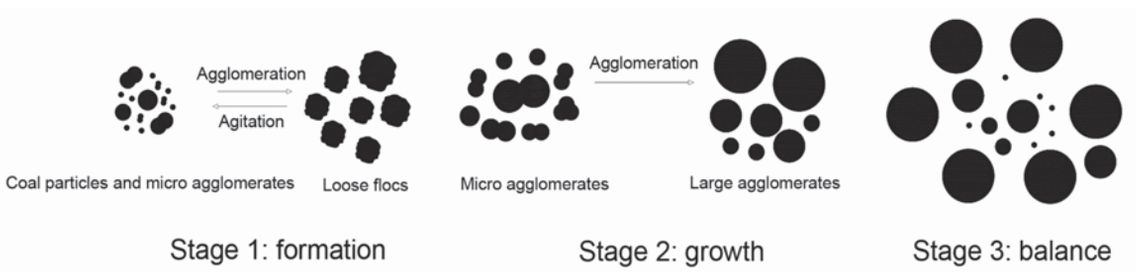

Figure 6—Three stages of the oil agglomeration process (Capes and Darcovich, 1984)

Effect of stirring time on oil agglomeration of fine coal

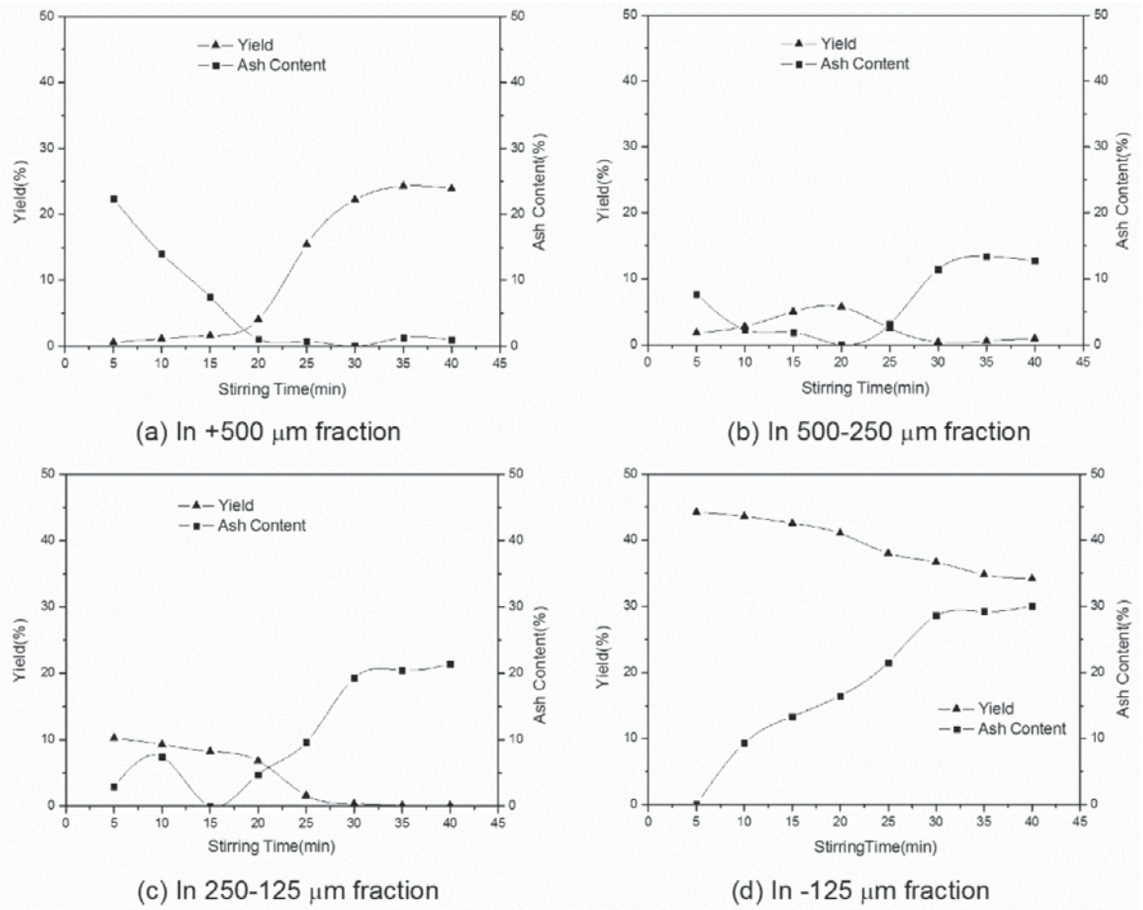

Figure 7—Yields and ash contents of particles finer than 45 μm in four different size fractions (kerosene concentration 16.7 wt.%, stirring speed 1450 r/min)

125 μm fractions was too loose and the agglomerates were broken up by agitation. During this stage, very few agglomerates larger than 500 μm were formed. The second stage began at 10 minutes, after which the yields of both the –125 and the 250–125 μm fraction decreased as larger agglomerates formed. The yields of +500 μm agglomerates increased sharply because of the formation of more stable agglomerates between 20 and 30 minutes. It is concluded that most of the agglomeration process took place during this stage. The third stage started from 30 minutes, after which the structure of stable agglomerates remained relatively unchanged and the whole suspension was in equilibrium.

Effect of stirring time on the behaviour of fine coal particles

In order to elucidate the behaviour of coal particles finer than 45 μm in the whole oil agglomeration process, the yields and ash contents of four different size fractions are discussed.

As shown in Figure7a, the yield of particles finer than 45 m in +500 μm agglomerates increased continuously while the ash content decreased with increasing stirring time up to 30 minutes. From 20 minutes, the ash content remained below 3% while the yield increased until 35 minutes. This indicates that the –45 μm particles with higher hydrophobicity or oleophilicity and lower ash content gradually transferred into the large agglomerates because of the more efficient collision between the –45 μm particles and the micro-agglomerates.

The yield and ash content of particles finer than 45 μm in the 500–250 μm fraction are shown in Figure 7b. The trends are similar to those for the +500 μm fraction (Figure 7a) for stirring times up to 20 minutes and after 30 minutes, and for the same reasons. However, between 20 and 30 minutes, the trends were opposite to those for the +500 μm fraction. This may be attributed to the intense formation of the +500 μm agglomerates during this period. The 500–250 μm agglomerates collided with fine particles and agglomerated further to form stronger and larger agglomerates. Therefore, fine coal particles with lower ash content were transferred from small agglomerates to large ones.

Unlike the variations in Figure 7b, the ash contents of particles finer than 45 m in the 250–125 μm fraction fluctuated at stirring times shorter than 20 minutes, as shown in Figure 7c. This is probably caused by a combination of constant agglomeration forming larger agglomerates and breaking of loosely structured agglomerates under continuous agitation. Between 20 and 30 minutes, the ash content and the yield displayed significant variations resulting from the drastic growth of agglomerates. After 30 minutes, very little change was observed.

Figure 7d shows that the yield of particles finer than 45 μm in the –125 μm fraction decreased constantly while the ash content increased with the increasing stirring time. This may be attributed to the sustained transfer of fine coal particles from small agglomerates to large agglomerates during the oil agglomeration process.

Conclusions

- The combustible recovery increased and the ash content of agglomerates decreased with increasing stirring time up to 30 minutes, after which the ash content increased slightly due to the entrapment of particles with high ash content. The results indicated that 80% of the coal could be recovered as a 7% ash product under optimum conditions.
- The entire oil agglomeration process can be divided into three stages. In the first stage, from 5 to 10 minutes, micro-agglomerates were formed, which could be easily broken by agitation, so the yield of agglomerates was low. In the second stage, from 10 to 30 minutes, the yield of agglomerates increased sharply due to enhanced contact of scattered particles and micro-agglomerates. In the third stage, from 30 to 40 minutes, the yield of agglomerates changed very little because of the stable structure of agglomerates, and the whole suspension was in equilibrium.
- The effect of coal particles finer than 45 μm on the oil agglomeration process was investigated. It was concluded that fine coal particles with lower ash content were transferred from small agglomerates to large ones with increasing stirring time. However, some particles with high ash content may contaminate the agglomerates with excessive stirring time.

The mechanism of high-ash particle contamination in the oil agglomeration process will be further investigated from thermodynamic or kinetic aspects in future studies. Some test methods may also be introduced to explore the structure of agglomerates.

Acknowledgements

This work was supported by the National Natural Science Foundation of China (Grants no. 51374205, 51474213, and 51704289. We also want to thank the General Financial Grant from the China Postdoctoral Science Foundation (2016M591963) and the support of 'A' Priority Academic Program Development of Jiangsu Higher Education Institutions.

References

Abakay, H., Ayhan, F.D., and Kahraman, F. 2004. Selective oil agglomeration in ırnak asphaltite beneficiation. *Fuel*, vol. 83. pp. 2081–2086.

Akta, Z. 2002. Some factors affecting spherical oil agglomeration performance of coal fines. *International Journal of Mineral Processing*, vol. 65. pp. 177–190.

Ayhan, F.D. 2009. Desulfurization and de-ashing of a mixture of subbituminous coal and gangue minerals by selective oil agglomeration. *Mineral and Metallurgical Processing*, vol. 26. pp. 203–207.

Capes, C.E. and Darcovich, K. 1984. A survey of oil agglomeration in wet fine coal processing. *Powder Technology*, vol. 40. pp. 43–52.

Cebeci, Y. and Eroglu, N. 1998. Determination of bridging liquid type in oil agglomeration of lignites. *Fuel*, vol. 77. pp. 419–424.

Cebeci, Y. and Sonmez, I. 2002. The investigation of coal-pyrite/lignite concentration and their separation in the artificial mixture by oil agglomeration. *Fuel*, vol. 81. pp. 1139–1146.

Cebeci, Y., Ulusoy, U.U., and Şimşek, S. 2002. Investigation of the effect of agglomeration time, pH and various salts on the cleaning of Zonguldak bituminous coal by oil agglomeration. *Fuel*, vol. 81. pp. 1131–1137.

Chary, G.H.V.C. and Dastidar, M.G. 2013. Comprehensive study of process parameters affecting oil agglomeration using vegetable oils. *Fuel*, vol. 106. pp. 285–292.

Duzyol, S. and Ozkan, A. 2014. Effect of contact angle, surface tension and zeta potential on oil agglomeration of celestite. *Minerals Engineering*, vol. 65. pp. 74–78.

Gürses, A., Doymu, K., and Bayrak Eken, S. 1997. Evaluation of response of brown coal to selective oil agglomeration by zeta potential measurements of the agglomerates. *Fuel*, vol. 76. pp. 1439–1444.

Laskowski, J.S. and Yu, Z.M. 2000. Oil agglomeration and its effect on beneficiation and filtration of low-rank/oxidized coals. *International Journal of Mineral Processing*, vol. 58. pp. 237–252.

Lin, S., Chen, B., Chen, W., Li, W., and Wu, S. 2012. Study on clean coal technology with oil agglomeration in Fujian Province. *Procedia Engineering,* vol. 45. pp. 986–992.

Mehrotra, V.P., Sastry, K.V.S., and Morey, B.W. 1983. Review of oil agglomeration techniques for processing of fine coals. *International Journal of Mineral Processing*, vol. 11. pp. 175–199.

Sahinoglu, E., and Uslu, T. 2008. Amenability of Muzret bituminous coal to oil agglomeration. *Energy Conversion and Management*, vol. 49. pp. 3684–390.

Sahinoglu, E. and Uslu, T. 2013a. Increasing coal quality by oil agglomeration after ultrasonic treatment. *Fuel Processing Technology*, vol. 116. pp. 332–338.

Sahinoglu, E. and Uslu, T. 2013b. Use of ultrasonic emulsification in oil agglomeration for coal cleaning. *Fuel*, vol. 113. pp. 719–725.

Sahinoglu, E. and Uslu, T. 2014. Effect of particle size on cleaning of high-sulphur fine coal by oil agglomeration. *Fuel Processing Technology*, vol. 128. pp. 211–219.

Sahinoglu, E. and Uslu, T. 2015. Cleaning of high sulphur coal by agglomeration with waste vegetable oil. *Energy Sources Part A*, vol. 37. pp. 2724–2731.

Sahinoglu, E. and Uslu, T. 2015. Role of recovery sieve size in upgrading of fine coal via oil agglomeration technique. *Fuel Processing Technology*, vol. 138. pp. 21–29.

Temel, H.A., Bozkurt, V., and Majumder, A.K. 2009. Selective oil agglomeration of lignite. *Energy and Fuels*, vol. 23. pp. 779–784.

Unal, I. and Ersan, M.G. 2005. Oil agglomeration of a lignite treated with microwave energy: Effect of particle size and bridging oil. *Fuel Processing Technology*, vol. 87. pp. 71–76.

Unal, I. and Gorgun Ersan, M. 2007. Factors affecting the oil agglomeration of Sivas-Divri i Uluçayır sivas-divrigi Ulucayir lignite. *Energy Sources Part A*, vol. 29. pp. 983–993.

Ünal, L. and Akta, Z. 2001. Effect of various bridging liquids on coal fines agglomeration performance. *Fuel Processing Technology*, vol. 69. pp. 141–155.

Wang, L., Peng, Y., Runge, K., and Bradshaw, D. 2015. A review of entrainment: Mechanisms, contributing factors and modelling in flotation. *Minerals Engineering*, vol. 70. pp. 77–91. ◆

NATIONAL & INTERNATIONAL ACTIVITIES

2018

25–28 February 2018 — **Infacon XV: International Ferro-Alloys Congress**
Century City Conference Centre and Hotel, Cape Town, South Africa
Contact: Gugu Charlie
Tel: +27 11 834-1273/7
Fax: +27 11 838-5923/833-8156
E-mail: gugu@saimm.co.za
Website: http://www.saimm.co.za

12–14 March 2018 — **Society of Mining Professors 6th Regional Conference 2018**
Overcoming challenges in the Mining Industry through sustainable mining practices
Birchwood Hotel and Conference Centre, Johannesburg, South Africa
Contact: Camielah Jardine
Tel: +27 11 834-1273/7
Fax: +27 11 838-5923/833-8156
E-mail: camielah@saimm.co.za
Website: http://www.saimm.co.za

23–26 April 2018—**Application of Multiple Point Statistics to Mineral Resource Estimation—School**
School of Mining Engineering at the University of the Witwatersrand
Contact: Camielah Jardine
Tel: +27 11 834-1273/7
Fax: +27 11 838-5923/833-8156
E-mail: camielah@saimm.co.za
Website: http://www.saimm.co.za

6–7 June 2018 — **Digitalization in Mining Conference**
'Mining business make-over –Exploiting the digital resolution'
Johannesburg, South Africa
Contact: Gugu Charlie
Tel: +27 11 834-1273/7
Fax: +27 11 838-5923/833-8156
E-mail: gugu@saimm.co.za
Website: http://www.saimm.co.za

11–14 June 2018 — **SAIMM: Diamonds — Source to Use 2018 Conference** *'Thriving in Changing Times'*
Birchwood Conference Centre (Jet Park)
Contact: Camielah Jardine
Tel: +27 11 834-1273/7
Fax: +27 11 838-5923/833-8156
E-mail: camielah@saimm.co.za
Website: http://www.saimm.co.za

9–12 July 2018 — **Copper Cobalt Africa in association with The 9th Southern African Base Metals Conference**
Avani Victoria Falls Resort, Livingstone, Zambia
Contact: Gugu Charlie
Tel: +27 11 834-1273/7
Fax: +27 11 838-5923/833-8156
E-mail: gugu@saimm.co.za
Website: http://www.saimm.co.za

6–8 August 2018—**Geometallurgy Conference 2018**
Cape Town, South Africa
Contact: Camielah Jardine
Tel: +27 11 834-1273/7
Fax: +27 11 838-5923/833-8156
E-mail: camielah@saimm.co.za
Website: http://www.saimm.co.za

10–11 September 2018 — **ASM Conference 2018**
'Fostering a regional approach to ASM transformation in sub-Saharan Africa'
Nasrec, Johannesburg (Electra Mining)
Contact: Gugu Charlie
Tel: +27 11 834-1273/7
Fax: +27 11 838-5923/833-8156
E-mail: gugu@saimm.co.za
Website: http://www.saimm.co.za

14–17 October 2018 — **Furnace Tapping 2018 Conference**
Nombolo Mdhluli Conference Centre, Kruger National Park, South Africa
Contact: Gugu Charlie
Tel: +27 11 834-1273/7
Fax: +27 11 838-5923/833-8156
E-mail: gugu@saimm.co.za
Website: http://www.saimm.co.za

Company Affiliates

The following organizations have been admitted to the Institute as Company Affiliates

3M South Africa (Pty) Limited
Atlas Copco (SA) (Pty) Limited
AECOM SA (Pty) Ltd
AEL Mining Services Limited
Air Liquide (PTY) Ltd
AMEC Foster Wheeler
AMIRA International Africa (Pty) Ltd
ANDRITZ Delkor(pty) Ltd
Anglo Operations Proprietary Limited
Anglogold Ashanti Ltd
Arcus Gibb (Pty) Ltd
Aurecon South Africa (Pty) Ltd
Aveng Engineering
Aveng Mining Shafts and Underground
Axis House Pty Ltd
Bafokeng Rasimone Platinum Mine
Barloworld Equipment -Mining
BASF Holdings SA (Pty) Ltd
BCL Limited (BCL001)
Becker Mining (Pty) Ltd
BedRock Mining Support Pty Ltd
BHP Billiton Energy Coal SA Ltd
Blue Cube Systems (Pty) Ltd
Bluhm Burton Engineering Pty Ltd(BLU003)
Bouygues Travaux Publics
CDM Group
CGG Services SA
Chamber of Mines
Coalmin Process Technologies CC
Concor Opencast Mining
Concor Technicrete
CRONIMET Mining Processing SA Pty Ltd
CSIR Natural Resources and the Environment (NRE)
Data Mine SA
Digby Wells and Associates
DMS Powders
DRA Mineral Projects (Pty) Ltd
Duraset
Elbroc Mining Products (Pty) Ltd
eThekwini Municipality
Expectra 2004 (Pty) Ltd
Exxaro Coal (Pty) Ltd
Exxaro Resources Limited
Filtaquip (Pty) Ltd
FLSmidth Minerals (Pty) Ltd (FFE001)
Fluor Daniel SA (Pty) Ltd
Franki Africa (Pty) Ltd-JHB
Fraser Alexander (Pty) Ltd
Geobrugg Southern Africa (Pty) Ltd
GHH Mining Machines (Pty) Ltd
Glencore
Hall Core Drilling (Pty) Ltd
Hatch (Pty) Ltd
Herrenknecht AG
HPE Hydro Power Equipment (Pty) Ltd
IMS Engineering (Pty) Ltd
Ivanhoe Mines SA
Joy Global Inc.(Africa)
Kudumane Manganese Resources
Leco Africa (Pty) Limited
Longyear South Africa (Pty) Ltd
Lonmin Plc
Lull Storm Trading (Pty) Ltd
Magotteaux (Pty) Ltd
MBE Minerals SA Pty Ltd
MCC Contracts (Pty) Ltd
MD Mineral Technologies SA (Pty) Ltd
MDM Technical Africa (Pty) Ltd
Metalock Engineering RSA (Pty)Ltd
Metorex Limited
Metso Minerals (South Africa) Pty Ltd
Minerals Operations Executive (Pty) Ltd
MineRP Holding (Pty) Ltd
Mintek
MIP Process Technologies (Pty) Limited
Modular Mining Systems Africa (Pty) Ltd
MSA Group (Pty) Ltd
Multotec (Pty) Ltd
Murray and Roberts Cementation
Nalco Africa (Pty) Ltd
Namakwa Sands(Pty) Ltd
Ncamiso Trading (Pty) Ltd
New Concept Mining (Pty) Limited
Northam Platinum Ltd - Zondereinde
PANalytical (Pty) Ltd
Paterson & Cooke Consulting Engineers (Pty) Ltd
Perkinelmer
Polysius A Division of Thyssenkrupp Industrial Sol
Precious Metals Refiners
Rand Refinery Limited
Redpath Mining (South Africa) (Pty) Ltd
Rocbolt Technologies
Rosond (Pty) Ltd
Royal Bafokeng Platinum
Roytec Global (Pty) Ltd
RungePincockMinarco Limited
Rustenburg Platinum Mines Limited
Salene Mining (Pty) Ltd
Sandvik Mining and Construction Delmas (Pty) Ltd
Sandvik Mining and Construction RSA(Pty) Ltd
SANIRE
Sebilo Resources (Pty) Ltd
SENET (Pty) Ltd
Senmin International (Pty) Ltd
Smec South Africa
Sound Mining Solution (Pty) Ltd
SRK Consulting SA (Pty) Ltd
Technology Innovation Agency
Time Mining and Processing (Pty) Ltd
Timrite Pty Ltd
Tomra (Pty) Ltd
Ukwazi Mining Solutions (Pty) Ltd
Umgeni Water
Webber Wentzel
Weir Minerals Africa
Worley Parsons RSA (Pty) Ltd

As another busy year comes to a close, we at

The Southern African Institute of Mining and Metallurgy

wish all of our members and those who supported us throughout this year, a heartfelt *Seasons greetings* to you and your families.

We point out to anyone who is interested in joining the SAIMM the benefits of being a member:

- Receipt of a monthly professional *Journal* with informative technical content of a high standard which serves as a communication medium to keep members informed on matters relating to their professional interests.
- Attendance at conferences, symposia, colloquia, schools and discussion groups at competitive prices with discounted rates for members.

- Invitations to participate in technical excursions and social events which create further opportunities for inter-active professional association and networking.
- The SAIMM is registered with ECSA as a Voluntary Association and all SAIMM members qualify for discounted ECSA fees as a result of their SAIMM membership.
- Members obtain valuable ECSA Continued Professional Development (CPD) points when they attend our accredited events.

SAIMM
THE SOUTHERN AFRICAN INSTITUTE OF MINING AND METALLURGY

MINING WITH

ELBROC
MINING PRODUCTS (PTY) LTD

ELBROC OMNI PROP

Dynamic Support

The Omni sacrificial and re-usable hydraulic prop performs in accordance with COMRO guidelines for rock-burst and rock-fall conditions.

- Safe remote installation
- Resilient in rock-burst conditions
- Superb energy absorption
- Can accommodate numerous seismic events
- Constant support resistance
- Reusable
- Light, easy and quick to install
- Cannot be over extended
- Standard attachments
- Controlled yielding

OMNI 89

- 89mm diameter
- 20 ton support resistance
- Blast on dynamic load bearing
- Covers stoping widths up to 2.0m
- Light weight

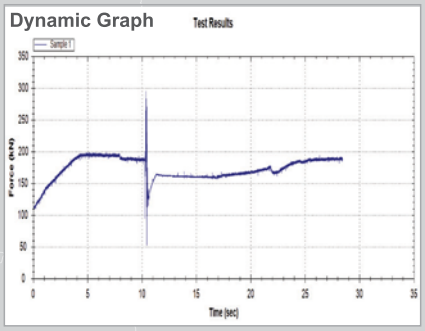

OMNI 127

- 127mm diameter
- 20 ton support resistance
- Blast on dynamic load bearing
- Covers stoping widths up to 4.5m

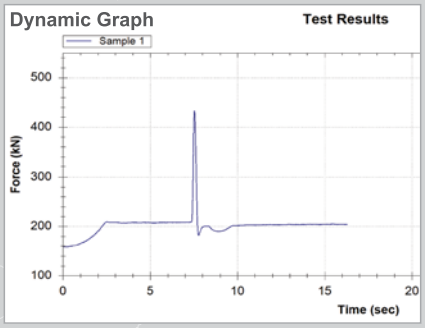

OMNI 150

- 150mm diameter
- 20 & 40 ton support resistance
- Blast on dynamic load bearing
- Covers stoping widths up to 6m
- Longer lengths available

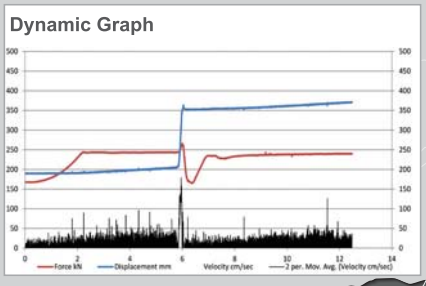

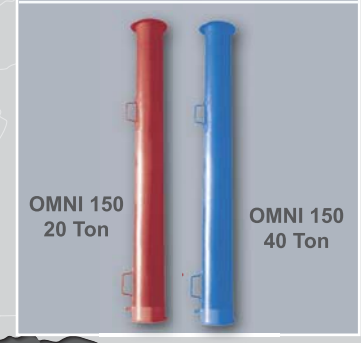

SABS ISO 9001

a member of the rbh royal bafokeng holdings

FOR OUR FULL PRODUCT RANGE PLEASE VISIT OUR WEBPAGE

Tel: 011 974-8013 • sales@elbroc.co.za

www.elbroc.co.za

mogs mining, oil and gas services